



*MANAS
JOURNAL OF
ENGINEERING*

MJEN



BISHKEK 2022



ISSN: 1694- 7398
Year: 2022
Volume: 10
Special Issue: 2
<http://journals.manas.edu.kg>
journals@manas.edu.kg

PUBLICATION PERIOD

Manas Journal of Engineering (MJEN) is published twice year, MJEN is a peer reviewed journal.

OWNERS Kyrgyz - Turkish Manas University
Prof. Dr. Alpaslan CEYLAN
Prof. Dr. Asilbek KULMIRZAYEV

EDITOR Prof. Dr. Nahit AKTAŞ

ASSOCIATE EDITOR Assit. Prof. Dr.Rita İSMAİLOVA

FIELD EDITORS

Prof. Dr. Asilbek ÇEKEEV	(Mathematics, Topology)
Prof. Dr. Anarkül URDALETOVA	(Mathematics)
Prof. Dr. Memet KOBYA	(Environmental Engineering)
Prof. Dr. Özgül SALOR DURNA	(Electrical and Electronics Engineering)
Prof. Dr. Ömer Faruk ÖZTÜRK	(Chemistry - Anorganic)
Assoc. Prof. Dr. Anarseyit DEYDİEV	(Food Engineering, Food Technology)
Assoc. Prof. Dr. Gülbübü KURMANBEKOVA	(Biology, Biochemistry)
Assoc. Prof. Dr. Raimbek SULTANOV	(Computer Engineering, Information Technology)
Assoc. Prof. Dr. Abdullah Erdal TÜMER	(Computer Engineering, Information Technologies)
Asist. Prof. Dr. Emil OMURZAKOĞLU	(Nanoscience, Nanotechnology, Nanomaterials)
Asist. Prof. Dr. Rita İSMAİLOVA	(Computer Engineering, Information Technology)

EDITORIAL BOARD

Prof. Dr. Nahit AKTAŞ	(Chemistry)
Prof. Dr. Mustafa DOLAZ	(Environmental Engineering)
Prof. Dr. Zarlyk MAYMEKOV	(Environmental Engineering)
Prof. Dr. Hilal Demir KIVRAK	(Chemical Engineering)
Prof. Dr. Fahreddin ABDULLAEV	(Applied Mathematics and Informatics)
Assoc. Prof. Dr. Tamara KARAŞEVA	(Physic)
Asist. Prof. Dr. Ayçürök MACİTOVA	(Food Engineering)

EDITORIAL ASSISTANTS Dr. Ruslan ADİL AKAI TEGİN
Kayahan KÜÇÜK
Yusuf GÜNDÜZ
Jumagul NURAKUN KYZY

CORRESPONDENCE ADDRESS

Kyrgyz Turkish Manas University
Chyngyz Aitmatov Avenue 56 Bishkek, KYRGYZSTAN
URL: <http://journals.manas.edu.kg>
e-mail: journals@manas.edu.kg
Tel : +996 312 492763- Fax: +996 312 541935



CONTENT

Tuba Ersen Dudu Duygu Alpaslan	<i>Eco-friendly and biodegradable dimethylacrylamide/starch hydrogels for controlled release of urea and its water retention</i>	116-128
Samir Abbas Ali Noma	<i>Immobilization of xylanase enzyme on poly-(HEMA-co-GMA) cryogel</i>	129-137
Sefika Kaya	<i>Development and application of bimetallic catalysts supported carbon nanotube for 1-propanol electrooxidation</i>	138-144
Damira Sambaeva Mirlan Moldobaev Kubat Kemelov Zarlık Maimekov	<i>Water is an effective additive to fuel oil to reduce the concentration of soot in the gas phase</i>	145-150
Mustafa Bilgin Mustafa Atasever	<i>Determining the enterotoxin genes and methicillin resistance in Staphylococcus Aureus isolated from goat milk and its products</i>	151-158
Yıldırım Özüpak	<i>Design and analysis of switched reluctance motor with FEM based Ansys-Maxwell</i>	159-164
Hasret Subak	<i>Electrochemical biosensor for simultaneously detection of Tamoxifen</i>	165-170
Mehmet Büyük	<i>Investigation and analysis of interleaved dc-dc boost converter for grid-connected photovoltaic energy system</i>	171-178
Pelin Demirçivi	<i>Synthesize of montmorillonite supported hydroxyapatite and determination of adsorption capacity by tetracycline removal</i>	179-186
Feride Ulu	<i>Solidification of tannery sludge with various binders</i>	187-193
Ella Abylaeva Asan omuraliev	<i>Asymptotics of the solution of the hyperbolic system with a small parameter</i>	194-198
Burak Uyar Cevdet Büyüksu	<i>Determining the factors affecting the happiness levels of divorced individuals by ordered logistics regression analysis</i>	199-208
Elsayed Elsayed Badriah Alofi	<i>Stability analysis and periodictly properties of a class of rational difference equations</i>	209-216
Yuksel Soykan Erkan Tasdemir Vedat Irge	<i>On Matrix Sequences of modified Tribonacci-Lucas Numbers</i>	217-227
Merve Aktay Murat Ozdemir	<i>On (α, ϕ)-weak Pata contractions</i>	228-240



MJEN



Eco-friendly and biodegradable dimethylacrylamide/starch hydrogels for controlled release of urea and its water retention

Tuba Ersen Dudu^{1,2,*}, Duygu Alpaslan^{1,2}

¹ Department of Chemical Engineering, Institute of Natural and Applied Science, Van Yuzuncu Yil University, Van, 65080, Turkey, tuba_ersen@hotmail.com, ORCID: 0000-0001-5564-2834

² Department of Mining Engineering, Faculty of Engineering, Van Yuzuncu Yil University, Van, 65080, Turkey

ABSTRACT

In this study, we focused on the synthesis of polymeric hydrogels that will support the sorption and controlled release of urea, which is a rich nitrogen source, from aqueous solutions and their usability in agricultural applications. N, N-Dimethylacrylamide (DMAAm) and Starch (St) were selected as monomers, and their superior properties, such as chemical stability, high sorption properties, biocompatibility, and the presence of modifiable groups, were utilized. A redox polymerization technique was used to create a poly(DMAAm-co-St)-based hydrogel that was then modified with acidic and basic agents to improve the properties of starch. The synthesized acid- and base-modified hydrogels were named DSt, DSt₁, and DSt₂, respectively. Swelling analyses were performed to examine the structural and morphological properties of DSt, DSt₁, and DSt₂ hydrogels, and Fourier-Transform Infrared Spectroscopy (FT-IR) and Thermogravimetric Analyzers (TGA) were used. Intense cross-linking, porosity, and the presence of hydrophilic groups were successfully detected by instrumental analysis and swelling results. The successful results of urea sorption by DSt, DSt₁, and DSt₂ hydrogels show that they can both minimize the harmful effects of urea in the environment and contain the nitrogen necessary for plants. At the same time, urea sorption behaviors were evaluated in terms of sorption isotherms and thermodynamic properties, and it was observed that urea sorption conformed to the Langmuir isotherm. The urea release results showed that DSt, DSt₁, and DSt₂ hydrogels exhibited different release properties in different pH solutions, and these results reached 94% at pH 6–8, 100% at pH 6, and 100% at pH 8–10, respectively. As a result of the gradual decrease in the water resources on the earth, the increase in the use of fertilizers in agricultural production, and the insufficient use of fertilizers, our study draws attention to the development and support of materials that absorb/store water, and forms of controlled release fertilizers and provides potential ease of application

ARTICLE INFO

Research article

Received: 26.10.2022

Accepted: 16.12.2022

Keywords:

controlled release hydrogel

nitrogen loss

starch

water retention

*Corresponding Author

1. Introduction

Nitrogen, phosphorus, and potassium fertilizers are especially used to increase and improve productivity in agricultural areas [1–2]. If these fertilizers, also known as mineral fertilizers, are used in accordance with the plant's request, type, soil characteristics, and climatic conditions, significant problems do not occur in the soil. However, with the development of agricultural practices, various chemicals, fertilizers, various wastes, and residues applied to the soil and plants pollute the soil and water resources, making them uninhabitable for living creatures [3–4]. Some of these substances, which mix with precipitation and irrigation water in the lower layers of the soil and from there into the groundwater, deteriorate the quality of the waters and make them undrinkable. Thus, both unnecessary economic losses

and important problems related to soil and water pollution arise [5–7]. Recently, various studies have been carried out on the capture and controlled release of nitrogen and phosphorus fertilizers, which play an important role in soil and water pollution, and attention has been drawn to various biocompatible polymeric materials for this purpose. Hydrogels, which are polymeric materials, provide advantages for use in agricultural applications due to their various properties, such as the presence of hydrophilic groups, cross-linked structures, and insolubleness in water [8–10]. Especially in the literature, the usability of hydrogels synthesized from many monomers, such as dimethylacrylamide, maleic acid, citric acid, acrylamide, cellulose, chitosan, alginate, and acrylic acid, in agricultural applications has been emphasized. The common point of all these studies is that the synthesized hydrogels have

hydrophilic properties and superabsorbent properties [11–16].

As a non-ionic monomer that polymerizes easily, DMAA's characteristics, such as high reactivity, low initiation temperature, chemical stability, and high sorption capacity, make it suitable for copolymerization reactions [17–18]. Due to its various properties, such as being produced from various sources, being an annually renewable resource, being water sensitive, and being biodegradable, starch has been used in most fields, such as thickening, gelling, and encapsulating agents in food products; coating binders and adhesives in papermaking; and the development of textiles, cosmetics, plastics, and polymeric materials [19–20]. Therefore, in this study, DMAAm and starch were chosen as monomers due to their biodegradability, excellent biocompatibility, chemical stability, and high water retention, and the sorption and release studies of urea fertilizer were focused on. Polysaccharide-based DSt hydrogels were synthesized by the free radical addition polymerization technique, and modified with acid and base agents to improve the positive properties of starch and minimize its negative properties. The chemical structure and morphological properties of DSt, DSt₁, and DSt₂ hydrogels were investigated with FT-IR and TGA devices. At the same time, their water sorption capacity was examined in distilled water and solutions at different pH values. Urea sorption and release experiments with DSt, DSt₁, and DSt₂ hydrogels were also examined. Urea sorption experiments were carried out at different urea concentrations, different pHs, and different temperatures, and the release behavior of urea-sorbed hydrogels was investigated in different pH environments.

2. Experimental

2.1. Materials

N, N-Dimethylacrylamide (Sigma Aldrich, 100%, DMAAm), and starch (Merck, 100%, St) were starting materials for the hydrogel synthesis. The crosslinking agent, accelerator, and initiator used were N, N'-methylene bis acrylamide (Merck, 99%, MBA), N, N, N', N'-tetramethylethylenediamine (Merck, 99%, TEMED), and ammonium persulfate (Merck, 98%, APS), respectively. Urea (Merck, 100%) was used as sorbat. Sodium hydroxide (Merck, 100%, NaOH) and hydrochloric acid (Sigma Aldrich, 37.5%, HCl) were used as the modification agents. The deionized water (DI water) was obtained from 18.2 MΩ.cm (Millipore Direct-Q3 UV). The pH measurements were carried out with a Thermo Scientific pH meter (USA). Ultra-Violet spectroscopy (UV-Vis, Thermo Scientific GENESYS 10S, USA) was used to quantify the amount of urea during sorption and release studies.

2.2. Preparation of hydrogels

DMAAm and St monomers were used to synthesize hydrogels via the redox polymerization technique. Briefly, 1.5.10⁻³ g of MBA crosslinker was dissolved in 1 mL of DMAAm monomer, and 1 mL of deionized water was added to the mixture and thoroughly mixed (at 2500 rpm) for one minute. To this mixture, 2 mL of a St solution (1 g/10 mL) was added and thoroughly mixed. Then 5 μL of TEMED and 0.2 mL of APS solution were added sequentially. The reaction mixture was carefully mixed for approximately one minute and allowed to polymerize and crosslink to complete the reaction (at about six hours). Then, the hydrogel was removed from the polymerization medium, cut into 6 mm long cylinders, cleaned by placing it in DI water, and named p(DMAAm-co-St) (DSt) hydrogel. After the cleaning procedure, the hydrogel was dried in an oven at 40°C to a constant weight and kept in sealed containers for further studies [11–21]. In the hydrogel modification process, the method applied by Ersen Dudu et al. (2019) was used and named p(DMAAm-co-St)/HCl (DSt₁) and p(DMAAm-co-St)/NaOH (DSt₂) hydrogels [8].

2.3. Characterization of Hydrogels

The Fourier-Transform Infrared Spectroscopy (FT-IR) investigation was performed using an Attenuated Total Reflection (ATR) built-in instrument (Thermo, model Nicolet iS10 FT-IR Spectrometer, USA). After being ground into powder, the hydrogel was arranged on the ATR sample plate. 4 cm⁻¹ of the resolution was used to examine the spectral range between 4000 and 650 cm⁻¹.

A Setaram Labsys Evo Gravimetric Analyzer (TGA/DSC 1600 model, France) was used to conduct TGA experiments on hydrogels. In ceramic crucibles, samples weighing 4–6 mg were put. Under an argon atmosphere, the samples were heated at a rate of 10°C/min from 50°C to 1000°C. A fixed 100 mL/min argon gas flow rate was used in the analyzer.

2.4. Swelling analysis

Swelling studies in water are a widely used technique for characterizing hydrogels. Both kinetic and balance swelling studies are based on the determination of the increase in mass or volume of a cross-linked gel held in a solvent. Swelling experiments were performed with the method specified in the literature, and swelling values (S%) were calculated using the equation given below.

$$S\% = \left(\frac{M_t - M_0}{M_0} \right) \cdot 100 \quad (1)$$

where M_0 is the beginning mass (g) of the hydrogel and is the mass of the hydrogel at the end of time t [22, 23]. The equilibrium swelling behavior of the synthesized hydrogels was also evaluated at different pH values. SR was also studied by adjusting the pH of the solutions with 0.1 M HCl and 0.1 M NaOH. Again, hydrogels were kept for 24 h in

acidic and basic solutions to determine the effect of medium pH on the swelling ratios.

Swelling is a characteristic feature of polymeric networks. Depending on the amount of crosslinking and the presence of hydrophilic groups, polymeric networks can absorb very large amounts of liquid without dissolving. The most basic way to describe the swelling behavior is to apply the swelling data to the equation below by accepting the swelling kinetic curves created as a result of the dynamic swelling tests as quadratic [24].

$$\frac{dS}{dt} = k_s \cdot (S_{\max} - S)^2 \quad (2)$$

where dS/dt is the swelling speed of hydrogels; S_{\max} is the swelling value of hydrogel at equilibrium ($g_{\text{water}}/g_{\text{hydrogel}}$); S is the swelling value at time t ($g_{\text{water}}/g_{\text{hydrogel}}$); k_s represents swelling speed constant ($g_{\text{hydrogel}}/(g_{\text{water}} \cdot \text{min})$); r_0 is the initial swelling speed ($g_{\text{water}}/(g_{\text{hydrogel}} \cdot \text{min})$).

Modeling the swelling kinetics of hydrogels is important for understanding the type and rate of diffusion of water into the hydrogel, as well as the forces acting on the swelling of the hydrogel. The most commonly used relations for modeling the swelling kinetics of hydrogels are Fick's laws. The following equation is the version of Fick's law applied to reticulated, swellable polymers [25].

$$F = \left(\frac{M_t}{M_e} \right) = k \cdot t^n \quad (3)$$

where M_e represents the mass of hydrogels that have reached equilibrium (g); k is a specific rate constant; n is a constant which shows diffusion exponent; t is time (min). The value of the diffusion exponent (n) is found from the slope of the graph between $\ln(M_t/M_e)$ and $\ln(t)$. The graph was drawn by applying it to data where the swelling has not yet reached equilibrium and the (M_t/M_e) ratio is less than 0.6.

2.5. Sorption experiments

Urea is a compound of physiological importance. It is both found in the bodies of mammals and excreted as waste, and it is also used in the production of fertilizer, animal feed, medicine, plastic, and paint. For this reason, it is in the class

of pollutants that cause pollution of environmental waters and soil, and it is a fertilizer that has great importance in the development of plants. The sorption experiments were carried out in a temperature-controlled magnetic stirrer in triplicate. To examine the effect of initial urea concentrations, the urea concentration was kept in the range of 10 to 1000 mg/L, while the hydrogel concentration, time, temperature, and stirring speed were kept constant at 1 g/L, 48 hours, 298 K, and 150 rpm, respectively. To examine the effect of pH change on urea sorption, pH was changed between 2 and 12, and urea concentration, amount of hydrogel, temperature, stirring speed, and time were kept constant at 100 mg/L, 1 g/L, 298 K, 150 rpm, and 24 hours. The effect of temperature on urea sorption was investigated by changing the temperature between 283 and 323 K while keeping the urea concentration, hydrogel amount, ambient pH, mixing speed, and time constant at 100 mg/L, 1 g/L, 12, 150 rpm, and 24 hours. In all sorption studies, the amount of urea in the solution was determined by a UV-Vis spectroscopy device, and the amount of urea loaded per unit mass of hydrogels, q_e (mg/g), was calculated with the following equation [26].

$$q_e = \frac{(C_o - C_e) \cdot V}{M} \quad (4)$$

where C_o represents the initial concentration of urea (mg/L); C_e is the equilibrium concentration of urea (mg/L); V represents the solution volume (L); and M is the hydrogel mass (g).

2.5.1. Urea sorption isotherms and thermodynamic studies

The urea sorption mechanism of hydrogels was evaluated using Langmuir (Eq. (5)) [27], Freundlich (Eq. (6)) [28], Temkin (Eq. (7)) [29], and Dubinin–Radushkevich (D–R) (Eq. (8)) [30] isotherm models (see Table 1a for equations).

In order to describe the thermodynamic behavior of urea sorption, thermodynamic parameters such as free energy change (ΔG° , J/mol), enthalpy change (ΔH° , J/mol), and entropy change (ΔS° , J/(mol.K)) were calculated using Equation 9 defined in the literature (see Table 1b for equations) [31–32].

Table 1. a) Sorption isotherm models for urea sorption, b) Thermodynamic parameters of urea sorption, and c) Mathematical models for urea release

a) Model	Mathematical Equation	
Langmuir (Eq. 5)	$\frac{C_e}{q_e} = \left(\frac{C_e}{q_{max}}\right) + \left(\frac{1}{q_{max} \cdot K_L}\right)$	
Freundlich (Eq. 6)	$\log q_e = \log K_f + \left(\frac{1}{n}\right) \log C_e$	
Temkin (Eq. 7)	$q_e = \frac{R \cdot T}{b_T} \ln A_T + \left(\frac{R \cdot T}{b_T}\right) \ln C_e$	
Dubinin–Radushkevich (D–R) (Eq. 8)	$\ln q_e = \ln q_s - \beta \cdot \varepsilon^2$ $\varepsilon = R \cdot T \cdot \ln \left(1 + \frac{1}{C_e}\right)$ $E = \frac{1}{\sqrt{2 \cdot \beta}}$	
b) Model	Mathematical Equation	
Thermodynamic parameters (Eq. 9)	$K^0 = \frac{C_t}{C_e}$ $\Delta G^0 = \Delta H^0 - T \cdot \Delta S^0$ $\ln K^0 = \frac{\Delta S^0}{R} - \frac{\Delta H^0}{R \cdot T}$	
c) Model	Mathematical Equation	Release Mechanism
Zero order kinetic model (Z-O) (Eq. 11)	$C_r = C_0 - k_0 \cdot t$	Diffusion Mechanism
First order kinetic model (F-O) (Eq. 12)	$\ln C_r = \ln C_0 - k_1 \cdot t$	Fick's first law, diffusion Mechanism
Higuchi Model (H) (Eq. 13)	$\frac{C_r}{C_\infty} = k_H \cdot \sqrt{t}$	Diffusion medium based Mechanism in Fick's first law
Korsmeyer-Peppas Model (K-P) (Eq. 14)	$\ln \frac{C_r}{C_\infty} = \ln k_{KP} + n \cdot \ln t$	Semi empirical model, diffusion-based mechanism

q_{max} is the monolayer sorption capacity of urea (mg/g); K_L is the L sorption equilibrium constant (L/mg) which can be determined via the linearized L isotherm; K_f (mg/g) and n are the F constants related to sorption capacity and sorption intensity, respectively; R is universal gas constant (8.314 J/(mol.K)); T is temperature at 298 K; A_T and b_T are T isotherm equilibrium binding constant (L/g) and T isotherm constant, respectively; q_s is the D-R monolayer sorption capacity (mg/g); ε is the Polanyi potential based upon equilibrium concentration; β is a constant based upon sorption energy (mol^2/J^2); E is sorption energy (kJ/mol). C_r is concentration of urea release in time t (mg/L); C_0 is the initial concentration of urea in the solution (most times, $C_0 = 0$) (mg/L); k_0 is the Z-O release constant expressed in units of concentration/time (mg/(L.min)); t is time (min); k_1 is the F-O release constant (1/min); C_∞ is concentration of urea release in equilibrium (mg/L); k_H is H release rate constant ($1/\sqrt{\text{min}}$); k_{KP} is K-P release rate constant; n is release exponent which is indicative of the transport mechanism ($M_t/M_\infty < 0.6$ should only be used); K^0 represents sorption equilibrium constant; and C_t represents the sorbed urea concentration at time t (mg/L); ΔG^0 is Gibbs free energy change (J/mol), ΔH^0 is enthalpy change (J/mol) and ΔS^0 is entropy change (J/(mol.K)).

2.6. Urea release in an aqueous medium and mathematical modeling

In this study, we focused on both the sorption of urea and the controlled release behavior. Although the loss of urea in

environmental waters causes pollution, its use as a controlled-release fertilizer is also of great importance. The usability of the DSt-based hydrogels we synthesized in the present study as a controlled urea release support material was also investigated and constituted the second pillar of this

study. Urea release experiments were performed in triplicate in different aqueous buffer solutions ranging from 2 to 12. Ambient temperature, stirring speed, and amount of urea-loaded hydrogel were kept constant at 298 K, 150 rpm, and 0.05 g, respectively. Release experiments were performed until the equilibrium value was reached as a function of time. To determine the amount of urea released, approximately 2 mL of sample was withdrawn from the solution at regular intervals, and the amount of released urea was measured using a UV-visible spectrophotometer. The cumulative urea release percentage was calculated with the following equation [33];

$$\text{Release\%} = \frac{Q_t}{Q_o} \cdot 100 \quad (10)$$

where Q_o represents the urea amount sorbed by the hydrogel (mg/L) and Q_t is the urea amount released into the solution medium at time t (mg/L).

In order to examine the release kinetics of urea in DSt-based swellable polymeric hydrogels, the release data were obtained experimentally and applied to four different release equations: the zero-order kinetic model (Z-O model) (Eq. 11) [34], the first-order kinetic model (F-O model) (Eq. 12) [34], the Higuchi model (H model) (Eq. 13) [35], and the Korsmeyer-Peppas model (K-P model) (the power law) (Eq. 14) [36]. They were displayed in Table 1c as model equations.

3. Results and discussion

3.1. Characterization

Fourier transform infrared (FT-IR) spectroscopy is a method frequently used to identify bonds in the structure of molecules, such as the determination of intramolecular bonds, the determination of molecular structure, the examination of intramolecular functional groups, and the determination of unknown molecules by library scanning. Figure 1a shown the FT-IR spectra of all hydrogels. Figure 1a, when analyzed, represented the broad peak -OH band observed in the 3678 to 3035 cm^{-1} region. The peaks occurring around 3429 cm^{-1} , 3434 cm^{-1} , and 3459 cm^{-1} in the three FT-IR spectra were assigned to the N-H stresses caused by the crosslinker. The aliphatic -CH bending vibration of DMAAm, starch, and MBA occurred at about 2926 cm^{-1} . It was determined that the peaks observed at approximately 1619 cm^{-1} in the same spectra correspond to the C = O stresses of DMAAm and MBA. It was determined that the peak determined around 1498 cm^{-1} belonged to the C-N tension of acrylamide, and the intensity of this tension increased after the modification. When all spectra were examined, it was determined that the strength of the structural bonds changed and the strength of the hydrogen bonds increased with the modification.

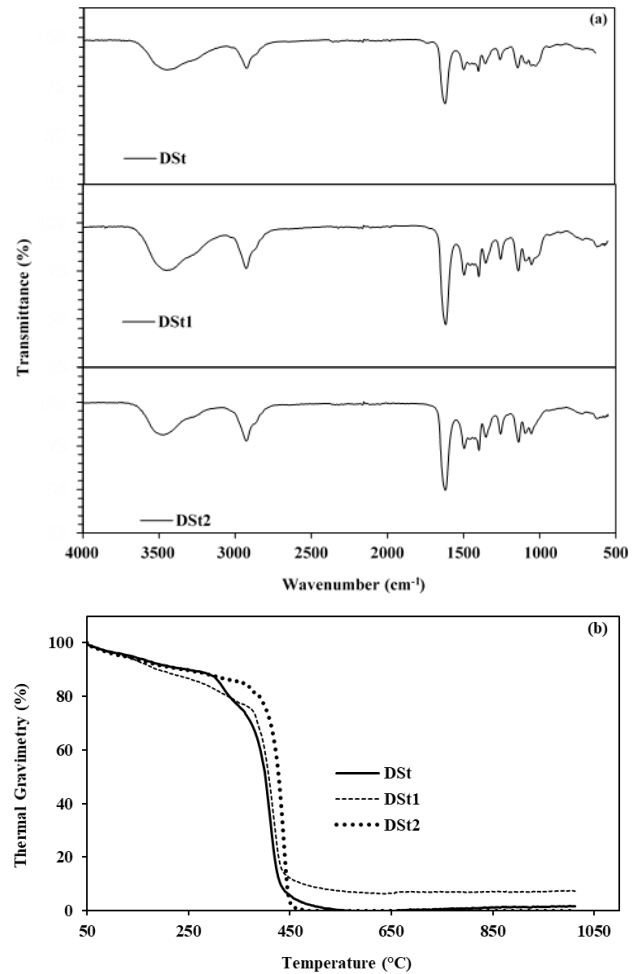


Figure 1. (a) FT-IR Spectra of DSt, DSt₁, and DSt₂ hydrogels, and (b) The Thermogravimetric Analysis of DSt, DSt₁, and DSt₂ hydrogels.

In the thermogravimetric analysis method, mass loss can be determined with temperature increases. For this reason, reactions such as oxidation, evaporation, sublimation, and desorption that may occur in the sample can be examined, and information about the degradation mechanism of the polymer can be provided. Thermogravimetric analysis results were presented in Figure 1b. In Figure 1b, it was seen that although DSt and DSt₁-based hydrogels degraded in four steps, the DSt₂-based hydrogel exhibited degradation behavior in two steps. When the temperature degradation curves were examined separately, it was determined that the DSt, DSt₁ and DSt₂ hydrogels had 100%, 6.4%, and 100% total mass loss, respectively, when temperatures of 597°C, 534°C, and 483°C were reached. Decomposition thermograms showed that after the modification of the DSt hydrogel with acid, its resistance to increasing temperature increased and its mass loss decreased. In addition, TGA thermograms showing the decomposition behavior with temperature explain that decompositions up to about 100–150 °C are caused by unbound water in the structure, losses between about 150–250 °C are caused by the removal of

bound water and slightly volatile compounds, and decomposition steps above 250°C were caused by structural deterioration and bond breaks.

3.2. Swelling analysis

The swelling behavior of hydrogels in pure water and in buffer solutions with different pH values can be explained by the presence of intense cross-linking, porosity, and hydrophilic groups. With the diffusion of the solvent into the polymeric lattice, swelling begins, and after a while, the rate of solvent transfer to the gel and the rate of release from the gel become equal. In this case, the gel reaches the equilibrium swelling ratio (S_{max}) [37]. In order to examine the swelling behavior of the synthesized hydrogels in a deionized water environment, dynamic swelling experiments were carried out at 25°C with a 0.05 g hydrogel amount at certain time intervals, and the results are given in Figure 2a. According to the data obtained, it was found that the DSt, DSt₁, and DSt₂ hydrogels reached the equilibrium swelling value after approximately 56 hours and were 1115%, 2364%, and 2629%, respectively. The equilibrium swelling values obtained indicate that the hydrophilicity of the DSt-based hydrogel increased after modification.

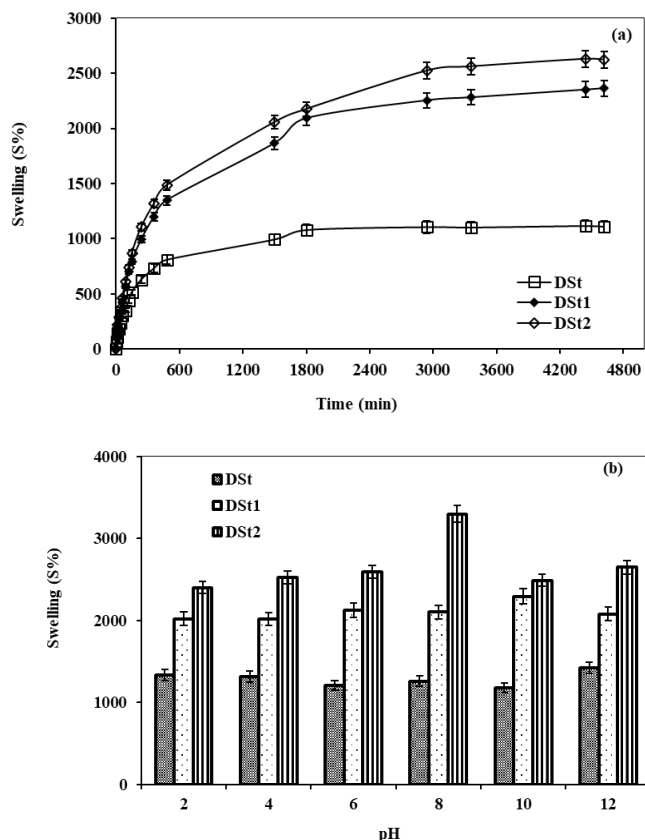


Figure 2. (a) Percent swelling degree of the DSt, DSt₁, and DSt₂ hydrogels with time in deionized water, and (b) Swelling % of the DSt, DSt₁, and DSt₂ hydrogels as a function of pH (pH is adjusted by the addition of 0.1 M HCl, 0.1 M NaOH; time: 24 h).

The water-holding capacity (swelling) of hydrogels containing anionic or cationic groups is significantly affected by pH change. The pH-dependent water holding capacities of DSt, DSt₁, and DSt₂-based hydrogels synthesized within the scope of this study were examined at 25°C and 0.05 g hydrogel amount in the pH = 2–12 range, and the results were reported in Figure 2b. When Figure 2b was examined, it was concluded that the nonionic structure of the DMAAm monomer was dominant in the DSt-based hydrogel. At the same time, it was determined that the swelling behavior of the DSt-based hydrogel was not significantly affected by the pH change, and the equilibrium swelling value was 1421% at pH 12. When the graphs showing the swelling behavior of DSt₁ and DSt₂-based hydrogels were examined, it was determined that the swelling capacity was affected by the pH change and that they reached different swelling values. The maximum equilibrium swelling values of DSt₁ and DSt₂-based hydrogels were observed to be 2294% at pH 10 and 3302% at pH 8, respectively. The different swelling behavior of DSt₁ and DSt₂-based hydrogels at different pH values is due to the fact that the ions in the external environment they are placed in penetrate the hydrogel and come into contact with more ionic groups, and as a result, they reach different equilibrium swelling values at different pH values.

While calculating the diffusion exponent and constant by drawing the $\ln F-t$ graph using the data expressing the weight change over time obtained as a result of the dynamic swelling experiments, the theoretical swelling percentage, swelling velocity, and rate constant values were calculated by drawing the $t/S-t$ curve. And then the results were summarized in Tables 2 and 3. When Table 2 was examined, the n values for DSt, DSt₁, and DSt₂ hydrogels were found to be 0.37, 0.45, and 0.45, respectively. These values comply with the $n \leq 0.45$ rule. In this case, it was concluded that the diffusion types of all three hydrogels fall into the Fickian type diffusion class. In this case, it can be said that swelling is controlled by the diffusion rate of water [38]. In addition, when Table 3 was examined, it was shown that the theoretical equilibrium swelling values (S_{max}) of the prepared cross-linked hydrogels were in harmony with the experimental equilibrium swelling values. This agreement in the swelling results was an indication that the swelling kinetics analysis was built on the right foundations. At the same time, it was observed that the initial swelling velocity (r_0) value and swelling capacity increased after the modification of the DSt hydrogel.

Table 2 Results of the diffusion exponent (n), correlation coefficient (R^2), and the specific rate constant (k) for the swelling kinetics in deionized water of the hydrogels

Water type	Hydrogels	Diffusion Exponent (n)	Specific Rate Constant (k)	Correlation Coefficient (R^2)
Deionized water	DSt	0.37	0.07	0.9873
	DSt ₁	0.45	0.04	0.9904
	DSt ₂	0.45	0.04	0.9906

Table 3 Results belonging to the swelling value at time t (S), the swelling value at equilibrium (S_{max}), the initial swelling speed (r_0) and swelling speed constant (k_s) in deionized water of the hydrogels

Water type	Hydrogels	S (%) ($\frac{g_{water}}{g_{hydrogel}}$)	S_{max} (%) ($\frac{g_{water}}{g_{hydrogel}}$)	r_0 ($\frac{g_{water}}{g_{hydrogel} \cdot \text{min}}$)	k_s ($\frac{g_{hydrogel}}{g_{water} \cdot \text{min}}$)
Deionized water	DSt	1115	1111	7.58	$6.14 \cdot 10^{-6}$
	DSt ₁	2364	2500	9.24	$1.48 \cdot 10^{-6}$
	DSt ₂	2629	2500	9.83	$1.57 \cdot 10^{-6}$

3.3. Sorption tests

In batch sorption studies, the effects of variables such as initial urea concentration, initial pH, and temperature on the sorption capacities of all sorbents were examined. The related graphics are given in Figure 3(a-c). The effect of initial urea concentration on urea sorption to dry DSt, DSt₁, and DSt₂ hydrogels was investigated at 48 hours, at 298 K, and in the range of 10–1000 mg/L urea. As seen in Figure 3a, it was determined that the sorption rate and capacity values increased as the initial urea concentration increased. It was determined that the urea sorption capacity of the DSt₂ hydrogel was higher than the other two hydrogels and was 128.5 mg/g. The results showed that the base modification made the hydrogel more sensitive to urea and increased its sorption capacity. At the same time, it was concluded that the hydrogel structure gave a remarkable attraction to urea in its modification with acid, and this value was 112.7 mg/g.

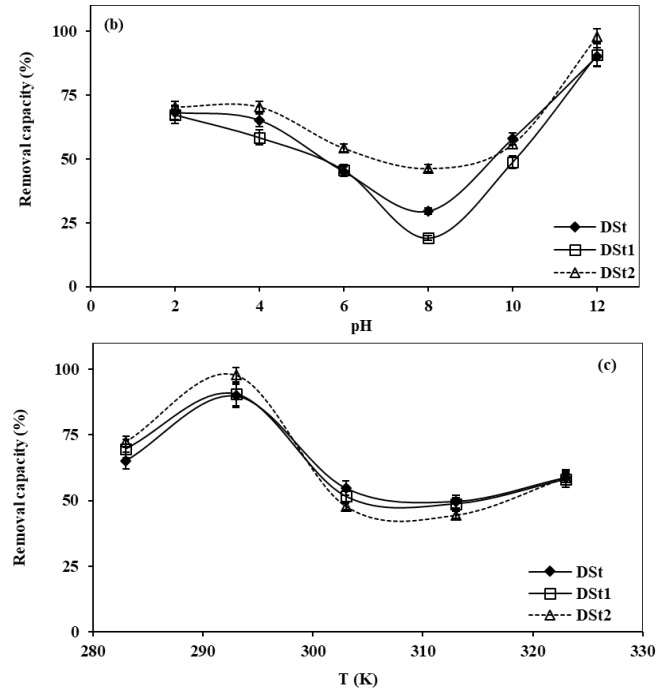
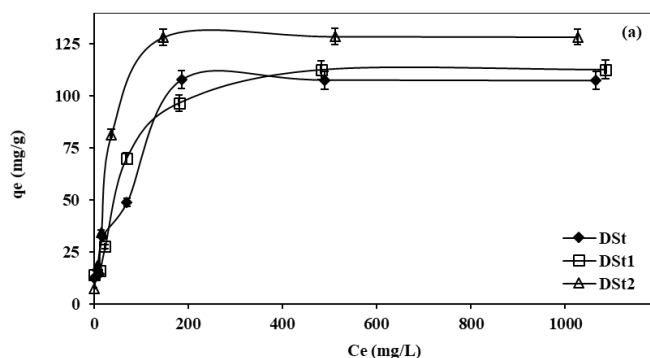


Figure 3. (a) The q_e vs C_e graphs at different urea concentrations of the hydrogels (urea concentration: 10-1000 mg/L (50 mL), sorbent dosage: 1 g/L, time: 48 h, temperature: 25 °C), (b) Effect of pH on the percent uptake of urea onto the hydrogels (pH: 2-12, urea concentration: 100 mg/L (50 mL), sorbent dosage: 1 g/L, time: 24 h, temperature: 25 °C), and (c) Effect of temperature on the percent uptake of urea onto the hydrogels (temperature: 10-50 °C, urea concentration: 100 mg/L (50 mL), sorbent dosage: 1 g/L, pH: 12, time: 24 h).

The urea removal potentials of dry DSt, DSt₁, and DSt₂ hydrogels from aqueous solutions were investigated in the pH 2–12 range for 24 hours at 298 K and 100 mg/L urea concentration. The amount of urea sorbed by all three sorbents was calculated as a percent, and the percent sorbed amounts against pH were shown in Figure 3b. It is seen from the graph that the sorption performances of each sorbent against urea are different from each other. Looking at Figure 3b, it was seen that the DSt₂-based hydrogel had a higher sorption ability against urea at different pHs than the other two hydrogels. DSt, DSt₁, and DSt₂ hydrogels reached the highest urea sorption capacity at pH 12; the results were 90%, 91%, and 98%, respectively. The fact that the surface functional groups of DSt₂ were higher than those of other sorbents caused an increase in sorption performance. In light of the sorption data obtained, it is concluded that the pH value is one of the most critical parameters affecting the sorption and that it significantly affects the sorption depending on the sorbate type and sorbent character of the solution.

In order to examine the effect of temperature on urea sorption from an aqueous solution on dry DSt, DSt₁, and DSt₂ hydrogels, sorption experiments between 283 and 323K were carried out. Initial urea concentration was chosen as

100 mg/L and pH 12, and sorption tests were applied under optimum conditions. Using the results obtained, the temperature–percent sorption graph was plotted in Figure 3c. When Figure 3c was examined in detail, as the temperature increased from 283 K to 293 K, the sorption efficiency increased from 65% to 89% for DSt, from 70% to 91 for DSt₁, and from 73% to 97% for DSt₂. It was seen that the sorption capacity for all hydrogels decreased with increasing the temperature from 293 K to 323 K. The positive effect of a temperature increase up to 293 K on sorption can be attributed to reasons such as increased sorbent-sorbate interaction with temperature, passive sites becoming more active, or intraparticle diffusion becoming more effective as a result of the enlargement of the pore structure of the sorbent. It was thought that the decrease after 293 K was due to the fact that the energy required for the sorption to take place was provided at 293 K and the increasing temperature affected the urea sorption negatively since the sorption exhibits exothermic properties after this temperature.

3.3.1. Sorption isotherms and thermodynamics

In order to explain the sorption behavior of DSt, DSt₁, and DSt₂ hydrogels against increasing initial urea concentrations, the four most known and applied sorption isotherms were examined, and the constants of the obtained sorption isotherms were given in Table 4. It was clear from Table 4 that the curves that best describe urea sorption by DSt, DSt₁, and DSt₂ hydrogels belong to the Langmuir isotherm, as confirmed by high R² values. In the Langmuir isotherm, the sorbent surface is considered to be similar in energy and is known to be used to explain monolayer homogeneous sorption. Thus, it is expected that these regions will form a monolayer by keeping the urea in equal numbers, irreversible adsorption, and high compatibility [39]. When the q_m values expressing the Langmuir sorption capacity were examined, it was observed that they were in good agreement with the experimental q_e values. The monolayer sorption capacities of urea for DSt, DSt₁, and DSt₂ were calculated as 111 mg/g, 119 mg/g, and 132 mg/g, respectively. Table 4 showed that the Freundlich, Temkin, and D–R isotherms exhibited a lower correlation with experimental sorption data compared to the Langmuir model.

Table 4 Isotherm results for sorption of urea by hydrogels

Model		Hydrogels		
		DSt	DSt ₁	DSt ₂
Langmuir	K _L (L/mg)	0.023	0.021	0.037
Isotherm	q _m (mg/g)	111.1	119.1	131.6
Constants	R ²	0.9930	0.9950	0.9981
Freundlich	K _f	10.3	10.9	13.2
Isotherm	n	2.71	2.76	2.66
Constants	R ²	0.8978	0.8746	0.8056
Temkin	b _T	145.9	142.3	103.8
Isotherm	A _T (L/g)	0.7	0.71	0.46
Constants	R ²	0.8456	0.8656	0.8758
D–R	E (kJ/mol)	0.13	0.11	0.16
Isotherm	R ²	0.3343	0.3559	0.8171
Constants				

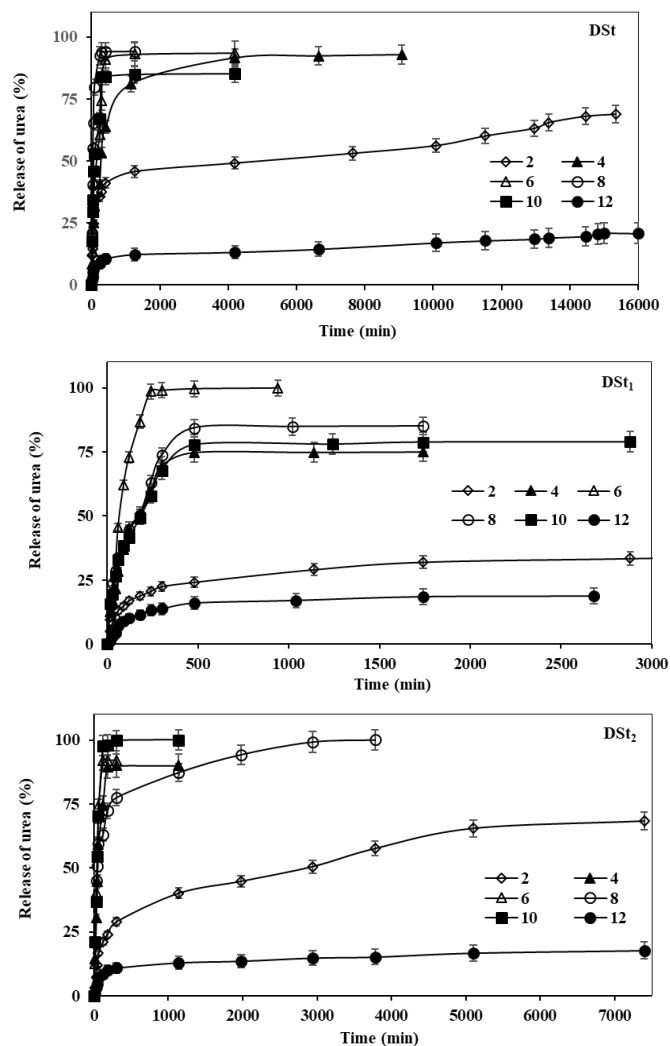
Equation 9 was used to determine the thermodynamic parameters ΔG° , ΔS° , and ΔH° , and $\ln K_c - 1/T$ graphs were drawn. The values calculated from the graph were given in Table 5. When the ΔG° values in the table were examined, it was observed that the ΔG° values increased with increasing temperature. Negative ΔG° values indicated that urea sorption occurs spontaneously and in a suitable process, while positive ΔG° values indicated that increasing temperature negatively affects urea sorption. The results showed that urea sorption was possible at low temperatures. Negative ΔH° values indicated that urea sorption on the three hydrogels was an exothermic process. ΔH° can also be helpful in deciding whether sorption is chemical or physical. While the enthalpy value is generally less than 4.2 kJ/mol in physical sorption, it has a value greater than 21.0 kJ/mol in chemical sorption [40]. Looking at the ΔH° values in the table, it can be said that urea sorption on hydrogels proceeds chemically. The negative ΔS° values indicated that the randomness of the sorption equilibrium occurring at the solid-liquid interface during urea sorption decreased [41].

Table 5 Thermodynamic parameters for sorption of urea by hydrogels

Hydrogels	Thermodynamic Parameters			
	Temperature (K)	ΔG° (J/mol)	ΔH° (J/mol)	ΔS° (J/(mol.K))
DSt	283	-	-	-
	293	2028.5	-	-
	303	-	21756.1	-69.1
	313	-634.3	-	-
	323	62.8	-	-
DSt ₁	283	-	-	-
	293	1979.7	-	-
	303	-	25060.1	-81.6
	313	1164.1	-	-
	323	-348.5	-	-
DSt ₂	283	-	-	-
	293	1987.4	-	-
	303	-1034	28967.6	-95.3
	313	-80.6	-	-
	323	872.7	-	-
323	1826.1	-	-	-

3.4. Cumulative urea release behavior

In the study, the release of urea, which has fertilizer properties, was monitored from the synthesized and modified hydrogels. Urea release from DSt, DSt₁, and DSt₂ hydrogels was investigated at room temperature and a pH range of 2–12, and the graphs of urea release were shown in Figure 4. As seen in Figure 4, it was observed that the amount of urea released from the DSt-based hydrogels increased after the modification of the hydrogels. It was thought that the functional groups and porosity in the structure of the DSt-based hydrogel increased after the modification process, and at the same time, its tight structure loosened a little more. In addition, while the DSt-based hydrogel exhibited similar urea release behavior in the 4–8 pH range, this situation changed in the DSt₁ and DSt₂-based hydrogels. It was observed that the maximum amount of urea released from DSt, DSt₁, and DSt₂-based hydrogels reached 94% at pH 6–8, 100% at pH 6, and 100% at pH 8–10, respectively. If the amount of urea released was evaluated in terms of time, it was determined that all hydrogels reached the equilibrium release value after about 17 hours, and there was a rapid release in the first four hours. In the first 4 hours, urea that adheres to the surface and binds with weak interactions was released, while urea attached to the pores was released slowly in the next process.

**Figure 4.** Release behavior of urea in different pHs from DSt, DSt₁, and DSt₂ hydrogels.

In the literature, various kinetic models have been proposed for drug release from the surface and pores of polymeric materials in the solution medium. Considering the slopes of the curves drawn according to the kinetic models, the model with the highest R^2 value is selected as the drug release kinetic model. In this study, the urea release mechanism from DSt, DSt₁, and DSt₂-based hydrogels was tried to be interpreted using Z-O model, the F-O model, the H model, and the K-P model, and the obtained kinetic model parameters were summarized in Table 6. Considering the R^2 values, it was seen that the best correlation for urea-loaded DSt, DSt₁, and DSt₂ hydrogels was obtained from the K-P model. When Table 6 was examined, it was observed that the diffusion exponent constants of DSt and DSt₁-based hydrogels at different pH values were both less than 0.45 and in the range of 0.45 to 0.89. In contrast to the DSt and DSt₁ hydrogels, the DSt₂ hydrogel was found to have diffusion exponent constants of less than 0.45 at all pH values. At n values less than 0.45, the release is diffusion-controlled and conforms to the Fickian diffusion type. At n values between

0.45 and 0.89, however, the release is affected by both the diffusion of water and the relaxation behavior of the hydrogel and conforms to the non-Fickian diffusion type [8, 42]. The release results supported the swelling analysis. One of the important parameters to be calculated while examining the release behavior of hydrogels is the diffusion coefficient.

When the diffusion coefficient values were examined, it was observed that the urea release behavior from hydrogels was different at each pH value. The high diffusion coefficients in Table 6 suggest that urea diffusion into the solution medium was greater.

Table 6. Release kinetic and mechanism of urea release

Kinetic Models		pH					
		2	4	6	8	10	12
Z-O	C _o	27.9	32.3	49.3	78.8	59.1	6.9
	k _o	-0.003	-0.012	-0.021	-0.020	-0.022	-0.001
	R ²	0.6895	0.7308	0.8923	0.7087	0.8436	0.5892
F-O	C _o	27.9	26.9	40.5	75.8	56.7	6.9
	k _i	-0.00009	-0.0002	-0.0002	-0.0001	-0.0002	-0.0001
	R ²	0.4057	0.4127	0.5658	0.4942	0.6231	0.4937
H	k _H	0.0054	0.0057	0.0074	0.007	0.0068	0.0057
	R ²	0.4785	0.8809	0.9786	0.8778	0.9723	0.8353
	n	0.23	0.53	0.45	0.25	0.37	0.2
K-P	K _{KP}	0.134	0.012	0.015	0.086	0.028	0.132
	D	3.1*10 ⁻⁷	1.2*10 ⁻⁵	3.6*10 ⁻⁶	2.2*10 ⁻⁷	1.1*10 ⁻⁶	2.6*10 ⁻⁸
	R ²	0.9383	0.9724	0.9776	0.9711	0.9688	0.9498
DS_{t1}		2	4	6	8	10	12
Z-O	C _o	11.9	45.7	71.8	56.3	45.2	8.3
	k _o	-0.023	-0.028	-0.035	-0.033	-0.03	-0.007
	R ²	0.6231	0.7493	0.6609	0.7715	0.8061	0.5316
F-O	C _o	16.4	42.6	54.8	33.5	44.5	7.4
	k _i	-0.0002	-0.0003	-0.0006	-0.0018	-0.0003	-0.0006
	R ²	0.4533	0.5354	0.3943	0.7635	0.6019	0.3108
H	k _H	0.0168	0.0108	0.0106	0.0154	0.0118	0.0182
	R ²	0.8892	0.9277	0.8582	0.9665	0.9621	0.7559
	n	0.39	0.49	0.41	0.46	0.45	0.47
K-P	K _{KP}	0.058	0.021	0.04	0.024	0.027	0.049
	D	1.7*10 ⁻⁵	2.1*10 ⁻⁵	1.1*10 ⁻⁵	1.2*10 ⁻⁵	1.4*10 ⁻⁵	6.3*10 ⁻⁵
	R ²	0.934	0.9775	0.9579	0.9914	0.9865	0.9406
DS_{t2}		2	4	6	8	10	12
Z-O	C _o	21.5	80.2	100.2	56.5	106.9	8.3
	k _o	-0.012	-0.031	-0.042	-0.035	-0.048	-0.003
	R ²	0.8083	0.7022	0.7319	0.7435	0.7365	0.6369
F-O	C _o	19.5	74.6	83.3	65.6	98.0	7.6
	k _i	-0.0003	-0.0002	-0.0003	-0.0003	-0.0003	-0.0002
	R ²	0.5176	0.4816	0.481	0.6383	0.5182	0.3772
H	k _H	0.011	0.011	0.011	0.012	0.0002	0.001
	R ²	0.9526	0.8944	0.9098	0.8732	0.8974	0.8265
	n	0.35	0.31	0.3	0.17	0.39	0.24
K-P	k _{KP}	0.050	0.073	0.077	0.122	0.041	0.124
	D	3.6*10 ⁻⁶	3*10 ⁻⁶	1.5*10 ⁻⁶	7.2*10 ⁻¹⁰	5.1*10 ⁻⁶	4.3*10 ⁻⁷
	R ²	0.9734	0.9424	0.9466	0.9527	0.9239	0.9261

4. Conclusions

Urea is a product that is naturally formed by the metabolism of proteins and can be excreted with feces. It is a

physiologically important compound used both as fertilizer in crops and as animal feed in the agricultural sector. Therefore, the conscious and correct use of urea is of great importance for the environment and plants. The present study focused on both the synthesis of new and

environmentally compatible hydrogels and the development and improvement of the urea absorption and release properties of these hydrogels. Dimethylacrylamide and starch-based hydrogels were synthesized by the free radical addition polymerization technique and separately modified with acid and base solutions. FT-IR, TGA, and swelling analyses were performed to determine whether hydrogel synthesis and modification took place. Intense cross-linking, porosity and the presence of hydrophilic groups were successfully detected by instrumental analysis and swelling results. In addition, urea sorption and release applications constituted the two important pillars of the presented study. The successful results of urea sorption by DSt, DSt₁ and DSt₂ hydrogels showed that they can both minimize the harmful effects of urea in the environment and contain the nitrogen necessary for plants. At the same time, the high swelling and urea sorption abilities of all hydrogels at different pH values give these hydrogels superior properties in terms of application area. When the urea release results were examined, it was determined that DSt, DSt₁, and DSt₂ hydrogels exhibited different release properties in different pH solutions, and these results reached 94% at pH 6–8, 100% at pH 6, and 100% at pH 8–10, respectively. The release results suggest that urea-loaded hydrogels in soils with different pH values will provide ease of application and positively affect plant growth. As a result, considering the synthesized hydrogels and their characterizations, urea sorption, and release results, it is predicted that the presented study will make important contributions to today's agriculture and that the damage that urea will cause in soil and environmental waters can be minimized.

Acknowledgements

This work is supported by the Van Yuzuncu Yil University BAP with grant # FBA-2019-7912.

Conflict of interest

There is no conflict of interest.

References

- [1]. Dawson C.J., Hilton J., "Fertiliser Availability in a Resource-Limited World: Production and Recycling of Nitrogen and Phosphorus", *Food Policy*, 36, (2011), S14-S22.
- [2]. Ghafoor I., Habib-ur-Rahman M., Ali M., Afzal M., Ahmed W., Gaiser T., Ghaffar A., "Slow-Release Nitrogen Fertilizers Enhance Growth, Yield, NUE In Wheat Crop and Reduce Nitrogen Losses Under an Arid Environment", *Environmental Science and Pollution Research*, 28, (2021), 43528–43543.
- [3]. Jarvis S.C., "Nitrogen Cycling and Losses from Dairy Farm", *Soil Use and Management*, 9(3), (1993), 99–105.
- [4]. Cruscio C.A.C., Almeida D.S., Alves C.J., Soratto R.P., Krebsky E.O., Spolidorio E.S., "Can Micronized Sulfur in Urea Reduce Ammoniacal Nitrogen Volatilization and Improve Maize Grain Yield?", *Journal of Soil Science and Plant Nutrition*, 19, (2019), 701–711.
- [5]. Rahman M.H., Ahmad I., Wang D. et al (2020) Influence of Semi-Arid Environment on Radiation Use Efficiency and Other Growth Attributes of Lentil Crop. *Environ Sci Pollut Res* 28:13697–13711. <https://doi.org/10.1007/s11356-020-11376-w>.
- [6]. Rao E.P., Puttanna K., "Nitrates, Agriculture and Environment", *Current Science*, 79(9), (2000), 1163–1168.
- [7]. Bowles T.M., Atallah S.S., Campbell E.E., Gaudin A.C.M., Wieder W.R., Grandy A.S., "Addressing Agricultural Nitrogen Losses in a Changing Climate", *Nature Sustainability*, 1, (2018), 399–408.
- [8]. Ersen Dudu T., Alpaslan D., Aktas N., "Urea Uptake and Release by Novel Macrogels from Dimethylacrylamide", *Communications in Soil Science and Plant Analysis*, 50(18), (2019), 2278–2293.
- [9]. Neethu T.M., Dubey P.K., Kaswala A.R., "Prospects and Applications of Hydrogel Technology in Agriculture", *International Journal of Current Microbiology and Applied Sciences*, 7(5), (2018), 3155-3162.
- [10]. Das D., Prakash P., Rout P.K., Bhaladhare S., "Synthesis and Characterization of Superabsorbent Cellulose-Based Hydrogel for Agriculture Application", *Starch – Stärke*, 73, (2021), 1900284.
- [11]. Ersen Dudu T., Alpaslan D., Aktas N., "Superabsorbent Hydrogels Based on N,N-Dimethylacrylamide and Maleic Acid for Applications in Agriculture as Water Purifier and Nitrogen Carrier", *Polymer Bulletin*, 79, (2022), 8551–8573.
- [12]. Ersen Dudu T., Alpaslan D., Aktas N., "Development of Urea Uptake and Release Studies Using N, N-Dimethylacrylamide/Maleic Acid/Citric Acid Based Macrogel", *Journal of Polymers and the Environment*, 29, (2021), 3636–3648.
- [13]. Song B., Liang H., Sun R., Peng P., Jiang Y., She D., "Hydrogel Synthesis Based on Lignin/Sodium Alginate and Application in Agriculture",

- International Journal of Biological Macromolecules, 144, (2020), 219–230.
- [14]. Cheng D., Liu Y., Yang G., Zhang A., “Water- and Fertilizer-Integrated Hydrogel Derived from the Polymerization of Acrylic Acid and Urea as a Slow-Release N Fertilizer and Water Retention in Agriculture”, *Journal of Agricultural and Food Chemistry*, 66, (2018), 5762–5769.
- [15]. Liu Y., Wang J., Chen H., Cheng D., “Environmentally Friendly Hydrogel: A review of Classification, Preparation and Application in Agriculture”, *Science of the Total Environment*, 846, (2022) 157303.
- [16]. Qu B., Luo Y., “Chitosan-Based Hydrogel Beads: Preparations, Modifications and Applications in Food and Agriculture Sectors – A Review”, *International Journal of Biological Macromolecules*, 152, (2020), 437–448.
- [17]. Akhmetzhan A., Myrzakmetova N., Amangeldi N., Kuanysheva Z., Akimbayeva N., Dosmagambetova S., Toktarbay Z., Longinos S.N., “A Short Review on the N,N-Dimethylacrylamide-Based Hydrogels”, *Gels*, 7, (2021), 234.
- [18]. Abdiyev K.Z., Toktarbay Z., Zhenissova A.Z., Zhursumbaeva M.B., Kainazarova R.N., Nuraje N., “The New Effective Flocculants Copolymers of N,N-Dimethyl-N,N-Diallyl-Ammonium Chloride and N,N-Dimethylacrylamide”, *Colloids Surf. A*, 480, (2015), 228–235.
- [19]. Soykeabkaew N., Thanomsilp C., Suwantong O., “A review: Starch-Based Composite Foams”, *Composites Part A: Applied Science and Manufacturing*, 78, (2015), 246-263.
- [20]. Kaewtatip K., Tanrattanakul V., Phetrat W., “Preparation and Characterization of Kaolin/Starch Foam”, *Applied Clay Science*, 80–81, (2013), 413–416.
- [21]. Alpaslan D., Ersen Dudu T., Aktas N., “Synthesis of Smart Food Packaging from Poly(Gelatin-co-Dimethyl Acrylamide)/Citric Acid-Red Apple Peel Extract”, *Soft Materials*, 19(1), (2021), 64–77.
- [22]. Gupta N.V., Shivakumar H.G., “Investigation of Swelling Behavior and Mechanical Properties of a pH-Sensitive Superporous Hydrogel Composite”, *Iranian Journal of Pharmaceutical Research*, 11 (2), (2012), 481-493.
- [23]. Sievers J., Sperlich K., Stahnke T., Kreiner C., Eickner T., Martin H., Guthoff R.F., Schünemann M., Bohn S., Stachs O., “Determination of Hydrogel Swelling Factors by Two Established and a Novel Non-Contact Continuous Method”, *Journal of Applied Polymer Science* 138, (2021), e50326.
- [24]. Adnadjevic B., Jovanovic J., “Novel Approach in Investigation of the Poly(Acrylic Acid) Hydrogel Swelling Kinetics in Water”, *Journal of Applied Polymer Science*, 107, (2008), 3579–3587.
- [25]. Peppas N.A., Franson N.M. “The Swelling Interface Number as a Criterion for Prediction of Diffusional Solute Release Mechanism in Swellable Polymers”, *Journal of Polymer Science Polymer Physics Edition*, 21, (1983), 983-997.
- [26]. Alpaslan D., Ersen Dudu T., “Removal of As(V), Cr(VI) and Cr(III) Heavy Metal Ions from Environmental Waters Using Amidoxime and Quaternized Hydrogels”, *MANAS Journal of Engineering*, 9(2), (2021), 104-114.
- [27]. Langmuir I., “The Adsorption of Gases on Plane Surfaces of Glass, Mica and Platinum”, *Journal of the American Chemical Society*, 40, (1918), 1361.
- [28]. Freundlich H.M.F., “Über Die Adsorption in Lösungen”, *Zeitschrift für Physikalische Chemie*, 57, (1906), 385-470.
- [29]. Tempkin M.I., Pyzhev V., “Kinetics of Ammonia Synthesis on Promoted Iron Catalyst”, *Acta Physicochimica URSS*, 12, (1940), 327-356.
- [30]. Dubinin M.M., “The Potential Theory of Adsorption of Gases and Vapors for Adsorbents with Energetically Non-Uniform Surface”, *Chemical Reviews*, 60, (1960), 235-266.
- [31]. Al-Degs Y.S., El-Barghouthi M.I., El-Sheikh A.H., Walker G.M., “Effect of Solution pH, Ionic Strength, and Temperature on Adsorption Behavior of Reactive Dyes on Activated Carbon”, *Dyes and Pigments*, 77, (2008), 16-23.
- [32]. Çakmak M., Taşar Ş., Selen V., Özer D., Özer A., “Removal of Astrazon Golden Yellow 7GL from Colored Wastewater Using Chemically Modified Clay”, *Journal of Central South University*, 24, (2017), 743–753.
- [33]. Alpaslan D., Ersen Dudu T., Aktas N., “Development of Onion Oil-Based Organo-Hydrogel for Drug Delivery Material”, *Journal Of Dispersion Science And Technology*, <https://doi.org/10.1080/01932691.2021.1974869>.
- [34]. Varelas C.G., Dixon D.G, Steiner C., “Zero-Order Release from Biphasic Polymer Hydrogels”, *Journal of Controlled Release*, 34, (1995), 185-192.

- [35]. Higuchi T., "Mechanisms of Sustained Action Medication: Theoretical Analysis of the Rate of Release of Solid Drugs Dispersed in Solid Matrices", *Journal of Pharmaceutical Sciences*, 52, (1963), 1145-1149.
- [36]. Korsmeyer R.W., Gurny R., Doelker E.M., Buri P., Peppas N.A., "Mechanism of Solute Release from Porous Hydrophilic Polymers", *International Journal of Pharmaceutics*, 15, (1983), 25-35.
- [37]. Peppas N.A., Bures P., Leobandung W., Ichikawa H., "Hydrogels in Pharmaceutical Formulations", *European Journal of Pharmaceutics and Biopharmaceutics*, 50, (2000), 27-46.
- [38]. Khare A.R., Peppas N.A., "Swelling/Deswelling of Anionic Copolymer Gels", *Biomaterials*, 16, (1995), 559-567.
- [39]. Swenson H., Stadie N.P., "Langmuir's Theory of Adsorption: A Centennial Review", *Langmuir*, 35(16), (2019), 5409-5426.
- [40]. Zhou X., Yi H., Tang X., Deng H., Liu H., "Thermodynamics for the Adsorption of SO₂, NO and CO₂ from Flue Gas on Activated Carbon Fiber", *Chemical Engineering Journal*, 200-202, (2012), 399-404.
- [41]. Edet U.A., Ifelebuegu A.O., "Kinetics, Isotherms, and Thermodynamic Modeling of the Adsorption of Phosphates from Model Wastewater Using Recycled Brick Waste", *Processes*, 8, (2020), 665. doi:10.3390/pr8060665.
- [42]. Rezk A.I., Obiwezuozor F.O., Choukrani G., Park C.H., Kim C.S., "Drug Release and Kinetic Models of Anticancer Drug (BTZ) from a pH-Responsive Alginate Polydopamine Hydrogel: Towards Cancer Chemotherapy", *International Journal of Biological Macromolecules*, 141, (2019), 388-400.



Immobilization of xylanase enzyme on poly-(HEMA-co-GMA) cryogel

Samir Abbas Ali Noma

Department of Chemistry, Faculty of Arts and Science, Bursa Uludağ University, Bursa, Türkiye, snoma@uludag.edu.tr,
ORCID: 0000-0003-4165-0045

ABSTRACT

In this study, a polyethyleneimine (PEI) coated poly-(HEMA-co-GMA), hybrid cryogel column (HCC), was designed. HCC was synthesized via polymerization of gel-former factors at minus temperatures. The characterization experiments of the HCC were conducted through SEM, and FTIR experiments. At the end of the experimental periods, there was no significant decrease in the performance of the HCC. Then HCC used as a novel support for xylanase immobilization for the first time. The successful immobilization of xylanase was confirmed by FT-IR, while biochemical properties and stability of the PHG/PI-Xyl were evaluated in terms of optimum pH, optimum temperature, thermostability, storage stability, reusability, and kinetic parameters. The optimum activities for both free and immobilized enzymes were recorded at pH 6.0, while the optimum temperature for free was 55 °C, and for PHG/PI-Xyl was 60 °C. PHG/PI-Xyl displayed remarkable thermal stability for 180 min at 60 °C, with 53.55%, and for free Xyl 32.05% from the initial activity. Meanwhile, it retained up to 49% and 69 % for free and immobilized xylanase of original activities after 4 weeks of storage at room temperature. PHG/PI-Xyl retained about 58% of its original activity after 10 consecutive reuses, while Km for the free Xyl and PHG/PI-Xyl were calculated 4.05 mg/mL and 2.62 mg/mL, whereas Vmax 133.33 U/mL and 188.68 U/mL, respectively. As envisioned, this study suggests a promising way to solve the problems of high price and poor operational stability of the enzyme during biocatalytic.

ARTICLE INFO

Research article

Received: 8.11.2022

Accepted: 12.12.2022

Keywords:

PHEMA,
cryogel,
adsorption,
xylanase,
enzyme immobilization

*Corresponding Author

1. Introduction

Cryogels are biomaterials that are in a subcategory of hydrogels and have perfect physical features [1,2]. Cryogels have 3D elastic interconnected macropores, spongy morphologies and good mechanical robustness [3]. They are extremely versatile tools when converted to desired purposes [4] such as purification/adsorption of biomolecules [5-8], and removal of some pollutants [9-11]. Increasing the existing properties while designing cryogels will further increase their potential use in different fields [4]. The weak side of cryogels is their low adsorption capacity. This is due to the low surface area of the super macropores in the matrix [12-14]. Improving the binding capacity in some processes based on cryogels is of great importance [15].

After cellulose, xylan, a straight homopolymer made of D-xylose monomers joined by 1,4-glycosyl linkages, is regarded as the second most prevalent biomass that is naturally renewable [16, 17]. In light of the plant source, glucuronopyranosyl, 4-o-methyl-d-glucopyranosyl, α -l-arabinofuranosyl acetyl. As well as, connected to feruloyl and coumaroyl components of lignin, are present to variable

degrees [18]. For a variety of commercial and industrial uses, xylanolytic enzymes use to convert xylan into shorter sugar residues is important [19]. Xylanase is one of these xylanolytic enzymes that are essential for xylan breakdown. Xylanase (EC 3.2.1.8), a hydrolytic enzyme employed in depolymerizing xylan, its used in a variety of industrial techniques, including whitening paper pulp with enzymes, juice clarification, oil extraction from plants, texture improvement in bakeries, bioconversion of agricultural wastes, bioscouring in textiles, and enhancing the animal feed digestibility [20, 21]. Bacteria, fungi, actinomycetes, and yeast have all been observed to produce xylanase [22]. With the use of commercially available substrates (xylan) or agricultural waste products (wheat bran, wheat straw, maize cob, sugar cane bagasse, etc.) as production substrates, xylanase can be produced both in submerged fermentation and in solid-state fermentation [23, 24]. To rise the brightness of the pulp, the paper and pulp companies utilized huge amounts of chlorine compounds, which resulted in the formation of harmful dioxins in the effluents. While on the other hand, pre-bleaching pulp with xylanase can preserve the brightness of the pulp while reducing chlorine usage by

20–30% [24]. For pulp bleaching, xylanase is recommended because it is most active at high temperatures and alkaline pH levels. Nevertheless, during industrial applications, free enzyme encounters challenges such as sensitivity and structural instability, as well as a failure to recover the active form of the enzyme from the reaction mixture for repeated use [25]. Enzyme immobilization offers a number of benefits, including the ability to process continuously and reuse the enzyme. At the industrial level, immobilized enzymes are preferable because they can be recycled and which lead to reduce production costs.

In this study, the cryogel of poly-(HEMA-co-GMA) coated with polyethyleneimine (PEI) hybrid cryogel column (HCC), a new kind of functional, low-cost was synthesized. Xylanase enzyme immobilization on PHG/PI-Xyl cryogel column was carried out by the interactions with the amino groups of PEI. The morphological structural of PHG/PI was investigated with Scanning Electron Microscopy (SEM), while the synthesized PHG/PI and enzyme-immobilized PHG/PI-Xyl were investigated by Fourier transform infrared (FT-IR). Biochemical parameters including optimum pH and temperature, thermal and storage stability, reusability, and kinetics (K_m and V_{max}) of free immobilized xylanase on PHG/PI cryogel column were investigated. The originality of this study to break down xylan into tiny sugar is further enhanced by the requirement for more work to translate the given approach to an industrial scale. The current study, to the best of our knowledge, the first attempt at immobilizing xylanase on a PHG/PI cryogel column for application in xylan degradation.

2. Materials and methods

2.1. Materials

HEMA (2-Hydroxyethyl methacrylate) was provided by Fluka A.G (Buchs, Switzerland). MBAAm (*N,N'*-methylene-bis-acrylamide), TEMED (*N,N,N',N'*-Tetramethylethylenediamine) and APS (ammonium persulfate), xylanase and beechwood xylan were purchased from Sigma–Aldrich Chemical Co. Other chemicals were purchased at reagent grade from Merck AG (Darmstadt, Germany).

2.2. Synthesis of poly-(HEMA-co-GMA) cryogel column

HEMA (174 μL) as monomer and MBAAm (10 mg) as the cross-linker were stirred within 1 mL of deionized water for cryo-polymerization technique. Then 20 μL of glycidyl methacrylate (GMA) was added to this prepared solution as a co-monomer. The mixture was then poured into a 2.5 mL plastic syringe. It was exposed to nitrogen gas for about 2 minutes to remove dissolved oxygen. After that, 100 μL (10% (w/v) APS as free radical generator and 20 μL

TEMED as catalyst was added to the resulting mixture and the mixture was left at -14°C for 24 hours. After 24 hours, the synthesized poly(HEMA-co-GMA) column was brought to room temperature for dissolution and washed with water, then with water-ethanol mixture to remove impurities.

2.3. PEI coating of poly-(HEMA-co-GMA) cryogel column

PEI molecules were immobilized on the prepared cryogel over reactive glycidyl groups in GMA. For this purpose, 15 mL of GMA (10%, w/v, pH 10.6) solution was prepared due to the viscosity of PEI. Then, the obtained poly (HEMA-co-GMA) cryogel was taken into the prepared solution (4 hours, 50°C , 100 rpm) for the interaction between reactive groups of GMA and PEI. After 4 hours, the product of PHG/PI cryogel was repeatedly washed with distilled water to remove the unreacted PEI molecules.

2.4. Xylanase immobilization on PHG/PI

100 mg PHG/PI were dropped in acetate buffer solution (50 mM, pH 6.0), then 5 mL xylanase enzyme solution was added to the PHG/PI cryogel column with continuous shaking for 24 h at 4°C . After 24 h, the PHG/PI cryogel column were removed from the solution and washed repeatedly three times with acetate buffer (50 mM, pH 6.0) to ensure the removal of unbound xylanase. Finally, the immobilized enzyme (PHG/PI-Xyl) was kept at $+4^\circ\text{C}$ for future use (Fig. 1).

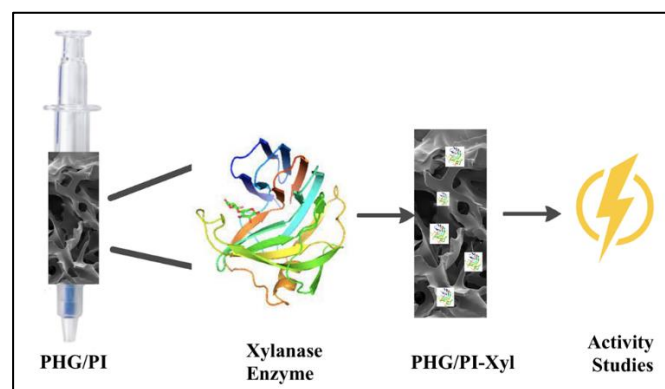


Figure 1. Schematic illustration immobilization of xylanase on PHG/PI and activity study.

2.5. Xylanase activity

The method described by Bailey et al. was used to determine the activity of xylanase by the increase in the formation of xylose [26], beechwood xylan was used as the substrate after employing a slightly modified. The xylanase activity was determined by the increase in production rate of xylose under the recommended conditions and DNS (3,5-dinitrosalicylic acid) was used as color indicator. Beechwood

xylan was dissolved in acetate buffer to create a xylan solution (1%, w/v) in (50 mM, pH 6.0). 1 mL of the substrate was added to 5 mg of cryogel containing xylanase, then the reaction mixture was incubated with heated to 50 °C for 10 minutes (under shaking). Then 1 mL of DNS was added and the reaction mixture was immediately cooled in cold water, after DNS additions the reaction mixture was boiled for 5 min at 100 °C. Furthermore, by using a UV-VIS spectrophotometer, the absorbance of complex between released reduce sugars and DNS reagent was determined at 540 nm. One unit (U) of xylanase activity was defined as the amount of enzyme catalyzed in the release of 1 μ mol of reducing sugar as xylose equivalent per minute under the specified assay conditions.

2.6. Effect of pH and temperature

The effect of pH on free xyl and PHG/PI-Xyl was investigated by dissolved xylan substrate in different buffers, the buffer pH changed from 3.0 to 10.0, while the effect of temperature on the free xyl and PHG/PI-Xyl activity was investigated at different temperatures scales from 30 °C to 70 °C. The highest activity was accepted as 100% and the results were converted to relative activities. The data with the highest activity was determined as the optimum value.

2.7. Thermal and storage stability

To examine the thermal stability of the PHG/PI-Xyl, free and immobilized xylanase were incubated at 60 °C at various times (from 0 to 180 min). At the end of each incubation period, a standard enzyme assay was conducted to determine the amount of remaining enzyme activity. The activity observed for 0 min was taken as control 100%.

The storage stability of the PHG/PI-Xyl and free xylanase enzyme were examined by storing them at 25 °C for four weeks. The Enzyme activity was evaluated on the first day and considered as control, 100%, and subsequent activities were transformed to relative activity.

2.8. Reusability

To determine the reusability of the PHG/PI-Xyl, the activity was measured under optimum conditions for 10 cycles. After each measurement, the cryogel was separate from the supernatant then DNS reagent was added. Further, the activity was restarted by adding a fresh substrate to the immobilized enzyme. The first measured enzyme activity

was accepted as 100% and this process was repeated for 10 successive reuses.

2.9. Values of K_m & V_{max}

To estimate the kinetic parameters (K_m & V_{max}), the activity of the PHG/PI-Xyl was measured at different xylan concentrations (1-5 %) under standard assay conditions. K_m and V_{max} values were estimated via the Lineweaver-Burk plot.

2.10. Characterization studies

The functional groups of HCC and enzyme bind to HCC were characterized by Fourier Transform Infrared Spectrometer (FTIR 8000 Series, Shimadzu, Japan). The surface morphology of cryogel was tested by using scanning electron microscopy (SEM, EVO LS 10 ZEISS 5600 SEM, Tokyo, Japan). For this aim, the samples were swollen in deionized water. Next, the samples were taken in to absolute (98%) ethanol to change the water with alcohol molecules in the pore structures. After this procedure, the alcohol is diffused. The samples were put inside an oven (60 °C) to eliminate the alcohol molecules from the samples without damaging their morphologies. The dehydrated cryogels were coated with gold-palladium (40:60). Afterward, they were taken to the SEM device for image acquisition.

3. Results and discussion

3.1. Characterization studies

The FTIR spectra of PHG/PI and PHG/PI-Xyl shows Fig.2. These spectra indicates that the broad peak about 3100-3200/cm was because of stretching bands of -OH and N-H groups. C-H stretching stretching stretching band was monitored at 2950/cm. In addition, a peak at 1717/cm of the stretching vibration of the C=O group was determined in the HEMA and GMA ester [1, 27]. After enzyme immobilization, the FTIR spectrum of the hybrid cryogel showed two new peaks at around 1550/cm and 1660/cm. These peaks can be attributed to amide I (vibration of C=O) amide II (a combination of C-N stretching and N-H vibration in the protein backbone), respectively [28]. Moreover, a small decrease in the asymmetric stretching of the epoxy group was also observed at about 900/cm with the immobilization of the enzyme. These results showed that the enzyme was successfully immobilized on the surface of the cryogel.

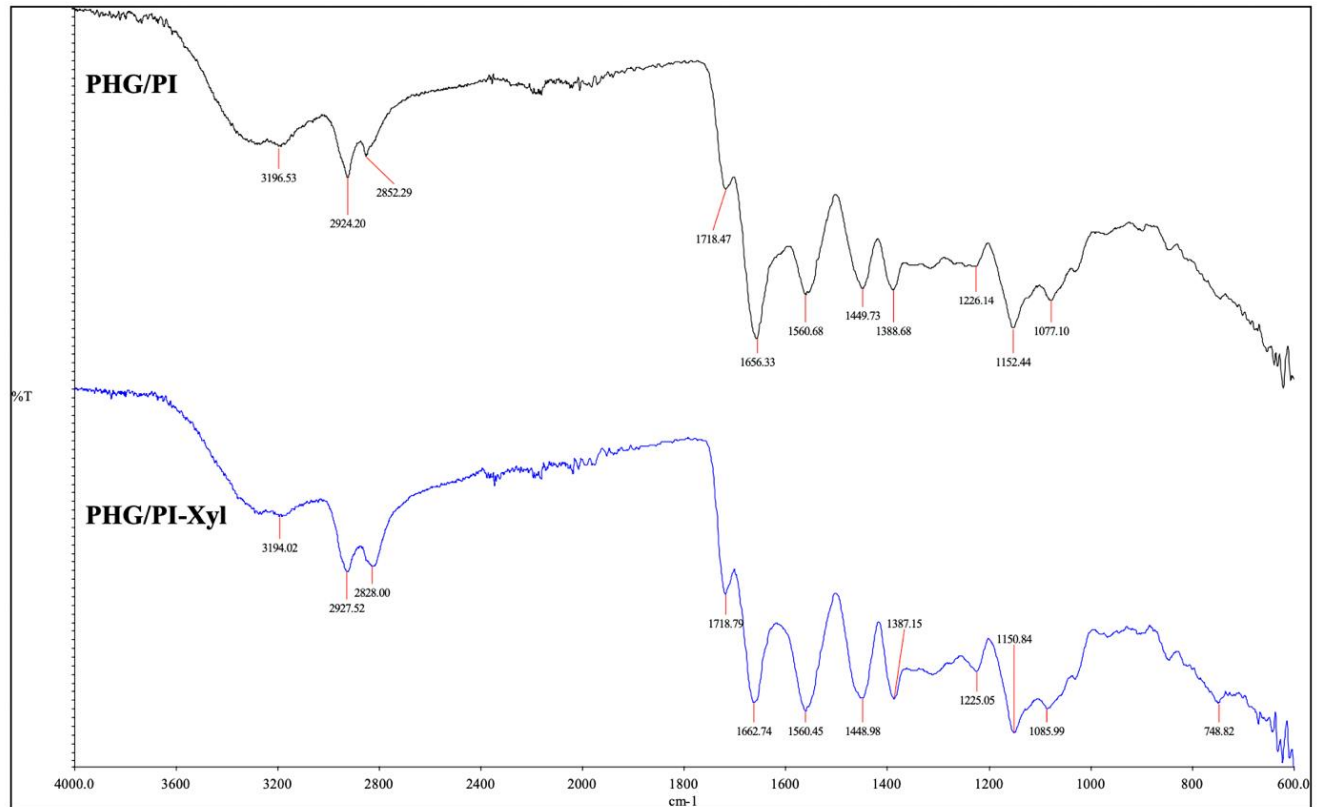


Figure 2. FTIR spectra of PHG/PI and PHG/PI-Xyl.

The SEM photos with magnified in different sizes of the PHG/PI cryogel column was shown in Fig.3. Integrated pores were observed in the PHG/PI cryogel structure. Thus, this structure created a high surface area for high immobilization performance. The reusability of HCC

cryogel column showed very important performance. All stages were repeated 10 times with the same cryogel column, and a important changing wasn't observed in cryogel column structure.

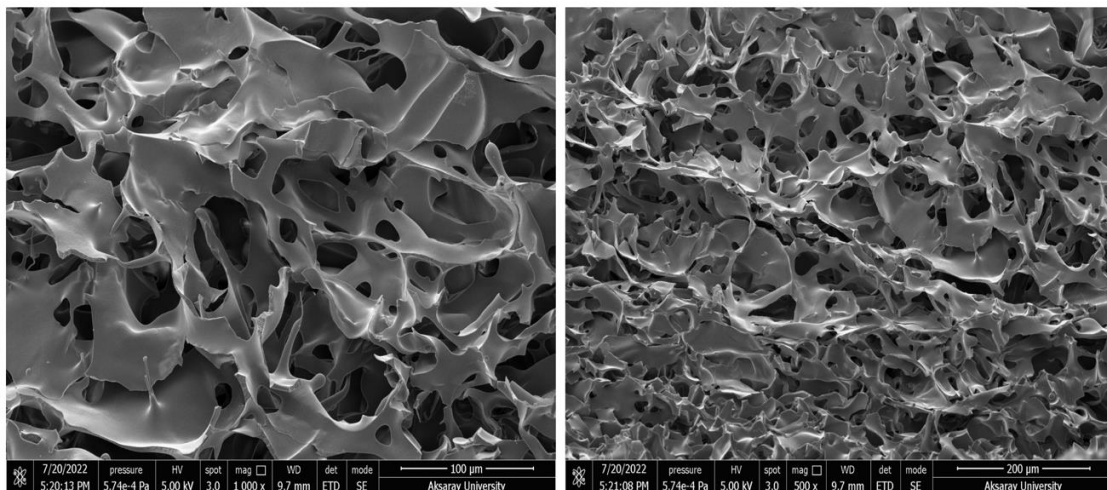


Figure 3. SEM images of PHG/PI.

3.2. Effect of change in pH and temperature on activity

The activity with varying pH is a significant parameter in the applications of enzymes immobilization. The activity of the

free and immobilized xylanase was monitored for the pH values ranging from 3.0 to 10.0. According to observed data (Fig. 4A), the maximal activity of the free Xyl and immobilized PHG/PI-Xyl were founded at pH 6.0. However, the residual activity of the PHG/PI-Xyl started to decrease above pH 6.0. For instance, only 64% of the PHG/PI-Xyl remained active at pH 10.0, while free xylanase enzyme was founded at 52 % at pH 10.0. It is observed that the PHG/PI-Xyl exhibited high relative activity in the pH ranges from 3.0–9.0. This excellent performance of the PHG/PI-Xyl could be due to the interactions between the xylanase and the PHG/PI cryogel column. In addition, compared to the free

enzyme, the activity of the immobilized enzyme was generally higher across the majority of pH ranges. In our earlier work, they determined the optimum pH of the xylanase enzyme which was founded as pH 6.0 [29]. Similarly, in our other study, the optimum pH for free and immobilized xylanase was found at pH 7.0 [30]. The possible reason for this slight shift in pH due to the charge of the support materials that they used. According to the pH stability tests, the immobilized xylanase was marginally more stable than the loose enzyme. The higher pH stability was probably advantageous for the immobilized enzyme to be used in the industrial application.

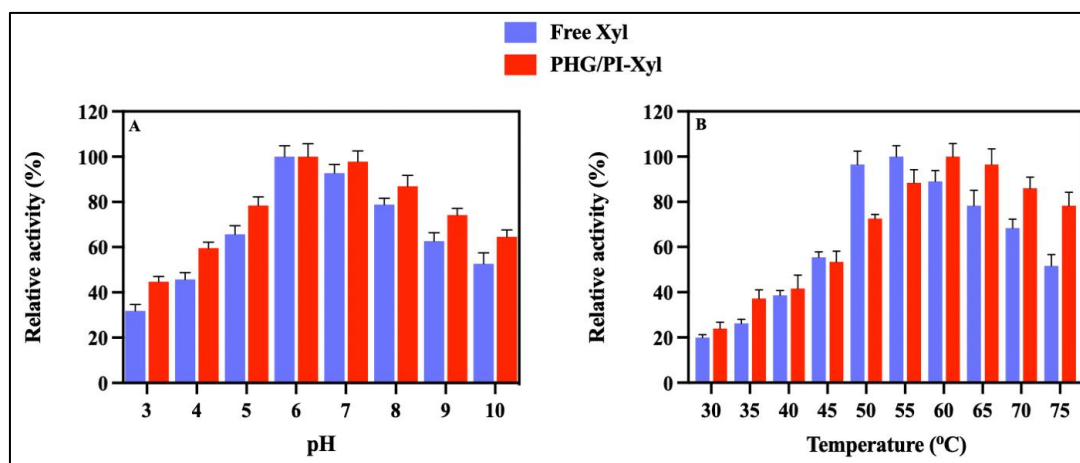


Figure 4. The effect of different pH (A) and temperature values (B) on the activity of free and immobilized xylanase.

The enzyme activity at various temperatures is also important for practical applications. Therefore, the activities of the free and immobilized xylanase enzyme were measured at various temperatures at pH 6.0 in order to examine the temperature dependence. The optimum temperature of free Xyl and PHG/PI-Xyl immobilized enzymes were measured to be 55 and 60 °C, respectively (Fig. 4B). In addition, the PHG/PI-Xyl maintained 95% and free Xyl maintained 78% of its activity at 65 °C. And the relative activity of free Xyl was only 51% while PHG/PI-Xyl was 78 % at 75 °C. The results indicated that the microenvironment of the support may have protected the enzyme from inappropriate changes at high temperature. Hence, the xylanase had better tolerance to high temperature. In prior investigations, a similar outcome of optimum temperature for immobilized enzymes and a very close result for free enzyme has been observed. However, depending on the type of interaction between the enzyme and the matrix as well as the matrix, the extent of displacement differed [31]. As a result of the intermolecular connections that form between the enzyme molecules and the matrix support, the structure of the enzyme molecule is made stiff and is therefore less susceptible to the denaturing effects of temperature [32].

3.3. Thermal and storage stability

The thermal stability study of free Xyl and PHG/PI-Xyl immobilized enzymes were carried out by measuring its activity at 60 °C and different incubation times (0, 10, 30, 60, 120, and 180 min) and were compared (Fig. 5A). The free Xyl and PHG/PI-Xyl showed 76.35%, and 90.48% of the relative activity at 30 min. On the other hand, after 60 min of incubation, the free Xyl and PHG/PI-Xyl preserved 61.13%, and 80.98% of their initial activity, respectively, while at the end of 180 min free Xyl and PHG/PI-Xyl preserved 32.05% and 53.55 % of its original activity, respectively. These findings revealed that the cryogel column provides a suitable microenvironment for the immobilized xylanase and provides protection against environmental factors such as high temperature that may reduce the activity. After immobilization, xylanase was adsorbed to the PHG/PI cryogel column, which inhibited changed in conformation and reduced molecular mobility due to hydrogen bonds, ionic, electrostatic and non-covalent interactions between the enzyme and carrier matrix. Overall, the thermal stability of xylanase enhanced after immobilization on the cryogel. The results obtained are comparable or even better than those reported in the literature using different supports [30].

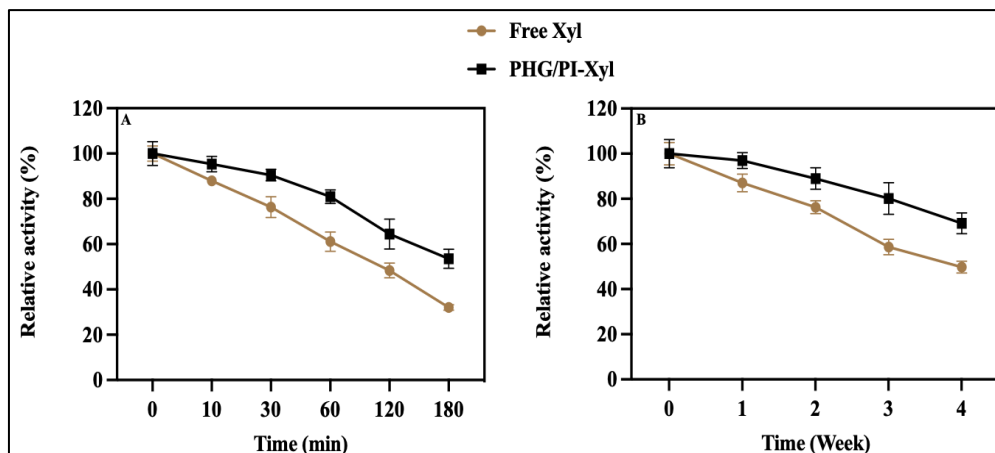


Figure 5. Thermal stability (A) storage stability (B) of free and immobilized xylanase.

The important advantages of immobilized enzymes in industrial areas have better storage stability compared to free enzymes. The storage stability of the free and immobilized xylanase was determined by measuring activity every single week for 4 weeks at 25 °C. As seen in (Fig. 5B), at the end of the 2 weeks the retained enzyme activity for free Xyl and immobilized PHG/PI-Xyl 76% and 88%, respectively of initial activities. Nevertheless, the activity was still above 49% and 69 % for free and immobilized xylanase, respectively at the end of the 4 weeks. A significant improvement in the enzyme activity after immobilization on cryogel column was observed with increasing storage time. The satisfactory ability of the cryogel column in long-term storage was owing to multiple linkages between the xylanase and the cryogel was present, which prevented enzyme denaturation or leaching from the support. Taken together, it is reasonable to conclude that the PHG/PI-Xyl displayed enhanced storage stability.

3.4. Reusability

The reusability of immobilized xylanase is the key to cost-effectiveness for industrial applications. Reusability of the PHG/PI-Xyl was investigated by hydrolyzing of xylan for 10 consecutive cycles. The residual activity was found out to be 90.5 % after 3 cycles, 81.38% after 5 cycles, 69.78% after 8 cycles, and even after 10 cycles the residual activity was still above 58% from the initial activity as shown in (Fig. 6). The relative activity of the PHG/PI-Xyl gradually decreased through the reaction cycles due to partial exhaustion of xylanase or its leaching from the carrier. Nonetheless, since the xylanase activity was maintained above half of the initial activity up to 10 reuse cycles, it can be considered that a highly stable biocatalyst is obtained by the immobilization of xylanase on PHG/PI. On the other hand, this PHG/PI-Xyl appears to be much more reusable than its counterparts reported in the literature using other support. For instance,

immobilized xylanase on a magnetic chitosan support retained about 22% of initial activity after 6 cycles [33], about 50% of residual activity was obtained after 4 cycles for immobilized covalent immobilization of xylanase from thermomyces lanuginosus on aminated superparamagnetic graphene oxide nanocomposite [34], and about 62% retained of its activity after six precipitations for immobilization of thermomyces lanuginosus SSBP xylanase using Eudragit S-100 [35]. Compared to these findings, immobilizing xylanase on PHG/PI could promising and bring a chance for xylanase to be used in industrial application and as biocatalysts in continuous reactors.

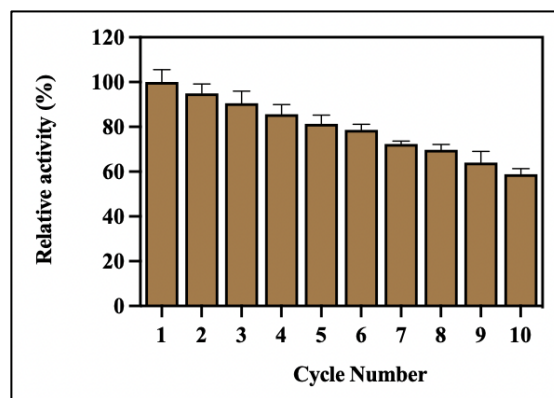


Figure 6: The reusability of the PHG/PI-Xyl using xylan as the substrate.

3.5. Values of K_m and V_{max}

The values of K_m and V_{max} from the Lineweaver–Burk plot were observed in (Fig. 7). Xylan was used to examine the relationship between substrate concentration and reaction rate of free and immobilized xylanase, different xylan concentrations of 0.5 –10 mg/mL were used and the enzyme activity assay has occurred at optimum condition. The K_m value of the PHG/PI-Xyl was founded 2.62 mg/mL which

was lower than the free xyl 4.05 mg/mL. This outcome means that the enzyme on the surface of PHG/PI-Xyl has more accessible potential active sites, thus increasing the affinity of xylanase to xylan substrate. In contrast, The V_{max} of the PHG/PI-Xyl was 188.68 U/mL, which was higher than free xyl 133.33 U/mL. Increased V_{max} of the PHG/PI-Xyl confirmed the enhanced biocatalytic activity of the enzyme after immobilization, which means a higher xylan hydrolysis rate than that free xyl. A study was reported for immobilized xylanase on a magnetic chitosan, according to the results of xylanase enzyme increased in V_{max} value from 6.31 ± 0.63 to 11.6 ± 0.26 U/mL, and increased in K_m concentration

from 1.89 ± 0.46 to 3.15 ± 0.16 mg/mL after immobilization [33]. According to reports, the main factor causing high V_{max} and lower K_m could be immobilization, which prevents conformational change and results in limited substrate diffusion. In another study, for covalent immobilization of xylanase on graphene oxide nanocomposite, they obtained K_m and V_{max} values 55.0 mM and 1.7 mM/min for free xylanase and 83.0 mM and 2.5 mM/min for immobilization of xylanase, respectively [34]. As a result, xylanase immobilization into the PHG/PI provided more efficient catalytic capability than that of the free one.

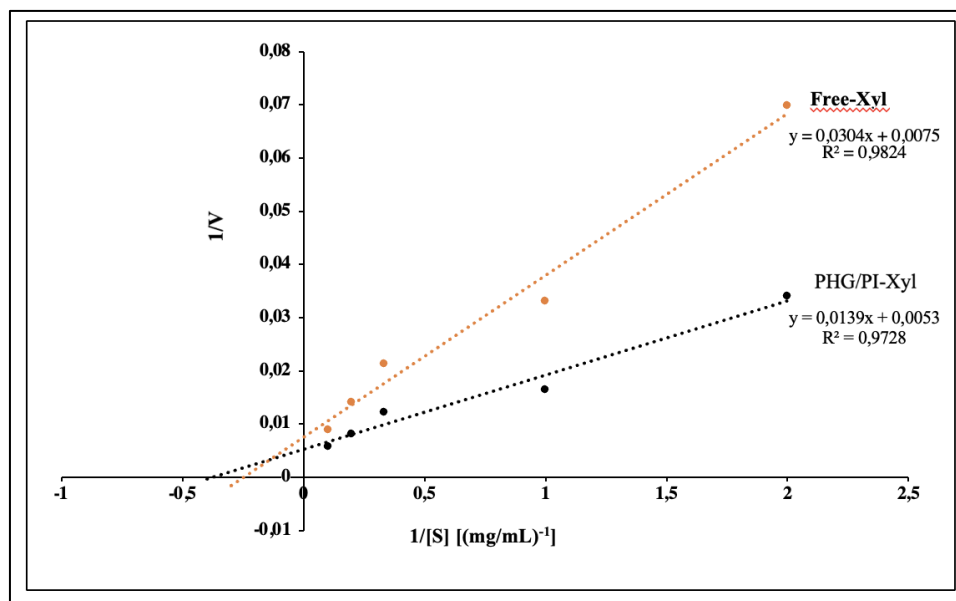


Figure 7. The Lineweaver-Burk plot of the of free and immobilized xylanase.

4. Conclusion

Herein, we demonstrated that PHG/PI cryogel column can be used as efficient as support materials for xylanase immobilization and its previously not reported in the literature. The materials were thoroughly characterized to investigate their structural and physicochemical properties before and after modification. Further, the successful immobilization of xylanase was verified by FT-IR. Significant enhancements of the xylanase stability after immobilization were observed. For instance, xylanase immobilized to the PHG/PI cryogel column structure exhibited broad tolerance against various pH and temperature conditions. The PHG/PI-Xyl showed good reusability as well as high thermal and storage stability. Moreover, the kinetic study reported a reduction in K_m values with an accompanying rise in V_{max} values, implying an increase in enzyme-substrate affinity. Taken together, improving the reuse of enzymes is a very important and targeted task since they contribute to the reduction of costs in

industrial processes and the economic viability of the application

Acknowledgements

The author would like to thank Prof. Dr. Bilgen Osman from Department of Chemistry, Faculty of Arts and Science, Bursa Uludağ University, for laboratory facilities.

References

- [1]. Noma, S. A. A., Acet, Ö., Ulu, A., Önal, B., Odabaşı, M., Ateş, B., "l-asparaginase immobilized p (HEMA-GMA) cryogels: A recent study for biochemical, thermodynamic and kinetic parameters", Polymer Testing, 93, (2021), 106980.
- [2]. Acet, Ö., "Investigation of BSA adsorption performances of metal ion attached mineral particles

- embedded cryogel discs”, *MANAS Journal of Engineering*, 9(Special 1), (2021), 65-71.
- [3]. Baran, N. Y., Acet, Ö., Odabaşı, M., “Efficient adsorption of hemoglobin from aqueous solutions by hybrid monolithic cryogel column”, *Materials Science and Engineering: C*, 73, (2017), 15-20.
- [4]. Eggermont, L. J., Rogers, Z. J., Colombani, T., Memic, A., & Bencherif, S. A., “Injectable cryogels for biomedical applications”, *Trends in biotechnology*, 38(4), (2020), 418-431.
- [5]. Acet, Ö., Aksoy, N. H., Erdönmez, D., Odabaşı, M., “Determination of some adsorption and kinetic parameters of α -amylase onto Cu⁺ 2-PHEMA beads embedded column”, *Artificial cells, nanomedicine, and biotechnology*, 46(sup3), (2018), S538-S545.
- [6]. Önal, B., Acet, Ö., Sanz, R., Sanz-Pérez, E. S., Erdönmez, D., Odabaşı, M., “Co-evaluation of interaction parameters of genomic and plasmid DNA for a new chromatographic medium”, *International journal of biological macromolecules*, 141, (2019), 1183-1190.
- [7]. Alacabey, İ., Acet, Ö., Önal, B., Dikici, E., Karakoç, V., Gürbüz, F., Alkan, H., Odabaşı, M., “Pumice particle interface: a case study for immunoglobulin G purification”, *Polymer Bulletin*, 78(10), (2021), 5593-5607.
- [8]. Önal, B., Odabaşı, M., “Design and application of a newly generated bio/synthetic cryogel column for DNA capturing”, *Polymer Bulletin*, 78(10), (2021), 6011-6028.
- [9]. Huseynli, S., Bakhshpour, M., Qureshi, T., Andac, M., Denizli, A., “Composite polymeric cryogel cartridges for selective removal of cadmium ions from aqueous solutions”, *Polymers*, 12(5), (2020), 1149.
- [10]. Gurbuz, F., Ozcan, A., Çiftçi, H., Acet, O., Odabasi, M., “Treatment of textile effluents through bio-composite column: Decolorization and COD reduction”, *International Journal of Environmental Science and Technology*, 16(12), (2019), 8653-8662.
- [11]. Gurbuz, F., Akpınar, Ş., Ozcan, S., Acet, Ö., Odabaşı, M., “Reducing arsenic and groundwater contaminants down to safe level for drinking purposes via Fe³⁺-attached hybrid column”, *Environmental monitoring and assessment*, 191(12), (2019), 1-14.
- [12]. Persson, P., Baybak, O., Plieva, F., Galaev, I. Y., Mattiasson, B., Nilsson, B., Axelsson, A., “Characterization of a continuous supermacroporous monolithic matrix for chromatographic separation of large bioparticles”, *Biotechnology and bioengineering*, 88(2), (2004), 224-236.
- [13]. Ünlü, N., Ceylan, Ş., Erzenin, M., & Odabaşı, M., “Investigation of protein adsorption performance of Ni²⁺-attached diatomite particles embedded in composite monolithic cryogels”, *Journal of separation science*, 34(16-17), (2011), 2173-2180.
- [14]. Bereli, N., Şener, G., Altıntaş, E. B., Yavuz, H., Denizli, A., “Poly (glycidyl methacrylate) beads embedded cryogels for pseudo-specific affinity depletion of albumin and immunoglobulin G”, *Materials Science and Engineering: C*, 30(2), (2010), 323-329.
- [15]. Yao, K., Yun, J., Shen, S., Wang, L., He, X., Yu, X., “Characterization of a novel continuous supermacroporous monolithic cryogel embedded with nanoparticles for protein chromatography”, *Journal of Chromatography A*, 1109(1), (2006), 103-110.
- [16]. Kumar, S., Haq, I., Prakash, J., Raj, A., “Improved enzyme properties upon glutaraldehyde cross-linking of alginate entrapped xylanase from *Bacillus licheniformis*”, *International journal of biological macromolecules*, 98, (2017), 24-33.
- [17]. Uday, U. S. P., Choudhury, P., Bandyopadhyay, T. K., Bhunia, B., “Classification, mode of action and production strategy of xylanase and its application for biofuel production from water hyacinth”, *International journal of biological macromolecules*, 82, (2016), 1041-1054.
- [18]. Kaur A, Mahajan R, Singh A, Garg G, Sharma J., “Application of cellulase free xylano-pectinolytic enzymes from the same bacterial isolate in biobleaching of kraft pulp”, *Bioresource Technology* 101, (2011), 9150-5.
- [19]. Shahrestani, H., Taheri-Kafrani, A., Soozanipour, A., Tavakoli, O., “Enzymatic clarification of fruit juices using xylanase immobilized on 1, 3, 5-triazine-functionalized silica-encapsulated magnetic nanoparticles”, *Biochemical engineering journal*, 109, (2016), 51-58.

- [20]. Butt MS, Tahir-Nadeem M, Ahmad Z, Sultan MT., "Xylanases in baking industry", *Food Technology Biotechnology*, 46, (2008), 22–31.
- [21]. Dhiman, S. S., Sharma, J., Battan, B., "Industrial applications and future prospects of microbial xylanases: a review", *BioResources*, 3(4), (2008), 1377-1402.
- [22]. Nagar, S., Gupta, V. K., Kumar, D., Kumar, L., Kuhad, R. C., "Production and optimization of cellulase-free, alkali-stable xylanase by *Bacillus pumilus* SV-85S in submerged fermentation", *Journal of Industrial Microbiology and Biotechnology*, 37(1), (2010), 71-83.
- [23]. Agnihotri, S., Dutt, D., Tyagi, C. H., Kumar, A., Upadhyaya, J. S., "Production and biochemical characterization of a novel cellulase-poor alkali-thermo-tolerant xylanase from *Coprinellus disseminatus* SW-1 NTCC 1165", *World Journal of Microbiology and Biotechnology*, 26(8), (2010), 1349-1359.
- [24]. Garg, G., Dhiman, S. S., Mahajan, R., Kaur, A., Sharma, J., "Bleach-boosting effect of crude xylanase from *Bacillus stearothermophilus* SDX on wheat straw pulp", *New Biotechnology*, 28(1), (2011), 58-64.
- [25]. Krajewska B., "Application of chitin- and chitosan-based materials for enzyme immobilizations: a review", *Enzyme Microbial Technol*, 35, (2004), 126–39.
- [26]. Bailey MJ, Biely P, Poutanen K., "Laboratory testing of method for assay of xylanase activity," *Journal of biotechnology*, 23, (1992), 257–70.
- [27]. Wan, B., Li, J., Ma, F., Yu, N., Zhang, W., Jiang, L., Wei, H., "Preparation and properties of cryogel based on poly (2-hydroxyethyl methacrylate-co-glycidyl methacrylate)", *Langmuir*, 35(9), (2019), 3284-3294.
- [28]. Li, G., Nandgaonkar, A. G., Lu, K., Krause, W. E., Lucia, L. A., Wei, Q., "Laccase immobilized on PAN/O-MMT composite nanofibers support for substrate bioremediation: a de novo adsorption and biocatalytic synergy", *RSC advances*, 6(47), (2016), 41420-41427.
- [29]. Dos Santos, J. P., da Rosa Zavareze, E., Dias, A. R. G., Vanier, N. L., "Immobilization of xylanase and xylanase- β -cyclodextrin complex in polyvinyl alcohol via electrospinning improves enzyme activity at a wide pH and temperature range", *International Journal of Biological Macromolecules*, 118, (2018), 1676-1684.
- [30]. Nagar, S., Mittal, A., Kumar, D., Kumar, L., Gupta, V. K., "Immobilization of xylanase on glutaraldehyde activated aluminum oxide pellets for increasing digestibility of poultry feed", *Process Biochemistry*, 47(9), (2012), 1402-1410.
- [31]. Gawande, P. V., & Kamat, M. Y., "Preparation, characterization and application of *Aspergillus* sp. xylanase immobilized on Eudragit S-100", *Journal of Biotechnology*, 66(2-3), (1998), 165-175.
- [32]. Ferrarotti, S. A., Bolivar, J. M., Mateo, C., Wilson, L., Guisan, J. M., Fernandez-Lafuente, R., "Immobilization and stabilization of a cyclodextrin glycosyltransferase by covalent attachment on highly activated glyoxyl-agarose supports", *Biotechnology Progress*, 22(4), (2006), 1140-1145.
- [33]. Amaro-Reyes, A., Díaz-Hernández, A., Gracida, J., García-Almendárez, B. E., Escamilla-García, M., Arredondo-Ochoa, T., Regalado, C. "Enhanced performance of immobilized xylanase/filter paper-ase on a magnetic chitosan support", *Catalysts*, 9(11), (2019), 966.
- [34]. Mehnati-Najafabadi, V., Taheri-Kafrani, A., Bordbar, A. K., Eidi, A. "Covalent immobilization of xylanase from *Thermomyces lanuginosus* on aminated superparamagnetic graphene oxide nanocomposite", *Journal of the Iranian Chemical Society*, 16(1), (2019), 21-31.
- [35]. Edward, V. A., Pillay, V. L., Swart, P., Singh, S., "Immobilization of xylanase from *Thermomyces lanuginosus* SSBP using Eudragit S-100: research in action", *South African journal of science*, 98(11), (2002), 553-554.

**MJEN**

Development and application of bimetallic catalysts supported carbon nanotube for 1-propanol electrooxidation

Sefika Kaya

Department of Chemical Engineering, Faculty of Engineering and Architectural Sciences, Eskisehir Osmangazi University, Eskisehir, 26040, Turkey, sefikakaya48@gmail.com, sefikakaya@ogu.edu.tr, ORCID: 0000-0003-3556-6461

ABSTRACT

Herein, carbon nanotube supported bimetallic catalysts (PtBi/CNT) are synthesized at various metals weight loadings by NaBH₄ reduction method. The surface morphology and crystal structure of the catalysts are investigated via X-ray diffraction (XRD) and electron microscopy with energy dispersive X-ray (SEM-EDX) advance surface methods. According to XRD results, the crystal size of PtBi(90:10)/CNT catalyst is determined as 4.66 nm. Cyclic voltammetry (CV), electrochemical impedance spectroscopy (EIS), and chronoamperometry (CA) electrochemical techniques are used to determine 1-propanol electrooxidation activities of the catalysts. The highest specific activity and mass activity are obtained with PtBi(90:10)/CNT catalyst as 5.663 mA/cm² and 447.21 mA/mg Pt, respectively. However, it is concluded that PtBi(90:10)/CNT catalyst can be used as an anode catalyst in 1-propanol electrooxidation with long-term stability and low resistance.

ARTICLE INFO

Research article

Received: 7.10.2022

Accepted: 8.12.2022

Keywords:

Pt,

Bi,

catalyst,

1-propanol, electrooxidation,

carbon nanotube

1. Introduction

In recent years, the increasing world population, the increase in energy demand, the depletion of fossil fuels and the damage to the environment have led to the search for renewable energy sources [1-4]. In this context, fuel cells come to the fore with their zero gas emission, high energy efficiency, sustainability and environmental friendliness [5-7]. Fuel cells are devices that convert chemical energy into electrical energy by electrochemical reactions in the presence of a fuel and an oxidizer [8]. Although hydrogen is a clean and efficient fuel for fuel cell, there are problems such as producing, transporting and storing pure hydrogen [9]. These problems have led research to liquid fuels such as alcohol. Alcohols with high energy density are easy to transport and process [10, 11]. Direct alcohol fuel cells work in both acidic and alkaline environments. However, the oxidation reaction is slow in acidic environment. The alkaline medium, where the oxidation reaction is faster and the corrosive effect is less, is more preferred [12-14]. 1-propanol is a three-carbon alcohol and 18 electrons are produced as a result of the complete oxidation reaction (Eq. 1)[15]. Compared to other alcohols, it has superior properties such as being less toxic and having a higher energy density [16, 17]. However, it is a cheap renewable fuel source that can be produced from biomass [18].



Nobel metals (e.g., Pt, Pd, Ru) and their alloys have been frequently investigated as anode and cathode catalysts in fuel

cell technology. Monometallic catalysts have superior physicochemical properties. However, bimetallic catalysts overcome the disadvantages of monometallic catalysts such as electrode poisoning and are more active [19, 20]. In addition, carbon-based materials with a large surface area and porous structure, which provide homogeneous dispersion of the catalyst, increase the catalytic activity, are preferred as support materials [21-23]. Carbon nanotubes (CNTs), one of the carbon-based materials, come to the fore in scientific studies with their high electrical conductivity, mechanical and thermal stability, large surface area and porosity [24, 25]. Etesami et al. prepared monometallic and bimetallic catalysts of Pt, Pd, and Au metals with pencil graphite support material for 1-propanol electrooxidation and compared catalytic activity of the catalyst in alkaline and acidic media. They reported that bimetallic catalysts have higher catalytic activity in alkaline media [19]. Kim et al. synthesized carbon supported monometallic and bimetallic catalysts at different atomic ratios of Pt and Sn. They emphasized that the addition of Sn metal to Pt/C catalyst reduces electrode poisoning and improves catalytic activity [26]. Synthesized Pt/RuO₂ catalyst was used to investigation 1-propanol electrooxidation activity by Spasojevic et al. They also declared that the increase in RuO₂ content increased the catalytic activity [27]. The different catalyst such as PdSn, PdRu, and PdIr [28], PtRh [29], PtAu/Ni [30], Pt/PANI/Au [31] were used for 1-propanol electrooxidation in literature.

In this study, 1-propanol electrocatalytic performances of bimetallic catalysts were investigated. The bimetallic

catalysts were synthesized at various Pt and Bi metals weight loadings by NaBH_4 reduction method. CV, EIS and CA electrochemical measurements were used to determine catalytic activities of the catalysts. The surface structure and crystal size of the catalysts were determined with SEM-EDX and XRD analyzes.

2. Experimental

2.1. Synthesis and characterization

Pt/CNT, Bi/CNT, and PtBi/CNT at different atomic ratios were prepared with NaBH_4 reduction method. The loaded metal was adjusted as 10 wt% on a support material (CNT). Precursor metal salts ($\text{Cl}_6\text{K}_2\text{Pt}$ and $\text{Bi}(\text{NO}_3)_3 \cdot 5\text{H}_2\text{O}$) were weighed and dissolved in pure water. After adding support material, prepared solution was stirred during 2 h. The NaBH_4 was added into the solution by dropwise. The solution was stirred for 1 h, filtered, washed and then dried in vacuum oven. Advanced surface characterization techniques such as SEM-EDX (Zeiss Sigma 300) and XRD (Panalytical Empyrean) were applied to determine the characterization of the catalysts.

2.2. Electrochemical measurements

CHI 660E potentiostat device with three electrode system was used for CV, CA, and EIS analyzes. The three-electrode system consisted of glassy carbon as working electrode, Pt wire as counter electrode, and Ag/AgCl as reference electrode. All electrochemical experiments were taken in 1 M KOH + 1 M 1-propanol solution. The 1-propanol electrooxidation activities of the catalyst were investigated by CV at -1.0-0.6 potential range V and 50 mV/s. The stability of the catalysts was defined with CA analyzes at -0.6, -0.4, -0.2, 0.0, and 0.2 V in 1000 s. EIS measurements were performed at different potential values (from -0.6 V to 0.2 V) in 300 kHz-0.04 Hz frequency range.

3. Results and Discussion

3.1. Physical characterization

The crystallinity of the Pt/CNT and PtBi(90:10)/CNT catalysts were determined with XRD analysis. Figure 1 presented the XRD patterns of the catalysts. Accordingly, the C (002) plane related hexagonal carbon structure was observed at 25.7° diffraction peak point [32]. The (111), (200), (220), and (311) planes were appeared at around 43.1° , 53.1° , 67.0° , and 78.5° belonging the face-centered cubic (fcc) Pt structure, respectively [33]. A positive shift was observed in the same Pt peaks for the PtBi(90:10)/CNT catalyst. The (112) planes of the Bi diffraction peak for the PtBi(90:10)/CNT catalyst was observed at 39.9° [34]. The crystal size of Pt/CNT and PtBi(90:10)/CNT catalysts were calculated by using Scherrer's equation and were found to be 2.81 nm and 4.66 nm, respectively.

The surface formation of PtBi(90:10)/CNT catalyst was explained via SEM-EDX analysis. SEM-EDX results of the catalyst are shown in Figure 2. In SEM images, it was observed that the metals were homogeneously dispersed without clumping. In addition, the EDX spectrum of the catalyst included peaks of Pt and Bi structures.

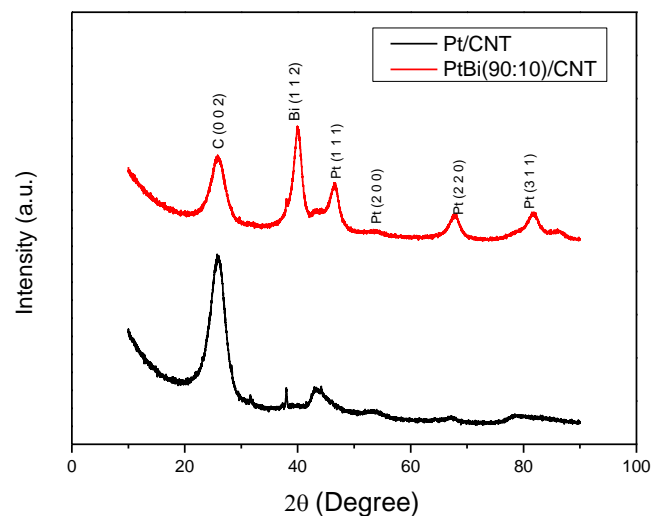


Figure 1. XRD patterns of the Pt/CNT and PtBi(90:10)/CNT catalysts.

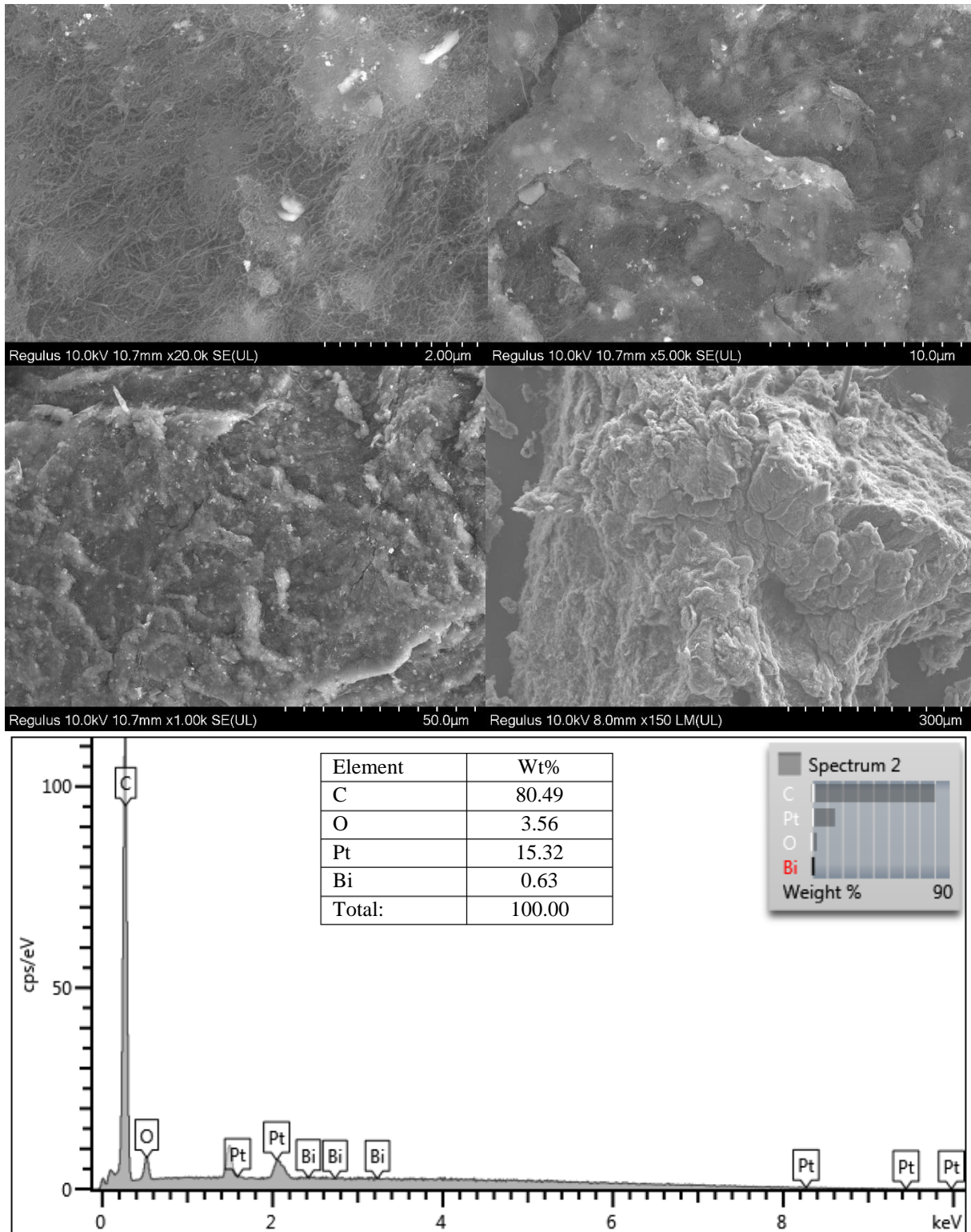


Figure 2. SEM-EDX results of PtBi(90:10)/CNT catalyst.

3.2. Electrochemical results

1-propanol electrooxidation performance of Pt/CNT, Bi/CNT, and PtBi/CNT at different atomic ratios were determined with CV measurements. The CV measurements were applied in 1 M KOH + 1 M 1-propanol solution in the potential range of -1.0 - 0.6 V. The obtained CV results are shown in Figure 3. In Figure 3, two characteristic peaks were observed between the potentials of -0.6 to 0.1 V in the forward scan and -0.5 to -0.2 V in the reverse scan. The observed peaks in the forward scan indicate 1-propanol oxidation. Table 1 includes the electrochemical properties of catalysts for 1-propanol electrooxidation. As the Pd metal ratio increased, the current value increased and the PdBi(90:10)/CNT catalyst showed the highest specific activity with 5.663 mA/cm² value.

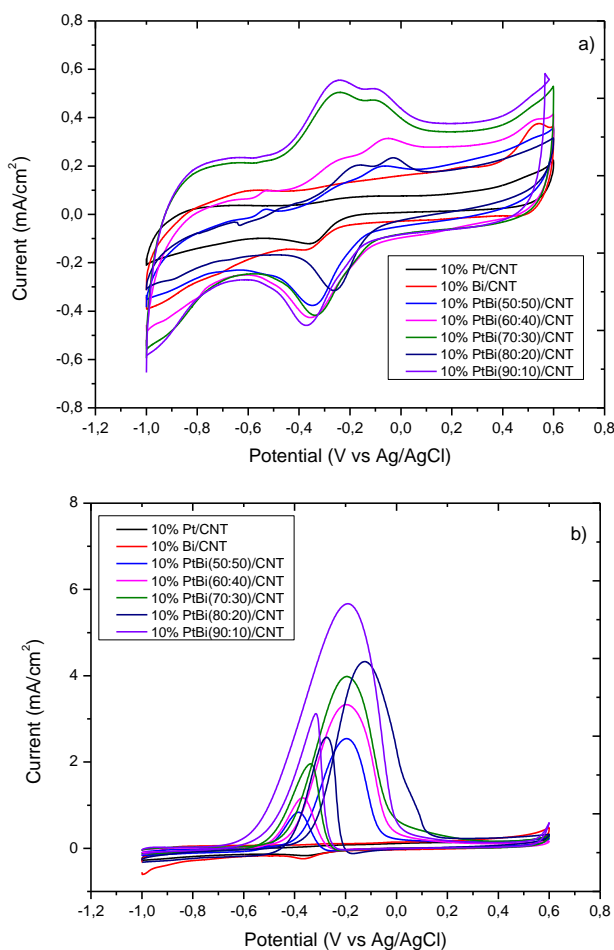


Figure 3. CV curves of 10% Pt/CNT, 10% Bi/CNT, and 10% PtBi/CNT at various atomic ratios in (a) 1 M KOH (b) 1 M KOH + 1 M 1-propanol.

CA measurements were applied to determine the stability of the 10% PtBi(90:10)/CNT catalyst at different potentials in 1000 s. The CA curves of the catalyst were shown in Figure 4. As seen in the Figure 4, there was a decrease at the beginning of the measurements as a result of electrode poisoning of intermediate species formed during electrooxidation. The catalyst was provided the highest catalytic activity and longest stability at -0.6 V potential.

The catalytic resistance of 10% PtBi(90:10)/CNT catalyst was explained by using Nyquist curves (Figure 5). Nyquist curves obtained with EIS measurements are usually semicircular. Since the diameter of the semicircle is proportional to the charge transfer resistance (R_{ct}), the smaller the diameter, the higher the catalytic activity [35, 36]. For 10% PtBi(90:10)/CNT catalyst, the best catalytic activity and lowest charge transfer resistance were provided at -0.2 V.

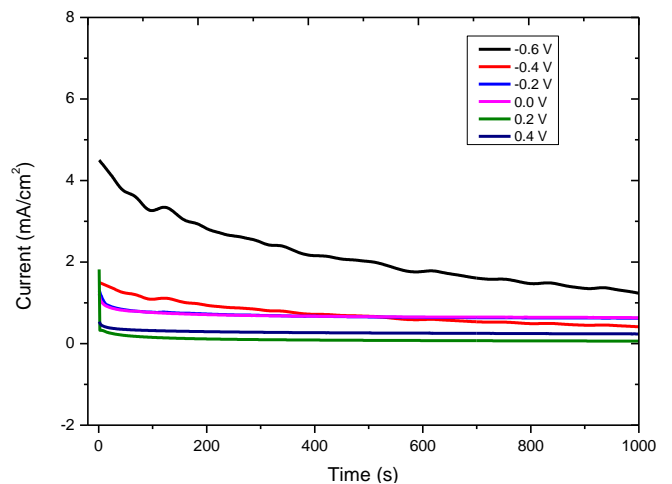


Figure 4. CA curves of 10% PtBi(90:10)/CNT catalyst at different potentials.

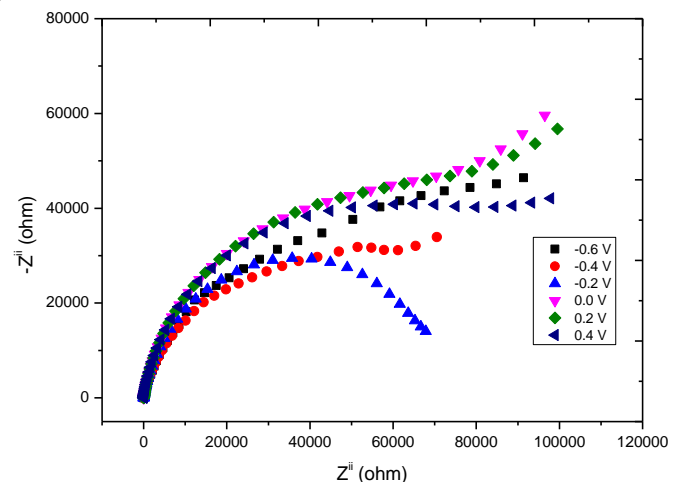


Figure 5. EIS profile of 10% PtBi(90:10)/CNT catalyst at different potentials.**Table 1.** The electrochemical properties of catalysts for 1-propanol electrooxidation.

Catalyst	Current, mA/cm ²	Peak Potential, V	Onset Potential, V	Mass Activity, mA/mg Pt
10% PtBi(50:50)/CNT	2.535	-0.199	-0.500	218.90
10% PtBi(60:40)/CNT	3.330	-0.196	-0.504	280.07
10% PtBi(70:30)/CNT	3.974	-0.196	-0.505	330.05
10% PtBi(80:20)/CNT	4.316	-0.124	-0.507	347.61
10% PtBi(90:10)/CNT	5.663	-0.189	-0.672	447.21

4. Conclusion

In this study, CNT supported bimetallic catalysts were prepared at different Pt and Bi metal ratios by using NaBH₄ reduction method. The synthesized catalysts were characterized via XRD and SEM-EDX characterization methods. CV, EIS, and CA electrochemical techniques were applied to determine the 1-propanol electrocatalytic activities of the catalysts. The following results were obtained from 1-propanol electrooxidation measurements and characterization results:

- The crystal size of PtBi/CNT catalyst from XRD results was found as 4.66 nm.
- In SEM images, it was observed that the metals were homogeneously dispersed without clumping.
- PtBi(90:10)/CNT catalyst exhibited the best catalytic activity and mass activity as 5.663 mA/cm² and 447.21 mA/mg Pt, respectively. This result can be explained by the synergistic effect between Pt and Bi metals.
- According to CA and EIS results, compared to other catalysts, PtBi(90:10)/CNT had the lowest long-term stability and lowest resistance in the 1-propanol electrooxidation reaction.
- PtBi(90:10)/CNT catalyst is promising as anode catalysts for 1-propanol fuel cells.

Acknowledgments

Eskisehir Osmangazi University Scientific Research Projects Commission (BAP Project No: FHD-2022-2346) supported this study.

References

For Journal Papers

- [1]. Wang C.Q., Zhang K., Xu H., Du Y.K., Goh M.C., "Anchoring gold nanoparticles on poly(3,4-ethylenedioxythiophene) (PEDOT) nanonet as three-dimensional electrocatalysts toward ethanol and 2-propanol oxidation", *Journal of Colloid and Interface Science*, 541, (2019), 258-268.

- [2]. Figueiredo M.C., Sorsa O., Doan N., Pohjalainen E., Hildebrand H., Schmuki P., Wilson B.P., Kallio T., "Direct alcohol fuel cells: Increasing platinum performance by modification with sp-group metals", *Journal of Power Sources*, 275, (2015), 341-350.
- [3]. Hu S.Z., Munoz F., Noborikawa J., Haan J., Scudiero L., Ha S., "Carbon supported Pd-based bimetallic and trimetallic catalyst for formic acid electrochemical oxidation", *Applied Catalysis B-Environmental*, 180, (2016), 758-765.
- [4]. Ulas B., Caglar A., Sahin O., Kivrak H., "Composition dependent activity of PdAgNi alloy catalysts for formic acid electrooxidation", *Journal of Colloid and Interface Science*, 532, (2018), 47-57.
- [5]. Kazici H.C., Yilmaz S., Sahan T., Yildiz F., Er O.F., Kivrak H., "A comprehensive study of hydrogen production from ammonia borane via PdCoAg/AC nanoparticles and anodic current in alkaline medium: experimental design with response surface methodology", *Frontiers in Energy*, 14(3), (2020), 578-589.
- [6]. Kivrak H., Atbas D., Alal O., Cogenli M.S., Bayrakceken A., Mert S.O., Sahin O., "A complementary study on novel PdAuCo catalysts: Synthesis, characterization, direct formic acid fuel cell application, and exergy analysis", *International Journal of Hydrogen Energy*, 43(48), (2018), 21886-21898.
- [7]. Baronia R., Goel J., Bajinath, Kataria V., Basu S., Singhal S.K., "Electro-oxidation of ethylene glycol on Pt-Co metal synergy for direct ethylene glycol fuel cells: Reduced graphene oxide imparting a notable surface of action", *International Journal of Hydrogen Energy*, 44(20), (2019), 10023-10032.
- [8]. Ulas B., Caglar A., Kivrak H., "Determination of optimum Pd:Ni ratio for Pd_xNi_{100-x}/CNTs formic acid electrooxidation catalysts synthesized via sodium borohydride reduction method", *International Journal of Energy Research*, 43(8), (2019), 3436-3445.
- [9]. Qi Z.G., Kaufman A., "Performance of 2-propanol in direct-oxidation fuel cells", *Journal of Power Sources*, 112(1), (2002), 121-129.

- [10]. Serov A., Martinez U., Falase A., Atanassov P., "Highly active Pd-Cu catalysts for electrooxidation of 2-propanol", *Electrochemistry Communications*, 22, (2012), 193-196.
- [11]. Zhou W.Q., Wang C.Y., Xu J.K., Du Y.K., Yang P., "Enhanced electrocatalytic performance for isopropanol oxidation on Pd-Au nanoparticles dispersed on poly(p-phenylene) prepared from biphenyl", *Materials Chemistry and Physics* 123(2-3), (2010), 390-395.
- [12]. Antolini E., Gonzalez E.R., "Alkaline direct alcohol fuel cells", *Journal of Power Sources* 195(11), (2010), 3431-3450.
- [13]. Wang Y., Li L., Hu L., Zhuang L., Lu J.T., Xu B.Q., "A feasibility analysis for alkaline membrane direct methanol fuel cell: thermodynamic disadvantages versus kinetic advantages", *Electrochemistry Communications*, 5(8), (2003), 662-666.
- [14]. Spendelov J.S., Wieckowski A., "Electrocatalysis of oxygen reduction and small alcohol oxidation in alkaline media", *Physical Chemistry Chemical Physics*, 9(21), (2007) 2654-2675.
- [15]. Modestov A.D., Tarasevich M.R., Pu H.T., "Study of 2-Propanol, 1-Propanol, and Acetone Electrochemical Oxidation on Pt in Gelled Phosphoric Acid at 170 degrees C", *Electrocatalysis*, 7(1), (2016), 42-49.
- [16]. Spasojevic M., Ribic-Zelenovic L., "Electrooxidation of 1-propanol on the mixture of nanoparticles of Pt and RuO₂", *Monatshefte Fur Chemie*, 152(5), (2021), 489-496.
- [17]. Wang D.Y., Liu J.P., Wu Z.Y., Zhang J.H., Su Y.Z., Liu Z.L., Xu C., "Electrooxidation of Methanol, Ethanol and 1-Propanol on Pd Electrode in Alkaline Medium", *International Journal of Electrochemical Science*, 4(12), (2009), 1672-1678.
- [18]. Yi Q.F., Chu H., Chen Q.H., Yang Z., Liu X.P., "High Performance Pd, PdNi, PdSn and PdSnNi Nanocatalysts Supported on Carbon Nanotubes for Electrooxidation of C₂-C₄ Alcohols", *Electroanalysis*, 27(2), (2015), 388-397.
- [19]. Etesami M., Mohamed N., "A comparative electrooxidation study on simply prepared nanoparticles in acidic and alkaline media", *Chemija*, 23(3), (2012), 171-179.
- [20]. Yu E.H., Krewer U., Scott K., "Principles and Materials Aspects of Direct Alkaline Alcohol Fuel Cells", *Energies*, 3(8), (2010), 1499-1528.
- [21]. Chiu W.T., Chiu Y.H., Hsieh P.Y., Chang T.F.M., Sone M., Hsu Y.J., Tixier-Mita A., Toshiyoshi H., "Nano-Au Catalysts Modified with TiO₂: Enhancement of Electrocatalytic Activity for 1-Propanol Oxidation in Alkaline Media", *Journal of the Electrochemical Society*, 166(12), (2019) F760-F767.
- [22]. Jafarian M., Mirzapoor A., Danaee I., Shahnazi S.A.A., Gopal F., "A comparative study of the electrooxidation of C₁ to C₃ aliphatic alcohols on Ni modified graphite electrode", *Science China-Chemistry*, 55(9), (2012), 1819-1824.
- [23]. King W.D., Corn J.D., Murphy O.J., Boxall D.L., Kenik E.A., Kwiatkowski K.C., Stock S.R., Lukehart C.M., "Pt-Ru and Pt-Ru-P/carbon nanocomposites: Synthesis, characterization, and unexpected performance as direct methanol fuel cell (DMFC) anode catalysts", *Journal of Physical Chemistry B*, 107(23), (2003), 5467-5474.
- [24]. Liu J.L., Lai L.F., Sahoo N.G., Zhou W.J., Shen Z.X., Chan S.H., "Carbon Nanotube-Based Materials for Fuel Cell Applications", *Australian Journal of Chemistry*, 65(9), (2012), 1213-1222.
- [25]. Ma M., You S.J., Gong X.B., Dai Y., Zou J.L., Fu H.G., "Silver/iron oxide/graphitic carbon composites as bacteriostatic catalysts for enhancing oxygen reduction in microbial fuel cells", *Journal of Power Sources*, 283, (2015), 74-83.
- [26]. Kim J.H., Choi S.M., Nam S.H., Seo M.H., Choi S.H., Kim W.B., "Influence of Sn content on PtSn/C catalysts for electrooxidation of C-1-C-3 alcohols: Synthesis, characterization, and electrocatalytic activity", *Applied Catalysis B-Environmental*, 82(1-2), (2008), 89-102.
- [27]. Spasojevic M., Markovic D., Ribic-Zelenovic L., "Electrooxidation of 2-propanol on the mixture of nanoparticles of Pt and RuO₂ supported on Ti", *Zeitschrift Fur Physikalische Chemie-International Journal of Research in Physical Chemistry & Chemical Physics*, 235(12), (2021), 1573-1588.
- [28]. Lim E.J., Kim Y., Choi S.M., Lee S., Noh Y., Kim W.B., "Binary PdM catalysts (M = Ru, Sn, or Ir) over a reduced graphene oxide support for electro-oxidation of primary alcohols (methanol, ethanol, 1-propanol) under alkaline conditions", *Journal of Materials Chemistry A*, 3(10), (2015), 5491-5500.
- [29]. Rodrigues I.A., Bergamaski K., Nart F.C., "Probing n-propanol electrochemical oxidation on bimetallic PtRh codeposited electrodes" *Journal of the Electrochemical Society*, 150(2), (2003), E89-E94.
- [30]. Funo S., Sato F., Cai Z.W., Chang G., He Y.B., Oyama M., "Codeposition of Platinum and Gold on Nickel Wire Electrodes via Galvanic Replacement Reactions for Electrocatalytic Oxidation of Alcohols", *Acs Omega*, 6(28), (2021), 18395-18403.

- [31]. Schwartz I., Jonke A.P., Josowicz M., Janata J., "Polyaniline-Supported Atomic Gold Electrodes: Comparison with Macro Electrodes", *Catalysis Letters*, 142(11), (2012), 1344-1351.
- [32]. Ulas B., Alpaslan D., Yilmaz Y., Dudu T.E., Er O.F., Kivrak H., "Disentangling the enhanced catalytic activity on Ga modified Ru surfaces for sodium borohydride electrooxidation", *Surfaces and Interfaces* 23, (2021), 100999.
- [33]. Kivrak H., Alal O., Atbas D., "Efficient and rapid microwave-assisted route to synthesize Pt-MnOx hydrogen peroxide sensor", *Electrochimica Acta*, 176, (2015), 497-503.
- [34]. Caglar A., Aldemir A., Kivrak H., "Alcohol electrooxidation study on carbon nanotube supported monometallic, Pt, Bi, and Ru catalysts", *Fullerenes Nanotubes and Carbon Nanostructures*, 26(12), (2018), 863-870.
- [35]. Ozok O., Kavak E., Er O.F., Kivrak H., Kivrak A., "Novel benzothiophene based catalyst with enhanced activity for glucose electrooxidation", *International Journal of Hydrogen Energy*, 45(53), (2020), 28706-28715.
- [36]. Caglar A., Cogenli M.S., Yurtcan A.B., Alal O., Kivrak H., "Remarkable activity of a ZnPdPt anode catalyst: Synthesis, characterization, and formic acid fuel cell performance", *Journal of Physics and Chemistry of Solids*, 156, (2021), 110163.



Water is an effective additive to fuel oil to reduce the concentration of soot in the gas phase

Damira Sambaeva¹, Mirlan Moldobaev^{2*}, Kubat Kemelov², Zarlık Maimekov²

¹Kyrgyz Mining and Metallurgical Institute Named after academician U. Asanaliev, Bishkek, Kyrgyz Republic, dsambaeva@gmail.com, ORCID: 0000-0002-9834-341X

²Kyrgyz-Turkish Manas University, Department of Environmental Engineering, Bishkek, Kyrgyz Republic, mirlan.moldobaev@manas.edu.kg, ORCID: 0000-0002-8710-5643, kubat.kemelov@manas.edu.kg, ORCID: 0000-0001-7375-6325, zarlyk.maymekov@manas.edu.kg, ORCID: 0000-0002-9117-262X

ABSTRACT

Soot is one of the products of incomplete combustion of hydrocarbon fuels. It has the property of adsorption of active and carcinogenic substances on the surface of soot particles. In this regard, in burner equipment of medium and small power, it is required to develop and implement effective environmental measures to reduce emissions of soot particles. In this paper, the fuel oil-water-air system at a wide temperature range ($T=500-3000K$) was studied and the ratio of gas-liquid flows (water content in fuel oil 5-15%) at the maximum entropy of the system and the formation of soot in flue gases was revealed. To reduce the concentration of soot in flue gases, a fuel oil-water emulsion was used. The particle sizes of the fuel oil-water emulsion were determined by sedimentation analysis. It is shown that they have a polydisperse character (diameter from 8.96 to 59.02 μm). The water content in fuel oil during the preparation of fuel oil-water emulsion in the boiler room was controlled by a capacitive sensor. The water flow was automatically maintained by an ejector-dosing device. The thermodynamic parameters of the system (entropy, enthalpy, internal energy) were calculated and their comparative characteristics were obtained. The concentration distribution of hydrogen, carbon, nitrogen, sulfur and oxygen containing molecules, particles and condensed phases in the gas phase has been established. During the combustion of the fuel oil-water emulsion, the concentration of soot in the gas phase decreased due to an increase in hydrogen-containing particles in the gas phase, i.e. an increase in the H/C ratio, as well as a change in the concentration of condensed carbon (mol/kg): (fuel oil without water $C_{(c)} = 63.3$ mol/kg); fuel oil with water: 5% H_2O , $C_{(c)} = 54.96$; 10% H_2O , $C_{(c)} = 50.45$; 15% H_2O , $C_{(c)} = 46.3$. It is noted that the H/C ratio in the case of burning fuel oil -water emulsion is 2.26 times higher. A technological scheme for the preparation and combustion of fuel oil in the form of fuel oil-water emulsions in industrial boilers of the E-1/9-M(3) type of the Bridge Construction Detachment of the Kyrgyz Railway, Bishkek, has been developed. It has been established that when burning fuel oil-water emulsions in boiler units, the soot content in flue gases is reduced by 75% due to the developed contact surface of the interacting phases and more complete combustion of particles of fuel oil-water emulsions.

1. Introduction

One of the atmospheric polluting components of hydrocarbon fuel combustion products are soot particles, which are highly stable and, therefore, capable of long-term preservation in ambient conditions [1-11]. This feature, as well as the possibility of adsorption of active and carcinogenic substances on the surface of soot particles, requires the development and implementation of effective environmental measures to reduce soot particle emissions, especially in medium and low power combustion equipment [12-20]. The formation and burnout of soot (change $C_{(c)}$ and

H/C) during the combustion of hydrocarbon fuels should be considered as a set of extremely complex physicochemical, heat and mass transfer processes, which require systematic scientific research and the implementation of environmental measures on their basis [16]. Taking into account the above circumstances, the paper considers the sources of pollution of the environment with technogenic soot, the processes of conversion of technogenic soot with water of fuel oil-water emulsions in a wide range of temperature changes and ratios of gas-liquid flows (5-15% of water in fuel oil).

2. Materials and methods

ARTICLE INFO

Research article

Received: 7.07.2022

Accepted: 1.12.2022

Keywords:

fuel oil,
water, air,
emulsion,
combustion,
concentration,
boiler unit,
thermodynamic modeling,
entropy,
technological scheme

*Corresponding Author

Experimental determination of the soot concentration in flue gases was carried out by sampling solid particles from the chimney of E-1/9M type boilers based on the Visit 01-L/LR multifunctional gas analyzer and the UG-2 type portable gas analyzer according to the standard methods 5506 and 5515 "NIOSH Manual of Analytical Methods" [2]; determination of the particle size of the fuel oil-water emulsion was carried out by the method of sedimentation analysis [21,22]; determination of the water content in the fuel oil-water emulsion was carried out by a capacitive sensor [16]; thermodynamic modeling of the process of burning fuel oil in the form of fuel oil-water emulsions at various ratios of gas-liquid flows, temperatures and the calculation of the concentration of carbon, hydrogen, oxygen, nitrogen and sulfur-containing particles, molecules and condensed phases in the gas phase was carried out at the maximum entropy of the system based on the software package "Terra" [23]. The development and making up of a basic technological scheme for the preparation and combustion of fuel oil-water emulsions took place in boiler units of the E-1 / 9M type of the Bridge Construction Detachment of the Kyrgyz Railway, Bishkek.

3. Results and discussion

The results of furnace practice show that the initial fuel oil contains from 3 to 5% of water, due to heating it with live steam in order to impart fluidity [12-14]. In this case, water in fuel oil has a lens distribution. Such a layered distribution of fuel oil -water does not lead to the formation of polydisperse inverse emulsions. In this case, water in fuel oil has a lens distribution. Such a layered distribution of fuel oil -water does not lead to the formation of polydisperse inverse emulsions. Taking into account these circumstances, an increase in the efficiency of the use of heating fuel oil in the boiler house was achieved by modifying it in the form of fuel oil-water emulsions (FWE). Accordingly, the model system is first considered: fuel oil-water-air at 5%, 10% and 15% of the content of fuel oil contaminated wastewater. Therefore, the following average composition of gas-liquid flows (%) was adopted in the calculations: fuel oil C (84.8) – H (11.2) – S (2.0) – N (0.5) – O (1.5); water (10) and air N (10.05) – O (2.67).

Table 1 shows the equilibrium concentrations of molecules, particles and the condensed phase formed during the oxidation of the fuel oil -water-air system at $\text{CH}_2\text{O}=10\%$ and within the limits of the theoretical fuel combustion temperature ($T=2000\text{ K}$).

Table 1. Equilibrium concentrations of molecules, particles, and condensed phase (mol/kg) formed in the gas phase during the oxidation of a fuel oil-water emulsion. Water content in fuel oil 10%, $T=2000\text{ K}$, $P=0.1\text{ MPa}$

$\text{O} = 0.15 \cdot 10^{-9}$	H = 0.088	$\text{S}_2 = 0.0068$	$\text{S}_2\text{O} = 0.39 \cdot 10^{-9}$
$\text{H}_2\text{O} = 0.64 \cdot 10^{-3}$	$\text{S} = 0.002$	$\text{SO}_2 = 0.38 \cdot 10^{-11}$	$\text{SOH} = 0.35 \cdot 10^{-9}$
$\text{S}_4 = 0.68 \cdot 10^{-11}$	$\text{SO} = 0.15 \cdot 10^{-6}$	$\text{HSO} = 0.25 \cdot 10^{-10}$	$\text{NO} = 0.94 \cdot 10^{-9}$
$\text{SH} = 0.039$	$\text{H}_2\text{S} = 0.321$	$\text{N}_2 = 2.96$	$\text{N}_2\text{H}_2 = 0.71 \cdot 10^{-11}$
$\text{H}_2\text{SO} = 0.4 \cdot 10^{-11}$	$\text{N} = 0.11 \cdot 10^{-7}$	$\text{NH}_3 = 0.20 \cdot 10^{-3}$	$\text{C}_2 = 0.13 \cdot 10^{-9}$
$\text{NH} = 0.18 \cdot 10^{-6}$	$\text{NH}_2 = 0.12 \cdot 10^{-5}$	C = 0.18 · 10⁻⁸	$\text{C}_2\text{O} = 0.13 \cdot 10^{-7}$
$\text{NS} = 0.34 \cdot 10^{-5}$	C_(c) = 50.45	CO₂ = 0.18 · 10⁻⁴	$\text{CH}_3 = 0.63 \cdot 10^{-3}$
$\text{C}_3 = 0.16 \cdot 10^{-8}$	CO = 6.64	$\text{CH}_2 = 0.14 \cdot 10^{-5}$	$\text{C}_2\text{H}_3 = 0.19 \cdot 10^{-4}$
$\text{C}_3\text{O}_2 = 0.17 \cdot 10^{-9}$	$\text{CH} = 0.88 \cdot 10^{-8}$	$\text{C}_2\text{H}_2 = 0.04$	$\text{C}_3\text{H} = 0.39 \cdot 10^{-4}$
CH₄ = 0.017	$\text{C}_2\text{H} = 0.49 \cdot 10^{-5}$	$\text{C}_2\text{H}_6 = 0.90 \cdot 10^{-7}$	$\text{C}_4\text{H} = 0.12 \cdot 10^{-8}$
$\text{C}_2\text{H}_4 = 0.21 \cdot 10^{-3}$	$\text{C}_2\text{H}_5 = 0.47 \cdot 10^{-7}$	$\text{C}_3\text{H}_8 = 0.10 \cdot 10^{-11}$	$\text{C}_6\text{H}_6 = 0.37 \cdot 10^{-10}$
$\text{C}_3\text{H}_4 = 0.36 \cdot 10^{-8}$	$\text{C}_3\text{H}_6 = 0.35 \cdot 10^{-10}$	$\text{C}_5\text{H}_6 = 0.94 \cdot 10^{-11}$	$\text{CH}_2\text{O}_2 = 0.2 \cdot 10^{-10}$
$\text{C}_4\text{H}_2 = 0.20 \cdot 10^{-3}$	$\text{C}_4\text{H}_4 = 0.73 \cdot 10^{-11}$	$\text{CH}_2\text{O} = 0.22 \cdot 10^{-5}$	$\text{COS} = 0.0018$
$\text{CHO} = 0.35 \cdot 10^{-5}$	$\text{CHO}_2 = 0.7 \cdot 10^{-11}$	$\text{CS}_2 = 0.02$	$\text{C}_2\text{N}_2 = 0.53 \cdot 10^{-5}$
$\text{CH}_3\text{O} = 0.1 \cdot 10^{-11}$	$\text{CS} = 0.072$	$\text{C}_2\text{N} = 0.15 \cdot 10^{-7}$	$\text{C}_2\text{HN} = 0.60 \cdot 10^{-7}$
$\text{CN} = 0.75 \cdot 10^{-5}$	$\text{CN}_2 = 0.95 \cdot 10^{-8}$	$\text{HNC} = 0.16 \cdot 10^{-4}$	$\text{C}_3\text{HN} = 0.46 \cdot 10^{-4}$
$\text{NCO} = 0.41 \cdot 10^{-10}$	$\text{HCN} = 0.21$	$\text{C}_7\text{HN} = 0.25 \cdot 10^{-3}$	$\text{NH}^{++} = 0.18 \cdot 10^{-10}$
$\text{C}_3\text{HN} = 0.0015$	$\text{C}_5\text{HN} = 0.0011$	$\text{SH} = 0.49 \cdot 10^{-11}$	
$\text{N}_2\text{C} = 0.30 \cdot 10^{-5}$	$\text{CN} = 0.10 \cdot 10^{-10}$	$\text{OH} = 0.11 \cdot 10^{-6}$	
$\text{CHO}^+ = 0.2 \cdot 10^{-11}$	$\text{H}_2 = 49.22$	$\text{S}_3 = 0.38 \cdot 10^{-6}$	

During the oxidation of a fuel oil-water emulsion, the formation of active particles and molecules in the gas phase (mol / kg) was established: hydrogen and oxygen containing - O, H, H₂, OH, H₂O, OH; sulfur containing - S₂, S₃, S₄, SO, SO₂, S₂O, SH, H₂S, HSO, SOH, H₂SO, CS, CS, COS, SH; nitrogen containing - N, N₂, NO, NH, NH₂, NH₃, N₂H₂, NS, NH₂, NCO, CN, HCN, HNC, C₂HN, C₃HN, C₅HN, C₇HN, C₉HN, N₂C, CN₂, C₂N, C₂N₂, NH₄⁺, CN⁻; carbon containing - C_(c), C, C₂, C, CO, CO₂, C₂O, C₃O₂, CH, CH₂, CH₃, CH₄, C₂H, C₂H₂, C₂H₃, C₂H₄, C₂H₅, C₂H₆, C₃H, C₃H₄, C₃H₆, C₃H₈, C₄H, C₄H₂, C₄H₄, C₅H₆, C₆H₆, CHO, CHO₂, CH₂O, CH₂O₂, CH₃O, CHO⁺ (table 1, figure 1).

The formation of condensed carbon and other gas components (mol/kg) was established: at **5%** water content in fuel oil, C_(c) = 54.96; H₂ = 48.96; CO = 4.56; CH₄ = 0.018; CO₂ = 0.9 · 10⁻⁵; H₂O = 0.46 · 10⁻³, the H/C ratio was 0.08/0.17 10⁻⁸; at **10%** water content in fuel oil C(c) = 50.45; H₂ = 49.22; CO = 6.64; CH₄ = 0.017; CO₂ = 0.18 10⁻⁴; H₂O = 0.64 10⁻³; N/C 0.088/0.18 10⁻⁸; at **15%** water content in fuel oil C(c) = 46.3; H₂ = 49.46; CO = 8.55; CH₄ = 0.017; CO₂ = 0.3 10⁻⁴; H₂O = 0.81 · 10⁻³; N/S 0.08/0.18 · 10⁻⁸.

It is shown that during the oxidation of the fuel oil-water-air system, the content of condensed carbon (significant change in H/C) in the gas phase decreases (mol/kg): fuel oil without water C_(c) = 63.3 mol/kg; with water 5% H₂O, C(c) = 54.96; 10% H₂O, C_(c) = 50.45; 15% H₂O, C_(c) = 46.3 (Fig. 1). The H/C ratio in the case of burning fuel oil-water emulsion was 0.088/0.18 10⁻⁸, i.e. The H/C is 2.26 times higher than the H/C of the fuel oil-air system.

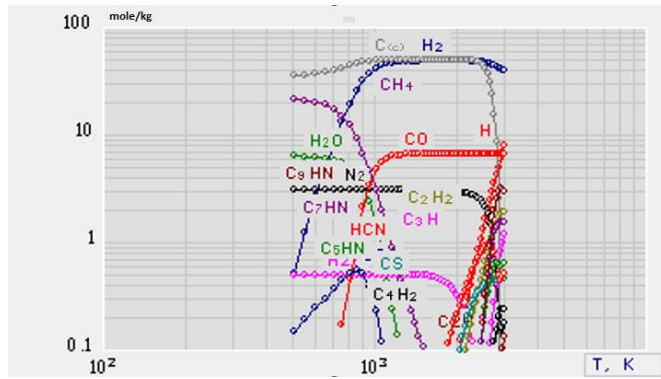


Figure 1. Concentration distribution of particles, molecules and condensed phase (mol/kg) in the gas phase depending on the oxidation temperature of the system: fuel oil-water-air, $C_{H_2O}=10\%$, $T=500-3000K$, $P=0.1 MPa$.

The concentration of condensed carbon in the gas phase increases with increasing temperature from 500 to 1750 K, and then decreases to zero (Table 2). Table 2. shows that combustible gases are present in the gas phase in various amounts: CO, H, H₂, CH₄, C₂H₆, C₃H₈, C₄H₁₀. Thus, the steam-oxygen conversion of fuel oil leads to the formation of a hydrogen-containing fuel gas. Therefore, the intensification of chemical processes for the conversion of hydrocarbon raw materials, in particular fuel oil into hydrogen-containing fuel synthesis gas based on the use and combustion of highly dispersed fuel oil-water emulsions, can be considered as a significant alternative to modern thermal catalytic processes for recycling liquid fuels.

Table 2. Concentration distribution of carbon, hydrogen containing particles, molecules and condensed phase (mol/kg) in the gas phase depending on the oxidation temperature of the system: fuel oil-water-air. $C_{H_2O}=10\%$, $T=500-3000K$ $P=0.1MPa$

T	C(e)	C	CO	CO ₂	CH ₄
500	36.18	1.92·10 ⁻²²	8.7·10 ⁻⁵	0.14	21,203
750	41.78	1.92·10 ⁻²²	0.17	0.44	15.12
1000	49.48	1.92·10 ⁻²²	4.74	0.23	3.06
1250	50.52	1.0·10 ⁻²⁰	6.54	0.07	0.44
1500	50.76	1.0·10 ⁻¹⁵	6.63	0	0.10
1750	50.74	3.81·10 ⁻¹²	6.64	0	0.037
2000	50.45	1.8·10 ⁻⁹	6.64	1.9·10 ⁻⁵	0.017
2250	49.50	2.1·10 ⁻⁷	6.64	6.6·10 ⁻⁶	0.009
2500	44.27	1.0·10 ⁻⁵	6.64	2.8·10 ⁻⁶	0.005
2750	15.77	0	6.64	1.4·10 ⁻⁶	0.003
3000	0	0	6.64	9.4·10 ⁻⁷	0.001

T	H	H ₂	C ₂ H ₆	C ₃ H ₈	C ₄ H ₁₀
500	2.83·10 ⁻²⁰	0,52	3,34·10 ⁻⁰⁵	5,63·10 ⁻¹⁰	1,37·10 ⁻¹⁴
750	7.2·10 ⁻¹²	13.4	0.0001	9.55·10 ⁻⁹	6.89·10 ⁻¹³
1000	1.08·10 ⁻⁷	41.7	4·10 ⁻⁵	1.85·10 ⁻⁹	1·10 ⁻¹³
1250	2.58·10 ⁻⁵	48.3	4.1·10 ⁻⁶	1.1·10 ⁻¹⁰	3.8·10 ⁻¹⁵
1500	9.5·10 ⁻⁴	49.06	7.6·10 ⁻⁷	1.4·10 ⁻¹¹	3.3·10 ⁻¹⁶
1750	0.012	49.2	2.2·10 ⁻⁷	3.3·10 ⁻¹²	5.8·10 ⁻¹⁷
2000	0.088	49.2	9·10 ⁻⁸	1·10 ⁻¹²	1.5·10 ⁻¹⁷
2250	0.40	48.9	4.36·10 ⁻⁸	4·33 ⁻¹³	5.26·10 ⁻¹⁸
2500	1.35	47.7	2.2·10 ⁻⁸	1.8·10 ⁻¹³	1.9·10 ⁻¹⁸
2750	3.57	44.0	1.1·10 ⁻⁸	6.8·10 ⁻¹⁴	5.8·10 ⁻¹⁹
3000	8.04	40.0	3.8·10 ⁻⁹	1.5·10 ⁻¹⁴	9.0·10 ⁻²⁰

Calculation and comparison of thermodynamic parameters of the system: fuel oil-air and fuel oil-water-air (Table 3) was

carried out. It is shown that in the fuel oil-water-air system the entropy value is higher, correspondingly, there are more particle interactions.

Table 3. Comparative characteristics of the thermodynamic parameters of the system: fuel oil-air and fuel oil-water-air

Temperature, K	System	
	Fuel oil -Air 500-750	Fuel oil -Water-Air 500-950
<i>Thermodynamic parameters:</i>		
Entropy <i>S</i> , kJ/(kg K)	2,49-3,28	7,44-11,49
Enthalpy <i>I</i> , kJ/kg	(-498) – (-94,7)	(-3252) – (-162)
Internal energy <i>U</i> , J/kg	(-510) – (-125)	(-3307) – (-452)
Prandtl number (<i>Pr</i> = γ/D)	0,68-0,59	0,69-0,47
Proportion of condensed phase (<i>z</i>)	0,79-0,78	0,41-0,54

The values of enthalpy and internal energy are negative within the temperature range from 500 to 750 K for the fuel oil-air system, and for the fuel oil-water-air system from 500 to 950 K, therefore, in the second system there are more chemical transformations. The Prandtl number for the fuel oil-water-air system is lower and more prone to dilution; in systems, the proportion of the condensed phase (*z*) is 0.79/0.41 at 500 K and 0.78/0.54 at 950 K, respectively, the formation of condensed carbon (C_e) is 2 times less in the fuel oil-water-air system. Thus, the thermodynamic parameters also showed the efficiency of using the fuel oil-water-air system in the processes of reducing gas emissions, including soot in boiler plants.

The results of thermodynamic modeling of the fuel oil-water-air system showed that the physical and chemical basis for the oxidation of fuel oil-water emulsions is the effective organization of the combustion process of the gas-vapor mixture due to microcrushing of the fuel mixture, i.e. in fact, on the replacement of the traditional catalyst - water inverse emulsions (water in fuel oil), leading to the acceleration of chemical processes by increasing the contact surface of the interacting phases. Taking into account the above circumstances, microcrushing of a mixture of fuel oil and waste water was achieved in the developed rotary pulsation apparatus (RPA) [16,24-26]. The resulting inverted emulsions in RPA had a polydisperse character with particle sizes from 8.92 to 75.12 μm (Table 4) and they were introduced in the boiler house of the Bridge Construction Detachment of the Kyrgyz Railway, Bishkek.

The processes of preparation and combustion of fuel oil-water emulsion, as noted above, were tested according to the

developed basic technological scheme in boiler units of the E-1/9M type of the Bridge Construction Detachment of the Kyrgyz Railway, Bishkek (Fig. 2). Fuel oil after passing through the fuel oil heater, coarse and fine filters, is pumped to the rotary pulsation apparatus (RPA). Water from the tank enters to the RPA and, based on a mixture consisting of 90% fuel oil and 10% water, polydisperse fuel oil-water emulsions are formed and they are sent to the combustion zone. The flow rates in pipelines are controlled by valves and check valves. Technical characteristics of the installation: electric motor, kW (rpm) - 4.0 (1500); fuel oil consumption 0.1-0.15 m³/hour; water consumption 0.01 - 0.015 m³/hour; water temperature and FWE 40 - 45°C (dashed line in the scheme: the path of the fuel oil-water emulsion).

Table 4. Distribution of particles of water-oil emulsion: $H=0.04m$, $\rho_K=775 \text{ kg/m}^3$, $\rho_{H_2O}=1000 \text{ kg/m}^3$, $\rho_{E+K}=820 \text{ kg/m}^3$, $\eta_{E+K}=2.46 \cdot 10^{-3} \text{ Pa} \cdot \text{s}$, $K=2.5 \cdot 10^{-3} \text{ m/s}$

Time, min	Sediment mass, mg	amount of precipitation over time, %	settling rate m/s	particle radius, μm	particle radius, μm
3	5	22,73	0,012	29,51	59,02
5	9	18,18	0,0091	22,79	45,57
8	12	12,63	0,0072	18,07	36,14
11	14	9,10	0,0061	15,41	30,82
15	16	9,09	0,0053	13,20	26,40
20	18	9,09	0,0046	11,43	22,86
30	19,5	6,82	0,0037	9,33	18,66
40	20	2,27	0,0032	8,08	16,16
50	20,5	2,27	0,0029	7,23	14,46
70	21	2,27	0,0024	6,11	12,22
90	21,5	2,28	0,0021	5,39	10,78
110	22	2,27	0,0019	4,87	9,75
130	22	0	0,0018	4,48	8,96

Measurements and calculation of concentrations of pollutants in flue gases were carried out in the processes of combustion of fuel oil (Table 5) and fuel oil-water emulsions (Table 6) taking into account the parameters of the chimney: $H=18m$, $D=0.5m$, the volume of the gas-air mixture $V_{g.cm}=0.889 \text{ m}^3/\text{s}$, flue gas temperature $t_{d.g.}=220^\circ\text{C}$, particle settling velocity $F=1$, wind speed $V=5.0 \text{ m/s}$. It should be noted here that in this work only soot was studied, and the gas components of boiler houses were considered in [16].

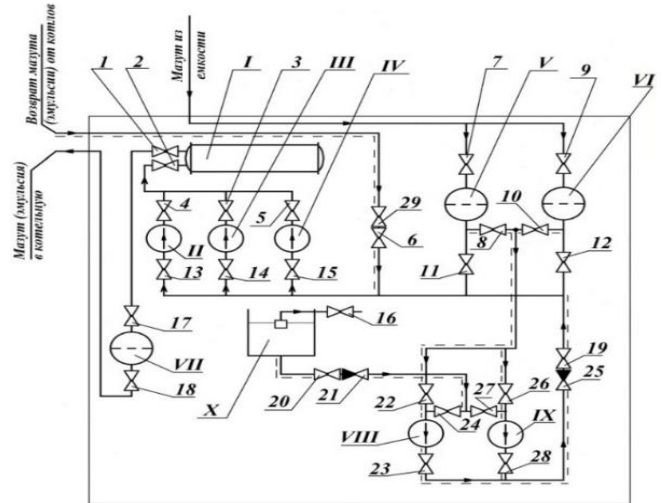


Figure 2. Principal technological scheme for the preparation and combustion of a water-oil emulsion in boiler units of the E-1/9-M type (3): I - fuel oil heater; II, III, IV - coarse filters; V, VI, VII - fine filters; VIII, IX - rotary-pulsation devices; X- water tank; 1-20, 22-24, 26-29-valves; 21, 25 - check valves.

Table 5. Fuel oil combustion and calculation of pollutant concentrations in the gas phase

Components of gas emissions	MPC, mg/m ³	The amount of substances emitted into the atmosphere		The sum of maximum surface concentrations (MAC shares) created by source emissions
		max., g/s	Total, t/year	
CO	3,0	0,071	2,242	0,00356
NO _x	0,085	0,069	2,186	0,12205
SO ₂	0,5	0,444	14,016	0,13351
C _x H _y	1,5	1,067	33,638	0,10695
soot	0,15	0,046	1,458	0,04611

Table 6. Fuel oil-water combustion and calculation of pollutant concentrations in the gas phase

Components of gas emissions	MPC*, mg/m ³	The amount of substances emitted into the atmosphere		The sum of Maximum Ground Level Concentration (MGLC) shares) created by source emissions
		max, g/s	Total, t/y	
CO	3,0	0,021	0,673	0,00145
NO _x	0,085	0,023	0,729	0,04953
SO ₂	0,5	0,427	13,455	0,12299
C _x H _y	1,5	0,391	12,334	0,04901
soot	0,15	0,012	0,364	0,02005

MPC - Maximum Permissible Concentration
MGLC - Maximum Ground Level Concentration

The results of the studies show that in reverse type emulsions (water in fuel oil), when water in the form of tiny droplets with a diameter of 10-100 microns is evenly distributed throughout the mass of fuel oil, it contributes to a more efficient process of burning liquid fuel, reducing soot formation and reducing the content of harmful substances in emissions (Table 7).

Table 7. Reducing the concentrations of pollutants in the flue gases of E-1/9M type boilers based on the combustion of fuel oil-water emulsions

Components of gas emissions	Amount of harmful substances						Reduction of gas emissions
	Fuel oil			MWE			
	mg/m ³	g/s	t/y	mg/m	g/s	t/y	
SO ₂	500	0,44	14,0	480	0,42	13,4	4,06
NO _x	78	0,06	2,18	26	0,02	0,72	66,67
CO	80	0,07	2,24	24	0,02	0,67	70,00
C _x H _y	1200	1,06	33,6	440	0,39	12,3	63,33
soot	52	0,04	1,45	13	0,01	0,36	75,00

An increase in the efficiency of combustion of a fuel oil-water emulsion in comparison with fuel oil is explained by the phenomenon of microexplosion [13–16]. Its essence lies in the fact that due to the large difference in the boiling points of water (100°C) and fuel oil (300°C), each drop of the inverse emulsion during the thermal effect increases in volume under the action of the water vapor formed inside, and then breaks into pieces. Intra-furnace crushing of droplets in boiler units, caused by microexplosions, sharply increases the reaction surface and improves the mixing of fuel with air. Accordingly, the water-oil emulsion droplets burn faster than the original fuel oil droplets. An increase in the concentration of active radicals (O, H, OH) in the combustion zone, due to the introduction of aqueous additives into liquid fuel, has a positive effect on the increase in the burnout rate of emulsions.

4. Conclusion

The fuel oil-air, fuel oil-water-air systems were studied at a wide range of temperature changes (T = 500-3000 K) and the ratio of gas-liquid flows (5-15% of water in fuel oil) at the maximum entropy of the system and a change in the concentration of condensed carbon and the ratio H/C, i.e. soot formation in flue gases. The particle sizes of the fuel oil-water emulsion were determined by sedimentation analysis and they have a polydisperse character. The water content in fuel oil during the preparation of fuel oil-water emulsion in the boiler room was controlled by a capacitive sensor. The

water flow was automatically maintained by an ejector-dosing device.

Thermodynamic modeling of the system: fuel oil-air, fuel oil-water-air has been carried out. The thermodynamic parameters of the system (entropy, enthalpy, internal energy) are calculated and their comparative characteristics are obtained. The concentration distribution of hydrogen, carbon, nitrogen, sulfur and oxygen containing molecules, particles and condensed phases in the gas phase has been established. During the combustion of the fuel oil-water emulsion, the concentration of soot in the gas phase decreased due to an increase in hydrogen-containing particles in the gas phase, i.e. an increase in the H/C ratio, as well as a change in the concentration of condensed carbon (mol/kg): (fuel oil without water C_(c) = 63.3 mol/kg); fuel oil with water: **5%** H₂O, C_(c) = 54.96; **10%** H₂O, C_(c) = 50.45; **15%** H₂O, C_(c) = 46.3. The H/C ratio in the case of burning fuel oil-water emulsion is 2.26 times higher.

A technological scheme for the preparation and combustion of fuel oil in the form of fuel oil-water emulsions in industrial boilers of the E-1/9-M (3) type of the Bridge Construction Detachment of the Kyrgyz Railway, Bishkek, has been developed. It is shown that when burning fuel oil-water emulsions in boilers, the soot content in flue gases is reduced by 75% due to the developed contact surface of the interacting phases and more complete combustion of particles of oil-water emulsions.

References

- [1]. Bakirov F. G. Zakharov V. M. Poleshchuk I. Z. Shaikhutdinov Z. G. Formation and burnout of soot during combustion of hydrocarbon fuels. M.: Mashinostroyeniye, (1989), 128.
- [2]. Kemelov K., Maimekov U., Sambaeva D., Maimekov Z.K. Reducing the Concentration of Benzo(a)pyrene in the Soot Particles in Gas Phase by Using and Burning Water Fuel Emulsions Polish Journal of Environmental Studies, 4, (2020), 2669-2677.
- [3]. Maimekov Z.K., Sambaeva D.A., Kemelov K.A. "Reducing the Concentration of Soot in Gas Phase by Using Water-Fuel Oil Emulsions. International Conference on Environmental Science and Technology - ICOEST" June 18-21, 2013, Cappadocia, Urgup, Turkey, 2013.
- [4]. Shiquan S., Kai S., Zhizhao C., Tianyou W., Ming J., Junqian C. Mechanism of micro-explosion of water-in-oil emulsified fuel droplet and its effect on soot generation. Energy, 191, (2020), 116-488.

- [5]. Garaniya V., Goldsworthy L., Heavy fuel oil combustion modelling using continuous thermodynamics. *Journal of the JIME*, 47(6), (2012), 871-877.
- [6]. Klaus H., Maximilian B., Roland B., Reduction of soot emissions in diesel engines due to increased air utilization by new spray hole configurations. *Automotive and Engine Technology*, 1, (2016), 69–79.
- [7]. Li G, Dai J, Li Y, Lee TH. Optical investigation on combustion and soot formation characteristics of isopropanol-butanol-ethanol (IBE)/diesel blends. *Energy Sci Eng.*, 9, (2021), 2311– 2320.
- [8]. Abhijit K., Jeroenvan O. Effects of hydrogen enrichment and water vapour dilution on soot formation in laminar ethylene counterflow flames. *Int. Journal of Hydrogen Energy*, 45, (43), (2020), 23653-23673.
- [9]. Shyam P. H, Joseph G., Vijay V. S., Effect of Introduction of Water into Combustion Chamber of Diesel Engines – A Review, *Energy and Power*, 5(1), (2015), 28-33.
- [10]. Strizhak, P. A., Piskunov, M. V., Kuznetsov, G. V., & Voytkov, I. S. Evaporation of oil-water emulsion drops when heated at high temperature, *Journal of Physics: Con. Ser.*, 891(1), (2017).
- [11]. Ying Y., Liu D. Effects of water addition on soot properties in ethylene inverse diffusion flames *Fuel*, 247 (2019), 187-197.
- [12]. Ivanov V.M. Fuel emulsions and suspensions. M.: Metallurgizdat, 1963, p. 102.
- [13]. Volikov A.N. Burning of gas and liquid fuels in low power boilers. L.: Nedra, 1989, p 128.
- [14]. Ivanov V.M. Fuel emulsions. Academy of Sciences of the USSR, (1961), 118-120.
- [15]. Maimekov Z.K. Development of a resource-saving and environmentally friendly technology for burning liquid fuels in the form of water-fuel emulsions. *Journal Engineer*, 1, (2010), 262-266.
- [16]. Maimekov Z.K. “Scientific basis for optimizing the processes of burning liquid fuels and recarbonization of water-salt systems”. Bishkek, 2015, p. 410.
- [17]. Maimekov Z.K. “Reducing the emission of gas emissions from boilers based on the preparation and combustion of water-fuel emulsions” In mat. "International Ecological Symposium-2009": - Bishkek: KTUM, (2009), 35.
- [18]. Moldobaev M.B., Sambaeva D.A., Maimekov Z.K., Bakanov K.T. Modification and combustion of liquid fuel in the form of water-fuel emulsions in boiler units of the DKVR-6.5-13 type and reduction of soot concentration in the gas phase. Materials of inter.scientific-practical conf. "Technosphere safety: science and practice" - KRSU, Bishkek (2015), 117-122.
- [19]. Moldobaev M.B., Sambaeva D.A., Maimekov Z.K. Reducing the concentration of soot in the gas phase based on the use of water-fuel emulsions in boiler units of the KEV-4-14 type. *Journal. Engineer*, 9, (2015), 354-363.
- [20]. Maimekov Z.K., Sambaeva D.A., Moldobaev M.B., Kemelov K.A. Influence of water in fuel emulsions on the formation and reduction of soot concentration in the gas phase. *Izvestiye Vuzov*,5, (2014), 8-11.
- [21]. Geller Z.I. Mazut as fuel - M.: Nedra, 1965, p.496.
- [22]. Sulin V.A. Waters of oil fields. M-L, ONTI, (1935), 367.
- [23]. Sinyarev G.B., Vatolin N.A., Trusov B.G., Moiseev G.K. The use of computers for thermodynamic calculations of metallurgical processes. - M.: Nauka, 1982, p. 264.
- [24]. Maimekov Z.K., Shcheredin V.A., Larin A.N., Bagimov N.I., Zholchubekov B.S., Doronova A.K., Sambaeva D.A. Rotary-pulsation apparatus for the preparation of water-fuel emulsions. *Intellectual Property*, 4, (1998), p. 33.
- [25]. Maimekov Z.K., Larin A.N., Bagimov N.I., Imanakunov S.B. Rotary pulsation apparatus for emulsifying water droplets in fuel. *Intellectual Property*, 3, (1997), p 24.
- [26]. Maimekov Z.K., Larin A.N., Bagimov N.I. Rotary-pulsation apparatus for emulsifying water droplets in fuel - Patent No. 146 No. 960352.1 dated 08.05.96.



Determining the enterotoxin genes and methicillin resistance in *Staphylococcus aureus* isolated from goat milk and its products

Mustafa Bilgin^{1,*}, Mustafa Atasever²

¹ Food Hygiene and Technology, Veterinary Faculty, Atatürk University, 25240, Erzurum, Turkey, bilqinm@gmail.com, ORCID: 0000-0001-9212-7823

² Food Hygiene and Technology, Veterinary Faculty, Atatürk University, 25240, Erzurum, Turkey, atasever@atauni.edu.tr, ORCID: 0000-0002-1627-5565

ABSTRACT

Milk and its products can be frequently contaminated with enterotoxigenic and methicillin-resistant *S. aureus*, and in such a case, it causes various diseases, especially staphylococcal food poisoning. In the present study, 100 sample materials (50 goat milk, 25 goat cream, and 25 goat cheese) were collected from 65 livestock farms in Erzurum. All samples were analyzed and tested selectively according to the EN ISO 6888-1 procedure standard. The obtained isolates were examined with the PCR in terms of nuc, Panton-Valentine Leukocidin (PVL), mecA, and enterotoxin genes. *S. aureus* was detected in 4 of 50 (8%) milk samples, 2 of 25 (8%) cream samples, 3 of 25 (12%) cheese samples, and 9 of the total samples (9%). While the incidence of methicillin resistance was found to be 3% by the disc diffusion method, the incidence of the mecA gene was found to be 2% by PCR. In terms of enterotoxin genes, 8% (4/50) of milk samples, 12% (3/25) of cheese samples, and 8% (2/25) of cream samples contained at least one enterotoxin gene. In total, 9% of 100 samples contained enterotoxigenic *S. aureus*. In conclusion, the consumption of enterotoxigenic and mecA positive *S. aureus*-containing raw milk, dairy products that have not been adequately heat-treated, or milk and products that are not kept in proper storage conditions pose a danger to public health.

ARTICLE INFO

Research article

Received: 7.10.2022

Accepted: 27.10.2022

Keywords:

Goat milk
methicillin resistance
staphylococcal
enterotoxins
Staphylococcus aureus

*Corresponding Author

1. Introduction

Microorganisms have been among us for centuries because they can adapt to changing environment. The foods consumed by us contain microbial loads whose composition varies greatly. Microorganisms, which usually originate from the surrounding flora, can also originate from stages such as animal slaughter and harvesting, processing, storage, and distribution of food [1]. *Staphylococcus aureus* belongs to the *Staphylococcaceae* family and is Gram-positive, facultatively anaerobic, cocci-shaped, immobile, and non-sporing [2]. *S. aureus* is a commensal, pathogenic bacterium and is colonized by almost 30% of people [3]. It causes food poisoning as well as bacteremia, endocarditis, skin, soft tissue, and pleuropulmonary infections [4].

S. aureus is especially detected in foods that contain protein such as ham, processed or unprocessed meat, puddings, tuna, chicken, cream fillings, meat salads, milk, and dairy products (primarily those that are not pasteurized) [5]. *S. aureus* food poisoning from milk and its products constitute 26% of all *S. aureus* food poisonings. Bacteria can be transmitted to milk

directly from the mammary glands of subclinically or clinically infected animals or environmentally during the processing of milk and its products [6].

Goat milk and products have an essential place in the treatment of people suffering from cow's milk allergies and gastrointestinal disorders, which are common in many countries, in meeting the gastronomic needs of consumers and in the nutrition of people who are malnourished from cow's milk in the developing world [7].

S. aureus has virulence factors causing many infections in humans and animals. These factors cause bacteria to adhere to the cell, collapse the immune mechanism, cause tissue invasion, sepsis, and toxic syndromes [8]. *S. aureus* produces staphylococcal enterotoxins (SEs) (A-E, G-I), which are potent gastrointestinal exotoxins. Food poisoning is seen as a result of the consumption of foods containing these toxins in sufficient amounts [9]. One of the characteristics of SEs is their resistance to temperature (121°C for 10 minutes)[10].

A total of 25 (A-V and X, three subtypes of C) types of SEs have been defined in a recent classification [11]. SEA is the

most common staphylococcal food poisoning worldwide, followed by SED and SEB [9].

The average methicillin-resistant *S. aureus* (MRSA) rate is between 60-70% worldwide. The Centers for Disease Control and Prevention in the USA reported that an average of 100.000 MRSA-related infections occur each year and result in around 19.000 deaths, which is higher than HIV death rates [12]. Unlike the penicillinase gene, *mecA*, a methicillin resistance gene, is found in the *S. aureus* chromosome. The detection of the *mecA* gene plays an essential role in determining resistance to β -lactam antibiotics [13].

According to the source of the infection, *S. aureus*, which causes various human infections, is divided into two community-acquired and hospital-acquired. These two types of infections are differentiated from each other by the genetic structure of the bacteria, antibiotic susceptibility, and clinical findings [14]. Previous studies showed that MRSA is associated with human consumption, whether it is Livestock-Associated (LA-MRSA), Community-Associated (CA-MRSA), or Hospital-Associated (HA-MRSA) [15].

This study aimed to investigate *nuc*, *PVL*, *mecA*, and enterotoxin genes in isolates after isolating *S. aureus* in raw goat milk and dairy products by the classical method. Thus, information was obtained about the prevalence of methicillin-resistant *S. aureus* and the types of staphylococcal enterotoxins in goat milk and products in the region.

2. Materials and methods

2.1. Collection of samples

In this investigation, 100 samples were gathered in June from 65 randomly chosen goat farms in the Erzurum province, including 50 goat milk samples, 25 goat cream samples, and 25 goat cheese samples. Samples taken from the milking containers were brought to the laboratory in sterile containers with ice packs within a few hours.

2.2. Isolation and identification of *S. aureus* with the classical method

In the present study, EN ISO 6888-1-2:1999 was used to isolate and identify *S. aureus* from dairy products. Under aseptic conditions, 10 ml of the milk samples and 25 grams of cheese and cream samples were weighed and placed into stomacher bags. 225 ml of sterile Ringer's solution was added to the cheese and cream samples, and 90 ml was added to the milk samples. Samples were homogenized in a stomacher machine for two minutes. The resulting homogenates were diluted until a decimal dilution of 10^{-3} was produced in tubes containing 9 ml of peptone water for

dilution. Prepared dilutions were inoculated on Baird Parker Agar with Egg Yolk Tellurite Emulsion added and incubated at 37°C for 24-48 hours under aerobic conditions. At the end of the incubation, black, shiny, convex colonies with a diameter of 1-3 mm with a transparent zone around them due to lecithinase activity and atypical colonies without halos were considered suspicious for *S. aureus*, and 3-5 samples were taken. Then, they were inoculated in Brain Heart Broth (BHI) and incubated at 37°C for 24 hours under aerobic conditions to identify coagulase-positive staphylococci. The clumping factor was searched with the Staph Rapid Latex Test Kit (Mascia Brunelli) in those who were positive for coagulase in the tube. As a result of the other tests, the isolates with hemolysis ability on blood agar, positive for catalase, acetoin, DNase test and Gram stain, oxidase negative, anaerobic glucose and mannitol fermenting ability were identified as *S. aureus* [16].

2.3. Determination of phenotypic methicillin resistance by disk diffusion method

To detect methicillin-resistant *S. aureus* isolates, oxacillin, cefoxitin antibiotic discs, and Mueller-Hinton agar medium were used based on Clinical and Laboratory Standards (CLSI). [17]. For this purpose, one loopful of isolates was taken from the isolates incubated for 24 hours at 37°C in TSB, and the turbidity of the bacterial suspension was adjusted to 0.5 McFarland standard with a densitometer in tubes containing 5 ml of 0.09% physiological saline. Then, 1 ml of suspension was taken and inoculated to the Mueller-Hinton agar medium. Antibiotic discs were placed by waiting for the agar to dry. Afterwards, the plates were incubated at 35°C for 24-48 hours and the inhibition zones formed were measured. The diameters of the inhibition zones were interpreted according to the CLSI guidelines. Oxacillin was considered susceptible if the inhibition zone diameter was ≥ 13 mm, moderately sensitive if 11-12 mm, and resistant if ≤ 10 mm. Cefoxitin was considered susceptible if the diameter of inhibition was ≥ 22 mm, and resistant if the diameter was ≤ 21 mm. [17]

2.4. The identification of *Nuc*, *PVL*, *mecA*, and Enterotoxin genes

2.4.1. Primers

The nucleotide sequence of the *mecA*, *PVL*, and *nuc* genes of *S. aureus* and the nucleotide sequence of the enterotoxin genes were obtained from the GenBank® database and used in Table 1 design of the primer sequences that were evaluated for specificity by using the standard nucleotide comparison tool.

Table 1. Primer list

Gen	Primer	Sequence
<i>mecA</i>	mecA fw	CAATGCCAAAATCTCAGGTAAAGTG
	mecA rev	AACCATCGTTACGGATTGCTTC
<i>PVL</i>	pvl fw	AAATGCTTTGCAGCGTTTTGTTTTTCG
	pvl rev	TGGACAAAACCTTCTTGG
<i>Nuc</i>	nuc fw	GGCATATGTATGGCAATTGTTTC
	nuc rev	CGTATTGCCCTTTCGAAACATT
<i>SEA</i>	SEA fw	TTGGAAACGGTTAAAACGAA
	SEA rev	GAACCTTCCCATCAAAAACA
<i>SEB</i>	SEB fw	TCGCATCAAACCTGACAAACG
	SEB rev	GCAGGTAATCTATAAGTGCC
<i>SEC</i>	SEC fw	GACATAAAAGCTAGGAATTT
	SEC rev	AAATCGGATTAACATTATCC
<i>SED</i>	SED fw	CTAGTTTGGTAATATCTCCT
	SED rev	TAATGCTATATCTTATAGGG

2.4.2. Total RNA Isolation

In total RNA isolation, 1 mL Qiazol (Qiagen, Germany) was added to the bacteria samples that were stored in a deep

Table 2. *Nuc*, *mecA*, and *PVL* prevalence on isolate basis

Samples	Classic Culture Method			PCR	
	BP	OT	<i>S. aureus</i>	<i>S. aureus</i>	Methicillin
	Isolate		(nuc)	(PVL)	Resistance Gene (mecA)
Milk (n=50)	43	5	5	5	-
Cream (n=25)	34	2	2	2	-
Cheese (n=25)	79	6	6	6	2
Total (n=100)	156	13	13	13	2

OT: Result of other biochemical tests

The application was made according to the protocol provided with the product. Then, 2-5 µg of these RNAs were translated into cDNA by using the miScript Reverse Transcription Kit (Qiagen) in line with the given protocol. The purity and amount of the resulting cDNA were determined with 260-280 nm absorbance measurements in the spectrophotometer and diluted at the same rates. It was stored at -20°C for later use in Real-Time PCR studies.

2.4.4. Quantitative Real-time PCR (qRT-PCR)

In the present study, the purpose was to determine the expressions of selected genes. The master mix content created in Real-Time PCR experiments (Qiagen Rotor-Gene HRM+) is as follows: Syber Green 2X Rox Dye Master Mix

freezer at -80°C, left for 5 minutes at room temperature, and centrifuged at 12.000 x g 4°C for 15 minutes. Then, the supernatant was taken into a new Eppendorf, 500 µl chloroform was added, mixed for 1 minute, and centrifuged at 12.000 x g 4°C for 15 minutes. The supernatant was taken again to a new Eppendorf, 200 µl isopropanol was added and centrifuged at 12.000 x g 4°C for 10 minutes. The supernatant was then discarded and 500 µl 75% ethanol was added to the pellet and centrifuged at 7.500 x g 4°C for 10 minutes. Finally, after the removal of the ethanol, the RNA pellet was dissolved with an appropriate volume of water without RNA-degrading enzymes (DEPC-treated RNase free).

The purity and amount of the resulting RNA were determined with 260-280 nm absorbance measurements in the spectrometer. The integrity and amount of RNA were checked by loading 1 µg RNA, which was quantified according to 260 nm absorbance, on a 1.5% agarose gel.

2.4.3. DNase I application and cDNA translation

DNase I (Thermo Scientific) was used against DNA contamination in the isolated total RNA samples.

(Qiagen), forward and reverse primers, cDNAs as templates, and nuclease-free water. The samples were placed in the Real-Time Device after the master mixes were prepared, and the results were evaluated. This way, the CT/CQ values of the genes were obtained. Melting Curve Analysis was performed in all reactions. The primer sequences of the relevant genes are given in Table 1.

2.5. Statistical Analysis

Statistical analyses were performed using SPSS software (Version 25.0, SPSS 167 Inc., Chicago, IL, USA) to evaluate *Staphylococcus aureus* in milk, cream and cheese. One-way ANOVA with *post hoc* Tukey's test was used to determine

significant differences. All statistical comparisons were performed at the significance level of $P < 0.05$.

3. Results

3.1 Prevalence of *S. aureus*

A total of 156 isolates were obtained from the BP agar in 100 samples, and 13 (8.3%) of them were found to be *S. aureus* as a result of the classical culture method and biochemical tests. The nuc and PVL genes were detected with PCR from those 13 samples (Table 2). *S. aureus* was detected in 4 of 50 milk samples, 2 of 25 cream samples, and 3 of 25 cheese samples. Statistical analysis revealed that there were no significant differences in the presence of *S. aureus* in the milk, cream, and cheese samples ($P = 0.612$).

3.2. Phenotypic Methicillin Resistance

In goat milk and dairy products, Cefoxitin and oxacillin resistance was observed in 1 of 5 isolates (20%) obtained from milk, 2 of 6 isolates (33.3%) obtained from cheese, and 3 (23%) of 13 isolates in total. No resistance was observed in 2 isolates obtained from cream samples.

3.3. *MecA* Gene Prevalence

In the *S. aureus* isolates, genotypic methicillin resistance is determined by the presence of the *mecA* gene. Also, methicillin resistance may be caused by the newly identified *mecA* homolog, the *mecC* gene, or other factors that provide resistance. There are studies in which *mecA* and *mecC* genes are absent, but methicillin resistance is seen [15]. It was observed with the PCR that 2 of 13 (15.3%) *S. aureus* isolates had the *mecA* gene, and they were obtained from cheese samples but not in isolates obtained from milk and cream samples (Table 2).

Table 3. Allocation of staphylococcal enterotoxin types

SEA/CT value	SEB/CT value	SEC/CT value	SED/Ct Value	Samples	İzolat No
14.12	Negative	24.17	25.26	Goat mik	130a-2
14.16	Negative	24.16	25.38	Goat mik	114a-2
14.25	Negative	24.18	25.46	Goat cream	163b-2
14.28	Negative	24.65	25.15	Goat cheese	199b-2
14.01	20.15	Negative	25.19	Goat cheese	199c-3
14.95	Negative	24.56	25.32	Goat mik	114a-3
14.25	Negative	24.02	Negative	Goat mik	145e--2
14.26	Negative	24.05	Negative	Goat cheese	184d-2
14.8	Negative	24.12	Negative	Goat mik	112a-2
14.13	Negative	Negative	Negative	Goat cheese	184b-2
14.23	Negative	Negative	25.01	Goat cream	168a-2
14.58	20.67	Negative	25.26	Goat cheese	178b-3
15.01	Negative	24.04	Negative	Goat cheese	199f-2

3.4. Staphylococcal Enterotoxin Gene Prevalence

Food poisoning caused by enterotoxigenic *S. aureus* has been reported previously due to consuming contaminated dairy products [18]. In this study, 8% (4/50) of goat milk samples, 12% (3/25) of cheese samples, and 8% (2/25) of cream samples contained at least one enterotoxin gene. In total, 9% of 100 samples contained enterotoxigenic *S. aureus* (Table 3, 4).

When the isolates were examined, it was found that one isolate had one enterotoxin gene, five isolates had two

enterotoxin genes, and seven isolates had three enterotoxin genes.

4. Discussion

In the present study, the incidence of *S. aureus* in goat milk and dairy products was 9%. This rate is close to the rate of 4.65% reported in the study of Günday [19] on 86 goat milk and the rate of 6.2% obtained by Mørk et al. from 5761 goat milk samples [20].

However, there are also studies reporting the presence of *S. aureus* at less than 3% in goat products [21]. Unlike these,

there are also studies reporting positive *S. aureus* rates in cow and goat milk samples, ranging from 75% to 96.2% [15].

These differences may be due to the collection of samples from animals with mastitis, milking hygiene conditions, milking equipment, storage, and transportation conditions.

When the samples were examined, it was seen that goat cheeses had the highest prevalence of *S. aureus*, which was isolated in 3 of 25 (12%) kind of goat cheese. Findings with similar rates were found as 20.2% in the study conducted by Yücel and Anıl [22] on 79 cheese samples, and as 16.7% in the study of Rahimi [23] conducted on 60 traditional cheese samples.

Table 4. Prevalence of the enterotoxin genes

Samples	Enterotoxin Genes				
	<i>S. aureus</i> Positive	sea	seb	sec	sed
Milk (n=50)	5	5	-	5	3
Cream (n=25)	2	2	-	1	2
Cheese (n=25)	6	6	2	3	3
Total (n=100)	13	13	2	9	8

Basanisi et al. [24] reported this rate to be 41.1% in a study conducted on sheep and goat cheeses in Italy, which was higher than the rates found in this study, and as 61% in the study of Özpınar and Gümüşsoy [25] on 100 kinds of Erzincan Tulum cheese.

These differences occur because of improper processing of foods, not applying enough heat to homemade cheese, obtaining raw milk from unhealthy animals, or contamination of production tools and equipment.

The prevalence of *S. aureus* was 8% in cream samples. One of the reasons for this low rate was the heat treatment (95°C) applied in obtaining cream from raw milk. This application is effective in the inactivation of bacteria present in raw milk. For this reason, no *S. aureus* was found in some cream studies [15].

The MRSA rate varies in disk diffusion studies on milk and dairy products. Turkyilmaz et al. [26] in their research conducted in Aydın province, 99 *S. aureus* isolates were obtained from milk collected from cows, and 16 (17%) were found to be MRSA by disc diffusion method. Can and Çelik [27] obtained 12 *S. aureus* isolates in a study of 200 Tulum and feta cheese samples, and they determined that 2 (16.6%) of them were MRSA by disc diffusion method. In their investigation of 400 samples (200 milk, 200 nasal swabs) taken from sheep and goats in Nigeria, Omshaba et al. [28] isolated *S. aureus* in 72 samples and found MRSA in 52 (72.2%) of them phenotypically

In the study, the presence of the *mecA* gene was 2% (2/100) based on all samples and 15.3% (3/13) based on the isolates obtained. Similar to these rates, Saka and Gulel [15] found the *mecA* gene in 9 of 99 (9%) *S. aureus* isolates (eight

isolate milk, one isolate cheese) obtained from 200 buffalo milk and products collected in the study that was conducted in Samsun. Basanisi et al. [24] obtained 37 *S. aureus* isolates from 90 sheep and goat cheeses and found the *mecA* gene in only 1 of them (2.7%). In another study, Obaidat et al. [29] found the *mecA* gene ratio to be 11.9% in the samples that were collected from 42 goat milk tanks in Jordan.

Methicillin resistance is classified as homogeneous and heterogeneous resistance. Homogeneous resistant bacteria have the *mecA* gene, and it is active. These bacteria can reproduce by resisting the presence of high levels of methicillin. On the other hand, Heterogeneous resistant bacteria have the *mecA* gene, but resistance is seen only in some. [30]

In the present study, Genotypic resistance was detected in 2 of 13 *S. aureus* isolates and phenotypic resistance in 3 (Table 5). In similar studies, it has been reported that phenotypic resistance is not only caused by the *mecA* gene but also by changes in PBP2a based on the production of beta-lactamase and methicillinase enzymes. In addition, it has been stated that strains that have the *mecA* gene but do not show resistance

Table 5. Methicillin resistance comparison

Nuc/CT value	MecA/CT value	Samples	İzolat No	Oxacillin	Cefoxitin
24.01	Negative	Goat milk	130a -2	Susceptible	Susceptible
23.12	Negative	Goat milk	114a-2	Susceptible	Susceptible
23.58	Negative	Goat cream	163b-2	Susceptible	Susceptible
23.16	Negative	Goat cheese	199b-2	Susceptible	Susceptible
22.16	26.15	Goat cheese	199c-3	Resistant	Resistant
23.17	Negative	Goat milk	114a-3	Susceptible	Susceptible
23.18	Negative	Goat milk	145e--2	Susceptible	Susceptible
23.16	Negative	Goat cheese	184d-2	Resistant	Resistant
23.18	Negative	Goat milk	112a-2	Resistant	Resistant
23.17	Negative	Goat cheese	184b-2	Susceptible	Susceptible
22.15	Negative	Goat cream	168a-2	Susceptible	Susceptible
22.02	26.15	Goat cheese	178b-3	Susceptible	Susceptible
23.14	Negative	Goat cheese	199f-2	Susceptible	Susceptible

phenotypically can cause serious health problems and are clinically significant. [31, 32] It is reported that many factors such as incubation time, temperature, amount of inoculum and pH of the medium can affect the analysis methods for determining phenotypic resistance. [33] Since detecting heterogeneous resistant MRSA strains does not provide accurate results by phenotypic methods, *mecA* gene detection is accepted as the gold standard in determining methicillin resistance [34].

Considering the studies on enterotoxin genes, in a study conducted in Norway, Jørgensen et al. [35] examined enterotoxin genes in 220 cattle, 213 goat tank milk, and 82 raw milk samples. They found enterotoxigenic *S. aureus* 52.5% in 101 cattle isolates, 55.8% in 95 goat isolates, and 72.4% in 29 raw milk isolates. Mørk et al. [20] found the rate of enterotoxigenic *S. aureus* as 71.9% in their study on 153 isolates obtained from dairy products. Rahimi [23] found this rate at 35% in 347 dairy products.

When the total number of samples was considered, the *seb* gene was detected only in 2 kinds of goat cheese. Less than synthetic chemicals are sufficient for this toxin, the strongest SE, to have a toxic effect. Even at low concentrations, death is observed because of multi-organ failure [36].

Although some studies on cow and goat milk only reported isolates with the *seb* gene, no isolates with the *seb* gene were reported in some other studies [15]. The ability of *S. aureus* to form toxins in foods can vary according to many factors, some of which are pH, salt content, contents of foods, competitive microflora, and the a_w value [37]. As can be seen,

the prevalence of enterotoxin-producing *S. aureus* in milk and its products varies among studies. This may be because of the source of the samples and geographical differences

5. Conclusion

The present study shows that goat milk and its products can be contaminated with enterotoxigenic and methicillin-resistant *S. aureus*. The presence of the *seb* gene, which produces high toxic SEB secretion, poses a danger to human health in milk and dairy products. Since the PVL gene was isolated from all samples, the possibility of human-to-animal transmission of *S. aureus* is high. Therefore, consuming milk and milk products that have not undergone adequate heat treatment or are stored under appropriate storage conditions must be avoided.

References

- [1]. Bezirtzoglou E., Maipa V., Voidarou C., Tsiotsias A., Papapetropoulou M., "Food-borne intestinal bacterial pathogens", *Microb. Ecol.*, 12(2), (2000), 96-104.
- [2]. Wieland B., Feil C., Gloria-Maercker E., Thumm G., Lechner M., Bravo J. M., Götz F., "Genetic and biochemical analyses of the biosynthesis of the yellow carotenoid 4, 4'-diaponeurosporene of *Staphylococcus aureus*", *J. Bacteriol.*, 176(24), (1994). 7719-7726.

- [3]. Wertheim, H. F., Melles, D. C., Vos, M. C., van Leeuwen W., Van Belkum A., Verbrugh H. A., Nouwen J. L., "The role of nasal carriage in *Staphylococcus aureus* infections", *Lancet Infect. Dis.*, 5(12), (2005), 751-762.
- [4]. Stryjewski M.E., G.R. Corey, "Methicillin-resistant *Staphylococcus aureus*: an evolving pathogen". *Clin. Infect. Dis.*, 58, (2014), 10-19.
- [5]. Xu Z., Peters B. M., Li B., Li L., Shirliff M. E., "Staphylococcal Food Poisoning and Novel Perspectives in Food Safety", in *Prevention and Control of Food Related Diseases*, vol. 1, M.H. Anthony, Eds. Croatia, InTech, 2016, 159.
- [6]. Di Giannatale E., Prencipe V., Tonelli A., Marfoglia C., Migliorati G., "Characterisation of *Staphylococcus aureus* strains isolated from food for human consumption", *Veterinaria Italiana*, 47(2), (2011), 165-173.
- [7]. Haenlein G., "Goat milk in human nutrition. Small ruminant research", 51(2), (2004), 155-163.
- [8]. Kim H.K., Falugi F., Missiakas D.M., Schneewind, O., "Peptidoglycan-linked protein A promotes T cell-dependent antibody expansion during *Staphylococcus aureus* infection", *Proc. Natl. Acad. Sci.*, 113(20), (2016), 5718-5723.
- [9]. Argudín M.Á., Mendoza M.C., Rodicio M.R., "Food poisoning and *Staphylococcus aureus* enterotoxins. Toxins", 2(7), (2010), 1751-1773.
- [10]. Tsutsuura S., Shimamura Y., Murata M., "Temperature dependence of the production of staphylococcal enterotoxin A by *Staphylococcus aureus*", *Biosci. Biotechnol. Biochem.*, 77, (2013) 30–37.
- [11]. Omoe K., Hu D. L., Ono H. K., Shimizu S., Takahashi-Omoe H., Nakane A., Imanishi K. I., "Emetic potentials of newly identified staphylococcal enterotoxin-like toxins", *Infect. Immun.*, 81(10), (2013), 3627-3631.
- [12]. Klevens R. M., Morrison M. A., Nadle J., Petit S., Gershman K., Ray S., "Invasive methicillin-resistant *Staphylococcus aureus* infections in the United States", *Jama*, 298(15), (2007), 1763-1771.
- [13]. Ito T., Katayama Y., Asada K., Mori N., Tsutsumimoto K., Tiensasitorn C., Hiramatsu K., "Structural comparison of three types of staphylococcal cassette chromosome mec integrated in the chromosome in methicillin-resistant *Staphylococcus aureus*", *Antimicrob. Agents Chemother.*, 45(5), (2001), 1323-1336.
- [14]. Archer, G.L., "Staphylococcus aureus: a well-armed pathogen" *Rev. Infect. Dis.*, 26(5), (1998), 1179-1181.
- [15]. Saka, E., G. Terzi Gulel, "Detection of enterotoxin genes and methicillin-resistance in *Staphylococcus aureus* isolated from water buffalo milk and dairy products", *J. Food Sci.*, 83(6), (2018), 1716-1722.
- [16]. Wald R., Hess C., Urbantke V., Wittek T., Baumgartner M., "Characterization of *Staphylococcus* Species Isolated from Bovine Quarter Milk Samples", *Animals*, 9(5), (2019), 200.
- [17]. Wayne, P.A., "Performance standards for antimicrobial susceptibility testing", *Clinical Laboratory Standard Institute*, 1, (2009), 19.
- [18]. Oliver S.P., Jayarao B.M., Almeida R.A., "Foodborne pathogens in milk and the dairy farm environment: food safety and public health implications", *Foodborne Pathogens & Disease*, 2(2), (2005), 115-129.
- [19]. Günday H., "Aydın bölgesinde ürüne işlenecek çiğ sütlerde staphylococcus aureus ve enterotoksin varlığının araştırılması," M.S. thesis, Institute of Health Sciences, Department of Microbiology, Adnan Menderes Üniversitesi, Aydın, Türkiye, 2017.
- [20]. Mørk T., Kvitle B., Mathisen T., Jørgensen H. J., "Bacteriological and molecular investigations of *Staphylococcus aureus* in dairy goats", *Vet. Microbiol.*, 141(1-2), (2010), 134-141.
- [21]. Menzies, P.I., Ramanoon S.Z., "Mastitis of sheep and goats", *Vet. Clin. North Am. Food Anim.*, 17(2), (2001), 333-358.
- [22]. Yücel N., Anıl Y., "Çiğ süt ve peynir örneklerinden *Staphylococcus aureus* ve koagülaz negatif stafilokokların identifikasyonu ve antibiyotik duyarlılığı", *Türk Hijyen ve Deneysel Biyoloji Dergisi*, 68(2), (2011), 73-78.
- [23]. Rahimi E., "Enterotoxigenicity of *Staphylococcus aureus* isolated from traditional and commercial dairy products marketed in Iran", *Brazilian Journal of Microbiology*, 44, (2013), 393-399.
- [24]. Basanisi M. G., Nobil, G., La Bella G., Russo R., Spano G., Normanno G., La Salandra G., "Molecular characterization of *Staphylococcus aureus* isolated from sheep and goat cheeses in southern Italy", *Small Rumin. Res.*, 135, (2016), 17-19.
- [25]. Özpınar N., Gümüşsoy K.S., "Phenotypic and genotypic determination of antibiotic resistant and biofilm forming *Staphylococcus aureus* isolated in Erzincan tulum cheese", *Kafkas Üniversitesi Veteriner Fakültesi Dergisi*, 19(3), (2013), 517-521.
- [26]. Türkyılmaz S., Tekbıyık S., Oryasin E., Bozdoğan B., "Molecular epidemiology and antimicrobial resistance mechanisms of methicillin-resistant *Staphylococcus*

- aureus isolated from bovine milk”, *Zoonoses and Public Health*, 57(3), (2010),197-203.
- [27]. Can H.Y., Celik T.H., “Detection of enterotoxigenic and antimicrobial resistant *S. aureus* in Turkish cheeses”, *Food Control*, 24(1-2), (2012), 100-103.
- [28]. Omoshaba E.O., Ojo O.E., Oyekunle M.A., Sonibare A. O., Adebayo A. O., “Methicillin-resistant *Staphylococcus aureus* (MRSA) isolated from raw milk and nasal swabs of small ruminants in Abeokuta”, *Nigeria. Trop. Anim. Health Prod.*, 52(5), (2020), 2599-2608.
- [29]. Obaidat M.M., Bani Salman A.E., Roess A.A., “High prevalence and antimicrobial resistance of *mecA* *Staphylococcus aureus* in dairy cattle, sheep, and goat bulk tank milk in Jordan”, *Trop. Anim. Health Prod.*, 50(2), (2018), 405-412.
- [30]. Jacoby G.A., Archer G.L., “New mechanisms of bacterial resistance to antimicrobial agents”, *N. Engl. J. Med.*, 324(9), (1991), 601-612.
- [31]. Oliveira D.C., Lencastre H.N.D., “Multiplex PCR strategy for rapid identification of structural types and variants of the *mec* element in methicillin-resistant *Staphylococcus aureus*”, *Antimicrob. Agents Chemother.*, 46(7), (2002), 2155-2161.
- [32]. Swenson J.M., Lonsway D., McAllister S., Thompson A., Jevitt L., Zhu W., Patel J.B., “Detection of *mecA*-mediated resistance using reference and commercial testing methods in a collection of *Staphylococcus aureus* expressing borderline oxacillin MICs”, *Diagn. Microbiol. Infect. Dis.*, 58(1), (2007), 33-39.
- [33]. Cauwelier B., Gordts B., Descheemaeker P., Van Landuyt H., “Evaluation of a disk diffusion method with cefoxitin (30 µg) for detection of methicillin-resistant *Staphylococcus aureus*”, *Eur. J. Clin. Microbiol. Infect. Dis.*, 23(5), (2004), 389-392.
- [34]. Tomasz A., Drugeon H.B., De Lencastre H.M., Jabes D., McDougall L., Bille, J., “New mechanism for methicillin resistance in *Staphylococcus aureus*: clinical isolates that lack the PBP 2a gene and contain normal penicillin-binding proteins with modified penicillin-binding capacity”, *Antimicrob. Agents Chemother.*, 33(11), (1989), 1869-1874.
- [35]. Jørgensen H.J., Mørk T., Rørvik L.M., “The occurrence of *Staphylococcus aureus* on a farm with small-scale production of raw milk cheese”, *J. Dairy Sci.*, 88(11), (2005), 3810-3817.
- [36]. Kashiwada T., Kikuchi K., Abe S., Kato H., Hayashi H., Morimoto T., Gemma A., “Staphylococcal enterotoxin B toxic shock syndrome induced by community-acquired methicillin-resistant *Staphylococcus aureus* (CA-MRSA)”, *Internal Medicine*, 51(21), (2012), 3085-3088.
- [37]. Lyra D.G., Sousa F.G., Borges M.F., Givisiez P.E., Queiroga R.C., Souza E.L., Oliveira C.J., “Enterotoxin-encoding genes in *Staphylococcus* spp. from bulk goat milk. *Foodborne Pathog. Dis.*, 10(2), (2013), 126-130.



Design and analysis of switched reluctance motor with FEM based Ansys-Maxwell

Yıldırım Özüpak

Dicle University, Silvan Vocational School, Electrical Department, Diyarbakır, yildirimozapak@gmail.com,
ORCID:0000-0001-8461-8702

ABSTRACT

In this study, radial forces that create noise, which is a fundamental problem in Switched Reluctance Motor (SRM), are investigated. Since radial force causes stator vibrations and noise caused by magnetic field, a new switched reluctance motor model with increased stator and rotor poles has been designed in order to reduce the radial force acting on the rotor poles. In addition, a structure with high torque and low leakage flux compared to conventional winding structure has been proposed for Switched Reluctance Motors (SRM). The windings of the designed SRM are placed in layers, insulated from each other. Rotor poles are formed to move on both sides of each phase winding. Thus, the flux that will occur in the phase windings axially completes its circuit from the stator poles and the rotor poles. This designed ARM model has been examined by Finite Element Method (FEM. The proposed motor geometry has been analyzed with ANSYS Maxwell-3D, which performs FEM-based solution), and parametric analysis with ANSYS-RMxpert.

ARTICLE INFO

Research article

Received: 19.08.2022

Accepted: 8.12.2022

Keywords:

SRM,

Maxwell-3D,

FEM

1. Introduction

Simple and robust construction, high efficiency and low cost are the generally accepted advantages of inverter circuit switched reluctance motors. Despite being extensively studied by researchers, the widespread use of switched reluctance motors in industry and household appliances has not yet been possible.

Switched reluctance motor has two drawbacks: torque ripple and acoustic noise. While the switched reluctance motor is running, vibrations occur in the stator as a result of radial forces and acoustic noise occurs. Compared to electronically controlled drives such as induction motors and permanent magnet synchronous motors, the acoustic noise level in ARM is higher.

The vibrations in the stator are caused by the torque generation mechanism of the switched reluctance motor. When current flows through a phase winding, a torque is produced that pulls the rotor to its smallest reluctance position. In order not to produce negative torque, the current is drawn to zero in a position close to the coincident position. The force acting on the rotor pole consists of two components, the tangential force component and the normal force component. The tangential force component produces torque in the rotor. The normal force component creates vibration in the stator. In the coincidence position, no moment is

produced, so the tangential force component is zero. However, in the coincident position, the normal force component reaches its maximum value. When the normal force pulling the rotor poles is small over the bearings on which the rotor shaft is placed, the change in inductance is larger, and thus large moments are produced. As the number of stator and rotor poles increases, the difference between the lowest phase inductance value and the largest phase inductance value becomes smaller, and therefore the torque produced for the same phase current becomes smaller.

Industrial interest in switched reluctance motors (ARM) dates back to the 1800s [1]. The switched reluctance machine was first used by Dawidson in Scotland in 1838 to move a locomotive [2, 3]. In the 1920s, a stepper motor was invented by C.L.Walker, which has the features of today's ARMs. In 1969 S.A. Nasar revealed the first basic features of the classical ARM [4]. Bedford and Hoft simultaneously switched stator winding currents to the rotor position, shaping today's modern ARMs and pioneering the effective use of semiconductor elements in ARM technology [5, 6]. They also conducted research on rotor and stator pole geometries and power electronics converter structures.

Miller brought the computer aided design approach to ARM design in 1991 and worked on optimum design

parameters [7]. A 6/4 pole ratio ARM operating with high voltage was designed by Miles [8]. Materu and Krishnan tried to find the losses of the 6/4 pole configuration prototype ARM produced, and tried to produce general expressions by obtaining the stator current and voltage waveforms. It is used for 100 HP ARM hybrid vehicles produced by Khwaja M.Rahman. It has been observed that the acceleration time of the designed ARM is much better than the asynchronous motor of the same power [9].

In recent years, significant developments have been made in switched reluctance motor designs, especially the design optimization results obtained in the stator structure have gained qualifications to lead to interesting designs. Significant developments in ARM design have caused these motors to take their place in robotic applications.

In this study, SRM was designed and analyzed on the ANSYS-RMxprt-Maxwell integrated platform. Maxwell-2D was used for RMxprt magnetic field analysis for parametric analyses. The results obtained were compared with the studies on this subject in the literature. The results were found to be satisfactory.

2. Material and method

2.1. Design SRM structure

One of the many studies on the optimum design of SRM was done by Miller. It is necessary to make the most appropriate choice by considering many criteria in switched reluctance motor designs made to reduce noise and prevent fluctuation in torque. One of the changes made on the geometric structure of the SRM in order to reduce the radial force was to increase the number of stator and rotor poles. When the number of stator and rotor poles is increased, the radial force acting on the rotor poles decreases for the same peak torque, so the noise generated as a result of vibrations in the SRM decreases. However, as the number of stator and rotor poles increases, the iron losses due to the increasing switching frequency of the phases increase somewhat. On the other hand, as the number of rotor and stator poles increases, the flux paths of the phases will shorten, and there will be a decrease in iron losses due to the path followed by the flux.

2.2. SRM Electrical equivalent circuit

In the designed SRM, the flux does not pass from the stator pole end to the air gap and then to the rotor pole, as in other conventional SRMs. Here, the flux passes from the winding to the stator pole and from there to the side surface of the rotor pole by air. Therefore, the flux path through which the flux can pass has been widened. Thus, the attraction force between the stator and rotor is

increased. The working principle of SRMs is based on the reluctance force, and it is realized in the form of pulling the flux in the magnetic circuit of the free-moving, protruding rotor by applying force to the smallest reluctance position where it can find the easiest way. Figure 1 shows the equivalent circuit for a single phase of the SRM.

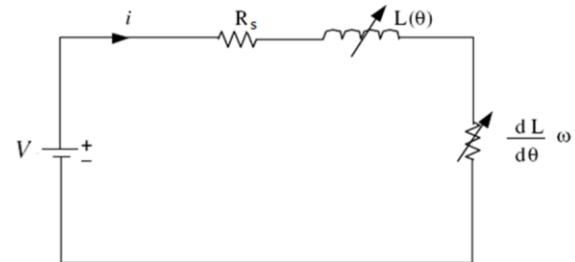


Figure 1. Equivalent circuit diagram of one phase of SRM

In the circuit given in Figure 1, R_s represents the stator winding resistance and L inductance value for each phase. Here, the voltage value applied to each phase can be given as in equation (1).

$$v = R_s i + \frac{d\lambda(\theta, i)}{dt} \tag{1}$$

$$\lambda = L(\theta, i) i \tag{2}$$

It can be expressed as. The input power can be expressed as given in equation 3.

$$P_i = v i = R_s i^2 + i^2 \frac{dL(\theta, i)}{dt} + L(\theta, i) i \frac{di}{dt} \tag{3}$$

$$\frac{d}{dt} \left(\frac{1}{2} L(\theta, i) i^2 \right) = L(\theta, i) i \frac{di}{dt} + \frac{1}{2} i^2 \frac{dL(\theta, i)}{dt} \tag{4}$$

Equations can be written. Starting from these equations, the input power can be written as in equation (5).

$$P_i = R_s i^2 + \frac{d}{dt} \left(\frac{1}{2} L(\theta, i) i^2 \right) + \frac{1}{2} i^2 \frac{dL(\theta, i)}{dt} \tag{5}$$

As can be clearly seen from Equation (5), the input power consists of the sum of the winding loss power given by the expression $R_s i^2$, the rate of change of the field energy given by the expression $p(\frac{1}{2} L(\theta, i) i^2)$, and the air gap power given by the $\frac{1}{2} i^2 pL(\theta, i)$ expression. If the rotor position and speed terms are substituted in the time expression for the air gap power;

$$T_e = \frac{\theta}{w_m} \tag{6}$$

$$P_{ag} = \frac{1}{2} i^2 \frac{dL(\theta, i)}{dt} = \frac{1}{2} i^2 \frac{dL(\theta, i)}{d\theta} \frac{d\theta}{dt} \tag{7}$$

$$P_{ag} = \frac{1}{2} i^2 \frac{dL(\theta, i)}{d\theta} w_m \tag{8}$$

expression is obtained.

Air gap power depends on electromagnetic torque and speed,

$$P_{ag} = T_e \omega_m \tag{9}$$

$$T_e = \frac{1}{2} i^2 \frac{dL(\theta,i)}{d\theta} \tag{10}$$

It is obtained as [7]

3. Result and discussion

3.1. SRM's magnetic analysis and results

Magnetic analyzes of SRM were carried out in two dimensions in Ansys Maxwell program. Transient analyzes were performed on the designed model. While creating the model, Dirichlet boundary condition is assigned to the outermost edge surfaces of a region, to the stator outer diameter and stator package length. In Figure 2, the designed model divided into networks is shown.

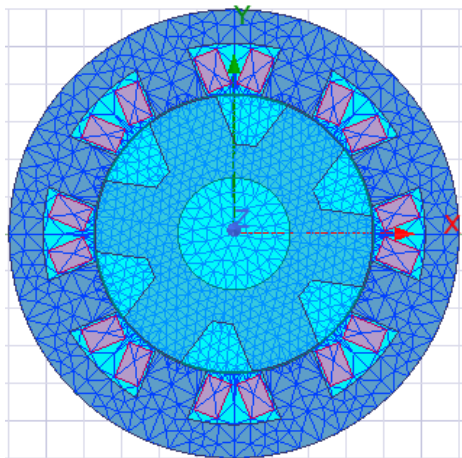


Figure 2. Mesh structure of the designed motor

SRM motors are motors that can be switched by position control. That is, after the first position information of the motor is received, a voltage is applied to the windings. The switching circuit drawn in the simplorer program in Figure 3 is used for transient analysis in magnetic simulation. This circuit performs a realistic analysis using the magnetic circuit model.

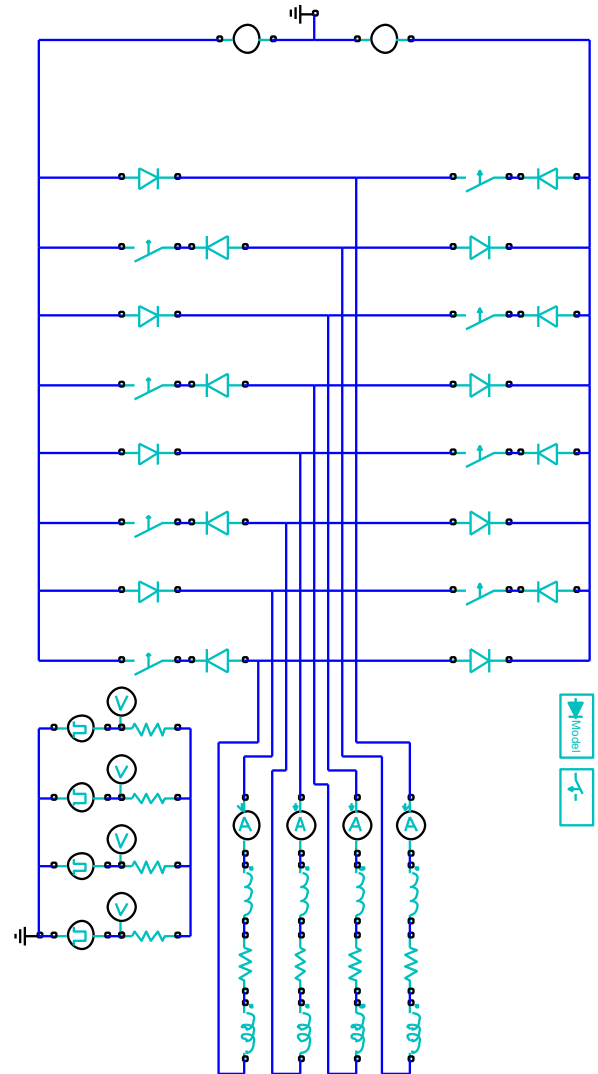


Figure 3. Driver circuit used for magnetic field analysis of SRM

Steel 1010 B-H curve of magnetic material used for rotor and stator in the model is given in Figure 9. In analytical calculations, the relative magnetic permeability (μ_r) of the magnetic material is taken as constant.

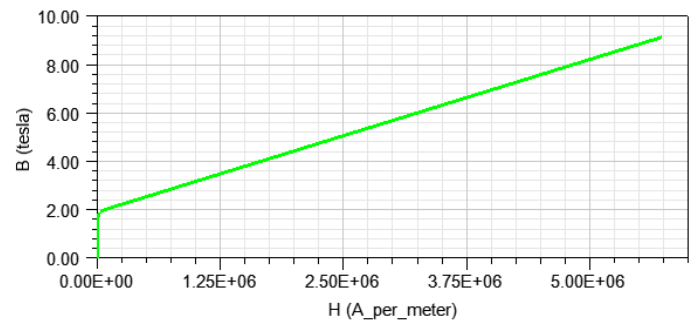


Figure 4. Steel 1010 B-H curve used as stator and rotor material

As a result of the magnetic analysis of the designed SRM, magnetic analysis results at different locations were obtained. The vectorial representation of the magnetic flux value in the case of the maximum gap between the stator and rotor poles is given in Figure 5.

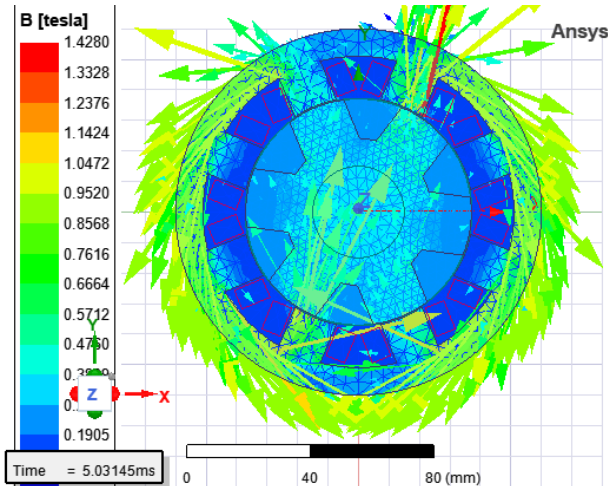


Figure 5. Vectorial distribution of magnetic flux values between stator and rotor poles

The windings of the SRM are triggered individually or together at certain angles to reduce torque fluctuations thanks to the designed encoder. In Figure 6, the magnetic flux in the rotor, stator and air gap is shown as vector when the windings are energized. If Figure 6 is examined, it can be seen that the leakage fluxes in the air gap are negligible.

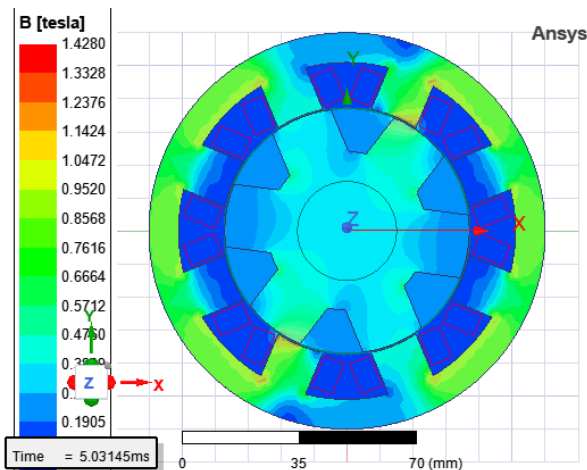


Figure 6. Magnetic flux distribution on model

As a result of the analysis of SRM, torque, inductance, flux, current and voltage curves were obtained. If the poles are too far from each other, the inductance is at the lowest value, and when the poles are in the same position, the inductance reaches its maximum value. The windings are energized by looking at the minimum and maximum values in this curve.

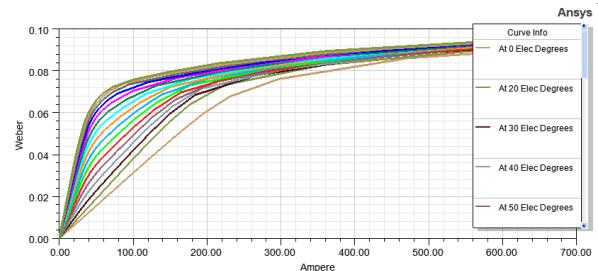


Figure 7. Flux-airgap of the SRM

The EMF values induced on the windings as a result of the parametric magnetic analysis are shown in Figure 8. The supply of the motor windings is provided by triggering the switches according to the angular velocity position information obtained in the driver circuit drawn in the Simplorer program. If the induced voltage curves are examined, the negative voltages are given back to the source together with the induced back emfs in the windings. Figure 9 shows the flux values of the windings as a result of the voltage applied to the windings of the SRM. The currents drawn by the motor windings are shown in Figure 10 as a current-time graph.

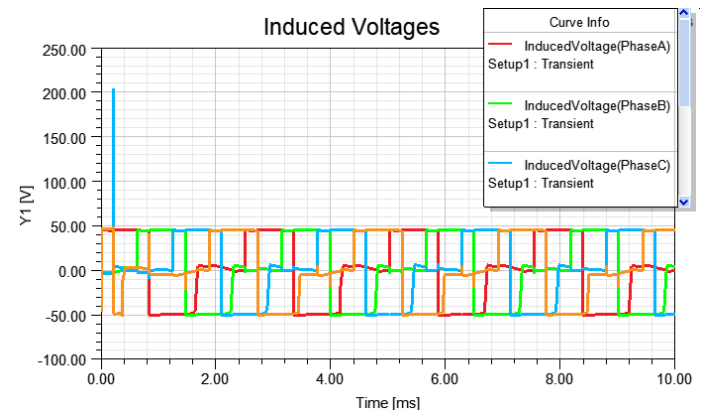


Figure 8. Graph of voltage induced in windings

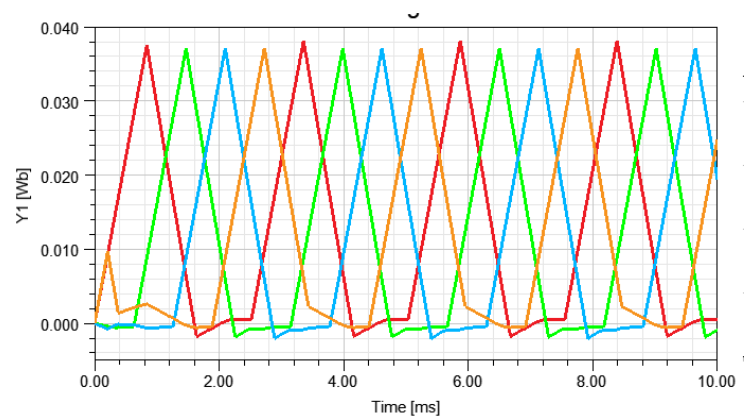


Figure 9. Flux values in the windings of the SRM

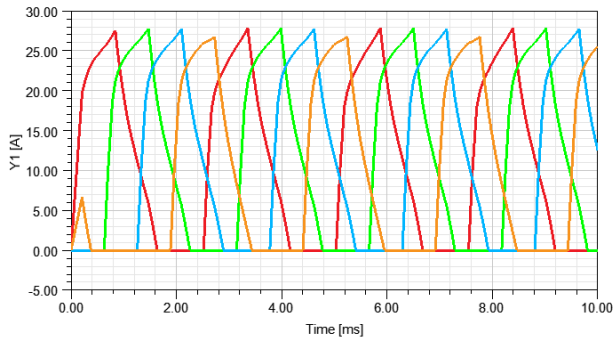


Figure 10. SRM windings current curves

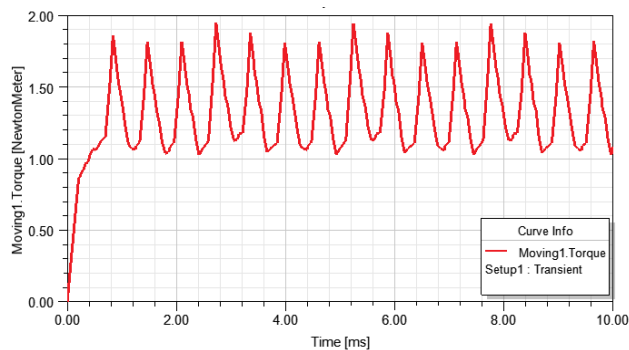


Figure 11. SRM speed-time curve

By energizing the SRM windings in this way, the motor speed reaches 429.77 rpm in a very short time and remains constant there. Velocity-time graph is given in Figure 11. While designing the SRM, parametric analyzes were carried out on motor dimensions, and parametric analyzes were made in the form of optimization of rotor and stator pole dimensions. Rotor and stator pole combinations that can give the most suitable torque value were tried and parametric analyzes were carried out. While performing the analysis, variables such as voltage, speed, and load were kept constant, and a parametric analysis was carried out by changing only the rotor and stator geometry. As can be seen in the figure, the torque value produced by the motor increased to the maximum at the peak values, but did not decrease to the minimum value too much. In other words, torque fluctuation is less compared to other structures.

4. Conclusion

Recently, many researches and studies are carried out on the design and application of switched reluctance motors. When the studies are examined, it can be concluded that these academic studies are on the structural design of the engine and the design of the control circuit. In this study, SRM was designed and analyzed. The designed SRM structure was modeled with the ANSYS-Maxwell 2D program. Rotor time transient analyzes were made and torque, phase inductance and magnetic flux density values were obtained. The torque SRM length is

maximized in the design. It has been observed that the torque graph obtained is in SRM torque characteristic and torque fluctuation occurs. It is recommended to switch phases together in certain positions to avoid torque fluctuations. It is possible to further reduce the ripples by increasing the number of phases of the motor. Controlling the prototype obtained by optimizing the design with a more skilled driver will be useful in demonstrating the capabilities of the SRM design.

References

- [1]. Irwin, J. D., 2001. "Switched Reluctance Motor Drives; Modeling, Simulation, Analysis, Design, and Applications", Series Editor, Auburn University, Alabama, A.B.D.
- [2]. Vijayraghavan, P., 2001. "Design of Switched Reluctance Motors and Development of a Universal Controller for Switched Reluctance and Permanent Magnet Brushless DC Motor Drives", Faculty of the Virginia Polytechnic Institute and State University, Blacksburg, Virginia,
- [3]. Miller, T.J.E., 1993. "Switched Reluctance Motors and their Control", Magna Physics Publishing and Clarendon Press, Oxford, İngiltere,
- [4]. Nasar, S.A., 1969. "DC Switched Reluctance Motor", Proc. IEE, Cilt 116, No 6, 1048–1049,
- [5]. Lawrenson, P.J., 1980. Stephenson, J.M., Blenkinsop, P.T., Corda, J. and Fulton, N.N., "Variable-speed Switched Reluctance Motors", Proc. IEE, Cilt 127, No 4, 253–265,
- [6]. Byrne, J. and Lacy, J.C.; 1976. "Electrodynamic system comprising a variable reluctance machine", U.S. Patent 3956678.
- [7]. Miller T. J. E., 2001. "Electronic Control of Switched Reluctance Machines", Oxford, İngiltere, 48-56,
- [8]. Miles A.R. 1991. "Design of a 5 MW, 9000V Switched Reluctance Motor", IEEE Trans. Energy Conversion, Cilt 6, 484–491,
- [9]. Khwaja M. R., 2000. "Advantages of Switched Reluctance Motor Applications to EV and HEV: Design and Control Issues", IEEE Transactions on Industrial Applications, Cilt 36, No 1, 1-4,
- [10]. S. S. Ahmad, E. Dhar, P. Kumar, and G. Narayanan, 2016. "Electromagnetic design of a 5-kW, 10,000 rpm switched reluctance machine," in 2016 7th India

- International Conference on Power Electronics (IICPE), 1–6.
- [11]. S. Allirani, H. Vidhya, T. Aishwarya, T. Kiruthika, and V. Kowsalya, 2018. “Design and Performance Analysis of Switched Reluctance Motor Using ANSYS Maxwell,” in 2018 2nd International Conference on Trends in Electronics and Informatics (ICOEI), pp. 1427–1432.
- [12]. Uzhegov, N.; Barta, J.; Kurfurst, J.; Ondrusek, C.; Pyrhonen, J. 2017. Comparison of High-Speed Electrical Motors for a Turbo Circulator Application. IEEE Trans. Ind. Appl., 53, 4308–4317.
- [13]. Lim, M.-S.; Kim, J.-M.; Hwang, Y.S.; Hong, J.-P. 2017. Design of an ultra-high-speed permanent-magnet motor for an electric turbocharger considering speed response characteristics. IEEE/ASME Trans. Mechatron., 22, 774–784.
- [14]. Kocan, S.; Rafajdus, P. 2019. Dynamic model of high speed switched reluctance motor for automotive applications. Transp. Res. Procedia, 40, 302–309..



Electrochemical biosensor for simultaneously detection of Tamoxifen

Hasret Subak

Yuzuncu Yil University, Department of Analytical Chemistry, Faculty of Pharmacy, Van, Türkiye,
hasretsubak@yyu.edu.tr, ORCID: 0000-0003-0100-2529

ABSTRACT

Cancer is described as the uncontrollably multiplying abnormal proliferation of cells. Cancer can affect everyone, and risk of which rises with age, lifestyle, and environmental toxins. Tamoxifen (TAM) which is a selective estrogen receptor modulator, has estrogenic or antiestrogenic effects on the breast tissue by binding to the estrogen receptors. The current study presents a voltammetric biosensor to identify the effect of Tamoxifen on DNA structure. In this study, the effect of TAM on the double-stranded DNA (dsDNA) was investigated electrochemically in both the presence and absence of antioxidants. For this purpose, TAM-dsDNA-antioxidant interaction investigated by using the pencil graphite electrode (PGE). The DNA modified sensor was created simply by wet-adsorption method. The prepared biosensor was examined electrochemically by square wave voltammetry (SWV) method, and its lowest concentration and optimum pH range were determined. The effect of TAM on dsDNA was investigated simultaneously for the first time in the literature.

ARTICLE INFO

Research article

Received: 17.10.2022

Accepted: 8.12.2022

Keywords:

tamoxifen,

DNA,

biosensors,

electrochemical biosensor

1. Introduction

The anti-estrogen tamoxifen was found by Beatson as an antineoplastic agent in the late nineteenth century. The anti-estrogen tamoxifen (TAM) found by Beatson is used in the treatment of breast cancer in pre-and post-menopausal women [1]. TAM which is a Selective Estrogen Receptor Modulator (SERM) has been used safely for more than 50 years as a single drug in the treatment of hormone-dependent breast cancer [2,3]. The chemical structure presented in fig 1 TAM has a benzothiophene core which is familiar with estrogen structure. Hence TAM effects the estrogen receptor like an agonist molecule [1,4]. There are two important pathways for using TAM in treatment which are blocking estrogen effect on cancer tissue and antiosteoporosis effect cause by increased bone mineral density. In light of TAM's effect mechanism, provide an agonistic effect as well as an antagonist effect by binding to estrogen receptors and causing estrogen-like effects [4,5]. In addition to these, TAM, known as a hormonal drug, is used in some hormone-sensitive cancers (pancreatic carcinoma, and in the treatment of benign breast disease) and in the treatment of male/female infertility due to this effect [2,6]. The certain inverse effects of TAM are hot flushes, nausea and/or vomiting, vaginal bleeding or discharge, and menstrual disturbances which are based on antiestrogenic activity of TAM. Besides these, according to cancer drugs and their side effects, TAM is a very well tolerated drug. In addition, due to the side effects of tamoxifen, discontinuation of the drug was not common

[2,6,7]. The cumulative use of TAM, which has been used by millions of women in cancer treatment and postmenopausal period due to its bone protection, makes it attractive to investigate. TAM's blockage by binding to the receptors and its agonist/antagonist effect allows it to be investigated with biological sensors. Chromatographic methods for TAM molecule determination [8,10], and electrochemical [4,11,12] determination methods were used. A reported study was used horseradish peroxidase immobilized on modified platinum electrode to define TAM by using CV and the EIS [11]. The antioxidants recommended together with chemotherapy in cancer treatment on tamoxifen, a chemotherapeutic, was investigated for the first time in our study. It is known that antioxidants reduce oxidative stress-induced carcinogenesis with their radical scavenging effect. For this reason, there are always questions about whether it is a correct practice for patients undergoing chemotherapy to take antioxidant-based food supplements during the treatment [13,15]. This is due to the fact that it is not known how the food supplements with high antioxidant content will affect the treatment protocol. If there is a patient in your neighborhood who is being treated for cancer or any diseases, you may have come across a patient's relative who says that you should eat these. The intense consumption of plants in the treatment of many diseases by the local people both in the world and in Turkey, and the centuries-old experience of folk medicine can guide various scientific studies. For this reason, the effect of the interaction of endemic antioxidant species that can be used as potential supplements by people who are treated for breast

cancer was investigated. In this study, the full electrochemical methods used in cancer treatment were investigated. In addition, it was desired to investigate how the anticancer effect changes or affects in an environment with antioxidants. For this, the effect on DNA and the change of its electrochemical behavior were investigated by using antioxidants.

1. Materials and methods

2.1 Chemicals

Tamoxifen citrate salt was obtained from the Sigma-Aldrich. were obtained from Sigma-Aldrich. Ultra-pure water was used for all buffer, stock and support buffer solutions preparations. In this work; NaOH (Riedel-de Haen), NaCl (Sigma), K_2HPO_4 (Merck), KH_2PO_4 (Merck), H_3PO_4 (Sigma), CH_3COOH (Riedel-de Haen, 99 %), tablet forms of CF (Sigma-Aldrich), H_3BO_3 (Sigma), fish sperm (dsDNA) (Sigma-Aldrich), single stranded from calf thymus (ssDNA) (Sigma) were used for analysing. The fish sperm dsDNA stock solutions were prepared as high concentration (such as 1000 $\mu\text{g/mL}$) and stored at -20°C . The antioxidant substance used in our study was obtained from Hypericum species found around the province of Van, which has a rich ethnomedical diversity. This species is still used by the local people for various medicinal purposes today.

2.2. Aparatus

All of the electrochemical measurements were performed with using an AUTOLAB 12 potentiostat/galvanostat analyzer (Eco Chemie, Netherlands). The voltammogram which obtained from the raw differential pulse (DP) was smoothed by Savitzky and Golay filter (level 2) of the General-Purpose Electrochemical Software (GPES) of Eco Chemie with moving average baseline correction, using a "peak width" of 0.01 V. PGE was used as a "working electrode" that contains 3 cm of graphite rod (0.5 mm diameter, Tombo, Japan) and a rotating model pencil was used as a holder. The 3-electrode system that includes of a pencil graphite electrode (GE, as a working electrode), an Ag/AgCl (KCl, 3M), (as a reference electrode) and a platinum wire auxiliary electrode obtained from Basi (USA).

2.3 Methods

In the study, all electrochemical analyzes of tamoxifen and antioxidant were carried out using the square wave stripping [16] voltammetry method. First, pencil graphite electrodes were activated in ABS buffer under 1.4 V for 30 seconds to form surface-active $-\text{COOH}$ functional groups. All measurements were made with activated electrodes. In the method, electrochemical studies of tamoxifen and antioxidant were firstly performed. In this direction, pH scanning, frequency scanning, amplitude and scan rate measurements were made. In the experiment performed for

stripping voltammetry, after the activated electrodes were immersed in the cell containing 10 ml of support solution, the appropriate concentration of tamoxifen was transferred to the cell. After adding tamoxifen, it was mixed for a certain time (30 sec). At the end of the period, measurements were made with square wave voltammetry. The general outline of the experiment is thus provided. Concentration study of tamoxifen Concentration study was carried out by measuring with 0.625/ 1.25/ 2.5/ 5/ 7.5/ 10/ 20 $\mu\text{g/mL}$ tamoxifen. All electrochemical optimization studies TAM were performed using PGE and square wave voltammetry. pH scanning, frequency, amplitude, scan rate scans were performed as optimization parameters. After the most suitable conditions were provided, calibration study was carried out. In the experiments, the change of the electrochemical signal depending on antioxidants was also examined.

2.4 Measurement conditions

The electrochemical measurement was performed by using SWV with 0 to +1.4 mV potential range; 5 mV step potential; 70 mV modulation amplitude; 0.05 s modulation time; 0.15 s interval time; 4 mV/s scan rate. The method indirectly detects the effect of the drug on the DNA structure.

2. Results and discussions

3.1 pH Scanning

Scanning was performed between pH 2/8 with BR buffer using PGE. The most suitable pH was determined as 5 in the obtained data. The voltammogram shows pH between 2 to 8.

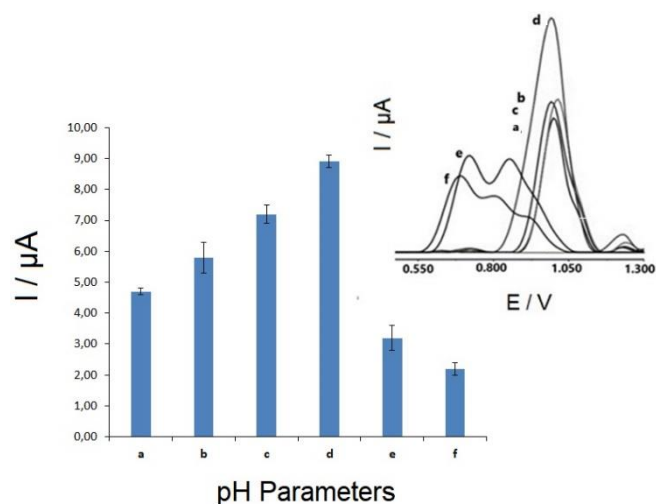


Figure 1. The oxidation peak current values obtained from DPV voltammograms of 100 μM TAM in the range changed from pH(a-d): 2.00 to 8.00 in 0.04 M B-R buffers at PGE

To determine optimal oxidation conditions of TAM, B-R buffers (pH: 2.00 to 8.00) were used as supporting electrolytes. DPV voltammograms of the 100 μM TAM in B-R electrolytes at different pH were recorded. The highest

current value related to the TAM oxidation was obtained in B-R buffer at pH=4.50 and this medium was chosen for further experiments. The oxidation peak current value of the 100 μM TAM obtained with the buffer solutions at different pH in the range changed from pH: 2.00 to 8.00 as shown in Fig.1.

3.2 Optimization parameters of TAM

After TAM was added to the measuring cell, it was mixed for a certain time (30 sec). At the end of the period, measurements were made with square wave voltammetry. The general outline of the experiment is thus provided. Concentration study of tamoxifen Concentration study was carried out by measuring with 0.725/1.25/2.5/5/10/20/30/40 $\mu\text{g/mL}$ tamoxifen amounts Fig.2.

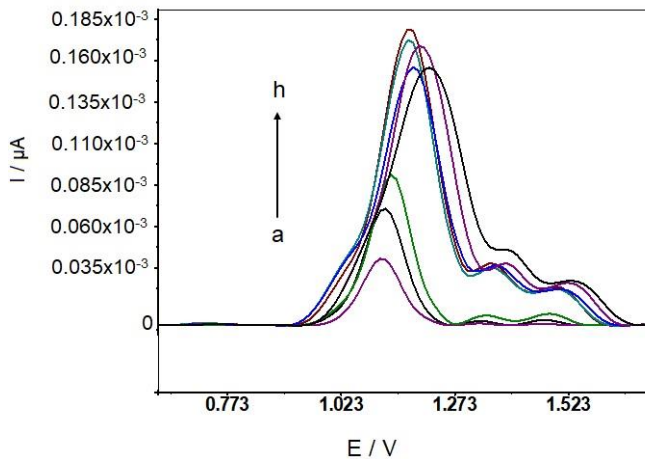


Figure 2. Concentration study of tamoxifen which were presented a: 0.725/b:1.25/c:2.5/d:5/e:10/f:1 20/g:30/h:40 $\mu\text{g/mL}$

Since the electrode surface reaches saturation after 5 $\mu\text{g/mL}$, the signal did not change or even decreased despite increasing concentration Fig 3.

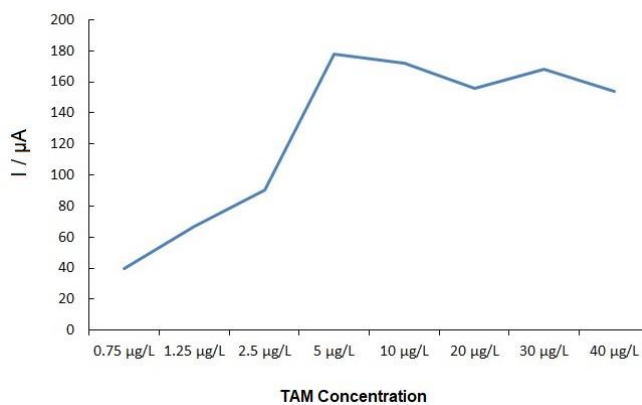


Figure 3. In the given histogram, signal changes are seen due to increasing TAM concentrations. The drug solutions which increasing concentration prepared were immobilized on the electrode surface by stripping method.

3.3 Biosensor preparation

PGEs were activated in an electrochemical cell which contains 4 mL of an acetate buffer solution (ABS; pH=4.80). Their 1 cm surface has applied to the buffer solution for 30 seconds at a potential of +1.40 V[17]. The activated PGE was modified with DNA by wet-adsorption technique. For the preparation of a biosensor under optimal conditions, time and concentration study was carried out with dsDNA. (Data not shown). The optimum condition for obtaining a DNA-modified biosensor was determined as a 20-minute adsorption of 20 $\mu\text{g/mL}$ dsDNA-activated electrodes.

3.4 TAM-DNA interaction

The selective analysis of cancer therapy drugs, especially TAM, could create the possibility to better control of the treatment process. Considering these, analytical sensors can be evaluated as an auxiliary device for such analysis in cancer patients. For this purpose, DNA modified electrodes were added at increased concentrations of TAM in the same solution medium and mixed for 30 seconds to interact. At the end of 20 minutes adsorption of dsDNA 2.5-5-10-10-10-10 μl 1000 mL is added to br buffer and mixed for 30 seconds, and then the measurement is taken in the same cell (4 mL B-R buffer medium). The interaction will also be evaluated in the dsDNA solution environment in the continuation of the study.

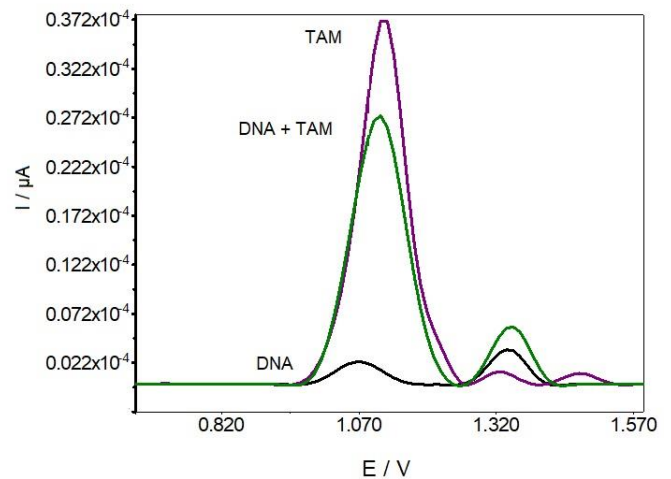


Figure 4. TAM-DNA interaction. Before the interaction dsDNA solution was analysed alone. After that dsDNA was modified at the electrode surface and interact with TAM. The electrochemical investigation of dsDNA and the TAM was detected.

Concentration study was carried out by square wave voltammetry method in B-R pH 5 buffer with PGE. Optimum concentration was found as 20 $\mu\text{g}/\text{mL}$ for DNA. % signal reduction was observed as increasing concentrations of TAM were added to the 20 $\mu\text{g}/\text{mL}$ DNA solution (Fig 4.).

3.5 Antioxidants – DNA interaction

The effect of antioxidant on tamoxifen and DNA interaction was also investigated. In this direction, the effect of antioxidant on DNA in the presence and absence of tamoxifen was investigated.

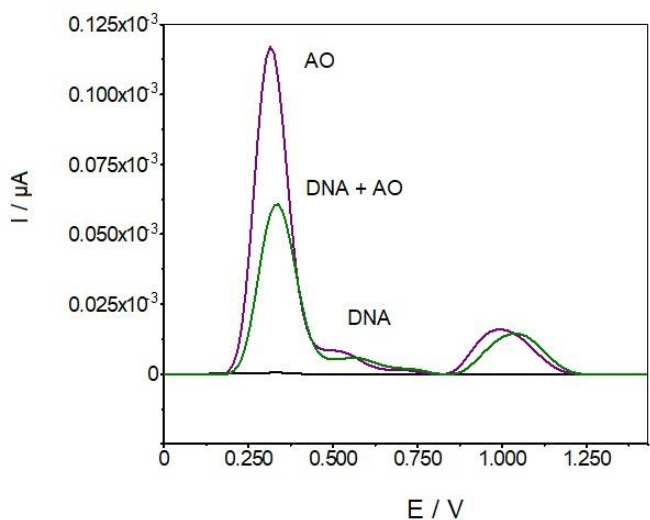


Figure 5. Antioxidant-DNA interaction. Before and after interaction The change in the oxidation signal of guanine (+1.0 V) and the extract (0.35 V) were measured using SWV method.

The experiment was carried out by applying the optimum conditions obtained with the PG electrode. AO gives signals at two potential area. Here is the effect with DNA at 1.0V which guanine oxidation potential area. There was a decrease in the signal around 0.30v and a shift towards the anodic region in the other signal. It is thought that there may be a reducing effect on the guanine oxidation signal by intercalation Fig 5.

3.6 Antioxidants – TAM interaction

In addition, the effect of antioxidant on the electrochemical behavior of tamoxifen in the absence of DNA was investigated in the study. In this direction, the signal change with increasing concentration of tamoxifen was investigated by measuring the AO and TAM oxidation potential points (Fig 6.).

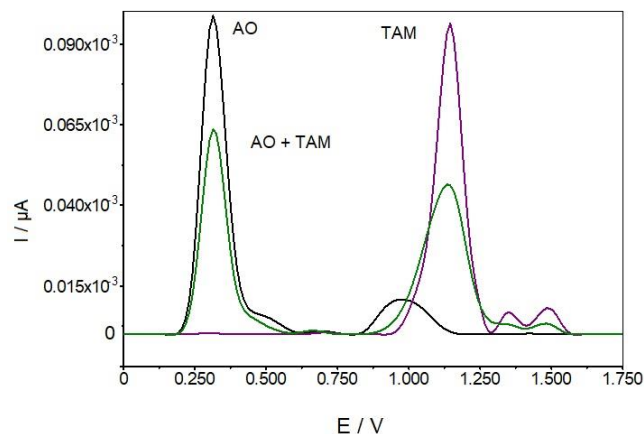


Figure 6. Antioxidant-TAM interaction. The interaction AO with TAM was examined in the study. The evaluated data show that there are different changes in both signals.

Despite the increasing concentration, the antioxidant signal reaches a maximum level of 120 μA and saturates on the electrode surface. When TAM is added to the environment, signal increase is observed. Concentration Studies of AO and TAM were also carried out separately. The concentration studies of TAM and AO were evaluated together with the concentration studies conducted separately. As a result of this study, a change was observed in the electrochemical behavior of AO in the presence of TAM. (Data not shown). Depending on the preliminary studies prepared for publication, the change in AO is indicated on the voltammogram (Fig 6.). Accordingly, AO and TAM were interacted electrochemically. The effects on the DNA concentration in the same medium were also be examined.

3.7 Antioxidants - TAM – DNA simultaneously interaction

Three electroactive materials, DNA, AO and TAM, were studied separately. In this step, these three electroactive substances were examined in the same electrochemical cell. In the measurement, the effect of AO and TAM on DNA was examined. The results of this examination were compared with the data obtained from the effect of both TAM and AO on DNA separately and together.

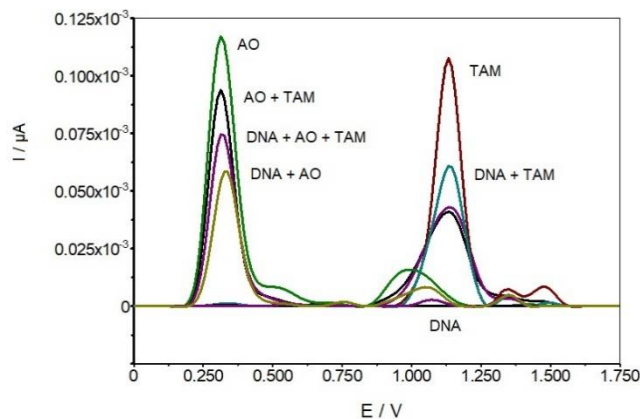


Figure 7. Antioxidant-TAM-DNA interaction. In the given voltammogram showed the effect of TAM and AO on DNA in the same time and separately.

Evaluation was made at three different oxidation points. The effects of AO and TAM on in the DNA medium were examined on the electrode surface separately and together. As a result of this; after interaction with DNA, the TAM and AO signal decreased separately. Here, the evaluation was made at two different points of the potential area. The decrease in the signal at 0.35 V is most distinct potential point which is belong AO interaction with DNA. The interaction of AO alone and with DNA has been compared. According to this, the change in the electrochemical signal of AO when it interacts with dsDNA alone is greater than the change obtained in the TAM environment. When the result is compared, it shows that AO interacts competitively with TAM in interaction with DNA. In the second signal, the overlap of TAM-AO and TAM-DNA-AO signals shows that the interaction with AO gives the same signal independent of DNA. The second electrochemical evaluation point, AO and TAM, was evaluated at the guanine oxidation area of DNA (1.0V). Accordingly, while TAM and AO do not change the guanine oxidation signal of DNA, it has been observed that AO alone changes the guanine oxidation signal of DNA. When TAM and AO were together, their signals at their oxidation sites did not change before and after the DNA interaction.

3. Conclusions

In this article, the simultaneously interaction of TAM with DNA and AO was investigated by electrochemical voltametric studies. The study of the interaction between the anticancer drug Tamoxifen and DNA is crucial to identify possible DNA damage during treatment. The research will also be valuable in the design of the molecule-specific electrochemical biosensor to be applied in diagnostic tests and the development of drugs for cancer treatment patients. A simple, fast and precise SWV method is recommended for the determination of Tamoxifen in pharmaceutical formulations. In conclusion, these studies in a new biosensor may play an important role in the

development of unknown drug-DNA interaction mechanisms.

References

- [1]. M. Clemons, S. Danson, and A. Howell, "Tamoxifen ('Nolvadex'): A review," *Cancer Treat. Rev.*, vol. 28, no. 4, pp. 165–180, 2002, doi: 10.1016/S0305-7372(02)00036-1.
- [2]. D. J. Bentrem and V. Craig Jordan, "Tamoxifen, raloxifene and the prevention of breast cancer.," *Minerva Endocrinol.*, vol. 27, no. 2, pp. 127–139, 2002, doi: 10.1210/edrv.20.3.0368.
- [3]. S. Mandlekar and A. N. T. Kong, "Mechanisms of tamoxifen-induced apoptosis," *Apoptosis*, vol. 6, no. 6, pp. 469–477, 2001, doi: 10.1023/A:1012437607881.
- [4]. M. Fouladgar, H. Karimi-Maleh, F. Opoku, and P. P. Govender, "Electrochemical anticancer drug sensor for determination of raloxifene in the presence of tamoxifen using graphene-CuO-polypyrrole nanocomposite structure modified pencil graphite electrode: Theoretical and experimental investigation," *J. Mol. Liq.*, vol. 311, p. 113314, 2020, doi: 10.1016/j.molliq.2020.113314.
- [5]. I. Girault, I. Bièche, and R. Lidereau, "Role of estrogen receptor α transcriptional coregulators in tamoxifen resistance in breast cancer," *Maturitas*, vol. 54, no. 4, pp. 342–351, 2006, doi: 10.1016/j.maturitas.2006.06.003.
- [6]. M. M. T. Buckley and K. L. Goa, "Tamoxifen: A Reappraisal of its Pharmacodynamic and Pharmacokinetic Properties, and Therapeutic Use," *Drugs*, vol. 37, no. 4, pp. 451–490, 1989, doi: 10.2165/00003495-198937040-00004.
- [7]. B. J. A. Furr and V. C. Jordan, "The pharmacology and clinical uses of tamoxifen," *Pharmacol. Ther.*, vol. 25, no. 2, pp. 127–205, 1984, doi: 10.1016/0163-7258(84)90043-3.
- [8]. K. Lee, B. A. Ward, Z. Desta, D. A. Flockhart, and D. R. Jones, "Q quantification of tamoxifen and three metabolites in plasma by high-performance liquid chromatography with fluorescence detection: application to a clinical trial," vol. 791, pp. 245–253, 2003.

- [9]. X. Liu, J. Zhang, J. Yin, and H. Duan, "Analysis of hormone antagonists in clinical and municipal wastewater by isotopic dilution liquid chromatography tandem mass spectrometry," pp. 2977–2985, 2010, doi: 10.1007/s00216-010-3531-0.
- [10]. S. Xiao, Y. Yang, J. Zhang, Y. Wu, and B. Shao, "[Determination of 6 antiestrogens in fish tissues by ultra performance liquid chromatography-tandem mass spectrometry]," *Se pu = Chinese J. Chromatogr.*, vol. 29, no. 11, p. 1055–1061, 2011, [Online]. Available: <http://europepmc.org/abstract/MED/22393691>.
- [11]. K. Radhapyari, P. Kotoky, and R. Khan, "Detection of anticancer drug tamoxifen using biosensor based on polyaniline probe modified with horseradish peroxidase," *Mater. Sci. Eng. C*, vol. 33, no. 2, pp. 583–587, 2013, doi: 10.1016/j.msec.2012.09.021.
- [12]. S. Yanik, D. Ozkan-ariksoysal, and S. Yilmaz, "ELECTROCHEMICAL BIOSENSOR FOR BRCA1 GENE AND TAMOXIFEN INTERACTION," vol. 4, no. 1, pp. 35–48, 2020.
- [13]. L. Dornelles, S. Hernandez, G. Marrazza, M. Mascini, and L. Tatsuo, "Investigations of the antioxidant properties of plant extracts using a DNA-electrochemical biosensor," vol. 21, pp. 1374–1382, 2006, doi: 10.1016/j.bios.2005.05.012.
- [14]. E. Küpeli Akkol, I. Süntar, M. İlhan, and E. Aras, "In vitro enzyme inhibitory effects of *Rubus sanctus* Schreber and its active metabolite as a function of wound healing activity," *J. Herb. Med.*, 2015, doi: 10.1016/j.hermed.2015.09.002.
- [15]. I. Erlund et al., "Pharmacokinetics of quercetin from quercetin aglycone and rutin in healthy volunteers," *Eur. J. Clin. Pharmacol.*, vol. 56, no. 8, pp. 545–553, 2000, doi: 10.1007/s002280000197.
- [16]. S. Allahverdiyeva, O. Yunusoğlu, Y. Yardım, and Z. Şentürk, "First electrochemical evaluation of favipiravir used as an antiviral option in the treatment of COVID-19: A study of its enhanced voltammetric determination in cationic surfactant media using a boron-doped diamond electrode," *Anal. Chim. Acta*, vol. 1159, 2021, doi: 10.1016/j.aca.2021.338418.
- [17]. H. Subak and D. Ozkan-Ariksoysal, "Label-free electrochemical biosensor for the detection of Influenza genes and the solution of guanine-based displaying problem of DNA hybridization," *Sensors Actuators, B Chem.*, vol. 263, 2018, doi: 10.1016/j.snb.2018.02.089

**MJEN**

Investigation and analysis of interleaved dc-dc boost converter for grid-connected photovoltaic energy system

Mehmet Büyük

Adıyaman University, Electrical and Electronics Engineering, 02300, Adıyaman, Türkiye, mbuyuk@adiyaman.edu.tr,
ORCID: 0000-0003-3026-4034

ABSTRACT

In this study, we focused on the synthesis of polymeric hydrogels that will support the sorption and controlled release of urea, which is a rich nitrogen source, from aqueous solutions and their usability in agricultural applications. N, N-Dimethylacrylamide (DMAAm) and Starch (St) were selected as monomers, and their superior properties, such as chemical stability, high sorption properties, biocompatibility, and the presence of modifiable groups, were utilized. A redox polymerization technique was used to create a poly(DMAAm-co-St)-based hydrogel that was then modified with acidic and basic agents to improve the properties of starch. The synthesized acid- and base-modified hydrogels were named DSt, DSt₁, and DSt₂, respectively. Swelling analyses were performed to examine the structural and morphological properties of DSt, DSt₁, and DSt₂ hydrogels, and Fourier-Transform Infrared Spectroscopy (FT-IR) and Thermogravimetric Analyzers (TGA) were used. Intense cross-linking, porosity, and the presence of hydrophilic groups were successfully detected by instrumental analysis and swelling results. The successful results of urea sorption by DSt, DSt₁, and DSt₂ hydrogels show that they can both minimize the harmful effects of urea in the environment and contain the nitrogen necessary for plants. At the same time, urea sorption behaviors were evaluated in terms of sorption isotherms and thermodynamic properties, and it was observed that urea sorption conformed to the Langmuir isotherm. The urea release results showed that DSt, DSt₁, and DSt₂ hydrogels exhibited different release properties in different pH solutions, and these results reached 94% at pH 6–8, 100% at pH 6, and 100% at pH 8–10, respectively. As a result of the gradual decrease in the water resources on the earth, the increase in the use of fertilizers in agricultural production, and the insufficient use of fertilizers, our study draws attention to the development and support of materials that absorb/store water, and forms of controlled release fertilizers and provides potential ease of application

ARTICLE INFO

Research article

Received: 26.10.2022

Accepted: 16.12.2022

Keywords:

controlled release, hydrogel,
nitrogen loss,
starch,
water retention

1. Introduction

In today's life, the applications of renewable energy sources have come into prominence by reduction of the fossil fuels and increasing greenhouse gas emissions [1, 2]. Photovoltaic (PV) panel systems attract further attention since their simple implementation and low maintenance cost. In addition, the power generation capacity of PV systems can be improved via implementation of industry 4.0 [3]. Besides, the systems are applicable for houses, industrial plants and commercial power plants [4-7]. Furthermore, the installed PV system capacity over the world has been increasing significantly in recent years [8]. Although standalone and grid-connected PV panel systems are available in applications, the grid-connected systems are more efficient and highly preferred systems in applications [5-7]. In general, a dc/dc converter and an inverter are used to connect the PV panels to the grid [9]. The dc/dc converter is applied to obtain the suitable dc

voltage level with the maximum power of PV panel [1, 10, 11]. The inverter is utilised to converter dc voltage into ac voltage [12].

There are several dc/dc converter topologies implemented in the grid-connected PV systems. However, a boost converter is usually preferred as a dc/dc converter in PV system and renewable energy systems [2, 13-16]. There are also a few boost converter circuits in literature studies and applications [13, 17, 18]. In earlier studies, conventional boost converter topology is used with PV system. However, the PV current has a high ripple ratio when the conventional boost converter is used [10, 11, 19, 20]. The high current ripple ratio in PV side effects total harmonic distortion (THD) value of current injected to the grid. Besides, the high ripple degrades the PV lifetime and overall system efficiency.

In this study, a three-leg interleaved boost converter is applied for the grid-connected PV system. The proposed system is modelled and analysed through a simulation environment. A grid-connected PV system in the rating of 10.6 kW is designed and constructed in the simulation environment, and the constructed model is simulated for conventional boost converter and IBC systems. The modelled system is examined under different irradiance and temperature values. The simulation results are presented by considering current ripple ratio and THD value.

The rest of the manuscript is organized as follows. In Section 2, the PV system model of the simulated system and its characteristics are introduced. In Section 3, the structure of the proposed system is presented. By this way, the model of the proposed system is explained in detail. In addition, the current ripple ratios are given for the conventional boost converter and IBC. In Section 4, the simulation results of the proposed system with the conventional boost converter and IBC topologies are presented. The results of IBC topology are discussed and compared with the results of the conventional topology. The conclusion is discussed in Section 5.

2. PV system model and characteristic

A PV module consists of small solar cells (approximately 1-2 W) to generate high output power and voltage. As well known that an ideal solar cell is modelled as a current source with parallel a diode. Besides, series and parallel resistors are included to ideal model to demonstrate power losses. The widespread equivalent circuit model of a single PV cell/module is illustrated in Figure 1. This model is called a single diode model and includes five parameters to be determined. The $I - V$ characteristic of the single diode model is acquired through Eq. (1) [21].

$$I = I_{pv} - I_0 \left[\exp \left(\frac{V + IR_s}{aV_T} \right) - 1 \right] - \frac{V + IR_s}{R_{sh}} \quad (1)$$

Where,

- I_{pv} : PV current
- I_0 : Saturation current
- R_s : Series resistor
- R_{sh} : Shunt resistor
- V_T : Diode thermal voltage

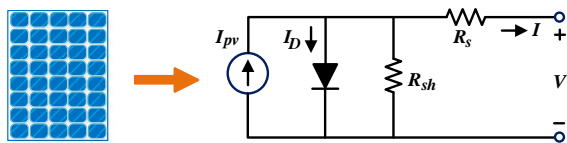


Figure 1. A single PV module and its equivalent circuit scheme

The parameters of the model are obtained by equations of short circuit, open circuit, MPP circuit and zero derivative for MPP circuit. The parameters for a single module are shown in Table 1. According to these parameters, PV current, series and shunt resistors and diode saturation current are obtained. Then, the $I - V$ and $P - V$ curves of this model are drawn for different irradiance values at 25 °C, as shown in Figure 2.

Table 1. The parameters for a single PV module

Parameter	Description	Value
P_{mp}	Maximum power	305.2 W
V_{oc}	Open circuit voltage	64.14 V
V_{mp}	Voltage at MPP	54.7 V
N_{cell}	# of cell per module	96
I_{sc}	Short-circuit current	5.94 A
I_{mp}	Current at MPP	5.56 A

The voltage level of the single module is low during the grid connection. Thus, in the present work, seven in series and five in parallel modules are connected to create a PV array with sufficient voltage level and high current value. The $I - V$ and $P - V$ curves of PV array are drawn for different irradiance values at 25 °C, as demonstrated in Figure 3.

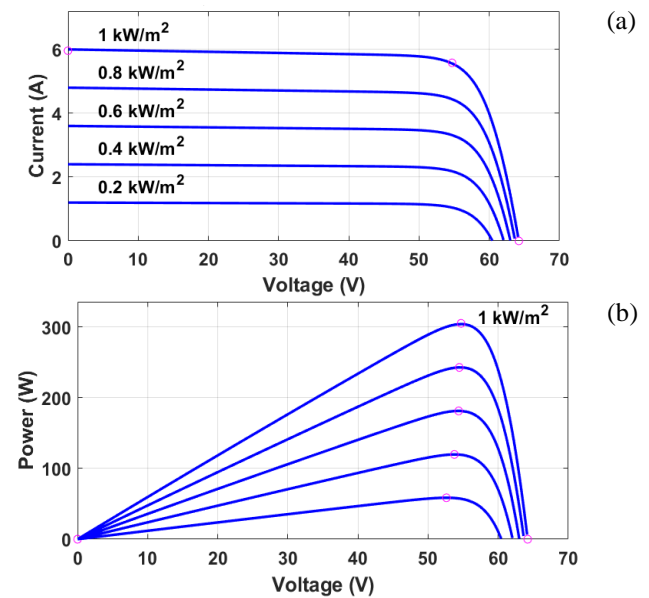


Figure 2. The $I - V$ and $P - V$ curves of single PV module under different irradiances

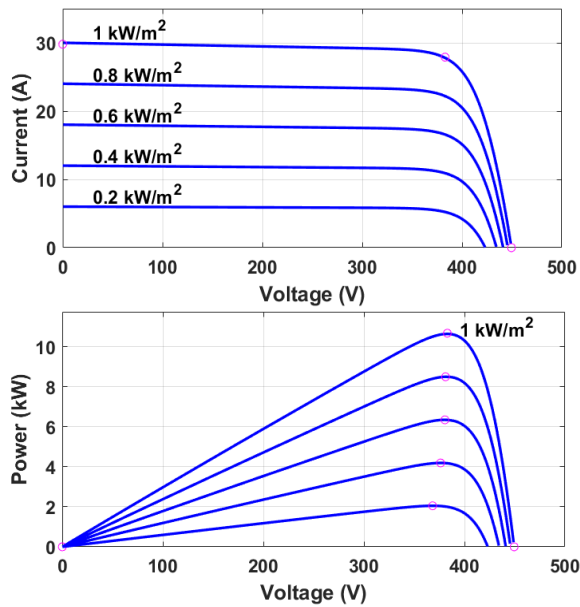


Figure 3. The $I - V$ and $P - V$ curves of PV array under different irradiances

3. Structure and control of the proposed system model

The general representation of the proposed system is demonstrated in Fig. 4. The proposed system consists of a PV array transferring solar energy into electric energy, a three-leg boost converter with MPPT controller, and a three-phase DC-AC inverter with the current controller and output LCL filter. Incremental conductance MPPT algorithm is applied to acquire maximum power [22,23].

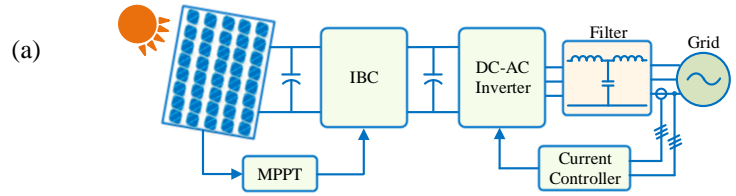


Figure 4. General structure scheme of the proposed system

3.1. Interleaved boost converter

The conventional boost converter and IBC structures with pulses and PV currents are shown in Figure 5. The structure and pulse signal of the conventional converter are demonstrated in Figure 5(a) and Figure 5(c). Besides, the structure and pulse signals of IBC topology are shown in Figure 5(b) and Figure 5(d).

The relation between input voltage and output voltage of the conventional boost converter is given in (2). The current flowing on the inductor is increasing once the switching component turns on and decreasing when turns off. The difference between the lower and upper points of the current is ripple current that has drawbacks on the PV system and output voltage. The ripple current is obtained by Eq. (3). To lessen the ripple current, the inductance value or switching frequency can be increased. However, higher inductance value results in bulky system and high switching frequency leads to efficiency degradation. In this study, instead, a three-leg boost converter is proposed to reduce the inductor current ripple and its negative effect [13, 24].

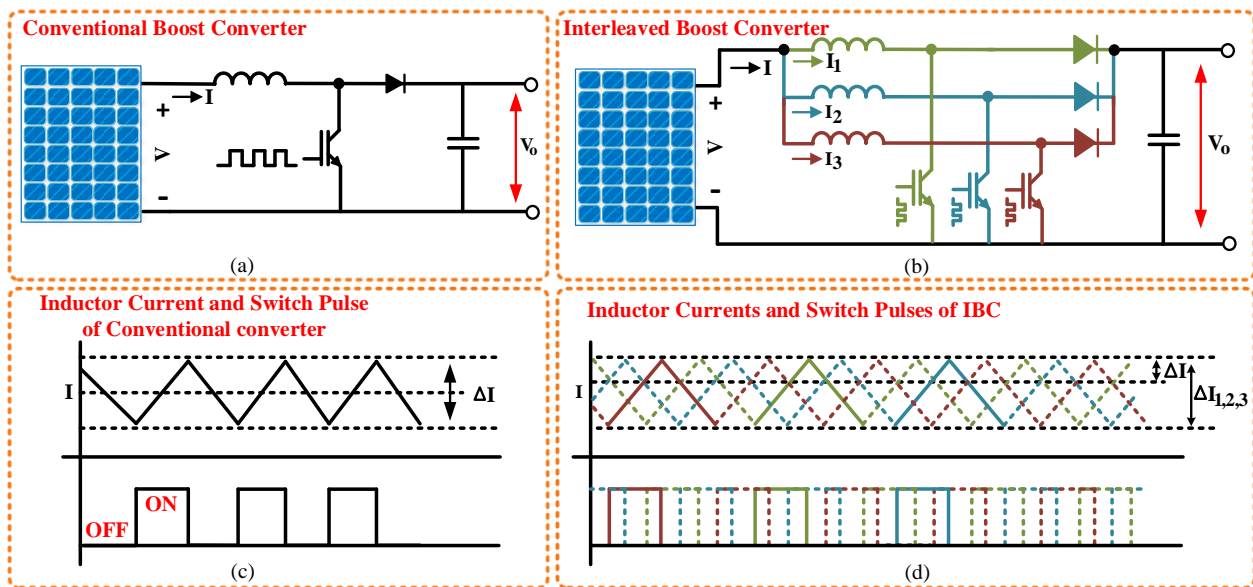


Figure 5. The structures, currents and pulse waveforms of the conventional boost converter and IBC

$$V_o = \frac{1}{(1-D)}V \tag{2}$$

$$\Delta I = \frac{DT_s}{L}V \tag{3}$$

Where, D is duty cycle and T_s is switching time.

In this study, a three-phase IBC is preferred to convert DC voltage level. Three parallel converters are used in this topology, as shown in Figure 5(b). The operation of IBC is based on applying identical pulses with shifting the pulses of the switches by 120° [19,24]. The switching signals and inductor currents are demonstrated in Figure 5(d). The switching signals may overlap depending on duty cycle, as shown in Figure 5(d). It is proposed to select the duty cycle higher than $1/3$ in order to obtain boosted input voltage. The input ripple current is obtained as Eq. (4). The input ripple current is obtained according to the duty cycle ratio [10].

$$\Delta I = \begin{cases} 0.34 < D < 0.66 ; & \frac{VT_s d}{3L} \left(\frac{2-3D}{D'} \right) \\ 0.67 < D < 1 & ; \frac{VT_s d}{L} \left(\frac{1-D}{D'} \right) \end{cases} \tag{4}$$

Where, d is the ratio of input current rising time to its period (t_r/τ).

3.1. DC/AC conversion

The PV system is connected to the grid through a DC-AC inverter. In this study, a three-phase inverter is used to convert DC voltage into AC voltage. The inverter includes three half-bridge inverter legs. The switching components of the inverter are modulated by SPWM method. The rms voltage value of inverter is obtained as in (5) for the fundamental component [25]. The circuit diagram of the grid-connected inverter is demonstrated in Figure 6. An LCL filter is tied between the inverter and the grid to effectively degrade the ripple harmonics generated from the modulation of the inverter [26]. Besides, a simple resistor connected in series with the filter capacitor suppresses the filter resonance.

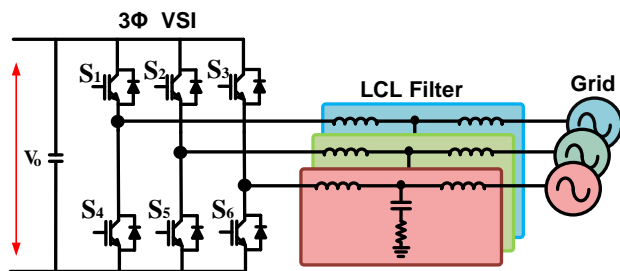


Figure 6. The circuit diagram of the three-phase grid-connected inverter

$$V_i = \frac{M}{2\sqrt{2}}V_o \tag{5}$$

Where, M index represents the modulation ratio of the reference sine signal to the carrier signal. V_i and V_o are inverter output fundamental voltage and capacitor dc voltage, respectively. The constant $M/(2\sqrt{2})$ gives the inverter gain value [25].

4. Case studies and discussion

The proposed system is modelled and analysed through a simulation program environment. The system parameters of the modelled system are given in Table 2. The proposed system is tested under various irradiance and temperature values. The changes in irradiance and temperature are shown in Figure 7. Besides, the mean powers obtained from PV array according to the irradiance and temperature variations for conventional boost converter and IBC are illustrated in Figure 8. The mean power obtained by the IBC topology is always higher than the conventional topology.

The modelled system is examined for conventional boost converter and three-phase IBC topologies. Figure 9 shows the current and voltage waveforms once the conventional boost converter and three-phase IBC are applied. It is obvious that the output current has high ripple current when the conventional method is used. On the other hand, the ripple current is reduced to almost $1/3$ ratio with IBC technique.

Table 2. The system parameters of the proposed system

Parameter	Description	Value
V_g	Grid voltage	380 V
f_g	Grid frequency	50 Hz
V_o	DC link voltage	750 V
P_{pv}	Max. PV power	10.6 kW
f_{sd}	IBC switching freq.	5 kHz
f_{si}	Inverter switching freq.	5 kHz

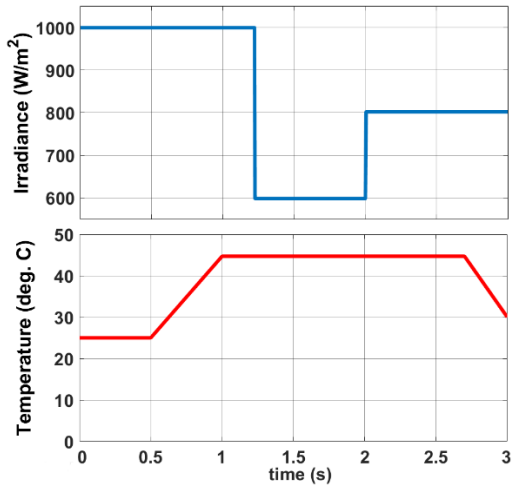


Figure 7. The changes in irradiance and temperature

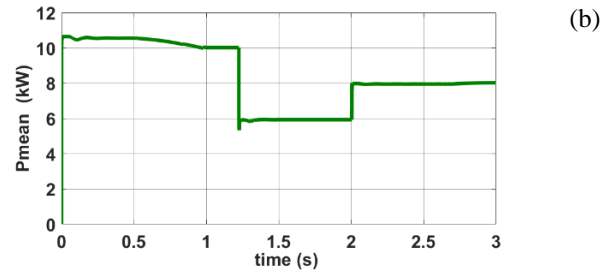


Figure 8. Mean power behaviour of PV array under irradiance and temperature changes for conventional converter and (b) IBC topology

The grid voltage and current supplied by PV to the grid under the variation of the irradiance and temperature are shown in Figure 10. This result is illustrated only for IBC based topology. It can be seen from the figure that the supplied current decreases with irradiance reduction and temperature increment.

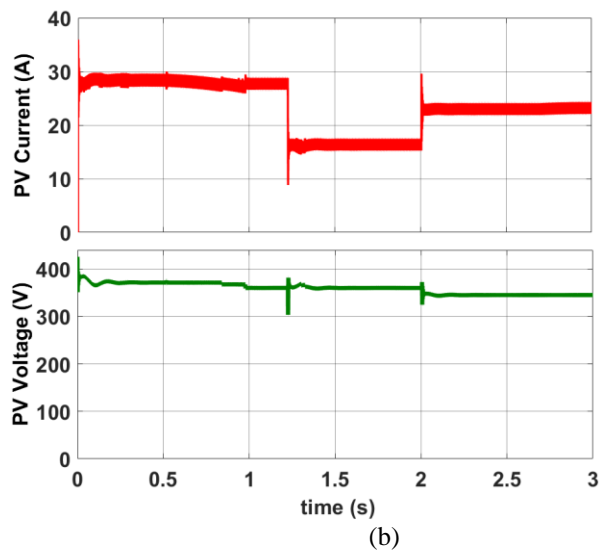
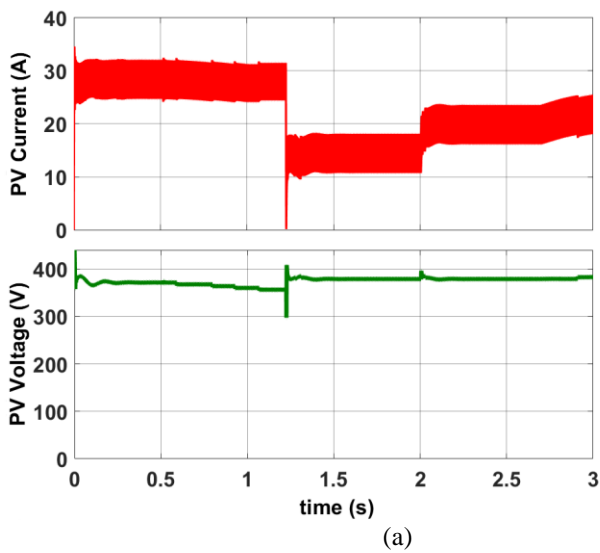
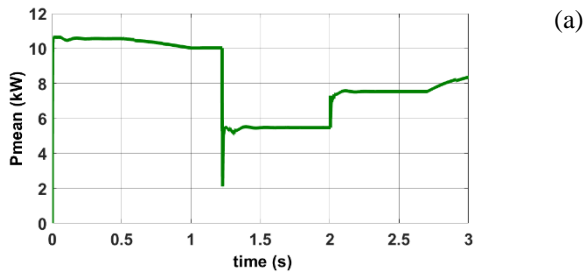


Figure 9. Output current and voltage waveforms of PV array for (a) conventional boost converter and (b) IBC

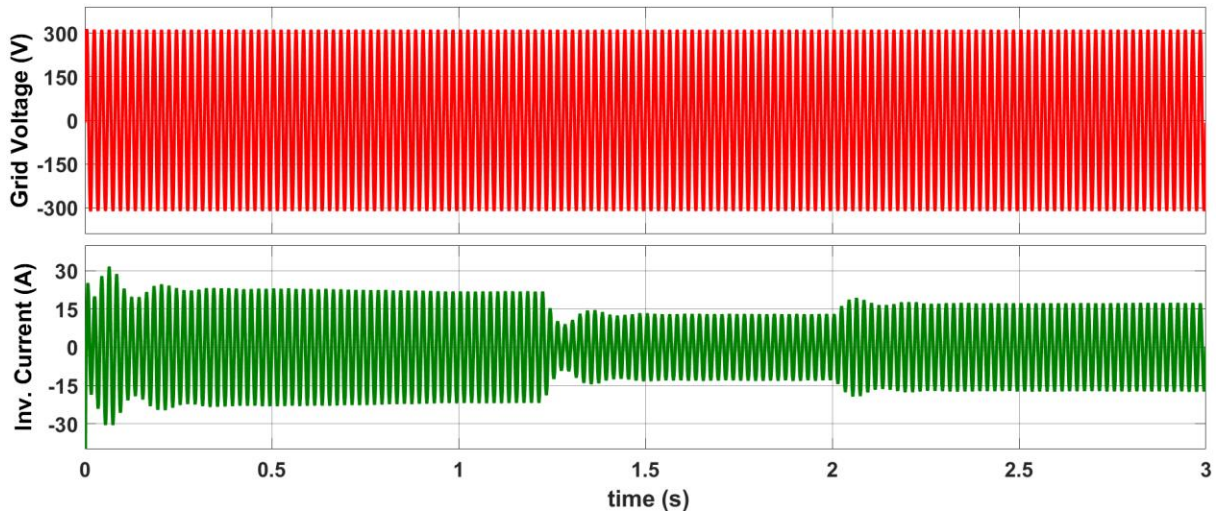


Figure 10. The waveforms of grid voltage and inverter current

The grid-side current waveforms with their harmonic spectra and THDs are shown in Figure 11. The results for conventional and IBC methods are given in Figure 11(a) and Figure 11(b), respectively. The THD values of the grid-side currents are 0.94 % and 0.87 % for the conventional method and IBC method, respectively. It is obvious from the simulation results that the proposed system injects current to the grid with lower THD value.

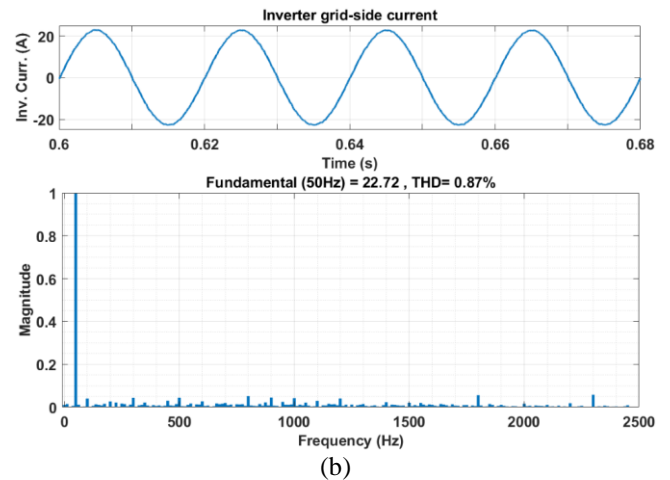
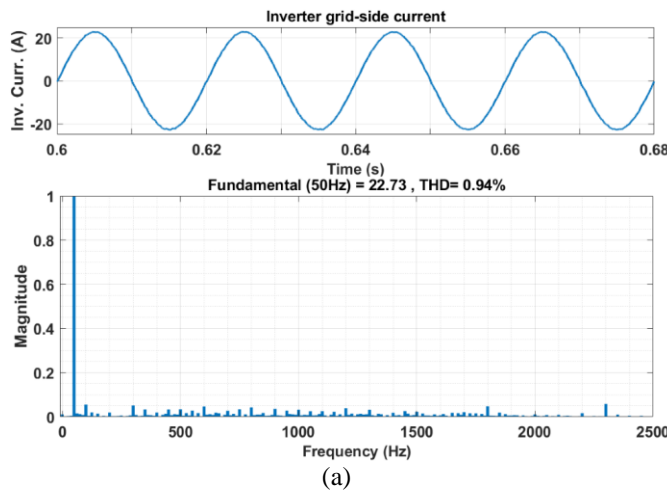


Figure 11. Waveforms of grid currents and FFTs with (a) conventional method and (b) IBC structure

5. Conclusion

A grid-connected PV system with IBC has been proposed in this study. In the proposed study, IBC is used as dc/dc converter to reduce the current ripple ratio. The IC MPPT algorithm is applied to obtain the maximum power from the PV array. A 10.6 kW grid-connected PV system is designed in this study. The proposed system has been modelled in simulation environment, and it is examined under variation of irradiance and temperature. The proposed system is compared with the conventional boost converter model. It is shown from the simulation results that the IBC topology has a lower PV current ripple in comparison with the conventional boost converter. The current ripple values are 7.2V and 2.1V for the conventional boost converter and the IBC topologies, respectively. Moreover, the THD values of the grid current are 0.94% and 0.87% for the conventional boost converter and the IBC topologies, respectively. It is

obvious from the results that the current ripple and THD value are reduced by the IBC model.

References

- [1]. M. İnci, "Interline fuel cell (I-FC) system with dual-functional control capability," *International Journal of Hydrogen Energy*, vol. 45, pp. 891-903, 2020/01/01/ 2020.
- [2]. Sudha R., Abishri P., and U. S., "Review of Coupled Two and Three Phase Interleaved Boost Converter (IBC) and Investigation of Four Phase IBC for Renewable Application," *International Journal of Renewable Energy Research*, vol. 6, 2016.
- [3]. H. H. ÇOBAN, "Accelerating renewable energy generation over industry 4.0 " *MANAS Journal of Engineering*, vol. 7, pp. 114-120, 2019.
- [4]. X. Cao, C. Zhang, Y. Zhang, Z. Gan, H. Li, W. Ni, et al., "The simulation study of the modulation method for PV grid-connected system," *Energy Procedia*, vol. 145, pp. 122-127, 2018/07/01/ 2018.
- [5]. M. İnci, "Design and Analysis of Dual Level Boost Converter Based Transformerless Grid Connected PV System for Residential Applications," in *2019 4th International Conference on Power Electronics and their Applications (ICPEA)*, 2019, pp. 1-6.
- [6]. F. Sedaghati, A. Nahavandi, M. A. Badamchizadeh, S. Ghaemi, and M. Abedinpour Fallah, "PV Maximum Power-Point Tracking by Using Artificial Neural Network," *Mathematical Problems in Engineering*, vol. 2012, p. 506709, 2012/03/01 2012.
- [7]. S. Zhang and Y. Tang, "Optimal schedule of grid-connected residential PV generation systems with battery storages under time-of-use and step tariffs," *Journal of Energy Storage*, vol. 23, pp. 175-182, 2019/06/01/ 2019.
- [8]. M. K. A. Rödl , H. Schaumburg, "Strategy For A Large Scale Introduction Of Solar Energy In Central Asia," *MANAS Journal of Engineering* vol. 5, pp. 48-56, 2017.
- [9]. M. S. Aygen and M. İnci, "Zero-sequence current injection based power flow control strategy for grid inverter interfaced renewable energy systems," *Energy Sources, Part A: Recovery, Utilization, and Environmental Effects*, pp. 1-22, 2020.
- [10]. G.-Y. Choe, J. Kim, H.-S. Kang, and B.-K. Lee, "An Optimal Design Methodology of an Interleaved Boost Converter for Fuel Cell Applications," *Journal of Electrical Engineering & Technology* vol. 5, pp. 319-328, 2010.
- [11]. M. Elsied, A. Oukaour, H. Chaoui, H. Gualous, R. Hassan, and A. Amin, "Real-time implementation of four-phase interleaved DC–DC boost converter for electric vehicle power system," *Electric Power Systems Research*, vol. 141, pp. 210-220, 2016/12/01/ 2016.
- [12]. M. İnci, "Performance Analysis of T-type Inverter Based on Improved Hysteresis Current Controller," *Balkan Journal of Electrical and Computer Engineering*, vol. 7, pp. 149-155, 2019.
- [13]. J. Seok and A. Parastar, "Modeling and Control of the Average Input Current for Three-Phase Interleaved Boost Converters," *IEEE Transactions on Industry Applications*, vol. 51, pp. 2340-2351, 2015.
- [14]. R. Seyezhai and B. L. Mathur, "Design and implementation of interleaved boost converter for fuel cell systems," *International Journal of Hydrogen Energy*, vol. 37, pp. 3897-3903, 2012/02/01/ 2012.
- [15]. F. Slah, A. Mansour, M. Hajer, and B. Faouzi, "Analysis, modeling and implementation of an interleaved boost DC-DC converter for fuel cell used in electric vehicle," *International Journal of Hydrogen Energy*, vol. 42, pp. 28852-28864, 2017/11/30/ 2017.
- [16]. P. Thounthong, P. Sethakul, S. Rael, and B. Davat, "Design and Implementation of 2-Phase Interleaved Boost Converter for Fuel Cell Power Source," in *2008 4th IET Conference on Power Electronics, Machines and Drives*, 2008, pp. 91-95.
- [17]. R. Saadi, M. Y. Hammoudi, O. Kraa, M. Y. Ayad, and M. Bahri, "A robust control of a 4-leg floating interleaved boost converter for fuel cell electric vehicle application," *Mathematics and Computers in Simulation*, vol. 167, pp. 32-47, 2020/01/01/ 2020.
- [18]. J. Choi, H. Cha, and B. Han, "A Three-Phase Interleaved DC–DC Converter With Active Clamp for Fuel Cells," *IEEE Transactions on Power Electronics*, vol. 25, pp. 2115-2123, 2010.
- [19]. D. S. G. Krishna and M. Patra, "Modeling of multi-phase DC-DC converter with a compensator for better voltage regulation in DC micro-grid application," in *2016 International Conference on Signal Processing*,

- Communication, Power and Embedded System (SCOPEs), 2016, pp. 989-994.
- [20]. M. Rezvanyvardom, E. Adib, and H. Farzanehfard, "New interleaved zero-current switching pulse-width modulation boost converter with one auxiliary switch," IET Power Electronics, vol. 4, pp. 979-983, 2011.
- [21]. J. Cubas, S. Pindado, and C. De Manuel, "Explicit Expressions for Solar Panel Equivalent Circuit Parameters Based on Analytical Formulation and the Lambert W-Function," Energies, vol. 7, pp. 4098-4115, 2014.
- [22]. S. Motahhir, A. El Hammoumi, and A. El Ghzizal, "The most used MPPT algorithms: Review and the suitable low-cost embedded board for each algorithm," Journal of Cleaner Production, vol. 246, p. 118983, 2020/02/10/ 2020.
- [23]. A. Loukriz, M. Haddadi, and S. Messalti, "Simulation and experimental design of a new advanced variable step size Incremental Conductance MPPT algorithm for PV systems," ISA Transactions, vol. 62, pp. 30-38, 2016/05/01/ 2016.
- [24]. S. Sakulchotruangdet and S. Khwan-on, "Three-phase Interleaved Boost Converter with Fault Tolerant Control Strategy for Renewable Energy System Applications," Procedia Computer Science, vol. 86, pp. 353-356, 2016/01/01/ 2016.
- [25]. M. Nabil, S. M. Allam, and E. M. Rashad, "Modeling and design considerations of a photovoltaic energy source feeding a synchronous reluctance motor suitable for pumping systems," Ain Shams Engineering Journal, vol. 3, pp. 375-382, 2012/12/01/ 2012.
- [26]. M. Büyük, A. Tan, M. Tümay, and K. Ç. Bayındır, "Topologies, generalized designs, passive and active damping methods of switching ripple filters for voltage source inverter: A comprehensive review," Renewable and Sustainable Energy Reviews, vol. 62, pp. 46-69, 2016/09/01/ 2016..



Synthesize of montmorillonite supported hydroxyapatite and determination of adsorption capacity by tetracycline removal

Pelin Demirci

Kimya Mühendisliği Bölümü, Mühendislik Fakültesi, Yalova Üniversitesi, Yalova, Türkiye, pepin.demircivi@yalova.edu.tr,
ORCID: 0000-0002-1068-9310

ABSTRACT

In this study, removal of organic pollutants in wastewater using HA/MMT composite material was studied. Tetracycline (TC) antibiotic was used as an organic pollutant. HA/MMT composites were synthesized in a ball mill at different ratios (1:1, 1:2 and 2:1). The synthesis time was fixed at 5 hours. As a result of the experiments, it was concluded that 1:2 ratio of HA/MMT composite has the highest adsorption capacity (147 mg g^{-1}) among the others. The isotherm experiments showed that the Langmuir isotherm model was compatible with the experimental data, and the maximum adsorption capacity was obtained as 150 mg g^{-1} , which indicated that TC was adsorbed to create a monolayer coverage on HA/MMT adsorption sites. In the light of kinetic data, pseudo-second-order kinetic model was the best suitable model for TC adsorption; moreover the calculated adsorption capacity ($q_e = 227.27 \text{ mg g}^{-1}$) was found suitable with experimental ($q_e = 223.47 \text{ mg g}^{-1}$). In addition, it has been observed that intra-particle diffusion takes place as a rate-determining step. It has been concluded that TC adsorption of HA/MMT composite was an endothermic ($\Delta H^\circ = +39.85 \text{ kJ mol}^{-1}$) and spontaneous process thermodynamically. It has been concluded that the synthesized HA/MMT composite has high adsorption capacity and can be used for the removal of organic pollutants such as TC from wastewater.

ARTICLE INFO

Research article

Received: 14.09.2022

Accepted: 12.12.2022

Keywords:

Hydroxyapatite,
montmorillonite,
clay composites,
removal of antibiotics

1. Introduction

Tetracycline (TC) is an antibiotic with broad-spectrum antimicrobial activity. Therefore, it is a type of antibiotic frequently used in the treatment of both human and animals [1]. TC, which is not fully metabolized in human and animal bodies, can easily penetrate into soil and water system. Antimicrobial resistance occurs with the increasing amount of TC in the environment and this situation is reflected in the food chain and causes environmental effects [2]. Therefore, TC removal from wastewater is of great importance.

Conventional methods for wastewater treatment are not sufficient for the removal of antibiotics. Therefore, advanced treatment methods are used in the treatment of wastewater. Adsorption is a widely used treatment method among advanced treatment methods with its low cost, high efficiency and easy applicability, which has also some disadvantages such as waste production and low selectivity [3]. Materials such as activated carbon, polymeric materials, clay, and biochar have been used as adsorbent in the removal of TC from wastewater [4-6].

Hydroxyapatite (HA) is a calcium phosphate material with the chemical formula $\text{Ca}_{10}(\text{PO}_4)_6(\text{OH})_2$. HA is a chemically

stable, low-solubility and non-toxic material with having high porosity. In addition, it is used in adsorption studies due to its high adsorption capacity [7]. Active adsorption sites on HA are cationic and anionic Ca^{2+} and PO_4^{3-} groups. The disadvantage of using HA in treatment processes is its low reusability due to its low mechanical strength. Various materials such as clay, chitosan, and carbon nanotubes are added to its structure to increase its mechanical strength [8-10]. Clay minerals are preferred due to their low cost, non-toxicity, and high adsorption capacity [11, 12]. Ofudje et al. (2021) studied removal of nickel using nano-rod hydroxyapatite, which was synthesized via thermal decomposition method. Adsorption studies showed that maximum removal of Ni^{2+} was found 183 mg g^{-1} while thermal decomposition temperature was 900°C [13]. Peng et al. (2023) investigated adsorption of Cu^{2+} by hydroxyapatite synthesized from marble sludge. Eco-friendly hydroxyapatite was synthesized by hydrothermal method and maximum adsorption capacity was achieved 256 mg g^{-1} [14]. Wei et al. (2021) examined adsorption of tannic acid by hydroxyapatite with a maximum adsorption capacity of 95 mg g^{-1} [15]. According to a brief literature research, hydroxyapatite and its clay modification form has not been used for removal of antibiotics from aqueous solution.

In this study, HA/MMT adsorbent was synthesized by adding montmorillonite (MMT) clay into the HA structure and used for TC removal. The effects of adsorbent amount, pH, contact time and temperature on TC removal were studied. In the light of the obtained data, adsorption capacity, kinetic and isotherm models were obtained and the adsorption mechanism was clarified.

2. Materials and methods

Montmorillonite (MMT) was received from Kalemaden Ceramic Factory at Canakkale (The chemical composition of MMT: SiO₂: 71%, Al₂O₃: 16%, TiO₂: 0.2%, Fe₂O₃: 1.5%, CaO: 2%, MgO: 2%, Na₂O: 1%, K₂O: 0.5%). The HA used in the experiments was obtained from Xi'an Realin Biotechnology. The HA used has a purity of 99% and the impurities in its structure are indicated in Table 1. All the reagents were in analytical grade.

Table 1. Impurities in the HA structure

Sulphate (%)	Chloride (%)	Heavy metals (mg L ⁻¹)
<0,048	<0,05	<10

Composites containing HA and MMT in different ratios (1:1, 1:2 and 2:1) were prepared. HA/MMT composites were obtained by grinding in a ball mill for 5 hours. In order to determine the amount of adsorbent and HA/MMT ratio to be used in the experiments, 1-30 mg of HA/MMT composites were weighed and shaken in an orbital shaker for 24 hours with 25 mL of 20 mg L⁻¹ TC solution. pH experiments were carried out using the determined HA/MMT ratio and adsorbent amount. In order to determine the most suitable pH value for TC adsorption, the pH value of the TC solution was adjusted between 2-12 using 0.1 M HCl and 0.1 M NaOH solutions. The determined amount of HA/MMT composite and 25 mL of 20 mg L⁻¹ TC solution was shaken in an orbital shaker for 24 hours. In contact time trials, samples were collected and analyzed between 0-300 min. In order to determine the thermodynamic parameters, adsorption experiments were carried out at 25, 35 and 45 °C. Samples taken at the end of all experiments were first filtered through a filter with a pore diameter of 0.45 µm and spectrophotometric measurements were made by UV-visible spectrophotometer (Shimadzu UV-Vis-1800) at 360 nm, the highest wavelength of the TC solution. Arithmetically averaging of triplicate experiments were utilized to fit

adsorption curves. Adsorption capacity was calculated using Eq.1 from obtained data.

$$q_e = \frac{C_o - C_e}{m} xV \quad (1)$$

Here, q_e is the adsorption capacity at equilibrium (mg g⁻¹), C_o and C_e are the TC concentration at initial and equilibrium (mg L⁻¹), m is the amount of adsorbent (g), and V is the solution volume.

3. Results and discussion

3.1. Effect of HA/MMT ratio and adsorbent amount on TC adsorption

In order to examine the effect of HA and MMT on TC adsorption, composites containing HA and MMT in 1:1, 1:2 and 2:1 ratios were synthesized. Experiments were carried out using 25 mL of 20 mg L⁻¹ TC solution and the amount of adsorbent was used between 1-30 mg. In Figure 1, the adsorption capacity and adsorption efficiency values against the amount of adsorbent were shown. According to Figure 1, the adsorption efficiency increased with the increase in the amount of adsorbent. Adsorption efficiency of 27%, 32% and 23% for 1 mg adsorbent amount was obtained for composites containing HA and MMT at 1:1, 1:2 and 2:1 ratios, while these values were 80%, 91% and 71%, respectively, for 30 mg adsorbent amount. Since the increase in the amount of adsorbent causes an increase in the adsorption surface, it also causes an increase in the active adsorption sites where TC adsorption will take place, and TC adsorption increases. In addition, the appropriate amount of adsorbent to be used in the experiments was determined as 20 mg, and the adsorption capacities were obtained as 24, 26 and 21 mg g⁻¹, respectively, against the amount of adsorbent. The reason for choosing the appropriate amount of adsorbent as 20 mg is that there is no change in adsorption efficiency despite increasing the amount of adsorbent and the adsorbent cannot adsorb more TC. Therefore, 20 mg adsorbent amount was used for all three adsorbents in the experiments.

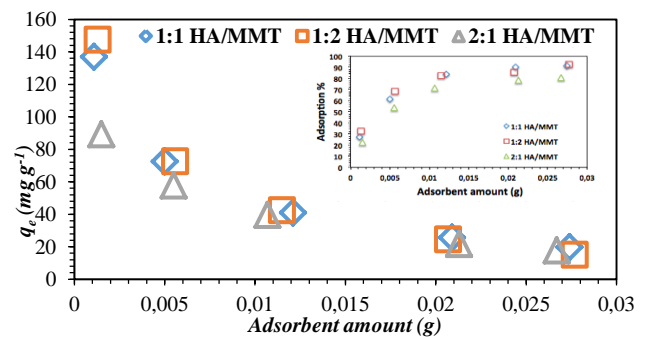


Figure 1. Adsorption capacity and adsorption efficiency against the amount of adsorbent belonging to different HA/MMT ratios

When HA/MMT ratios were compared, the highest yield was obtained at 1:2 ratio (91%), while lower adsorption efficiency was obtained at 1:1 and 2:1 ratios (80% and 71%), respectively. Since TC has both positive and negative sites due to its structure, it was concluded that adsorption occurred with electrostatic interaction on the MMT surface and hydroxyl (-OH), calcium (Ca^{2+}) and phosphate (PO_4^{3-}) groups in the HA structure were also effective in adsorption. 1:2 HA/MMT adsorbent, where the highest adsorption efficiency was obtained, was used in parameter trials.

3.2 Effect of pH on TC adsorption

One of the most important parameters affecting the adsorption is the pH value of the solution, as it causes changes in both the adsorbate types and the surface properties of the adsorbent. The initial solution pH values of 25 mL of 20 mg L^{-1} TC solution were changed in the range of 2-12 and adsorption experiments were carried out using $20 \text{ mg HA/MMT}(1:2)$ adsorbent. As a result of the experiments, it was observed that the highest removal was realized around pH 6 and the adsorption efficiency was obtained as 95% at this pH value (Figure 2). While the adsorption efficiency in strongly acidic solution (pH=2) was 67%, respectively, it was observed that it decreased to 49% in strongly basic area (pH=12). The adsorption capacity was obtained as 19 mg g^{-1} and 20 mg g^{-1} at pH 2 and 12, respectively. At pH 6, where the highest removal was achieved, the adsorption capacity was 26 mg g^{-1} .

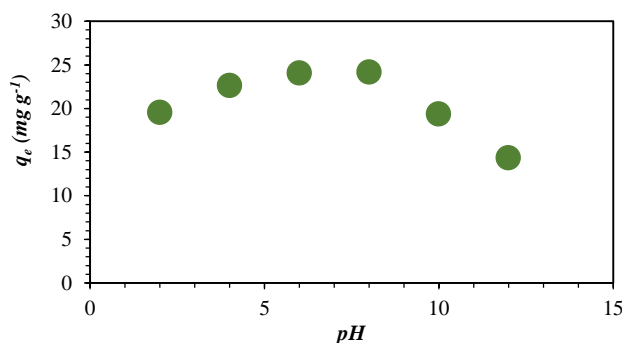


Figure 2. Effect of solution pH value on TC adsorption

In TC aqueous solution, it can exist in different structural forms depending on the pH of the solution. TC has three different dissociation constants; these are designated as $pK_{a1}=3.3$ (dimethylamino group), $pK_{a2}=7.3-7.7$ (phenolic diketone group), and $pK_{a3}=9.1-9.7$ (tri-carbonylamide group) [4]. While the cationic TC form (TCH_3^+) is dominant in the aqueous solution at pH 3.3, it comes to the TCH_2^\pm form where the positive and negative charge density is equal between pH 3.3-7.7. In the basic environment where the pH value is higher than 7.7, TCH^- and TC_2^- forms are present in the aqueous solution as negatively charged ions [16, 17]. In the light of this information, at pH 6, where the highest removal is achieved, C contains both positive and negative

charges and it is known that the total charge density is zero. The isoelectric point for HA/MMT adsorbent is around 6.6. The HA/MMT adsorbent is positively charged when the solution pH is lower than the isoelectric point, and negatively charged when it is higher. The adsorption value was found to be low, as there would be an electrostatic repulsion force between the positively charged adsorbent and the positively charged TC molecule (TCH_3^+) in an acidic environment. Adsorption increased when the pH value was around the isoelectric point. In this region, TC is in the TCH_2^\pm structure in aqueous solution and adsorption takes place by electrostatic attraction between its charged groups and HA/MMT adsorbent. In addition, TC, which has high hydrophobicity, can be adsorbed on the adsorbent surface with the hydrophobic interactions it will form. In basic media, adsorption decreases partially due to the repulsive force between the negatively charged adsorbent surface and TCH^- and TC_2^- molecules [18].

3.3 Adsorption isotherm

Adsorption isotherms were created to determine the TC adsorption capacity of HA/MMT adsorbent. As indicated in Figure 3, while the adsorption capacity of the 1:2 ratio HA/MMT composite was the highest (147 mg g^{-1}), the lowest adsorption capacity was obtained at the 2:1 HA/MMT ratio (89 mg g^{-1}). Experimentally obtained data were analyzed using Langmuir, Freundlich and Temkin isotherm models and the mechanism of TC adsorption at the solid/liquid interface was revealed.

Langmuir isotherm model assumes that the adsorption occurs on homogenous surface sites on the adsorbent and monolayer coverage occurs on the same adsorption energy sites. The linear form of the Langmuir isotherm equation is given in Eq. (2);

$$\frac{C_e}{q_e} = \frac{1}{Qb} + \frac{C_e}{Q} \quad (2)$$

where q_e is the amount of TC adsorbed at equilibrium (mg g^{-1}), C_e is the equilibrium TC concentration in the solution (mg L^{-1}), Q is the monolayer capacity of the adsorbent (mg g^{-1}) and b is the Langmuir adsorption constant (L mg^{-1}).

Freundlich isotherm model takes place on heterogeneous surface sites with non-uniform distribution of sorption heat. Multilayer coverage occurs on heterogeneous surface sites. The linear form of the Freundlich isotherm equation is given in Eq. (3);

$$\log q_e = \log K_f + \frac{1}{n} \log C_e \quad (3)$$

where q_e is the amount of TC adsorbed at equilibrium (mg g^{-1}), C_e is the equilibrium TC concentration in the solution (mg L^{-1}), K_f is Freundlich constant related to the adsorption

capacity ($L g^{-1}$) and n is the Freundlich constant related to adsorption intensity.

Temkin isotherm model describes linear decline of adsorption heat instead of logarithmic decline. Linearized form of Temkin isotherm expressed as (4);

$$q_e = \frac{RT}{b} \ln K_t + \frac{RT}{b} \ln C_e \quad (4)$$

where q_e is the amount of boron adsorbed at equilibrium ($mg g^{-1}$), C_e is the equilibrium boron concentration in the solution ($mg L^{-1}$), K_t is the equilibrium binding constant ($L g^{-1}$), b is the Temkin constant, R is the ideal gas constant and T is the temperature.

According to the obtained data, when the correlation coefficients (R^2) of the studied models were compared, it was found that the Langmuir isotherm model (0.98) was compatible with TC adsorption (Table 2). In this case, it was concluded that the TC molecule was adsorbed on the HA/MMT surface as a single layer. It was concluded that the maximum adsorption capacity ($150 mg g^{-1}$) obtained from Table 2. Isotherm models of different HA/MMT ratios

Adsorbent	Langmuir isotherm			Freundlich isotherm		Temkin isotherm			
	Q_m ($mg g^{-1}$)	b	R^2	K_F ($mg g^{-1}$)	n	R^2	K_t ($L g^{-1}$)	b	R^2
1 HA : 1 MMT	138,89	0,0153	0,97	11,292	1,13	0,98	0,0005	0,045	0,91
1 HA : 2 MMT	150,00	0,1782	0,85	3,285	0,74	0,88	0,0012	0,030	0,86
2 HA : 1 MMT	100,11	0,0019	0,93	3,548	0,87	0,95	0,0012	0,048	0,99

Electrostatic and hydrophobic interactions dominate the adsorption of the TC molecule on the HA/MMT surface, while hydrogen bonds are also effective in TC adsorption. The oxygen atoms in the carboxyl and hydroxyl groups in the TC structure provide the formation of dipole-dipole H bonds on the HA/MMT surface. In addition, Si-OH, Al-OH groups and Ca-OH, P-OH groups in the HA/MMT structure play an important role in TC adsorption [23, 24].

3.4 Adsorption kinetics

In order to examine the adsorption kinetics, samples were taken at different time intervals (0-300 min) and a graph of adsorption capacity at equilibrium was obtained (Figure 4). It was observed that the adsorption on the HA/MMT (1:2) surface of the TC molecule reached equilibrium in 180 minutes. In the first 120 minutes, the TC molecule was adsorbed on the HA/MMT surface rapidly, while the amount of adsorption did not change at the end of 180 minutes. In the first 120 minutes, when rapid adsorption is observed, empty adsorption sites are quickly filled with TC molecules, and as the time progresses, the adsorption capacity decreases as all of the adsorption sites are filled.

the Langmuir isotherm model was in agreement with the experimentally obtained data ($147 mg g^{-1}$). Moreover, tetracycline adsorption capacity of 1:2 HA/MMT was much higher than $32 mg g^{-1}$ on illite [19], $140 mg g^{-1}$ on rectorite [20], $4 mg g^{-1}$ on kaolinite [21] and $11 mg g^{-1}$ on MMT-biochar [22].

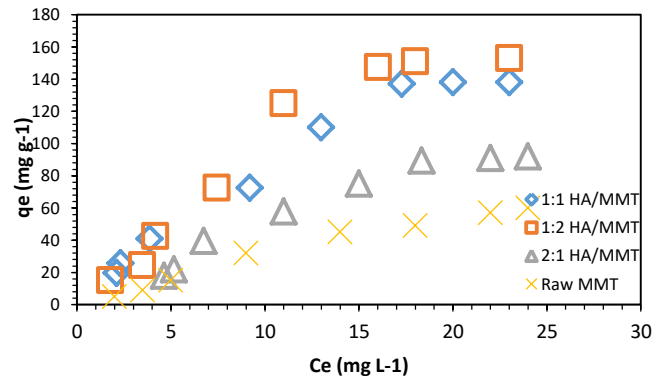


Figure 3. Isotherm plot of different HA/MMT ratios

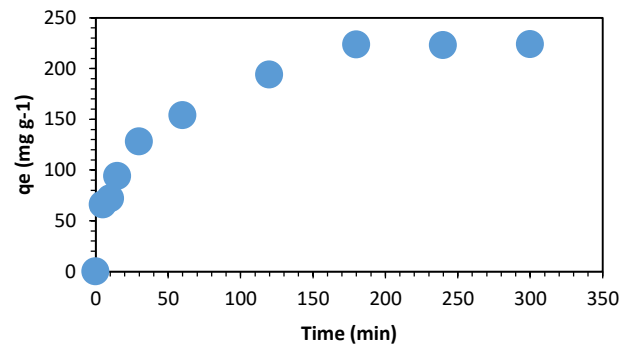


Figure 4. Variation of HA/MMT adsorption capacity versus time Pseudo-first-order, pseudo-second-order kinetic models and intra-particle diffusion model were applied to analyze the kinetic data. The pseudo-first order rate equation of Lagergren is given in Eq. (5);

$$\log(q_e - q_t) = \log q_e - \frac{k_1}{2.303} t \quad (5)$$

where q_e and q_t are the amounts of adsorbed TC at equilibrium and at time t (mg g^{-1}) and k_1 is the pseudo-first-order rate constant (min^{-1}).

The pseudo-second-order rate equation is given in Eq. (6);

$$\frac{t}{q_t} = \frac{1}{k_2 q_e^2} + \frac{1}{q_e} t \tag{6}$$

where q_e and q_t are the amounts of adsorbed TC at equilibrium and time t (mg g^{-1}) and k_2 is the pseudo-second-order rate constant ($\text{g mg}^{-1} \text{min}^{-1}$).

The intra-particle diffusion model is given in Eq. (7);

$$q_t = k_{int} t^{1/2} + c \tag{7}$$

where q_t is the amount of adsorbed TC at time t (mg g^{-1}), k_{int} is the intra-particle-diffusion rate constant ($\text{mg g}^{-1} \text{min}^{-1/2}$), t is the time (min) and c is the intercept (mg g^{-1}).

The parameters of the kinetic models are given in Table 3. When the correlation coefficients (R^2) are compared, it is seen that the correlation coefficient (0.99) of the pseudo-second-order kinetic model is considerably higher than (0.91) of the pseudo-first-order kinetic model. In addition, it was concluded that the adsorption capacity calculated using the kinetic model ($q_e = 227.27 \text{ mg g}^{-1}$) was compatible with the experimentally obtained adsorption capacity ($q_e = 223.47 \text{ mg g}^{-1}$). With the intra-particle diffusion model, the mass transfer mechanism of the TC molecule from the liquid phase to the HA/MMT surface has been elucidated. According to the intra-particle diffusion model, TC adsorption consists of two steps. In the first step, diffusion of the TC molecule from the liquid phase to the HA/MMT outer surface (border layer diffusion) takes place. The second step involves diffusion and adsorption of the TC molecule into the pores on the HA/MMT surface. One of these two steps can control TC adsorption kinetically. When the k_{int1} and k_{int2} rate constants of intra-particle diffusion are compared, it is seen that the k_{int2} rate constant is much lower than the k_{int1} rate constant. Accordingly, it was concluded that intra-particle diffusion is the rate-determining step in TC adsorption [25].

Table 3. Isotherm models of TC adsorption of HA/MMT adsorbent

Pseudo first order kinetic model		
k_1 ($L dk^{-1}$)	q_e ($mg g^{-1}$)	R^2
$2,55 \cdot 10^{-2}$	25,73	0,92
Pseudo second order kinetic model		
k_2 ($g mg^{-1} dk^{-1}$)	q_e ($mg g^{-1}$)	R^2
$2,93 \cdot 10^{-3}$	227,27	0,99
Intraparticle diffusion model		
k_{int1} ($g mg^{-1} dk^{-1}$)	c	R^2
2,43	200,58	0,99
k_{int2} ($g mg^{-1} dk^{-1}$)		
0,36		

3.5 Adsorption thermodynamics

The adsorption of the TC molecule on the HA/MMT surface was investigated at different temperatures (25, 35 and 45 °C) and thermodynamic parameters were calculated from the data obtained (Table 4). Change in standard enthalpy (ΔH°) was calculated according to Van't Hoff equation;

$$\ln \left(\frac{C_{e2}}{C_{e1}} \right) = \frac{\Delta H^\circ}{R} \left(\frac{1}{T_2} - \frac{1}{T_1} \right) \tag{8}$$

Change in standard Gibbs free energy (ΔG°) was given as;

$$\Delta G^\circ = -RT \ln K \tag{9}$$

$$K = \frac{C_{ads}}{C_e} \tag{10}$$

Change in standard entropy (ΔS°) was calculated;

$$\Delta G^\circ = \Delta H^\circ - T \Delta S^\circ \tag{11}$$

Positive ΔH° value indicates that TC adsorption occurs endothermically. The fact that the ΔH° value is lower than 40 kJ mol^{-1} indicates that physical adsorption has taken place [26]. A positive ΔS° value indicates an increase in disorder at the solid/liquid interface. The negative Gibbs free energy (ΔG°) at all temperatures indicates that TC adsorption occurs spontaneously. The ΔG° value decreases as the temperature increases. This shows that the TC molecule meets the energy required to increase its diffusion and adsorb onto the HA/MMT surface [27].

Table 4. Thermodynamic parameters of HA/MMT adsorbent for TC adsorption

T	ΔH	ΔG	ΔS
---	------------	------------	------------

(K)	(kJ mol ⁻¹)	(kJ mol ⁻¹)	(J mol ⁻¹ K ⁻¹)
298		-5.49	
308	39.85	-6.61	0.165
318		-8.26	

3.6 Reusability of the adsorbent

Adsorbent stability tests were performed for 180 min using HA/MMT. At the end of each cycle, the adsorbent was separated, washed with distilled water and adsorption test was repeated at the same conditions. After third cycle, tetracycline degradation was decreased to 75%, while it was 96% for the first cycle (Fig. 5). Tetracycline adsorption after third cycle remained constant at around 64% and a decreased was observed at third cycle that could be cause of occupation of active adsorption sites by TC.

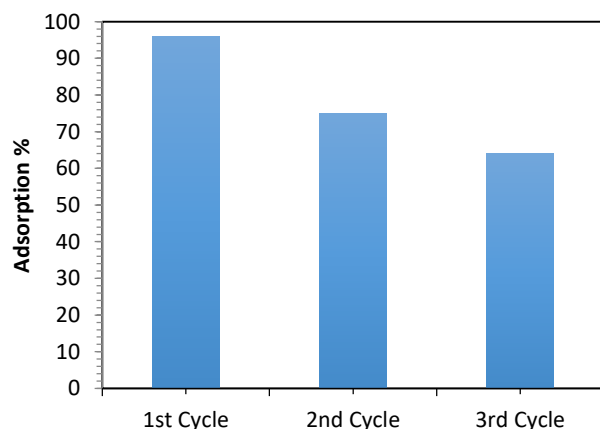


Figure 5. Reusability of 1:2 HA/MMT adsorbent

4. Conclusion

As a result of the study, it has been shown that HA/MMT adsorbent can be synthesized and used effectively in the adsorption of TC antibiotic from aqueous solutions. 1:1, 1:2 and 2:1 HA/MMT composites were synthesized and isotherm experiments were showed that 1:2 HA/MMT composite exhibited the highest adsorption capacity (147 mg g⁻¹). Moreover, the results of isotherm models were proved that 1:2 HA/MMT composition has the adsorption capacity of 150 mg g⁻¹ indicated more adsorption sites than among the other composites. As a result of kinetic models it was found that the pseudo-second order kinetic model was in agreement with the experimental data of TC adsorption ($R^2=0.99$). Thermodynamic analysis was showed that TC adsorption was a spontaneous endothermic process. It was concluded that the adsorption of the TC molecule on the HA/MMT surface occurs through electrostatic interactions, hydrophobic interactions and H-bonds. As a result of the study, it could be stated that HA-supported adsorbents can be

used effectively in the removal of antibiotics such as TC from wastewater.

References

- [1]. Chopra I., Roberts M., "Tetracycline antibiotics: Mode of action, applications, molecular biology, and epidemiology of bacterial resistance", *Microbiology and Molecular Biology Reviews*, 65, (2001), 232–260.
- [2]. Chang P.H., Jiang W.T., Li Z., Jean J.S., Kuo C.Y., "Antibiotic tetracycline in the environments-a review", *Journal of Pharmaceutical Analysis*, 4, (2015), 86-111.
- [3]. Aarab N., Hsini A., Laabd M., Essekre A., Laktif T., Ait Haki M., Lakhmiri R., Albourine A., "Theoretical study of the adsorption of sodium salicylate and metronidazole on the PANi", *Materials Today: Proceedings*, 22, (2020), 100–103.
- [4]. Anton-Herrero R., Garcia-Delgado C., Alonso-Izquierdo M., Garcia-Rodriguez G., Cuevas J., Eymar E., "Comparative adsorption of tetracyclines on biochars and stevensite: Looking for the most effective adsorbent", *Applied Clay Science*, 160, (2018), 162-172.
- [5]. Yeşilova E., Osman B., Kara A., Özer E.T., "Molecularly imprinted particle embedded composite cryogel for selective tetracycline adsorption", *Separation and Purification Technology*, 200, (2018), 155-163.
- [6]. Acosta R., Fierro V., Martínez de Yuso A., Narbalatz D., Celzard A., "Tetracycline adsorption onto activated carbons produced by KOH activation of tyre pyrolysis char," *Chemosphere*, 149, (2016), 168–176.
- [7]. Ragab A., Ahmed I., Bader D., "The removal of brilliant green dye from aqueous solution using nano hydroxyapatite/chitosan composite as a sorbent," *Molecules*, 24, (2019), 847.
- [8]. Le V.T., Doan V.D., Nguyen D.D., Nguyen H.T., Ngo Q.P., Tran T.K.N., Le H.S., "A novel cross-linked magnetic hydroxyapatite/chitosan composite: Preparation, Characterization, and Application for Ni(II) Ion Removal from Aqueous Solution", *Water, Air and Soil Pollution*, 229, (2018), 101.
- [9]. Cziko M., Bogy E.S., Paizs C., Katona G., Konya Z., Kukovecz Á., Barabás R., "Albumin adsorption study onto hydroxyapatite-multiwall carbon nanotube based

- composites”, *Materials Chemistry and Physics*, 180, (2016), 314–325.
- [10]. Hokkanen S., Doshi B., Srivastava V., Puro L., Koivula R., “Arsenic (III) removal from water by hydroxyapatite-bentonite clay-nanocrystalline cellulose”, *Environmental Progress and Sustainable Energy*, 38, (2019), 13147. ^[1]_[SEP]
- [11]. Zabihi O., Ahmadi M., Nikafshar S., Chandrakumar Preyeswary K., Naeb M., “A technical review on epoxy-clay nanocomposites: Structure, properties, and their applications in fiber reinforced composites”, *Composites Part B: Engineering*, 135, (2018), 1–24.
- [12]. El Ouardi M., Laabd M., Abou Oualid H., Brahmi Y., Abaamrane A., Elouahli A., Ait Addi A., Lakinifli A., “Efficient removal of p-nitrophenol from water using montmorillonite clay: insights into the adsorption mechanism, process optimization, and regeneration”, *Environmental Science and Pollution Research*, 26, (2019), 19615–19631.
- [13]. Ofudje E.A., Adedapo A.E., Oladeji O.B., Sodiya E.F., Ibadin F.H., Zhang D., “Nano-rod hydroxyapatite for the uptake of nickel ions: Effect of sintering behaviors on adsorption parameters”, *Journal of Environmental Chemical Engineering*, 9, (2021), 105931.
- [14]. Peng S.Y., Lin Y.W., Lee W.H., Lin Y.Y., Hung M.J., Lin K.L., “Removal of Cu²⁺ from wastewater using eco-hydroxyapatite synthesized from marble sludge”, *Materials Chemistry and Physics*, 293, (2023), 126854.
- [15]. Wei W., Li J., Han X., Yao Y., Zhao W., Han R., Li S., Zhang Y., Zheng C., “Insights into the adsorption mechanism of tannic acid by a green synthesized nano-hydroxyapatite and its effect on aqueous Cu(II) removal”, *Science of Total Environment*, 778, (2021), 146189.
- [16]. Leeson L.J., Krueger J.E., Nash R.A., “Concerning the structural assignment of the second and third acidity constants of tetracycline antibiotics”, *Letters Tetrahedron*, 4, (1963), 1155–1160.
- [17]. Chen Y., Wang F., Duan L., Yang H., Gao J., “Tetracycline adsorption onto rice husk ash, an agricultural waste: Its kinetic and thermodynamic studies”, *Journal of Molecular Liquids*, 222, (2016), 487–494.
- [18]. Laabd M., Brahmi Y., El Ibrahim B., Hsini A., Toufik E., Abdellaoui Y., Abou Oualid H., El Ouardi M., Albourine A., “A novel mesoporous hydroxyapatite@montmorillonite hybrid composite for high-performance removal of emerging ciprofloxacin antibiotic from water: Integrated experimental and Monte Carlo computational assessment”, *Journal of Molecular Liquids*, 338, (2021), 116705.
- [19]. Chang P.H., Li Z., Jean J.S., Jiang W.T., Wang C.J., Lin K.H., “Adsorption of tetracycline on 2:1 layered non-swelling clay mineral illite”, *Applied Clay Science*, 67-68, (2012), 158-163.
- [20]. Chang P.H., Jean J.S., Jiang W.T., Li Z., “Mechanism of tetracycline sorption on rectorite”, *Colloids and Surfaces A*, 339, (2009), 94-99.
- [21]. Li Z., Schulz L., Ackley C., Fenske N., “Adsorption of tetracycline on kaolinite with pH-dependent surface charges”, *Journal of Colloid and Interface Science*, 351, (2010), 254-260.
- [22]. Borthakur P., Aryafard M., Zara Z., David R., Minofar B., Das M.R., Vithanage M., “Computational and experimental assessment of pH and specific ions on the solute solvent interactions of clay-biochar composites towards tetracycline adsorption: Implications on wastewater treatment”, *Journal of Environmental Management*, 283, (2021), 111989.
- [23]. Afzal M.Z., Yue R., Sun X.F., Song C. Wang S.G., “Enhanced removal of ciprofloxacin using humic acid modified hydrogel beads”, *Journal of Colloid and Interface Science*, 543, (2019), 76–83.
- [24]. Parker H.L., Hunt A.J., Budarin V.L., Shuttleworth P.S., Miller K.L., Clark J.H., “The importance of being porous: polysaccharide-derived mesoporous materials for use in dye adsorption,” *RSC Advances*, 2, (2012), 8992.
- [25]. Laabd M., El Jaouhari A., Bazzaoui M., Albourine A., El Jazouli H., “Adsorption of benzene-polycarboxylic acids on the electrosynthesized polyaniline films: ^[1]_[SEP]Experimental and DFT calculation,” *Journal of Polymers and Environment*, 25, (2017), 359–369.
- [26]. Peng X., Hu F., Dai H., Xiong Q., Xu C., “Study of the adsorption mechanisms of ciprofloxacin antibiotics onto graphitic ordered mesoporous carbons”, *Journal of Taiwan Institute of Chemical Engineers*, 65, (2016), 472–481. ^[1]_[SEP]
- [27]. Abdellaoui Y., Abou Oualid H., Hsini A., El Ibrahim B., Laabd M., El Ouardi M., Giacomán-Vallejos G.,

Gamero-Melo P., “Synthesis of zirconium- modified Merlinoite from fly ash for enhanced removal of phosphate in aqueous medium: Experimental studies

supported by Monte Carlo/SA simulations”, *Chemical Engineering Journal*, 404, (2021), 126600.



Solidification of tannery sludge with various binders

Feride Ulu

Gebze Technical University, Environmental Engineering Department, 41400, Gebze-Kocaeli, Turkey, fulu@gtu.edu.tr,
ORCID: 0000-0002-9495-3958

ABSTRACT

The treatment of tannery sludge is an issue that has received considerable attention due to the potential of tannery sludge to cause severe environmental damage. In this study, the solidification process of the waste sludge of the Istanbul Tannery Organize Industry Wastewater Treatment Plant was investigated for safe disposal. The solidification technique was applied using various binders and their different mixtures, such as active carbon, gypsum ($\text{CaSO}_4/2\text{H}_2\text{O}$), fly ash, lime (CaO), zeolite, and different cement-sand mixtures on the laboratory scale. The essential parameters such as TOC, fluoride (F^- mg/l), chloride (Cl^- mg/l), sulfate (SO_4^{2-} mg/l), chromium (VI) (Cr^{6+} mg/l), and ammonium (NH_4^+ mg/l) were determined after solidification process at certain conditions. The analysis results of treated sludge samples were compared to the criteria for storage in the landfills in the Hazardous Waste Control Regulation (HWCR) as well as cost-calculation was done at optimum conditions. After the addition of 10% wt. CaSO_4 in the solidification study, the eluate concentration of TOC, Cl^- and SO_4^{2-} was below the limit values. When tannery sludge was solidified using CaO , the necessary criteria could not be obtained. On the other hand, with the addition of 33% CaO and 5% AC mixture TOC and AOX were observed below the limit values. The solidification was occurred with mortar + portland cement and 5% activated carbon additives and the desired limit values in HWCR were succeeded for all parameters. Besides, with the addition of 30% zeolite, all parameters declined below the limit values.

ARTICLE INFO

Research article

Received: 26.10.2022

Accepted: 16.12.2022

Keywords:

Tannery sludge,
tannery industry,
solidification,
stabilization.

1. Introduction

Tannery industry wastewaters have severe hazards to the environment due to their high concentration of suspended solids, organic matter (COD and BOD values), inorganic compounds such as chlorides, sulfides, nitrogen-containing compounds (ammonia, nitrites, and nitrates), toxic metals complexes, especially chromium (used as tanning agent) and deep color content [1]. Generally, conventional processes such as adsorption [2], biological process [3,4], and advanced processes [5, 6, 7], etc. are carried out to remove these pollutants from tannery industry wastewaters. Tanneries in Europe usually discharge their wastewater effluents to large wastewater treatment plants. In contrast, in developing countries, those effluents are directly discharged without treatment into surface waters, rivers, lakes, and marine ecosystems [1]. Because of the widespread use of leather around the world, the sustainable management of produced wastewater and waste sludge from the tannery industry need to be highlighted more.

The tanning operation results in a high amount of waste sludge which is known a threat to the ecological biota [8].

Especially, the metal-containing sludges in tannery are one of the primary environmental problems due to the leaching of toxic metals into surface and groundwater. Since each wastewater treatment plant has different features, the character and amount of sludge produced change. Also, each country has different regulations regarding the utilization and/or safe disposal of tannery wastewater sludge. Because of these reasons, the optimal sludge utilization/application methods solution would differ from case to case.

In the literature, various techniques such as landfill, composting, anaerobic digestion [9], thermal treatment [10], aerobic stabilization and compaction and drying [11], pyrolysis [12], solidification and stabilization (S/S) process [13,14] for utilization and/or safe disposal of waste sludge have been studied.

S/S technologies use binders and additives to reduce pathogens, liquid volume, offensive odors, the mobility and toxicity of the pollutants in waste sludge, and transform a final product before its reuse or disposal in a landfill [15, 16].

Solidification refers to techniques that mechanically bind the waste and solidification reagents using organic and inorganic binders such as polyesters and epoxy resins; lime, gypsum, or zeolites, respectively [15, 17]. It does not necessarily involve a chemical interaction between the contaminants and the solidifying additives. On the other hand, stabilization refers to techniques that chemically reduce the hazard potential of waste by converting the contaminants into less soluble, mobile, or toxic forms. The stabilization mechanism of a solidified matrix can be chemisorption, adsorption, ion exchange, precipitation, surface complexation, passivation, chemical incorporation, and inclusion [15, 13].

In addition, as mentioned above, the other most common methods of sludge stabilization are biological processes of anaerobic mesophilic digestion and aerobic digestion under ambient conditions.

The aim of this study is to research the most appropriate solidification process for the waste sludge of the Istanbul Tannery Organize Industry Wastewater Treatment Plant, in order to make the waste sludge comply with the criteria for storage in the landfills in the Hazardous Waste Control Regulation. Different substances such as active carbon,

gypsum ($\text{CaSO}_4/2\text{H}_2\text{O}$), fly ash, lime (CaO), zeolite, and different cement-sand mixtures were used for the solidification process on the laboratory scale. Besides, the cost analysis of the solidification process was done.

2. Materials and experimental procedure

2.1. Materials

The wastewater of all facilities in the Istanbul Leather Organized Industrial Zone is collected with a closed sewage system and treated at the Istanbul Tannery Organize Industry Wastewater Treatment Plant, before discharging.

Sludges were collected in the form of filter cakes from the Istanbul Tannery Organize Industry Wastewater Treatment Plant. The samples were taken from the outlet of the dewatering unit (belt press) and primary and secondary settling outlets. Two different commercial types of cement, mortar (MC) and Portland (PC) cement, $\text{CaSO}_4/2\text{H}_2\text{O}$, CaO , fly ash (FA), and zeolite as additives were used to perform the solidification process of the tanning sludge. Table 1 shows composition of MC and PC.

Table 1 Composition of MC and PC

Additive	TOC [mg/L]	AOX [mg/L]	F ⁻ [mg/L]	Cl ⁻ [mg/L]	pH	Conductivity [$\mu\text{S}/\text{cm}$]
MC	<10	<0.02	<2	0	13	9670
PC	<10	<0.02	<2	0	13.3	14430

2.2. Characterization of the tannery sludge leachate

Turkish environmental regulations made the leaching test obligatory according to DIN 38414-S4 Standard [18]. The standard states that 100 g of dry waste sample is extracted by shaking with 1 liter of distilled water for 24 hours. After extraction, the solid and liquid phases are separated from

each other by centrifugation or filtration method. The composition of sludge was analyzed according to the criteria of HWCR for safe disposal. Table 2 shows the analysis results of the tannery waste sludge eluate.

Table 2 Comparison of eluate analysis results of tannery sludge sample with the criteria of HWCR

1.1.1. Parameter / Sample	26.08.2021	07.09.2021	20.09.2021	10.10.2021	HWCR Hazardous Waste
pH	8.00	7.7	7.45	7.92	4 – 13
TOC, mg/l	823	403.5	550	393	40 – 200
Arsenic (As mg/l)	0.008	0.005	0.003	<0.003	0.2 – 1
Lead (Pb mg/l)	1.17	0.95	0.146	<0.1	0.4 – 2
Cadmium (Cd mg/l)	< 0.02	< 0.02	<0.02	<0.02	0.1 – 0.5
Chromium (VI) (Cr ⁶⁺ mg/l)	0.1	0.5	0.081	0.15	0.1 – 0.5
Copper (Cu mg/l)	0.18	0.11	0.05	0.030	2 – 10
Nickel (Ni mg/l)	0.2	0.16	0.064	0.0760	0.4 – 2
Mercury (Hg mg/l)	0.001	0.0015	<0.0001	0.001	0.02 – 1
Zinc (Zn mg/l)	0.51	0.35	0.406	0.225	2 – 10
Phenols (C ₆ H ₅ OH mg/l)	1.25	0.32	12.22	1.31	20 – 100
Fluoride (F ⁻ mg/l)	73.8	13.5	38.57	5.6	10 – 50
Ammonium (NH ₄ ⁺ mg/l)	178	129.7	257	146	200 – 1000
Chloride (Cl ⁻ mg/l)	1437	1527	1644	1133	1200 - 6000
Cyanide (CN ⁻ mg/l)	0.13	0.12	<0.05	<0.05	0.2 - 1
Sulfate (SO ₄ ⁼ mg/l)	90	21.4	152	342	200 – 1000
Nitrite (NO ₂ ⁻ mg/l)	0.13	0.18	0.082	0.013	6 – 30
(AOX mg/l)	2.09	1.25	1.09	1.25	0.6 – 3

2.3. Mixture preparation and characterization

Tannery sludge and the additives such as active carbon, gypsum (CaSO₄/2H₂O), fly ash, lime (CaO), cement, and zeolite were mixed in different proportions by following the addition of water to form homogenous mixtures. Mixing was carried out on a rotary mixer with a capacity of 3 to 5 kg per charge. After mixing, each mixture was placed in a tray 30 cm long, 24 cm wide, and 6 cm high. Afterward, they were weighed and left for 28 days under room temperature and humidity conditions. After 28 days of curing, the mixtures were weighed again. The leachate characteristics, TOC, chromium (Cr⁶⁺), fluoride (F⁻), chloride (Cl⁻ mg/l), sulphate (SO₄⁼ mg/l), and AOX, after each solidification experiment were determined for all the cured mixtures.

2.4. Analytical methods

The concentration of metals was determined by Flame Atomic Absorption Spectrophotometry, using the Perkin-Elmer Analyst 800 instrument. The organic matter content was measured by the TOC- Shimadzu, Japan analyzer. Ammonium nitrogen, AOX, nitrite, and sulfate were measured in accordance to Standard Methods (APHA, 1999) [19].

3. Results

3.1. Solidification studies with CaSO₄ and fly ash

The reaction of waste sludge with water results in an excessive amount of halogenated organic compounds, chloride, fluoride, and total organic carbon which can pass into the liquid phase. These pollutants leaching can be prevented by an appropriate solidification process using a mixture of sludge and additives materials such as activated carbon, zeolite, CaSO₄.2H₂O (gypsum), fly ash, CaO, and cement.

The waste sludge was mixed with 4% and %10 of CaSO₄ and 10% of fly ash. The analysis results of the solidification processes at different ratios were given in Table 3. When the results were examined, it was seen that TOC, chloride, and fluoride parameters declined below acceptable values with %10 CaSO₄. It was observed that the concentration of SO₄ in the eluate was above the limit value. The lowest CaSO₄ concentration succeed in reducing fluoride and chlorine values below the limit values.

Table 3 Eluate composition of different solidification matrixes containing CaSO_4 and fly ash at different ratios

1.1.2. Parameter / Sample	Raw sample	4 wt.% CaSO_4	10 wt.% CaSO_4	10 wt.% Fly ash	Belt pres sludge	HWRC Hazardous Waste
26.08.2021						
TOC, mg/l	823	207	33	520	823	40 – 200
Fluoride, mg/l	73.8	<0.2	<0.2	13	73.8	10 – 50
Chloride, mg/l	1437	517	571	574	1437	1200 - 6000
Sulfate, mg/l	90	2010	1982	2182	90	200 – 1000
AOX, mg/l	2.09	1.11	0.07	1.37	2.09	0.6 – 3

3.2. Solidification study with CaO

As a result of the solidification study performed with the addition of 5%, 7%, and 10% CaO, it was observed that the eluate concentration of fluoride and ammonium parameters decreased at all applied rates, and the chloride parameter

declined below the limit values in the studies when 5% and 7% CaO were added, as seen in Table 4.

In addition, it was observed that the eluate concentrations of Cr^{6+} and total organic carbon parameters increased and exceeded the limit values.

Table 4 Eluate composition of solidification matrixes at different CaO ratios

1.1.3. Parameter / Sample	Raw sample	5 % CaO	7 % CaO	10 % CaO	Belt Pres Sludge	HWRC Hazardous Waste
07.09.2021						
TOC, mg/l	403.5	895	1732	1995	403.5	40 – 200
Fluoride, mg/l	13.5	<0.2	<0.2	<0.2	13.5	10 – 50
Chloride, mg/l	1527	732	1024	1395	1527	1200 – 6000
Sulfate, mg/l	21.4	58.2	101.6	97.6	21.4	200 – 1000
Cr^{+6} , mg/l	0.5	0.27	0.21	0.21	<0.01	0.1-0.5
Ammonium	129.7	28.4	42.4	43.2	129.7	200-1000

As shown in Table 5, the total organic carbon parameter, which increased as a result of the addition of CaO, could be reduced with the addition of 5% activated carbon.

Table 5 Eluate composition of solidification matrixes containing CaO and active carbon at different ratios

1.1.4. Parameter / Sample	Raw sample	8 % CaO	16 % CaO	33 % CaO	8 % CaO + 5 % active carbon	16 % CaO + 5 % active carbon	33 % CaO + 5 % active carbon	Belt Pres Sludge
20.09.2021								
TOC, mg/l	550	1075	950	750	800	400	275	550
AOX, mg/l	1.09	0.28	0.356	<0.02	<0.02	0.042	<0.02	1.09

3.3. Solidification study with different cement mixtures

Solidification results with different cement mixtures were shown in Table 6 and Table 7. Mörtel cement contains 10% cement and 90% sand by weight, while Portland cement contains 100% cement. Mörtel cement and portland cement

mixture were prepared as 75% Mörtel cement and 25% Portland cement. The cement and sand ratio of the mixture were 32.5% and 67.5%, respectively. The solidification process containing PC and MC could not achieve the limit value of TOC as 200 mg/l in the HWCR.

Table 6 Eluate composition of solidification matrixes containing MC and PC at different ratios

1.1.5. Para meter / Sample	Raw sample	16 % MC	33 % MC	50 % PC	16 % PC	33 % MC+PC	50 % MC+PC	Belt Press Sludge
20.09.2021								
TOC, mg/l	550	200	600	550	325	600	300	550
AOX mg/l	1.09	0.16	0.10	0.10	0.18	0.232	<0.02	1.09
Chloride, mg/l	1644	850	845	474	905	875	683	1644
Fluoride, mg/l	38.57	4.55	<2	12.5	<2	4.8	22.2	38.57

The literature states ordinary PC and sludge with certain other additive including fly ash or other aggregates improves the physical characteristics and decreases the leaching losses from the resulting solidified waste [20]. As seen in Table 7, in the study carried out with the addition of

16% mörtel+portland cement + 5% activated carbon, the solidification results comply with the limit values specified in HWCR.

Table 7 Eluate composition of solidification matrixes containing active carbon and Mörtel+Portland cement at different ratios

1.1.6. Para meter / Sample	Raw sample	16% MC+PC+ AC	33% MC+PC + 5% AC	16% MC+PC	33% MC+PC	Belt Press Sludge
20.09.2021						
TOC, mg/l	550	175	178	600	300	550
AOX mg/l	1.09	<0.02	0.218	0.232	<0.02	1.09
Chloride	1644	935	1000	875	683	1644
Fluoride	38.57	7.4	<2	4.8	22.2	38.57

The additives used in the study are cost-effective and widely available. Also, the equipment required for processing is simple to operate. The estimated cost for the solidification process using additives such as PC, MC, and AC is given below.

The additive of 16% includes 32.5% cement and 67.5% sand. The amount of additive content required for 200

tons/day of treatment sludge was 32 tons/day, and the amount of active carbon was 10 tons/day.

Cement amount= 32 ton/day x 0.325 = 10.4 ton/day

Sand amount = 32 ton/day x 0.675 = 21.6 ton/day

Active carbon amount = 10 ton/day

Cement cost= 10400 kg/day x 0.5 Euro/kg = 5200 Euro/day

Sand cost = 21.6 ton/day x 1.5 Euro/ton = 32 Euro/day
 Active carbon cost = 10 000 kg/day x 5 Euro/kg = 50 000 Euro/day
 Total cost = 5200 + 32 + 50 000 = 55 232 Euro/day

3.4. Solidification study with zeolite

As shown in Table 8, in the study carried out with the addition of 30% and 40% zeolite, the concentration of all

parameters declined above the limit values specified in HWRC. The estimated cost for the solidification process to be made by preparing a 30% zeolite mixture is given below.

Zeolite amount: 200 ton/day x 0.30 = 60 ton/day

Zeolite cost: 60 ton/day x 444 Euro/ton = 26 666 Euro/day

Table 8 Eluate composition of solidification matrixes containing zeolite at different ratios

1.1.7. Parameter /Sample	Raw sample	10 wt.% zeolite	20 wt.% zeolite	30 wt.% zeolite	40 wt.% zeolite	50 wt.% zeolite	Belt Press Sludge
10.10.2021							
TOC, mg/l	393	315	219	175	110	2	393
AOX mg/l	1.25	0.84	0.66	0.37	0.32	0.025	1.25
Chloride	1133	771	685	613	485	2	1133
Fluoride	5.6	4.4	4.5	3.8	3.7	0.35	5.6
Sulphate	342	371	220	199	18	4	342
Chromium ⁶⁺	0.15	<0.03	<0.03	<0.03	<0.03	<0.03	0.04

4. Conclusions

The solidification process converts the pollutants into an immobile phase and obtains easy handling. In the study, the solidification process using substances such as CaSO₄, fly ash, CaO, cement, and zeolite was applied to tannery sludge to find the most appropriate way to comply with the criteria for Storage in the Landfills in the Hazardous Waste Control Regulation. The efficiency of the process was determined in terms of halogenated organic compounds, chloride, fluoride, and total organic carbon concentration of leachate.

As a result of the study with the addition of CaSO₄, it was observed that all parameters, TOC, chloride, and fluoride declined below the limit value but the sulfate parameter reached above the limit values.

When the fly ash was used as an additive, a slight decrease was observed in the eluate concentrations of the chloride, TOC, and fluoride parameters, and an increase in concentration of the sulfate parameter exceeding the limit values was detected.

In the study conducted with CaO, it was observed that the concentration of the TOC parameter increased significantly, and concentrations of fluoride and chloride parameters declined below the limit values. But concentration of the chromium (Cr⁶⁺) parameter increased. In the experiments with CaO, 20% TOC removal was achieved in the study

with the addition of 5% activated carbon, but the removal at this rate was not successful in reaching the 200 mg/l level determined by HWCR for the TOC parameter.

In addition, in the solidification study performed with mortar + portland cement and 5% activated carbon additives, all parameters complied with the criteria of HWCR.

The active carbon seems to be a successful absorbent that can be incorporated into cement. Also, the zeolite is a suitable and cost-effective material to form a solid product for safe disposal. It is more economical than another alternative, the mixture of PC, CM, and AC. ent ripple and THD value are reduced by the IBC model.

References

- [1] Jallouli S., Wali A., Buonerba A., Zarra T., Belgiorno V., Naddeo V., & Ksibi M. "Efficient and sustainable treatment of tannery wastewater by a sequential electrocoagulation-UV photolytic process". Journal of Water Process Engineering, 38, (2020), 101642.
- [2] Mia A. S., Ahmad F., Rahman M. "Adsorption of chromium (Cr) from tannery wastewater using low-cost spent tea leaves adsorbent". Applied Water Science, (2018), 8(5), 1-7.

- [3] Zou X., Ma F., Yu J., Su Q., Gai L., Zhao W., & Xiao, S. "Pilot-scale Study on Removal of Pollutants in Tannery Wastewater and Sludge Reduction by Biological Synergist Effect". In IOP Conference Series: Earth and Environmental Science, 546 (3), (2020), 032041. IOP Publishing.
- [4] Tran L. L., Tran T. T., Nguyen B. D., & Nguyen T. T. P. "Study of the treatment of tannery wastewater after biological pretreatment by using electrochemical oxidation on BDD/Ti anode". Desalination and Water Treatment, 137, (2019), 194-201.
- [5] Isari, A. A., Mehregan M., Mehregan S., Hayati F., Kalantary R. R., & Kakavandi, B. "Sono-photocatalytic degradation of tetracycline and pharmaceutical wastewater using WO₃/CNT heterojunction nanocomposite under US and visible light irradiations: a novel hybrid system". Journal of hazardous materials, 390, (2020), 122050.
- [6] Rodriguez J., Ochando-Pulido J. M., & Martinez-Ferez A. "The effect of pH in tannery wastewater by Fenton vs. heterogeneous Fenton process". Chemical Engineering Transactions, 73, (2019), 205-210.
- [7] Mohammed K., Sahu O. "Recovery of chromium from tannery industry waste water by membrane separation technology: health and engineering aspects". Science African, 4, (2019), e00096.
- [8] Juel, M. A. I., Chowdhury, Z. U. M., & Ahmed, T. (2016, July). Heavy metal speciation and toxicity characteristics of tannery sludge. In AIP Conference Proceedings, 1754 (1),(2016), 060009. AIP Publishing LLC.
- [9] Mpofu A. B., Welz P. J., & Oyekola, O. O. "Anaerobic digestion of secondary tannery sludge: optimisation of initial pH and temperature and evaluation of kinetics". Waste and Biomass Valorization, 11(3), (2020), 873-885.
- [10] Kokkinos E., Proskynitopoulou V., & Zouboulis A. "Chromium and energy recovery from tannery wastewater treatment waste: Investigation of major mechanisms in the framework of circular economy". Journal of Environmental Chemical Engineering, 7(5), (2019), 103307.
- [11] Alibardi L., & Cossu R. "Pre-treatment of tannery sludge for sustainable landfilling". Waste Management, 52, (2016), 202-211.
- [12] Pietrelli L., Ippolito N., Reverberi, A., & Vocciante, M. "Heavy metals removal and recovery from hazardous leather sludge". Chemical Engineering, 76, (2019).
- [13] Arthy M., & Phanikumar B. R. "Solidification/stabilization of tannery sludge with iron-based nanoparticles and nano-biocomposites. Environmental Earth Sciences, 76(4), (2017), 1-17.
- [14] Lin H., Zeng L., Zhang P., Jiao B., Shiao Y., & Li D. "Solidification of chromium-containing sludge with attapulgite combined alkali slag". Environmental Science and Pollution Research, 29(9), (2022), 13580-13591.
- [15] Montañés M. T., Sánchez-Tovar R., & Roux M. S. "The effectiveness of the stabilization/solidification process on the leachability and toxicity of the tannery sludge chromium". Journal of Environmental Management, 143, (2014), 71-79.
- [16] Jayasankar R., & Mohan S. "Experimental studies on solidification and stabilization of tannery sludge". International Journal for Research in Applied Science and Engineering Technology, 6(4), (2018), 856-864.
- [17] Pantazopoulou E., Zebiliadou O., Mitrakas M., & Zouboulis A. "Stabilization of tannery sludge by co-treatment with aluminum anodizing sludge and phytotoxicity of end-products". Waste Management, 61, (2017), 327-336.
- [18] DIN 38 414 S4, German Standard Methods for Researching Water, Effluent Water and Sludge, Group S: Sludge and Sediments; Determining Leaching with Water (S4), (1984).
- [19] Rodger B., and Bridgewater L. "Standard Methods for the Examination of Water and Wastewater. 23rd edition". Washington, D.C.: American Public Health Association, (2017).
- [20] Juel Md A. I., Stabilization of Tannery Sludge Through Brick Production, Department of Civil Engineering Bangladesh University of Engineering and Technology, (2016).



Asymptotics of the solution of the hyperbolic system with a small parameter

Ella Abylaeva*, Asan omuraliev

Kyrgyz-Turkish Manas University, Department of Applied Mathematics and Informatics, Bishkek, Kyrgyz Republic, abylaeva.ella@gmail.com, ORCID: 0000-0002-8680-6675

ABSTRACT

Asymptotic study of singularly perturbed differential equations of hyperbolic type has received relatively little attention from researchers. In this paper, the asymptotic solution of the singularly perturbed Cauchy problem for a hyperbolic system is constructed. In addition, the regularization method for singularly perturbed problems of S. A. Lomov is used for the first time for the asymptotic solution of a hyperbolic system. It is shown that this approach greatly simplifies the construction of the asymptotics of the solution for singularly perturbed differential equations of hyperbolic type.

ARTICLE INFO

Research article

Received: 05-11-2021

Accepted: 08-08-2022

Keywords:

Asymptotics, singularly perturbed hyperbolic system, Cauchy problem

*Corresponding author

1. Introduction

As mentioned above, the asymptotic study of singularly perturbed problems of hyperbolic type has been studied not so much. Almost half of the researchers paid attention to the following equation:

$$\varepsilon^2(\partial_t^2 u - \partial_x^2 u) + \varepsilon^k a(x, t) \frac{\partial u}{\partial t} + b(x, t)u = f(x, t) \quad (A)$$

The case when $k = 0$ was studied in [1], where the asymptotics of the solution of the Cauchy problem and the mixed problem was constructed, which contains exponential and parabolic boundary layer functions.

The work [2] is devoted to the construction of the asymptotics of the solution to equation (A) in the case when the small parameter is absent at the time derivative and $a(x, t) = 0$. It is shown that the solution contains only a hyperbolic boundary layer.

The work [4] is devoted to the study of the boundary value problem for the equation:

$$\varepsilon^2(a(x)\partial_t^2 u - b(x)\partial_x^2 u) + u_x + u_t = 0,$$

here the second derivative of the solution to the degenerate equation has a discontinuity in the characteristic of the

boundary emerging from the corner point (0,0). This leads to the appearance of an inner transition layer. The smoothing procedure is used to construct the asymptotics of the solution.

The Darboux problem for equation (A) in the case $k = 0$ was studied in [6], where the asymptotics of the solution of the boundary layer type was constructed. The works [7] - [12] are devoted to systems of hyperbolic equations.

In [7], a system of two equations with constant coefficients is studied, one of the eigenvalues is equal to zero and has an inner transition layer in the vicinity of the discontinuity of the solution of the degenerate equation.

A feature of the system studied in [8], [9] is the fact that the small parameter $\varepsilon > 0$ in the first equation is contained in the derivative with respect to t , and in the second equation - in the derivative with respect to x . This leads to interesting features of the solution and its asymptotics as $\varepsilon \rightarrow 0$. In [9], the same problem with a nonlinear term is studied and an existence theorem for a classical solution is proved. As a result the asymptotic solution of arbitrary order with respect to a small parameter is constructed.

Papers [10] - [14] are devoted to the study of scalar and multidimensional systems of hyperbolic equations in the critical case. In [10] a formal asymptotic representation of the solution of an initial-boundary value problem for a

singularly perturbed system of first order partial differential equations with small nonlinearity is constructed. The aim of the work is to construct a formal asymptotic representation of the solution to the initial-boundary value problem.

The work [11] is devoted to the construction of an asymptotic expansion of the solution of the Cauchy problem for a singularly perturbed hyperbolic system of linear equations in the critical case. A feature of the problem is the presence of asymptotic terms described by parabolic equations. The degenerate solution has a discontinuity along the line due to the corner points of the boundaries. In the vicinity of such discontinuity lines, the solution has the character of a transition layer, the form of which can change depending on the initial setting.

In [12] a complete asymptotic expansion of the solution to the initial problem for a singularly perturbed hyperbolic system of equations was constructed and justified.

In the solution of this problem, splash zones arise, in the vicinity of which the asymptotics is described by a parabolic equation.

In [13] the boundary layer method is generalized to systems with an arbitrary number of spatial variables and the behavior of problem solving in the far field is described for large values of x, t .

The work [14] is devoted to the construction of an asymptotic expansion of the solution of the Cauchy problem for one class of hyperbolic weakly nonlinear systems with many spatial variables. A parabolic quasilinear equation is obtained, which describes the behavior of the solution for asymptotically large values of independent variables.

2. Asymptotic construction

2.1. Statement of the problem

In this work, we study the Cauchy problem for a hyperbolic system:

$$\begin{aligned} \varepsilon(\partial_t u + A(x)\partial_x u) + B(t)u &= f(x, t), \quad x \in \Omega, \\ u|_{t=0} &= u^0(x), \end{aligned} \tag{1}$$

where $\varepsilon > 0$ – is a small parameter, $\Omega = (0 \leq x \leq 1) \times (0 < t \leq T)$, $A(x), B(t), f(x, t)$ - are known.

The problem is solved under the following assumptions: $A(x) \in C^\infty([0,1], \mathbb{C}^{n \times n}), B(t) \in C^\infty([0, T], \mathbb{C}^{n \times n}), f(x, t) \in C^\infty(\bar{\Omega}, \mathbb{C}^n)$,

$$B(t)\psi_i(t) = \lambda_i(t)\psi_i(t), \operatorname{Re} \lambda_i(t) \geq 0, \lambda_i(t) \neq \lambda_j(t),$$

$$\forall i \neq j, \quad t \in [0, T], i, j = \overline{1, n}.$$

2.2. Regularization of the problem

Under such assumptions for the regularization of the problem (1) we introduce regularizing independent variables using methods described in [15]:

$$\xi_i = \frac{1}{\varepsilon} \varphi_i(t), i = \overline{1, n}, \varphi_i(0) = 0.$$

Here, for now, $\varphi_i(t)$ -is an arbitrary function that satisfies $\varphi_i(0) = 0$. Then for the extended function $\tilde{u}(x, t, \xi, \varepsilon)|_{\xi=\varepsilon^{-1}\varphi(t)} \equiv u(x, t, \varepsilon)$ we set the problem as:

$$\begin{aligned} T_0 \tilde{u} &\equiv \sum_{i=1}^n \varphi_i'(t) \partial_{\xi_i} \tilde{u} + B(t) \tilde{u} \\ &= f(x, t) - \varepsilon \partial_t \tilde{u} - \varepsilon A(x) \partial_x \tilde{u}, \\ \tilde{u}|_{\xi=0} &= c(x, t), c(x, t)|_{t=0} = u^0(x). \end{aligned} \tag{2}$$

2.3. Solution of iterative problems

The solution of this extended problem is determined in the form of a series:

$$\tilde{u}(x, t, \xi, \varepsilon) = \sum_{k=0}^{\infty} \varepsilon^k u_k(x, t, \xi). \tag{3}$$

On the basis of (2) for the coefficients of series (3) we obtain the following iterative problems:

$$\begin{aligned} T_0 u_0 &= f(x, t), \\ T_0 u_k &= -\partial_t u_{k-1} - A(x) \partial_x u_{k-1}, \\ u|_{\xi=0} &= d_0(x, t), d_0(x, 0) = u^0(x), \\ u_k|_{\xi=0} &= d_k(x, t), d_k(x, 0) \\ &= 0, \end{aligned} \tag{4}$$

here $d_k(x, t)$ – is an arbitrary function.

Where $T_0 \equiv \sum_{i=1}^n \varphi_i'(t) \partial_{\xi_i} + B(t)$, $k \geq 0$.

We introduce a class of functions in which the iterative problems (4) are solved:

$$U = \left\{ u(x, t, \varepsilon): u = \sum_{i=1}^n \left[\sum_{j=1}^n c_{ij}(x, t) \exp(-\xi_j) + v_{ii}(x, t) \right] \psi_i(t) \right\},$$

$c_{ij}(x, t), v_i(x, t) \in C^\infty(\bar{\Omega})$.

The vector function $\psi_i(t)$ included in U is an eigenvector of the matrix $B(t)$ which corresponds to the eigenvalue $\lambda_i(t)$ $i = \overline{1, n}$.

2.4. Solvability of intermediate tasks

Let the eigenvectors $\psi_i^*(t)$ of the matrix $B^*(t)$ – matrix is conjugate to $B(t)$ which corresponds to the eigenvalue $\bar{\lambda}_i(t)$:

$$B^*(t) \psi_i^*(t) = \bar{\lambda}_i(t) \psi_i^*(t), i = \overline{1, n},$$

moreover:

$$(\psi_i(t), \psi_j^*(t)) = \delta_{ij}, \quad i, j = \overline{1, n}.$$

The scalar product of elements $u \in U$ and elements $v \in U^*$ is conjugate space which is defined as:

$$\langle u, v \rangle = \sum_{i,j=1}^n u_{ij} \bar{v}_{ij} + \sum_{i=1}^n u_i \bar{v}_i.$$

Theorem 1. Suppose the above assumption and $H(x, t, \xi) \in U$ are satisfied. Then equation (5) is solvable

$$T_0 u(M) = H(M), \quad M = (x, t, \xi) \tag{4}$$

in U if and only if $H(x, t, \xi) \perp \text{Ker } T_0^*$.

Proof. With using the (6)

$$H(x, t, \xi) = \sum_{i=1}^n \left[\sum_{j=1}^n h_{ij}(x, t) \exp(-\xi_j) + h_i(x, t) \right] \psi_i(t), \tag{5}$$

and substituting the function $u(x, t, \xi) \in U$ into equation (5), with respect to $c_{ij}(x, t), v_i(x, t)$, we get:

$$\begin{aligned} & \sum_{ij=1}^n \{ -\varphi_j'(t) c_{ij}(x, t) + \lambda_i(t) c_{ij}(x, t) \} \exp(-\xi_j) \psi_i(t) \\ & + \sum_{i=1}^n v_i(x, t) \lambda_i(t) \psi_i(t) \\ & = \sum_{i,j=1}^n h_{ij}(x, t) \exp(-\xi_j) \psi_i(t) \\ & + \sum_{i=1}^n h_i(x, t) \psi_i(t). \end{aligned}$$

We choose a regularizing function in the form:

$$\varphi_j'(t) = \lambda_j(t), \quad \varphi_j(t) = \int_0^t \lambda_j(s) ds, \quad j = \overline{1, n},$$

then the previous ratio will be rewritten as:

$$\begin{aligned} & \sum_{i,j=1}^n (\lambda_i(t) - \lambda_j(t)) c_{ij}(x, t) \psi_i(t) \exp(-\xi_j) \\ & + \sum_{i=1}^n \lambda_i v_i(x, t) \psi_i(t) \\ & = \sum_{i,j=1}^n h_{ij}(x, t) \psi_i(t) \exp(-\xi_j) \\ & + \sum_{i=1}^n h_i(x, t) \psi_i(t). \end{aligned}$$

Multiplying the obtained relation by $\psi_i^*(t) \exp(-\xi_i) \in \text{Ker } (T_0^*)$, T_0^* is operator adjoint to T_0 . We will make sure

that the function $u(x, t, \xi) \in U$ is a solution of the equation

$$(5) \text{ for arbitrary } c_{ii}(x, t), \text{ if and only if } < H(x, t, \xi), \psi^*(t) \exp(-\xi_i) > \equiv 0 \Rightarrow h_{ii}(x, t) \equiv 0.$$

The theorem is proved.

Theorem 2. Suppose that the conditions of Theorem 1 are satisfied. Then equation (5) is uniquely solvable in U , which satisfying the following conditions:

$$u|_{t=\xi=0} = u^0(x), \quad < \partial_t u + A(x) \partial_x u, u_i^* > = 0, \\ i = \overline{1, n}. \tag{6}$$

Proof.

By Theorem 1 the function $u(x, t, \xi) \in U$ is the solution of equation (5) with an accuracy up to arbitrary functions $c_{ii}(x, t)$. Subjecting it to the initial conditions from (7), we define $c_{ii}(x, 0)$:

$$c_{ii}(x, 0) = (u^0(x), \psi_i^*(0)) - \sum_{j=1, i \neq j}^n c_{ij}(x, 0) - v_i(x, 0), \\ i = \overline{1, n}. \tag{7}$$

The second condition in (7) is written as:

$$\partial_t c_{ii}(x, t) + \sum_{k=1}^n \alpha_{ki}(x, t) \partial_x c_{kk}(x, t) + \sum_{k=1}^n \beta_{ki}(t) c_{kk}(x, t) = \rho_i(x, t), \tag{8}$$

where $\alpha_{ki}(x, t) = (A(x) \psi_k(t), \psi_i^*(t))$, $\beta_{ki}(t) = (\psi_k'(t), \psi_k^*(t))$, $\rho_i(x, t)$ – is a known function.

Having solved (8), (9) we uniquely define the function $u(x, t, \xi) \in U$.

The theorem is proved.

Applying Theorems 1 and 2, we successively determine the solutions of iterative problems (4).

2.5 Assessment of the remainder term.

Theorem 3. Suppose that the conditions of Theorems 1 and 2 are satisfied. For the remainder term $R_{\varepsilon n}(x, t, \xi)|_{\xi=\frac{\varphi(x)}{\varepsilon}} = u(x, t, \varepsilon) - \sum_{k=1}^n \varepsilon^k u_k(x, t, \xi)|_{\xi=\frac{\varphi(x)}{\varepsilon}}$ for sufficiently small $\varepsilon > 0$ the following estimate is fair:

$$\| R_{\varepsilon n} \left(x, t, \frac{\varphi(x)}{\varepsilon} \right) \| < c \varepsilon^{n+1}.$$

The proof of this theorem is based on the using of the energy integral [16].

3. Conclusion

The regularization method for singularly perturbed problems of S. A. Lomov was first used for the asymptotic solution of a hyperbolic system. By choosing a regularizing function as a solution of the Cauchy problem for a first-order partial differential equation, the process of constructing the asymptotic of a solution of any order of the problem is significantly simplified. This approach makes it possible to easily solve the studied problems in works [7]-[14].

References

- [1]. Su Yu-cheng, “Asymptotics of solutions of some degenerate quasilinear hyperbolic equations of the second order”, Reports of the USSR Academy of Sciences, 138(1), (1961), 63-66.
- [2]. Trenogii V. A., “On the asymptotics of solutions of quasilinear hyperbolic equations with a hyperbolic boundary layer”, Proceedings of the Moscow Institute of Physics and Technology, 9, (1962), 112-127.
- [3]. Butuzov V. F., “Angular boundary layer in mixed singularly perturbed problems for hyperbolic equations”, Mathematical Collection, 104(146), (1977), 460-485.

- [4]. Butuzov V. F., Nesterov A. V., “On some singularly perturbed problems of hyperbolic type with transition layers”, *Differential Equations*, 22(10), (1986), 1739–1744.
- [5]. Valiev M. A., “Asymptotics of the solution of the Cauchy problem for a hyperbolic equation with a parameter”, *Proceedings of the Moscow Energy Institute*, 142, (1972), 2-12.
- [6]. Abduvaliev A. O., “Asymptotic expansions of solutions of the Darboux problem for singularly perturbed hyperbolic equations”, *Fundamental Mathematics and Applied Informatics*, 1(4), (1995), 863–869.
- [7]. Vasileva A. B., “On the inner transition layer in the solution of a system of partial differential equations of the first order”, *Differential Equations*, 21, (1985), 1537-1544.
- [8]. Butuzov V. F., Karashchuk A. F., “On a singularly perturbed system of partial differential equations of the first order”, *Mathematical Notes*, 57(3), (1995), 338–349.
- [9]. Butuzov V. F., Karashchuk A. F., “Asymptotics of the solution of a system of partial differential equations of the first order with a small parameter”, *Fundamental and Applied Mathematics*, 6(3), (2000), 723–738.
- [10]. Nesterov A. V., Shuliko O. V., “Asymptotics of the solution of a singularly perturbed system of first order partial differential equations with small nonlinearity in the critical case”, *Journal of Computational Mathematics and Mathematical Physics*, 47(3), (2007), 438–444.
- [11]. Nesterov A. V., “Asymptotics of the solution of the Cauchy problem for a singularly perturbed system of hyperbolic equations”, *Chebyshev collection*, 12(3), (2011), 93–105.
- [12]. Nesterov A.V., “On the asymptotics of the solution of a singularly perturbed system of partial differential equations of the first order with small nonlinearity in the critical case”, *Journal of Computational Mathematics and Mathematical Physics*, 52(7), (2012), 1267-1276.
- [13]. Nesterov A. V., Pavlyuk T. V., “On the asymptotics of the solution of a singularly perturbed hyperbolic system of equations with several spatial variables in the critical case”, *Journal of Computational Mathematics and Mathematical Physics*, 54(3), 2014, 450-462.
- [14]. Nesterov A. V., “On the structure of the solution of one class of hyperbolic systems with several spatial variables in the far field”, *Journal of Computational Mathematics and Mathematical Physics*, 56(4), (2016), 639–649.
- [15]. Lomov S. A., *Introduction to the general theory of singular perturbations*, Moscow, USSR: Nauka, 1981.
- [16]. Mizohata S., *Theory of partial differential equations*, Moscow, USSR: Mir, 1977.



MJEN



Determining the factors affecting the happiness levels of divorced individuals by ordered logistics regression analysis

Burak Uyar^{1,*}, Cevdet Büyüksu²

¹Van Yüzüncü Yıl University, Faculty of Economics and Administrative Sciences, Department of Econometrics, Van, Turkey, burak.uyar@yyu.edu.tr, ORCID: 0000-0002-3178-4157

²Van Yüzüncü Yıl University, Graduate School of Natural and Applied Sciences, Department of Statistics, Van, Turkey, cevdet_buyuksu@hotmail.com, ORCID: 0000-0003-3448-3699

ABSTRACT

In cases where the dependent variable is categorical and ordinal, the Ordinal Logistic Regression Model is used for model estimation. In order to predict the Ordinal Logistic Regression Model, it must provide the parallel lines assumption. In the study, the happiness levels of divorced individuals were estimated with the ordinal logistic regression model. The data set used in the analysis was obtained from the Life Satisfaction Survey implemented by the Turkish Statistical Institute in 2020. Brant's Wald Test and Likelihood Ratio Test were applied for the parallel lines assumption and the null hypothesis could not be rejected. In this context, the model ordinal logistic regression model was estimated. The statistically significant gender variable shows that divorced women are happier than divorced men. It has been determined that success and job variables tend to decrease happiness levels in divorced individuals compared to other factors. In general, when the education level is examined, it is seen that the level of happiness of divorced individuals increases as the education level increases. It has been concluded that divorced individuals who are satisfied with their health, education, income and social life are happier than divorced individuals who are not satisfied with their health, education, income and social life. It has been determined that divorced individuals are registered with the Social Security Institution and their happiness levels are higher than those who are not registered.

ARTICLE INFO

Research article

Received: 9.10.2021

Accepted: 7.06.2022

Keywords:

Ordered logistic regression model,
parallel lines assumption,
life satisfaction research

1. Introduction

Some dependent variables encountered in data analysis can take categorical values. Many special statistical methods have been developed for the analysis of categorical data. Categorical data can be multi-class or ordered. The statistical method used when the dependent variable is categorical and ordinal is defined as the Ordered Logistic Regression Model.

The dependent variable, which is considered in many types of research and practices, can be in an ordinal structure. E.g.; There may be dependent variables in at least 3 categories such as life satisfaction level (dissatisfied, moderate, satisfied), happiness level (unhappy, moderate, happy), disease severity (mild, moderate) and in an ordered structure. In this case, the statistical method to be used should be determined as the Sequential Logistic Regression Model. In cases where the dependent variable is categorical and ordinal, using other regression models will result in erroneous results.

Sequential logistic regression models have been widely used in many fields such as medicine, economics, biology, zoology, education, and social sciences in recent years. In this study, the dependent variable was determined as the happiness levels of divorced individuals. In this context, some studies in the literature examining the factors that may affect the happiness or life satisfaction levels of individuals are as follows:

In Akın and Şentürk's studies; They used the 2007 European Quality of Life Survey dataset. They used happiness level as a dependent variable in the study, independent variables are Gender, Marital Status, Age, Educational Status, Occupational Status, Income, Work Sector, Lived Area/Settlement and Health. In the conclusion part of the study; it has been observed that as the income level increases, happiness also increases, students and retirees are generally happy, and individuals between the ages of 18-24 and 65 and over have a high level of happiness. In addition, the increase in the level of education caused a decrease in the level of happiness with the effect of not reaching the level of

welfare that the individual expected after a certain level [3].

In the works of Boxwood and Generous; They used the 2010 Life Satisfaction Survey data set. They used happiness level as a dependent variable in the study, independent variables are Income level, Employment, Employment status, Sector, Gender, Age, Marital status, and Settlement status. In the conclusion part of the study; It has been determined that those with low-income levels are less happy than those with high income, men are less happy than women, and individuals aged 65 and over are happier than other age categories. It has been concluded that married individuals are happier than individuals living separately. It has been determined that those living in the city are less happy than those living in the countryside. It was concluded that employment, job status and industry variables did not affect happiness [18].

In Bee and Star studies; They used the 2014 Life Satisfaction Survey data set. The level of happiness was taken as the dependent variable in the study. Independent variables; gender, marital status, last completed school, employment status, health, education, residence, income, social life, relations with relatives, relations with friends, relations with neighbors, health services, public order services, legal services, education services, SGK services, transportation services determined as satisfaction. In the study, the Proportional Ratio Model, the Non-Proportional Ratio Model and Partial Proportional Ratio Model, which are sequential logistic models, were applied and these models were compared in terms of goodness of fit. As a result of the application, it was found significant in all three models. However, although the Proportional Ratio Model was found to be significant, the Parallel Lines Assumption required for the use of this model was not provided. When the Non-proportional Ratio Model and Partial Proportional Ratio Model were evaluated in terms of goodness of fit criteria, it was determined that the Partial Proportional Ratio Model was the most suitable model for the data set [5].

In his study, Servet used the 2004 and 2014 Life Satisfaction Survey datasets. He used happiness level as a dependent variable in the study, independent variables are household income, age, gender, education level, health satisfaction, welfare level, and need satisfaction. In the study, the years 2004 and 2014 were examined comparatively. As a result of the analysis, it was determined that the happiness levels of men increased in the intervening time. It has been concluded that individuals are happier as they get older. It has been determined that the happiness levels of married individuals decrease over time [15].

Sönmez and Altınsu Sönmez used the World Values Survey (WVS) Turkey data set in their studies. They used life satisfaction as a dependent variable in the study, independent variables are happiness, age, gender, being married, number

of children, employment status, educational status, income status, skill, satisfaction with income, world citizen, social class, the importance of God, participation in religious services, destiny or control, cognitive task. In the study, individuals with high skills and higher income are less satisfied with life than individuals with no skills and low income. It has been determined that individuals with higher education levels, employed individuals and cognitively working individuals who believe that they shape their own destiny have higher life satisfaction. It has been determined that women have higher life satisfaction than men. It has been determined that individuals who participate in religious activities more frequently have higher life satisfaction than those who do not. In addition, it has been concluded that individuals with high social class are more satisfied with their lives than individuals with low social class. It is also among the results that the elderly people have higher life satisfaction than the young people [16].

Yılmaz used the 2018 Life Satisfaction Survey data set in his study. He used life satisfaction as a dependent variable in the study, and independent variables are happiness, employment status, marital status, and gender. In the study, it was concluded that individuals who are very happy and happy have higher life satisfaction than unhappy individuals. Another result obtained in the study is that working individuals have higher life satisfaction than non-working individuals [20].

Some studies in which life satisfaction or happiness levels were determined as dependent variables in the literature review and these dependent variables were estimated by ordinal logistic regression model are given above. The dependent variable in this study is the happiness levels of divorced individuals. No study has been found in the literature on the happiness levels of divorced individuals.

In the next part of the study, the ordinal logistic regression model, which is one of the logistic regression models and the analysis method of the study, is introduced in detail.

In the application part of this thesis, it is aimed to determine the factors affecting the happiness levels of divorced individuals. In the application section, the data set used in the analysis was introduced and descriptive statistics were given by the purpose. The results of the assumptions and estimation of the ordinal logistic regression model are also included in this section.

In the conclusion part of the study, a general evaluation was made and suggestions were made for future studies.

2. Materials and methods

2.1. Ordered logistic regression model

The ordinal logistic regression model is a logistic regression model used when the dependent variable has more than two categories and is sortable. Many examples such as satisfaction level (from dissatisfied to satisfied), happiness level (from unhappy to happy), disease severity (from least severe to most severe), and income level (from low to high) can be given to the dependent variable in the ordinal structure. Ordinal logistic regression is a logistic regression model used to model the relationship between categorical dependent variables in an ordinal structure and continuous or discrete independent variables. Assuming that the dependent variable in the ordinal structure has j categories, there are $j-1$ logistic model variations used to predict this model. This situation reveals whether the estimated regression coefficients and probability values differ according to the categories of the dependent variable of the model [10].

Since there is a hierarchy between the categories of the dependent variable in the ordinal logistic regression model, the model differs from the multinomial logistic regression model in this respect. Another difference between these two multi-category models concerns the selection of reference categories. In the multinomial logistic regression model, the reference category can be selected as any category of the dependent variable. However, since the ordinal logistic regression model uses the assumption that the categories of the dependent variable are parallel to each other, the reference category is usually determined as the reference category with the highest value [6].

Since non-linear models are used in models created with ordinal structure and categorical dependent variables, the Maximum Likelihood method is used when estimating the model. Odds (difference) ratios are generally used in the interpretation of the ordinal logistic regression model [14].

2.1.1. Hidden variable theory

In the ordinal logistic regression model, it is assumed that there is an unobserved latent variable y^* , which varies between $-\infty$ and $+\infty$, under the dependent variable y in the ordinal and categorical structure. The dependent variable y is shown in Eqn. 2.1 [13].

$$\text{When } y_i = j \text{ then } \tau_{j-1} \leq y_i^* < \tau_j \quad j = 1, 2, \dots, J \quad (2.1)$$

“ j ” indicates the category number of the dependent variable. τ represents the breakpoints or thresholds. i and J represent extreme categories. In this context, it is defined as $\tau_{j-1} =$

$\tau_0 = -\infty$ and $\tau_j = \tau_j = +\infty$ E.g.; Suppose that individuals' happiness levels are determined as an ordinal categorical variable. Suppose that happiness levels are divided into 5-point Likert-type categories as “1-Not at all happy”, “2-Not happy”, “3-Medium”, “4-Happy” and “5-Very happy”. This ordinal categorical dependent variable is assumed to be associated with a continuous latent variable y^* . The relationship between the observed y and the latent variable y^* is expressed as in Eq. 2.2 [13].

$$y_i^* = \begin{cases} 1 = \text{Hiçmutluedeğil} & \tau_0 = -\infty \leq y_i^* < \tau_1 \\ 2 = \text{Mutluedeğil} & \tau_1 \leq y_i^* < \tau_2 \\ 3 = \text{Orta} & \tau_2 \leq y_i^* < \tau_3 \\ 4 = \text{Mutlu} & \tau_3 \leq y_i^* < \tau_4 \\ 5 = \text{Çokmutlu} & \tau_4 \leq y_i^* < \tau_5 = +\infty \end{cases} \quad (2.2)$$

The relationship between the y categories observed from the y^* latent variable is shown in Figure 2.1 [13].

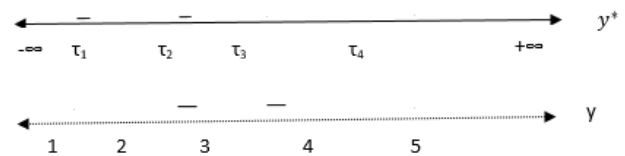


Figure 2.1 Obtaining y observed categories from the hidden variable y^*

The τ_j values shown in Figure 2.1 are the breakpoints. In the example, since the dependent variable has 5 categories, 4 cut-off points are calculated while creating the model. The cut-off point varies depending on the category number of the dependent variable. The number of breakpoints is one less than the number of categories of the dependent variable [11].

2.1.2. Distribution assumptions

The Maximum Likelihood method is used to estimate the model established with the latent variable y^* [13]. To use the Maximum Likelihood method, the error term must have a certain distribution. The logit model is used when the error term has a logistic distribution. The ordered logit model shows a logistic distribution with ε error term mean zero and variance $\pi^2/3$ [13]. The probability density function is shown in Eqn. 2.3.

$$f(\varepsilon) = \frac{e^{-\varepsilon}}{[1 + e^{-\varepsilon}]^2} \quad (2.3)$$

The cumulative distribution function is shown in Eqn. 2.4.

$$F(\varepsilon) = \frac{e^{-\varepsilon}}{1 + e^{-\varepsilon}} \quad (2.4)$$

2.1.3. The probabilities of the observed categories

After determining the distribution of the errors, the probabilities of the observed values of the dependent variable y can be calculated for the given values of the independent

variable x . The distribution of the latent variable for the three values of the independent variable x is shown in Figure 2.2.

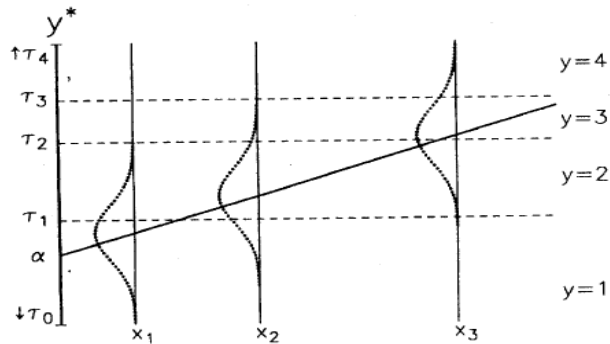


Figure 2. 2. Scatter plot of Hidden Variable (y^*) Given x Values for Ordinal Logistic Regression Model [13]

The errors are either logistic or normally distributed around the regression line $E(y^*|x) = \alpha + \beta x$. The probability of m corresponds to the area between the cut-off points τ_{j-1} and τ_j . For the probability of the first category of the categorical dependent variable in the ordinal structure, it is expressed as $\tau_0 = -\infty \leq y_i^* < \tau_1$ as shown earlier in Eqn. 2.2 where variable y^* is between τ_0 and τ_1 while $y=1$.

Here, if one independent univariate $y^* = \beta x + \varepsilon$ is substituted, Eqn. 2.5 is obtained [13].

$$P(y = 1|x) = P(\tau_0 \leq \beta x + \varepsilon < \tau_1|x) \quad (2.5)$$

Here, when βx is removed in the inequality, Eqn. 3.6 is obtained.

$$P(y = 1|x) = P(\tau_0 - \beta x \leq \varepsilon < \tau_1 - \beta x|x) \quad (2.6)$$

It is shown in Eqn. 2.7 that the probability of a random variable being between two values is equal to the difference between the cumulative distribution function evaluated at these values.

$$P((y = 1|x)) = P(\varepsilon_i < \tau_1 - \beta x|x) - P(\varepsilon_i < \tau_0 - \beta x|x) \\ F(\tau_1 - \beta x) - F(\tau_0 - \beta x) \quad (2.7)$$

In this context, the probability of the observed y dependent variable being in m th categories is shown in Eqn. 2.8 [9].

$$P(y = j) = F(\tau_j - \beta x) - F(\tau_{j-1} - \beta x) \quad (2.8)$$

The probability of the observed y dependent variable being in the last category is shown in Eqn. 3.9.

$$P(y = J) = F(\tau_J - \beta x) - F(\tau_{J-1} - \beta x) \quad (2.9)$$

Since $\tau_j = +\infty$ is in the $F(\tau_j - \beta x)$ term in Eqn. 2.9, it is taken as $F(\infty - \beta x) = 1$ [1].

2.2. Parallel Lines Conjecture and Test

The parallel lines assumption assumes that the determining regression coefficients are equal in all categories of the ordinal and categorical dependent variable [7]. If the parallel lines assumption is met, the relationship between the independent variables and the dependent variable does not change according to the categories of the dependent variable. In order to explain the parallel lines assumption, the cumulative probability model of the category with a level equal to or lower than j , which is the number of categories of the dependent variable, is shown in Eqn. 2.10 [13].

$$P(y \leq j|x) = F(\tau_j - \beta x) \quad (2.10)$$

The cumulative probability is the cumulative distribution function value in $\tau_j - \beta x$. Since β does not change according to the categories of the dependent variable, Eqn. 2.12 defines the models in which the dependent variable has two categories with different cut-off points. This situation is shown in Eqn. 2.11.

$$\tau_j - \beta x = (\tau_j - \beta_0) - \sum_{i=1}^N \beta_i x_i \quad i = 1, 2, \dots, Nj \\ = 1, 2, \dots, J \quad (2.11)$$

In this case, the model for $y \leq 1$ is shown in Eqn. 2.12 and for $y \leq 2$ in Eqn. 2.13.

$$P(y \leq 1|x) = F\left(\tau_1 - \beta_0 - \sum_{i=1}^N \beta_i x_i\right) \quad (2.12)$$

$$P(y \leq 2|x) = F\left(\tau_2 - \beta_0 - \sum_{i=1}^N \beta_i x_i\right) \quad (2.13)$$

When Eqn. 2.12 is examined, the model for $y \leq 1$ is with $\tau_1 - \beta_0$ the cut-off point, when Eqn. 2.13 is examined, the model for $y \leq 2$ is with $\tau_2 - \beta_0$ cut-off point. When the Eqn. 2.12 and Eqn. 2.13 equations are examined, and it is seen that the regression coefficients for the variable x_i with different cut-off points remain the same. The graphical representation of the parallel lines assumption for the change in the breakpoints is given in Figure 2.3.

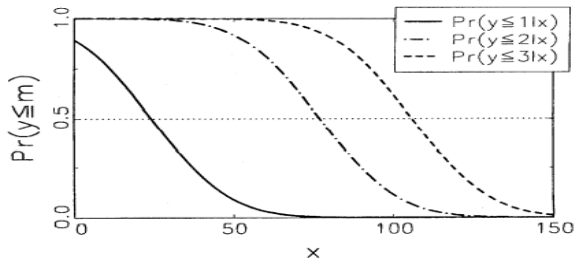


Figure 2.3. Graphical Representation of the Parallel Lines Conjecture

As seen in Figure 2.3, the change in the cut-off points shifts the probability curve to the right or left, but does not change the shape of the curve [13]. When Figure 2.3 is examined, it is seen that cumulative probability lines are belonging to 3 categories. In this case, since it is known that 1 more of the correct number in the graph gives the category of the dependent variable, it is concluded that the dependent variable consists of 4 categories. In Figure 2.3, probability 0.5 is shown with a horizontal line as the midpoint. At this point, Eqn. 2.14 is obtained when 3 probability curves are determined [13].

$$\frac{\partial(y \leq 1|x)}{\partial x} = \frac{\partial(y \leq 2|x)}{\partial x} = \frac{\partial(y \leq 3|x)}{\partial x} \quad (2.14)$$

Eq 2.14 shows that all regression lines are parallel.

The accuracy and reliability of the results obtained from the created model vary depending on whether the parallel lines assumption is provided or not. Therefore, the parallel lines assumption should be tested. To test this assumption, tests such as the Likelihood Ratio test and Brant's Wald Test are used. Under the assumption of parallel lines, hypotheses are established as shown in Eqn. 2.15 [17].

$$\begin{aligned} H_0: \beta_1 = \beta_2 = \dots = \beta_{j-1} = \beta \\ H_1: \text{Enaz bir } \beta \text{ farklıdır.} \end{aligned} \quad (2.15)$$

While the null hypothesis (H_0) in Eqn. 2.15 states that the regression coefficients in the model are the same in all categories of the dependent variable, the alternative hypothesis (H_1) states that the regression coefficients in the model differ in at least one category of the dependent variable.

2.2.1. Likelihood ratio (lr) test

The likelihood ratio test, which is used to test the parallel lines assumption, makes a constrained model estimation and shows how the likelihood function changes when these constraints are removed [7]. In other words, the likelihood ratio test measures the performance of the unconstrained model compared to the constrained model [19]. The proportional ratio model with parallel lines assumption is the restricted version of the non-proportional ratio model. The

likelihood of the proportional ratio model is expressed as LR, and the likelihood of the non-proportional ratio model is expressed as LUR. The likelihood ratio test statistic is shown in Eqn. 2.16.

$$LR = -2[\ln L_R - \ln L_{UR}] \quad (2.16)$$

The log-likelihood function of the $\ln L_R$ the constrained model given in Eqn. 2.16 is the log-likelihood function of the $\ln L_{UR}$ unconstrained model. For the LR test statistic, logarithmic transformation and multiplying with the value of -2 is to provide an approximate χ^2 distribution [4]. The degrees of freedom for the χ^2 distribution is $k(j-2)$. Here k represents the number of independent variables and j represents the category number of the dependent variable. The LR test statistic is compared with the χ^2 table value. If the LR test statistic is greater than the χ^2 table value, the H_0 hypothesis is rejected and it is concluded that at least one regression coefficient is different from the others. In this case, the assumption of parallel lines is not satisfied [4].

2.2.2. Brant's Wald test

With the Wald test developed by Brant, it is generally tested that the regression coefficients are equal in all categories of the dependent variable, and it is also shown which variable or variables break the parallel lines assumption [13]. Wald test statistics are obtained by the ratio of the coefficients of the predicted model to their standard errors [2]. The Wald test statistic fits the χ^2 distribution with 1 degree of freedom. The Wald test statistic is shown in Eqn. 2.17 [10].

$W = \frac{\hat{\beta}_i - \beta_0}{sh(\hat{\beta}_i)}$	(2.17)
---	--------

There is no definite information about which test should be used for the test of the parallel lines assumption, but it is stated that the Wald test proposed by Brant is slightly more powerful than the LR test [13].

2.3. Measuring goodness of fit in the ordered logistic regression model

The determination of how adequate and effective the model estimated in the regression analysis is in explaining the dependent variable can be measured by goodness-of-fit tests. By testing the goodness of fit of the model, it is aimed to obtain a statistical value representing all observation values. Measures such as the deviation measure and the so-called R^2 are used to test the goodness of fit of the model.

2.3.1. Deviance measure

One of the criteria used for the goodness of fit of the model is the measure of deviation. The deviation measure gives the

magnitude of the deviation from the actual values. The deviation measure is expressed as shown in Eqn. 2.18 [8].

$$D = -2(\ln L_M - \ln L_S) \tag{2.18}$$

The L_M is shown in Eqn. 2.18 represents the maximum likelihood value of any sub-model of the saturated model formed with the independent variables considered to be important, and L_S the maximum likelihood value of the saturated model. The small deviation measure is a condition that should be preferred for the goodness of fit of the model.

2.3.2. Pseudo R^2 value

The R^2 statistic is unsuitable for use with the logistic model. It may appear as a result of some logistic regression analysis but should be ignored. Because the R^2 value obtained in the logistic regression analysis does not give accurate information about the power of the independent variables to explain the dependent variable. Statisticians suggest pseudo- R^2 values suitable for logistic regression models. One of the so-called R^2 values developed for logistic regression models is the McFadden R^2 value developed by McFadden. Eqn. 2.19 is used to calculate the McFadden R^2 value [12].

$$R_{McFadden}^2 = 1 - (\ln L / \ln L_0) \tag{2.19}$$

L_0 given in Eqn. 2.19 represents the maximum likelihood value of the model with only the constant term, and L represents the maximum likelihood value of the model with both the constant term and the independent variables.

3. Application

In this study, data from the Life Satisfaction Survey (YMA) implemented by the Turkish Statistical Institute (TUIK) in 2020 were used. In practice, it was aimed to determine the factors affecting the happiness levels of divorced individuals who participated in the survey. The Ordered Logistic Regression Model was used in the study due to the nature of the dependent variable. The Chi-Square Independence test was applied to 18 variables that could affect the happiness levels of divorced individuals, and 9 statistically significant variables were determined as independent variables (Table 3.1).

Table 3.1 Chi-Square Test of Independence Results

Variable Name	Chi-Square Value	Likelihood	Relationship Status
Gender	6.6873	0.035**	Yes
Educational status	32.7106	0.036**	Yes
Working status	0.8401	0.657	No
How Happy	34.7413	0.000***	Yes
Health Satisfaction	30.5174	0.000***	Yes
Housing Satisfaction	2.2339	0.973	No
Neighborhood Satisfaction	3.9597	0.861	No
Education Satisfaction	26.9324	0.000***	No
Income Satisfaction	39.5058	0.000***	No
Social Life Satisfaction	43.4395	0.000***	No
Job Satisfaction	9.6103	0.293	No
Relative Satisfaction	6.0829	0.638	No
Friend Satisfaction	11.3570	0.182	No
Neighbor Satisfaction	7.3039	0.504	No
Workplace relationship satisfaction	7.7943	0.454	No
Future Life	6.8316	0.337	No
SSI Registration	18.8296	0.000***	Yes
Hope	1.2171	0.544	No

In practice, it is "happiness" in adaptation. Independent abilities; age, war, education status, what makes you happy, health, education, income, social environment, Social Security Institution (SGK) registration requests. Stata 15.0 statistical package program was used in the study. 10103 people participated in the 2020 Life Satisfaction Survey. By the purpose of the study, individuals who stated their marital status as divorced were selected from the individuals who participated in the survey. It has been determined that 364 divorced individuals participated in the survey.

3.1. Results

3.1.1. Descriptive Statistics

The frequency table of the variables used in the study is shown in Table 3.2.

Table 3. 2. Frequency table of variables

Variables	Number of Observations	Percentage (%)
Happiness		
1: Unhappy	98	26.92
2: Fair	159	43.68
3: Happy	107	29.40
Gender		
1: Male	134	36.81
2: Female	230	63.19
Education Status		
1: None	16	4.4
2: Primary School	119	32.69
3: Middle School	65	17.86
4: High School	88	24.18
5: College-University	63	17.31
6: Postgraduate	13	3.57
How Happy		
2: Success	23	6.32
3: Job	9	2.47
4: Health	252	69.23
5: Love	52	14.29
6: Money	25	6.87
98: Other	3	0.82
Health Satisfaction		
1: Satisfied	206	56.59
2: Fair	109	29.95
3: Dissatisfied	49	13.46
Education Satisfaction		
1: Satisfied	192	53.78
2: Fair	79	22.13
3: Dissatisfied	86	24.09
Income Satisfaction		
1: Satisfied	100	27.47
2: Fair	93	25.55
3: Dissatisfied	171	46.98
Social Life Satisfaction		
1: Satisfied	123	33.79
2: Fair	107	29.40
3: Dissatisfied	134	36.81
SSI Registration		
1: Yes	289	79.40

2: No	75	20.60
-------	----	-------

When Table 3.2 is examined, 26.92% of divorced individuals state that they are unhappy, 29.4% state that they are happy, and 43.68% state that they are moderately happy. It has been determined that 36.81% of divorced individuals participating in the Life Satisfaction Survey in 2020 are male and 63.19% are female. When the educational status of the divorced individuals participating in the survey was examined, it was determined that the individuals who did not complete a school were .4.4%, primary school graduates 32.69%, primary school graduates 17.86%, high school graduates 24.18%, college-faculty graduates 17.31% and postgraduate graduates 3.57%. In the question asked about what makes divorced individuals happy, 6.32% of divorced individuals state that they are a success, 2.47% work, 69.23% health, 14.29% love, 6.87% money and 0.82% other factors. While 56.59% of divorced individuals state that they are satisfied with their health, 13.46% state that they are not satisfied. While 53.78% of divorced individuals state that they are satisfied with the education they have received, 24.09% state that they are not satisfied. While 27.47% of divorced individuals state that they are satisfied with their monthly income, 46.98% state that they are not satisfied. While 33.79% of divorced individuals state that they are satisfied with their social life, 36.81% state that they are not satisfied. 79.4% of divorced individuals are registered with the Social Security Institution and 20.6% are individuals who are not registered with the Social Security Institution.

3.1.2. Ordinal logistic regression model prediction results

There are three assumptions to consider before using the ordinal logistic regression model. After the model estimation, there is no multicollinearity problem in the model, there is no specification error in the model, and the assumption of parallel lines is provided. First of all, there is no multicollinearity problem since there is no more than one continuous variable in the model created. After the created model was estimated with ordinal logistic regression, it was tested whether there was a specification error in the model with the link test, and the results are shown in Table 3.3.

H₀: The model has no specification errors.

H₁: The model has specification errors.

Table 3. 3. Link Test result

Variable	Test Statistics	Likelihood Value (p)
Hatsq	0.09	0.927

When Table 3.3 is examined, it is seen that the probability value of the Hatsq variable is 0.846. Since p>0.01, the coefficient of the Hatsq variable is not statistically significant and the null hypothesis cannot be rejected. In this case, there is no specification error in the model. Another and most important assumption of the ordinal logistic regression model is the parallel lines assumption. The parallel lines

assumption was tested with Brant's Wald test and likelihood ratio test, and the results are shown in Table 3.4.

H₀: The regression coefficients of the model are the same in each category of the dependent variable.

H₁: The regression coefficients of the model are different in at least one category of the dependent variable.

Table 3. 4 Parallel lines assumption test results

Tests	Test Statistics	Likelihood Value
Brant's Wald Test	14.07	0.170
Likelihood Ratio Test	15.55	0.113

When Table 3.4 is examined, it is seen that the probability values of all tests used to test the parallel lines assumption are $p > 0.01$. In this case, the null hypothesis cannot be rejected. It was concluded that the regression coefficients of the model were the same in each category of the dependent variable. In this context, it can be said that the parallel lines assumption is provided and the ordinal logistic regression model can be used in the analysis.

The model created to determine the factors affecting the happiness levels of divorced individuals was estimated by ordinal logistic regression and the results are shown in Table 3.5.

Table 3. 5. Sıralı Lojistik Regresyon Tahmin Sonuçları

Independent Variables	Coefficient	Odds Ratio	Likelihood Value (p)	Marginal Effects
Age	.0100864	1.010137	0.337	.0015753
Gender (Basic Level: Male) 2: Female	.6937311	2.001168	0.003***	.102536
How Happy (Basic level: Other) 2: Success 3: Work 4: Health 5: Love 6: Money	-2.821646 -3.526317 -1.095435 -1.19982 -1.923653	.0595079 .029413 .3343941 .3012484 .1460724	0.018** 0.011** 0.319 0.289 0.103	-.4406809 -.5507355 -.1710836 -.1873863 -.3004335
Education Status (Basic Level: Ph.D.) 2: Primary 31: General Middle School 32: Vocational or Technical Secondary School 33: Middle School 41: General High School	.5626191 .1898603 .8542974 .2199049 .6386383 .8276271 1.563182 .1824859 1.709674 .0816342	1.755264 1.209081 2.349723 1.245958 1.8939 2.287883 4.773987 1.200197 5.527161 1.085059	0.321 0.753 0.421 0.816 0.287 0.206 0.032** 0.772 0.080* 0.933	.0878691 .0296521 .133423 .0343445 .0997417 .1292577 .2441356 .0285004 .2670146 .0127495

42: Vocational or Technical High School 511: 2 or 3-year college 512: 4-year College or University 52: Master Degree 53: PhD				
Health Satisfaction (Basic Level: Dissatisfied) 1: Satisfied 2: Fair	1.144636 .386973	3.141297 1.472517	0.004*** 0.322	.1787677 .0604369
Education Satisfaction (Basic Level: Dissatisfied) 1: Satisfied 2: fair	1.023683 1.055584	2.783427 2.873653	0.001*** 0.002***	.1598774 .1648597
Income Satisfaction (Basic Level: Dissatisfied) 1: Satisfied 2: Fair	.949581 .235221	2.584627 1.265188	0.001*** 0.418	.1483043 .0367365
Social Life Satisfaction (Basic Level: Dissatisfied) 1: Satisfied 2: Fair	1.06721 .6959409	2.907257 2.005595	0.000*** 0.019**	.1666755 .1086911
SSI Registration (Basic Level: No) 1: Yes	1.189545	3.285587	0.000***	.1857816

A level of gender segregation is "Male" basic. 1% is significant as the point score of the "Woman" award. It is the "Other" at the basic level as if to be divorced. In this regard, it has been evaluated as important at a level that can be evaluated within the scope of "Success" and "Work". "He did not finish school" is expected at the basic level regarding the education level. In terms of education, 3-year college "5% point degree" and "master's degree" is important at 10% importance.

The baseline level of compliance with health is estimated as "Not satisfied". In this election, "Satisfied" is meaningful as a 1% point score.

Not very good as a basic level of expectation regarding adjustment from education. In this selection, "Satisfied" points and "Average" points are significant at 1% points.

The basic level of the income satisfaction variable was determined as the "Dissatisfied" category. In this variable, the "Satisfied" category is statistically significant at the 1% significance level.

The basic level of satisfaction with the social life variable was determined as the "Dissatisfied" category. In this variable, the "Satisfied" category is statistically significant at the 1% significance level and the "Medium" category at the 5% significance level.

The basic level of the SGK registry variable is the "No" category. In this variable, it was concluded that the "Yes" category was statistically significant at the 1% significance level.

The odds ratios of the model estimated by ordinal logistic regression are given in Table 3.5. Statistically, significant odds ratios are interpreted as follows:

- When the gender variable is examined, it is concluded that the happiness level of divorced individuals is 2.001168 times higher than that of men.
- When the variable about what makes divorced individuals happy is examined, it is concluded that the happiness level of the "success" factor is approximately 0.06 times less than the reference category "other" factors.
- It was concluded that the happiness level of the "work" factor, which is one of the factors that make divorced individuals happy, is approximately 0.03 times less than the reference category "other" factors.
- When the educational status variable was examined, it was concluded that the divorced individuals graduated from a "2 or 3-year college" and their happiness level was approximately 4.77 times higher than the divorced individuals who did not "complete a school".
- It has been concluded that the divorced individuals being a "master's degree" and their happiness level is 5.53 times higher than the divorced individuals who have not "finished a school".
- When the health satisfaction variable was examined, it was concluded that the happiness levels of the divorced individuals who were "satisfied" with their health were approximately 3.14 times higher than the divorced individuals who were "not satisfied" with their health.
- When the variable of satisfaction with education is examined, it has been concluded that the happiness level of divorced individuals who are "satisfied" with the education they have received so far is approximately 2.78 times higher than the "Dissatisfied" divorced individuals.
- It has been concluded that the happiness level of divorced individuals who are "moderately" satisfied with the education they have received so far is approximately 2.87 times higher than the "Dissatisfied" divorced individuals.

- When the income satisfaction variable is examined, it is concluded that the happiness level of divorced individuals who are "satisfied" with their monthly income is approximately 2.58 times higher than the divorced individuals who are "not satisfied" with their monthly income.
- When the variable of satisfaction with social life was examined, it was concluded that the happiness levels of divorced individuals who were "satisfied" with their social life were approximately 2.91 times higher than those of divorced individuals who were "not satisfied" with their social life.
- It has been concluded that the happiness level of divorced individuals who are "moderate" satisfied with their social life is approximately 2.01 times higher than those who are "Dissatisfied" with their social life.
- It has been concluded that the happiness level of divorced individuals who are "moderate" satisfied with their social life is approximately 2.01 times higher than those who are "Dissatisfied" with their social life.

4. Results

In the model estimated by ordinal logistic regression, it was determined that the "age" variable was not statistically significant. The statistically significant gender variable shows that divorced women are happier than divorced men. It has been determined that success and job variables tend to decrease happiness levels in divorced individuals compared to other factors. When the education level is examined in general, it has been concluded that as the education level of divorced individuals increases, their happiness levels also increase. It has been concluded that divorced individuals who are satisfied with their health are happier than divorced individuals who are not satisfied with their health. It has been determined that the divorced individuals are more satisfied with the education they have received so far and their happiness levels are higher than the dissatisfied individuals. It has been concluded that divorced individuals who are satisfied with their income and social life are happier than those who are not satisfied. It is one of the results obtained as a result of the analysis that divorced individuals are registered with the Social Security Institution and their happiness levels are higher than those who are not registered.

To our best knowledge, there is no research or application on the happiness of divorced individuals in the literature. In this context, it is thought that this thesis study can guide the studies on the factors affecting the happiness levels of divorced individuals.

References

- [1]. Agresti, A. (2015). Foundations of Linear and Generalized Linear Models. New Jersey: John Wiley & Sons, Inc.
- [2]. Agresti, A. (2019). An Introduction to Categorical Data Analysis (Third Edition b.). Hoboken, NJ: John Wiley & Sons, Inc.
- [3]. Akın, H. B., & Şentürk, E. (2012). Bireylerin Mutluluk Düzeylerinin Ordinal Lojistik Regresyon ile İncelenmesi. *Öneri Dergisi*, 10(37), 183-193.
- [4]. Arı, E. (2013). Sıralı Lojistik Regresyonda Paralel Doğrular Varsayımı ve Çözümleme Yaklaşımları. Doktora Tezi. Eskişehir: Eskişehir Osmangazi Üniversitesi, Fen Bilimleri Enstitüsü.
- [5]. Arı, E., & Yıldız, Z. (2016). Bireylerin Yaşam Memnuniyetini Etkileyen Faktörlerin Sıralı Lojistik Regresyon Analizi ile İncelenmesi. *Uluslararası Sosyal Araştırmalar Dergisi*, 9(42), 1362-1374.
- [6]. Aslan, H. (2006). Bireylerin Otomobil Seçiminin Çoklu Tercih Modelleri ile Analizi. Yüksek Lisans Tezi. İstanbul: Marmara Üniversitesi, Sosyal Bilimler Enstitüsü.
- [7]. Ayhan, S. (2006). Sıralı Lojistik Regresyon Analiziyle Türkiye'deki Hemşirelerin İş Bırakma Niyetini Etkileyen Faktörlerin Belirlenmesi. Yüksek Lisans Tezi. Eskişehir: Osmangazi Üniversitesi, Fen Bilimleri Enstitüsü.
- [8]. Barak, N. A. (2005). Sıralı (Ordinal) ve Multinomial Logit Modeller Üzerine Bir Uygulama. Yüksek Lisans Tezi. Ankara: Hacettepe Üniversitesi, Sağlık Bilimleri Enstitüsü.
- [9]. Cramer, J. S. (2003). Logit Models from Economics and Other Fields. New York: Cambridge University Press.
- [10]. Harrell, F. E. (2015). Regression Modeling Strategies with Applications to Linear Models, Logistic and Ordinal Regression, and Survival Analysis (Second Edition b.). Switzerland: Springer International Publishing.
- [11]. Hayat, E., & Sözen Özden, A. (2021). Genelleştirilmiş Sıralı Lojistik Regresyon Analizi ile Bireylerin Mutluluk Düzeylerine Etki Eden Faktörlerin Belirlenmesi. *OPUS Uluslararası Toplum Araştırmaları Dergisi*, 18(40), 2288-2316.
- [12]. Hilbe, J. M. (2009). Logistic Regression Models. Chapman & Hall .
- [13]. Long, J. S. (1997). Regression Models for Categorical and Limited Dependent Variables. California: Sage Publications, Inc.
- [14]. O'Connell, A. A. (2006). Logistic Regression Models for Ordinal Response Variables . California: Sage Publications, Inc.
- [15]. Servet, O. (2017). Mutluluğun Türkiye'deki Belirleyicilerinin Zaman İçinde Değişimi. *Akdeniz İİBF Dergisi*, 17(35), 16-42.
- [16]. Sönmez, A., & Altınsu Sönmez, Ö. (2018). Life Satisfaction and Happiness with Regard Human Capital and Religiosity in Turkey. *Bingöl Üniversitesi Sosyal Bilimler Enstitüsü Dergisi*, 8(16), 217-234.
- [17]. Şerbetçi, A. (2012). Sıralı Lojistik Regresyon Analizi ile İstatistik ve Ekonometri Derslerinde Başarıyı Etkileyen Faktörlerin Belirlenmesi: Atatürk Üniversitesi İktisadi ve İdari Bilimler Fakültesi Öğrencileri Üzerine Bir Uygulama . Yüksek Lisans Tezi. Erzurum: Atatürk Üniversitesi, Sosyal Bilimler Enstitüsü.
- [18]. Şimşir Cömertler, N. (2013). Türkiye'de Mutluluk Ekonomisinin Belirleyicilerinin Ekonometrik Analizi. *Finans Politik & Ekonomik Yorumlar*, 50(579), 7-22.
- [19]. Yerdelen Tatoğlu, F. (2020). Ekonometri Stata Uygulamalı. İstanbul: Beta Basım Yayım Dağıtım A.Ş.
- [20]. Yılmaz, A. (2020). Yaşam Memnuniyeti ve Yaşam Memnuniyetini Etkileyen Faktörlerin Sıralı Lojistik Analiziyle İncelenmesi. Yüksek Lisans Tezi. İstanbul: Marmara Üniversitesi, Sosyal Bilimler Enstitüsü..

Stability analysis and periodictly properties of a class of rational difference equations

Elsayed Elsayed^{1,2}, Badriah Alofi^{2,*}

¹Department of Mathematics, Faculty of Science, Mansoura University ²,King Abdulaziz University, Faculty of Science, Mathematics Department, P. O. Box 80203, Jeddah 21589, Saudi Arabia, emmelsayed@yahoo.com, ORCID: [HTTPS://ORCID.ORG/0000-0003-0894-8472](https://ORCID.ORG/0000-0003-0894-8472), badoora2al3ofi@gmail.com, ORCID: <https://orcid.org/0000-0002-8330-8910>

ABSTRACT

The goal of this study is to investigate the global, local, and boundedness of the recursive sequence

$$T_{\eta+1} = r + \frac{p_1 T_{\eta-l_1}}{T_{\eta-m_1}} + \frac{q_1 T_{\eta-m_1}}{T_{\eta-l_1}} + \frac{p_2 T_{\eta-l_2}}{T_{\eta-m_2}} + \frac{q_2 T_{\eta-m_2}}{T_{\eta-l_2}} + \dots + \frac{p_s T_{\eta-l_s}}{T_{\eta-m_s}} + \frac{q_s T_{\eta-m_s}}{T_{\eta-l_s}},$$

where the initial values $T_{-l_1}, T_{-l_2}, \dots, T_{-l_s}, T_{-m_1}, T_{-m_2}$ and T_{-m_s} are arbitrary positive real numbers. It also investigates periodic solutions for special case of above equations.

ARTICLE INFO

Research article

Received: 24.10.2021

Accepted: 11.03.2022

Keywords: difference equations, stability, boundedness, periodictly

*Corresponding author

1. Introduction

The main proposal of this paper gets the behavior of the solutions such as local Stability, global stability and boundedness character of the following difference equation

$$T_{\eta+1} = r + \frac{p_1 T_{\eta-l_1}}{T_{\eta-m_1}} + \frac{q_1 T_{\eta-m_1}}{T_{\eta-l_1}} + \frac{p_2 T_{\eta-l_2}}{T_{\eta-m_2}} + \frac{q_2 T_{\eta-m_2}}{T_{\eta-l_2}} + \dots + \frac{p_s T_{\eta-l_s}}{T_{\eta-m_s}} + \frac{q_s T_{\eta-m_s}}{T_{\eta-l_s}}, \quad \eta \geq 0, \quad (1)$$

where $l_1, l_2, \dots, l_s, m_1, m_2, \dots, m_s, s$, are positive constants and the initial values $T_{-l_1}, T_{-l_2}, \dots, T_{-l_s}, T_{-m_1}, T_{-m_2}$ and T_{-m_s} are arbitrary positive real numbers. In addition, numerical results are provided to confirm theorems. Let $L = \max\{l_1, l_2, \dots, l_s, m_1, m_2, \dots, m_s\}$.

Let us introduce some basic definitions and some theorems that we need in the sequel.

Let I be some interval of real numbers and let

$$g : I^{k+1} \rightarrow I,$$

be a continuously differentiable function. Then for every set of initial values $T_{-k}, T_{-k+1}, \dots, T_0 \in I$, the difference equation

$$T_{\eta+1} = g(T_{\eta}, T_{\eta-1}, \dots, T_{\eta-k}), \quad \eta = 0, 1, \dots, \quad (2)$$

has a unique solution $\{T_{\eta}\}_{\eta=-k}^{\infty}$ [13].

A point $\bar{T} \in I$ is called an equilibrium point of Eq.(2) if

$$\bar{T} = g(\bar{T}, \bar{T}, \dots, \bar{T}).$$

That is, $T_{\eta} = \bar{T}$ for $\eta \geq 0$, is a solution of Eq. (2), or equivalently, \bar{T} is a fixed point of g .

(Stability)

(i) The equilibrium point \bar{T} of Eq.(2) is locally stable if for every $\epsilon > 0$, there exists $\delta > 0$ such that for all $T_{-k}, T_{-k+1}, \dots, T_{-1}, T_0 \in I$ with

$$|T_{-k} - \bar{T}| + |T_{-k+1} - \bar{T}| + \dots + |T_0 - \bar{T}| < \delta,$$

we have

$$|T_{\eta} - \bar{T}| < \epsilon \quad \text{for all } \eta \geq -k.$$

(ii) The equilibrium point \bar{T} of Eq.(2) is locally asymptotically stable if \bar{T} is locally stable solution of Eq.(2) and there exists $\gamma > 0$, such that for all $T_{-k}, T_{-k+1}, \dots, T_{-1}, T_0 \in I$ with

$$|T_{-k} - \bar{T}| + |T_{-k+1} - \bar{T}| + \dots + |T_0 - \bar{T}| < \gamma,$$

we have

$$\lim_{\eta \rightarrow \infty} T_\eta = \bar{T}.$$

(iii) The equilibrium point \bar{T} of Eq.(2) is global attractor if for all $T_{-k}, T_{-k+1}, \dots, T_{-1}, T_0 \in I$, we have

$$\lim_{\eta \rightarrow \infty} T_\eta = \bar{T}.$$

(iv) The equilibrium point \bar{T} of Eq.(2) is globally asymptotically stable if \bar{T} is locally stable, and \bar{T} is also a global attractor of Eq.(2).

(v) The equilibrium point \bar{T} of Eq.(2) is unstable if \bar{T} is not locally stable.

The linearized equation of Eq.(2) about the equilibrium \bar{T} is the linear difference equation

$$y_{\eta+1} = \sum_{i=0}^k \frac{\partial g(\bar{T}, \bar{T}, \dots, \bar{T})}{\partial T_{\eta-i}} y_{\eta-i}. \quad (3)$$

Theorem A [12]: Assume that $p, q \in \mathbb{R}$ and $k \in \{0, 1, 2, \dots\}$. Then

$$|p| + |q| < 1,$$

is a sufficient condition for the asymptotic stability of the difference equation

$$T_{\eta+1} + pT_\eta + qT_{\eta-k} = 0, \quad \eta = 0, 1, \dots$$

Theorem A can be easily extended to a general linear equations of the form

$$T_{\eta+k} + p_1T_{\eta+k-1} + \dots + p_kT_\eta = 0, \quad \eta = 0, 1, \dots, \quad (3)$$

where $p_1, p_2, \dots, p_k \in \mathbb{R}$ and $k \in \{1, 2, \dots\}$. Then Eq.(4) is asymptotically stable provided that

$$\sum_{i=1}^k |p_i| < 1.$$

Consider the following equation

$$T_{\eta+1} = h(T_\eta, T_{\eta-1}, T_{\eta-2}). \quad (4)$$

The following theorem will be useful for the proof of our results in this paper.

Theorem B [13]: Let $[a, b]$ be an interval of real numbers and assume that

$$h : [a, b]^3 \rightarrow [a, b],$$

is a continuous function satisfying the following properties :

(a) $h(x, y, z)$ is non-decreasing in x and z in $[a, b]$ for each $y \in [a, b]$, and is non-increasing in $y \in [a, b]$ for each x and z in $[a, b]$;

(b) If $(n, N) \in [a, b] \times [a, b]$ is a solution of the system

$$N = h(N, n, N) \quad \text{and} \quad n = h(n, N, n),$$

then

$$n = N.$$

Then Eq.(4) has a unique equilibrium $\bar{T} \in [a, b]$ and every solution of Eq.(4) converges to \bar{T} .

The increasing worldwide attention paid to the study of many characteristics, of behaviors and dynamics of difference equations, such as stability, periodicity, boundedness character, is not a coincidence. The applications of distinction equations have recently been the basic of numerous sciences and that is the cause why the principle of difference equations stays the important thing participant not only in mathematics however also in different sciences that employ its implementations. Many mathematicians find the research on difference equations interesting and fruitful because it supports the analysis and modeling of various phenomena in everyday life [15]. For example, Elsayed [15] discovered a new technique to get second and third periodic solution of the recursive sequence that is given by

$$T_{\eta+1} = a + \frac{bT_\eta}{T_{\eta-1}} + \frac{bT_{\eta-1}}{T_\eta},$$

Chatzarakis et al. in [5] focused on study periodic and boundedness, local and global stability of a class of non-linear difference equations given by

$$T_{\eta+1} = a + \frac{bT_\eta^2}{(T_\eta + d)T_{\eta-1}},$$

The dynamical analysis of the following difference equations

$$T_{\eta+1} = a_\eta + \frac{T_\eta^p}{T_{\eta-1}^p},$$

is examined by Khan and El-Metwally [18].

The global attractivity and local stability of the difference equation

$$T_{\eta+1} = \frac{T_{\eta-1}}{c + dT_{\eta-1}T_{\eta-2}},$$

have investigated by Yang et al. [24].

Khaliq et al. [17] studies the dynamical behavior of solutions of the seventh order difference equation

$$T_{\eta+1} = aT_{\eta-3} + \frac{\alpha T_{\eta-3} T_{\eta-7}}{\beta T_{\eta-3} + \gamma T_{\eta-7}}.$$

Cinar [6] has figured out how to obtain solution of the difference problem

$$T_{\eta+1} = \frac{aT_{\eta-1}}{1 + bT_{\eta}T_{\eta-1}}.$$

Alayachi et al. [7] studied qualitative behavior and boundedness of the difference equation

$$T_{\eta+1} = aT_{\eta-1} + \frac{\alpha T_{\eta-1} T_{\eta-3}}{\beta T_{\eta-3} + \gamma T_{\eta-5}}.$$

Another associated papers on rational difference equations see [1-25].

2. Behavior of the Solutions of Eq. (1)

In this section we investigated the behavior of the solution of Eq. (1).

2.1. Local Stability

In this subsection we investigate the local stability character of the solutions of Eq.(1).

Theorem 1 Assume that $2[|p_1 - q_1| + |p_2 - q_2| + \dots + |p_s - q_s| < r + p_1 + q_1 + p_2 + q_2 + \dots + p_s + q_s$, then the equilibrium point $\bar{T} = r + p_1 + q_1 + p_2 + q_2 + \dots + p_s + q_s$, of Eq.(1) is Locally asymptotically stable.

proof: The equilibrium point of Eq. (1) is given by

$$\bar{T} = r + p_1 + q_1 + p_2 + q_2 + \dots + p_s + q_s. \quad (5)$$

Define a function $g : (0, \infty) \rightarrow (0, \infty)$ as

$$g(x_1, y_1, x_2, y_2, \dots, x_s, y_s) = r + \frac{p_1 x_1}{y_1} + \frac{q_1 y_1}{x_1} + \frac{p_2 x_2}{y_2} + \frac{q_2 y_2}{x_2} + \dots + \frac{p_s x_s}{y_s} + \frac{q_s y_s}{x_s}.$$

Hence we obtain,

$$\begin{aligned} \frac{\partial g}{\partial x_1}(x_1, y_1, x_2, y_2, \dots, x_s, y_s) &= \frac{p_1}{y_1} - \frac{q_1 y_1}{x_1^2}, \\ \frac{\partial g}{\partial y_1}(x_1, y_1, x_2, y_2, \dots, x_s, y_s) &= -\frac{p_1 x_1}{y_1^2} + \frac{q_1}{x_1}, \\ \frac{\partial g}{\partial x_2}(x_1, y_1, x_2, y_2, \dots, x_s, y_s) &= \frac{p_2}{y_2} - \frac{q_2 y_2}{x_2^2}, \\ \frac{\partial g}{\partial y_2}(x_1, y_1, x_2, y_2, \dots, x_s, y_s) &= -\frac{p_2 x_2}{y_2^2} + \frac{q_2}{x_2}, \dots, \\ &\dots, \\ \frac{\partial g}{\partial x_s}(x_1, y_1, x_2, y_2, \dots, x_s, y_s) &= \frac{p_s}{y_s} - \frac{q_s y_s}{x_s^2}, \\ \frac{\partial g}{\partial y_s}(x_1, y_1, x_2, y_2, \dots, x_s, y_s) &= -\frac{p_s x_s}{y_s^2} + \frac{q_s}{x_s}. \end{aligned}$$

It follows that

$$\begin{aligned} \frac{\partial g}{\partial x_1}(\bar{T}, \bar{T}, \bar{T}, \bar{T}, \dots, \bar{T}, \bar{T}) &= \frac{p_1}{\bar{T}} - \frac{q_1}{\bar{T}} = -a_1, \\ \frac{\partial g}{\partial y_1}(\bar{T}, \bar{T}, \bar{T}, \bar{T}, \dots, \bar{T}, \bar{T}) &= -\frac{p_1}{\bar{T}} + \frac{q_1}{\bar{T}} = -b_1, \\ \frac{\partial g}{\partial x_2}(\bar{T}, \bar{T}, \bar{T}, \bar{T}, \dots, \bar{T}, \bar{T}) &= \frac{p_2}{\bar{T}} - \frac{q_2}{\bar{T}} = a_2, \\ \frac{\partial g}{\partial y_2}(\bar{T}, \bar{T}, \bar{T}, \bar{T}, \dots, \bar{T}, \bar{T}) &= -\frac{p_2}{\bar{T}} + \frac{q_2}{\bar{T}} = -b_2, \dots, \\ &\dots, \\ \frac{\partial g}{\partial x_s}(\bar{T}, \bar{T}, \bar{T}, \bar{T}, \dots, \bar{T}, \bar{T}) &= \frac{p_s}{\bar{T}} - \frac{q_s}{\bar{T}} = -a_s, \\ \frac{\partial g}{\partial y_s}(\bar{T}, \bar{T}, \bar{T}, \bar{T}, \dots, \bar{T}, \bar{T}) &= -\frac{p_s}{\bar{T}} + \frac{q_s}{\bar{T}} = -b_s. \end{aligned}$$

Therefore, the linearized equation becomes

$$S_{\eta+1} = a_1 S_{\eta-l_1} + b_1 S_{\eta-m_1} + a_2 S_{\eta-l_2} + b_2 S_{\eta-m_2} + \dots + a_s S_{\eta-l_s} + b_s S_{\eta-l_s},$$

using Theorem A, we get that the equilibrium point is asymptotically stable if

$$|a_1| + |a_1| + \dots |a_1| + |b_1| + |b_1| + \dots + |b_1| < 1,$$

and hence

$$2[|p_1 - q_1| + |p_2 - q_2| + \dots + |p_s - q_s|] < r + p_1 + q_1 + p_2 + q_2 + \dots + p_s + q_s,$$

which means the prove is complete.

2.2. Global Attractor

In this subsection we investigate the global attractivity character of solutions of Eq. (1).

Theorem 2 The equilibrium point of Eq. (1) is global Attractor if $\gamma(1 - \alpha) \neq \beta$.

proof: Let a, b are real number and define $f : [a, b]^{2s} \rightarrow [a, b]$ a function $f(x_1, y_1, x_2, y_2, \dots, x_s, y_s) = r + \frac{p_1x_1}{y_1} + \frac{q_1y_1}{x_1} + \frac{p_2x_2}{y_2} + \frac{q_2y_2}{x_2} + \dots + \frac{p_sx_s}{y_s} + \frac{q_sy_s}{x_s}$. Since $p_1x_1^2 - q_1y_1^2 \geq 0, p_2x_2^2 - q_2y_2^2 \geq 0, \dots, p_sx_s^2 - q_sy_s^2 \geq 0$, for $x_1, y_1, x_2, y_2, \dots, x_s, y_s \geq 0$, the function f is increasing in x_1, x_2, \dots, x_s and decreasing in y_1, y_2, \dots, y_s , hence

$$N = f(N, n, N, n, \dots, N, n) \text{ and } n = f(n, N, n, N, \dots, n, N).$$

Hence we get

$$N = r + \frac{p_1N}{n} + \frac{q_1n}{N} + \frac{p_2N}{n} + \frac{q_2n}{N} + \dots + \frac{p_sN}{n} + \frac{q_sn}{N},$$

$$n = r + \frac{p_1n}{N} + \frac{q_1N}{n} + \frac{p_2n}{N} + \frac{q_2N}{n} + \dots + \frac{p_sn}{N} + \frac{q_sN}{n},$$

or

$$N^2n = rNn + p_1N^2 + q_1n^2 + p_2N^2 + q_2n^2 + \dots + p_sN^2 + q_sn^2,$$

$$Nn^2 = rNn + p_1n^2 + q_1N^2 + p_2n^2 + q_2N^2 + \dots + p_sn^2 + q_sN^2,$$

subtracting these two equations, we get

$$(N - n)Nn = p_1(N^2 - n^2) + q_1(n^2 - N^2) + p_2(N^2 - n^2) + q_2(n^2 - N^2) + \dots + p_s(N^2 - n^2) + q_s(n^2 - N^2)$$

$$0 = (N - n)[Nn + (N + n)(q_1 + q_2 + \dots + q_s - p_1 - p_2 - \dots - p_s)]$$

Under the conditions $q_1 + q_2 + \dots + q_s \geq p_1 + p_2 + \dots + p_s$, we obtain

$$N = n,$$

we obtain by theron (B) that he equilibrium point \bar{T} of Eq.(1) is global Attractor.

2.3. Boundness of solutions

In this subsection we study the boundedness of solutions of Eq. (1).

Theorem 3 Every solution of Eq. (1) is bounded and prsists if $r > p_1 + q_1 + p_2 + q_2 + \dots + p_s + q_s$.

proof: Sppose $\{T_\eta\}_{-L}^\infty$ be solution of Eq. (1). It follows from Eq. (1) that

$$T_{\eta+1} = r + \frac{p_1T_{\eta-l_1}}{T_{\eta-m_1}} + \frac{q_1T_{\eta-m_1}}{T_{\eta-l_1}} + \frac{p_2T_{\eta-l_2}}{T_{\eta-m_2}} + \frac{q_2T_{\eta-m_2}}{T_{\eta-l_2}} + \dots + \frac{p_sT_{\eta-l_s}}{T_{\eta-m_s}} + \frac{q_sT_{\eta-m_s}}{T_{\eta-l_s}} > r,$$

thus

$$T_{\eta+1} > r, \text{ for } \eta \geq 0.$$

Also, it follows from Eq. (1) that

$$T_{\eta+1} \leq r + \frac{p_1T_{\eta-l_1}}{r} + \frac{q_1T_{\eta-m_1}}{r} + \frac{p_2T_{\eta-l_2}}{r} + \frac{q_2T_{\eta-m_2}}{r} + \dots + \frac{p_sT_{\eta-l_s}}{r} + \frac{q_sT_{\eta-m_s}}{r},$$

using Comparisons Theroms, we get

$$\lim_{\eta \rightarrow \infty} \text{sub}T_\eta \leq \frac{r^2}{(r - p_1 - p_2 \dots - p_s - q_1 - q_2 \dots - q_s)}.$$

Therefore $\{T_\eta\}_{-L}^\infty$ is bounded and persists.

3. Periodic two solution of Eq. (1):

In this section, we investigate the periodic two solutions of special cases of Eq. (1). We states theorem that gives us necessary and sufficient conditions of the following equation

$$T_{\eta+1} = r + \frac{p_1T_\eta}{T_{\eta-1}} + \frac{q_1T_{\eta-1}}{T_\eta} + \frac{p_2T_{\eta-2}}{T_{\eta-3}} + \frac{q_2T_{\eta-3}}{T_{\eta-2}} + \dots + \frac{p_sT_{\eta-2l}}{T_{\eta-(2l+1)}} + \frac{q_sT_{\eta-(2l+1)}}{T_{\eta-2l}}, \quad \eta = 0, 1, \dots, \tag{6}$$

where $T_{\eta-2l} = \dots = T_{\eta-2} = T_\eta = u$, and $T_{\eta-(2l+1)} = \dots = T_{\eta-3} = T_{\eta-1} = v$, has a prime period solution of periodic two.

Theorem 4

Assume that $p_1 + p_2 + \dots + p_s \neq q_1 + q_2 + \dots + q_s$ and $c \in R/\{0, \pm 1\}$, then Eq. (6) has a periodic solution of prime periodic two if and only if $r = q_1 + q_2 + \dots + q_s - (p_1 + p_2 + \dots + p_s) \left(\frac{c^2+c+1}{c}\right)$, where $c = \frac{u}{v}$ such that u, v, u, v, \dots is a periodic solution of Eq. (6).

Proof: From Eq. (6), we obtain

$$u = r + \frac{p_1v}{u} + \frac{q_1u}{v} + \frac{p_2v}{u} + \frac{q_2u}{v} + \dots + \frac{p_sv}{u} + \frac{q_su}{v}, \text{ and}$$

$$v = r + \frac{p_1u}{v} + \frac{q_1v}{u} + \frac{p_2u}{v} + \frac{q_2v}{u} + \dots + \frac{p_su}{v} + \frac{q_sv}{u}.$$

Since $c = \frac{u}{v} \neq 0, \pm 1$. Then, it follows

$$u = r + \frac{p_1}{c} + q_1c + \frac{p_2}{c} + q_2 + \dots + \frac{p_s}{c} + q_sc, \tag{7}$$

and

$$v = r + p_1c + \frac{q_1}{c} + p_2c + \frac{q_2}{c} + \dots + p_sc + \frac{q_s}{c},$$

or

$$vc = rc + p_1c^2 + q_1 + p_2c^2 + q_2 + \dots + p_sc^2 + q_s, \quad (8)$$

subtracting Eq. (8) from Eq. (7) gives the following equation

$$u - vc = r(c - 1) + (p_1 + p_2 + \dots + p_s) \left(c^2 - \frac{1}{c} \right) + (q_1 + q_2 + \dots + q_s) (1 - c),$$

hence

$$r(c - 1) + (p_1 + p_2 + \dots + p_s) \left(\frac{c^3 - 1}{c} \right) + (q_1 + q_2 + \dots + q_s) (1 - c) = 0.$$

Since $c \neq 0$, we conclude

$$r = q_1 + q_2 + \dots + q_s - (p_1 + p_2 + \dots + p_s) \left(\frac{c^2 + c + 1}{c} \right), \quad (9)$$

which is the condition of this theorem holds.

Furthermore, we rewrite Eqs. (8) and Eq. (7) as follows

$$\begin{aligned} u &= q_1 + q_2 + \dots + q_s - (p_1 + p_2 + \dots + p_s) \left(\frac{c^2 + c + 1}{c} \right) \\ &+ \frac{p_1}{c} + q_1c + \frac{p_2}{c} + q_2 + \dots + \frac{p_s}{c} + q_sc, \\ &= (q_1 + q_2 + \dots + q_s) (c + 1) \\ &- (p_1 + p_2 + \dots + p_s) (c + 1) \\ &= [(q_1 + q_2 + \dots + q_s) - (p_1 + p_2 + \dots + p_s)] (c + 1), \end{aligned} \quad (10)$$

and

$$\begin{aligned} v &= \left(q_1 + q_2 + \dots + q_s - (p_1 + p_2 + \dots + p_s) \left(\frac{c^2 + c + 1}{c} \right) \right) \\ &+ p_1c + \frac{q_1}{c} + p_2c + \frac{q_2}{c} + \dots + p_sc + \frac{q_s}{c} \\ &= \left((q_1 + q_2 + \dots + q_s) \left(1 + \frac{1}{c} \right) \right) \\ &- (p_1 + p_2 + \dots + p_s) \left(\frac{c + 1}{c} \right) \\ &= [(q_1 + q_2 + \dots + q_s) - (p_1 + p_2 + \dots + p_s)] \left(\frac{c + 1}{c} \right), \end{aligned} \quad (11)$$

therefore, u, v distinct real numbers. Let $T_{\eta-2l} = \dots = T_{\eta-2} = T_{\eta} = u$, and $T_{\eta-(2l+1)} = \dots = T_{\eta-3} = T_{\eta-1} = v$. According Eq. (6), we state

$$T_1 = u, T_2 = v.$$

$$\begin{aligned} T_1 &= r + \frac{p_1u}{v} + \frac{q_1v}{u} + \frac{p_2u}{v} + \frac{q_2v}{u} + \dots + \frac{p_su}{v} + \frac{q_sv}{u} \\ &= q_1 + q_2 + \dots + q_s - (p_1 + p_2 + \dots + p_s) \left(\frac{c^2 + c + 1}{c} \right) \\ &+ \frac{(p_1 + p_2 + \dots + p_s)}{c} + c (q_1 + q_2 + \dots + q_s) \\ &= (c + 1) [(q_1 + q_2 + \dots + q_s) - (p_1 + p_2 + \dots + p_s)] \\ &= u, \\ T_2 &= r + \frac{p_1v}{u} + \frac{q_1u}{v} + \frac{p_2v}{u} + \frac{q_2u}{v} + \dots + \frac{p_sv}{u} + \frac{q_su}{v} \\ &= q_1 + q_2 + \dots + q_s - (p_1 + p_2 + \dots + p_s) \left(\frac{c^2 + c + 1}{c} \right) \\ &+ c (p_1 + p_2 + \dots + p_s) + \frac{(q_1 + q_2 + \dots + q_s)}{c} \\ &= \frac{(c + 1)}{c} [(q_1 + q_2 + \dots + q_s) - (p_1 + p_2 + \dots + p_s)] \\ &= v. \end{aligned}$$

Hence similar T_1, T_2 , we get $T_{2\eta+1} = u, T_{2\eta} = v$, for $\eta \geq 0$, therefore the proof is completed.

4. Numerical results:

Example 1 For confirming the results of subsection (2.1), we consider difference equation

$$T_{\eta+1} = 2 + \frac{T_{\eta-2}}{T_{\eta-3}} + \frac{4T_{\eta-3}}{T_{\eta-2}} + \frac{2T_{\eta-1}}{T_{\eta}} + \frac{5T_{\eta}}{T_{\eta}}, \quad (13)$$

with the initial conditions $T_{-3} = 14.5, T_{-2} = 13.5, T_{-1} = 14.5$ and $T_0 = 13.5$, where the equilibrium point is $\bar{T} = 14$. (See Fig. 1).

Example 2 For confirming the results of subsection (2.1), we consider difference equation

$$T_{\eta+1} = 2 + \frac{T_{\eta-2}}{T_{\eta-3}} + \frac{4T_{\eta-3}}{T_{\eta-2}}, \quad (14)$$

with the initial conditions $T_{-3} = 7.5, T_{-2} = 6.5, T_{-1} = 7.4$ and $T_0 = 6.5$, where the equilibrium point is $\bar{T} = 7$. (See Fig. 2).

2005/06/28ver : 1.3subfigpackage

Example 3 For confirming the results of subsection (2.2), we consider numerical example for Eq. (13) with the initial conditions

IC1: $T_{-3} = 14, T_{-2} = 13, T_{-1} = 14, T_0 = 13,$

IC2: $T_{-3} = 13, T_{-2} = 12, T_{-1} = 11, T_0 = 10,$

IC3: $T_{-3} = 12, T_{-2} = 11, T_{-1} = 10, T_0 = 9,$

IC4: $T_{-3} = 11, T_{-2} = 10, T_{-1} = 9, T_0 = 8.$

(See Fig. 3).

Example 4 For confirming the results of subsection (2.2), we consider numerical example for Eq. (14) with the initial conditions IC1-IC4. (See Fig. 4).

Example 5 For confirming the results of section (3), we consider difference equation

$$T_{\eta+1} = r + \frac{p_1 T_{\eta}}{T_{\eta-1}} + \frac{q_1 T_{\eta-1}}{T_{\eta}} + \frac{p_2 T_{\eta-2}}{T_{\eta-3}} + \frac{q_2 T_{\eta-3}}{T_{\eta-2}} + \frac{p_s T_{\eta-4}}{T_{\eta-5}} + \frac{q_s T_{\eta-5}}{T_{\eta-4}}, \quad (15)$$

where $p_1 = 2, q_1 = 6, p_2 = 3, q_2 = 7, p_3 = 4, q_3 = 8, c = 3,$ with the initial condition $T_{-5} = 48, T_{-4} = 16, T_{-3} = 48, T_{-2} = 16, T_{-1} = 48$ and $T_0 = 16.$ (See Fig. 5).

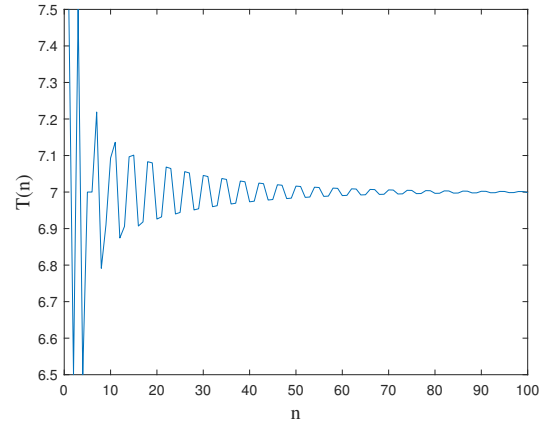


Figure 2: The figure shows the local stability of $\bar{T} = 7$ in Eq. (14).

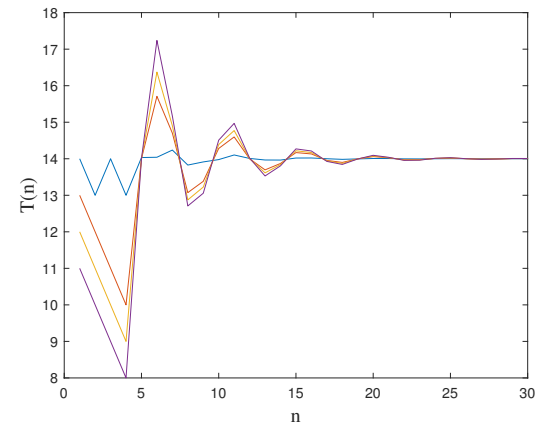


Figure 3: The figure shows the global stability of $\bar{T} = 7$ in Eq. (14).

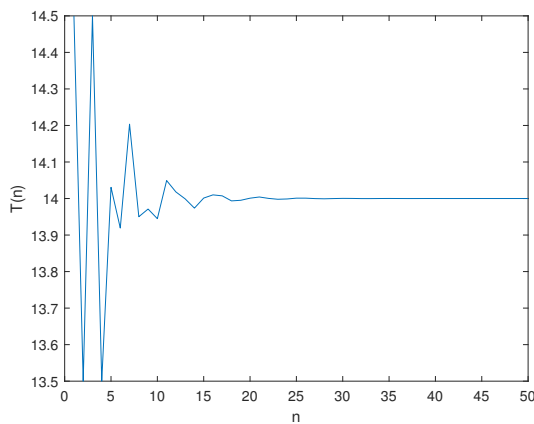


Figure 1: The figure shows the local stability of $\bar{T} = 14$ in Eq. (13).

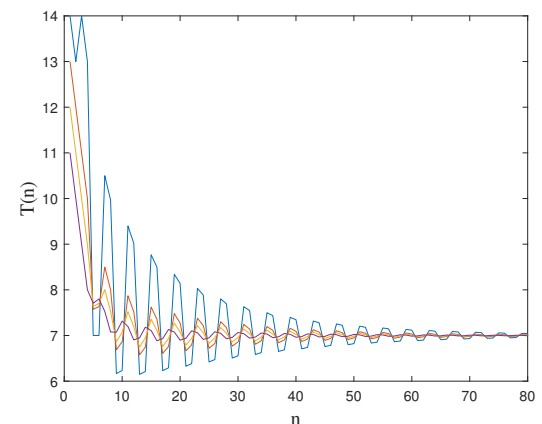


Figure 4: The figure shows the global stability of $\bar{T} = 14$ in Eq. (13).

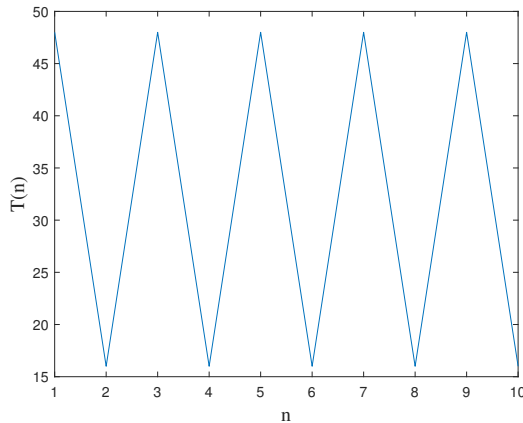


Figure 5: The figure shows Eq. (15) has period two solutions where $p_1, q_1, p_2, q_2, p_3, q_3$ and initial condition satisfies the condition of Theorem 4.

References

- [1] H. S. Alayachi, M. S. M. Noorani, A. Q. Khan, and M. B. Almatrafi, Analytic Solutions and Stability of Sixth Order Difference Equations, *Mathematical Problems in Engineering*, 2020 (2020), 12 pages.
- [2] A. M. Amleh, V. Kirk and G. Ladas, On the dynamics of $x_{\eta+1} = \frac{a + bx_{\eta-1}}{A + Bx_{\eta-2}}$, *Math. Sci. Res. Hot-Line*, 5 (2001), 1–15.
- [3] E. Camouzis, G. Ladas and H. D. Voulov, On the dynamics of $x_{\eta+1} = \frac{\alpha + \gamma x_{\eta-1} + \delta x_{\eta-2}}{A + x_{\eta-2}}$, *J. Differ. Equations Appl.*, 9 (8) (2003), 731-738.
- [4] E. Chatterjee, E. A. Grove, Y. Kostrov and G. Ladas, On the trichotomy character of $x_{\eta+1} = \frac{\alpha + \gamma x_{\eta-1}}{A + Bx_{\eta} + x_{\eta-2}}$, *J. Differ. Equations Appl.*, 9(12) (2003), 1113–1128.
- [5] G. Chatzarakis, E. Elabbasy, O. Moaaz and H. Mahjoub, Global analysis and the periodic character of a class of difference equations, *Axioms*, 2019, 8(4), 131.
- [6] C. Cinar, On the positive solutions of the difference equation $x_{\eta+1} = \frac{ax_{\eta-1}}{1 + bx_{\eta}x_{\eta-1}}$, *Appl. Math. Comp.*, 156 (2004) 587-590.
- [7] D.S.Dilip, S. M. Mathew and E. M. Elsayed, Asymptotic and boundedness behaviour of a second order difference equation, *Journal of Computational Mathematics*, 4 (2)(2020), 68 - 77.x
- [8] E. M. Elabbasy, H. El-Metwally and E. M. Elsayed, Global attractivity and periodic character of a fractional difference equation of order three, *Yokohama Math. J.*, Vol. 53, 2007, 89-100.
- [9] E. M. Elabbasy, H. El-Metwally and E. M. Elsayed, On the difference equation $x_{\eta+1} = ax_{\eta} - \frac{bx_{\eta}}{cx_{\eta} - dx_{\eta-1}}$, *Adv. Differ. Equ.*, Volume 2006, Article ID 82579, 1–10.
- [10] E. M. Elabbasy, H. El-Metwally and E. M. Elsayed, On the difference equations $x_{\eta+1} = \frac{\alpha x_{\eta-k}}{\beta + \gamma \prod_{i=0}^k x_{\eta-i}}$, *J. Conc. Appl. Math.*, 5(2), (2007), 101-113.
- [11] E. M. Elabbasy, H. El-Metwally and E. M. Elsayed, Qualitative behavior of higher order difference equation, *Soochow Journal of Mathematical*, Vol. 33, No. 4, (2007), 861-873.
- [12] H. El-Metwally, E. A. Grove and G. Ladas, A global convergence result with applications to periodic solutions, *J. Math. Anal. Appl.*, 245 (2000), 161-170.
- [13] H. El-Metwally, E. A. Grove, G. Ladas and McGrath, On the difference equation $y_{\eta+1} = \frac{y_{\eta-(2k+1)} + p}{y_{\eta-(2k+1)} + qy_{\eta-2l}}$, *Proceedings of the 6th ICDE*, Taylor and Francis, London, 2004.
- [14] H. El-Metwally, E. A. Grove, G. Ladas and H. D. Voulov, On the global attractivity and the periodic character of some difference equations, *J. Differ. Equations Appl.*, 7 (2001), 1-14.
- [15] E. M. Elsayed, New method to obtain periodic solutions of period two and three of a rational difference equation, *Non-linear Dyn.* (2015) 79:241-250.
- [16] E. M. Elsayed, F. Alzahrani, I. Abbas and N. H. Alotaibi, Dynamical behavior and solution of nonlinear difference equation via fibonacci sequence, *Journal of Applied Analysis & Computation*, 10 (2020), 281-288.
- [17] A. Khaliq, S. S. Hassan, M. Saqib and D. S. Mashat, Behavior of a seventh order rational difference equation, *Dynamic Systems and Applications*, 28, No. 4 (2019), 809-825.

- [18] A. Khan and H. El-Metwally, Global dynamics, boundedness, and semicycle analysis of a difference equation, *Discrete Dynamics in Nature and Society*, 2021(2021)1,0 pages.
- [19] V. L. Kocic and G. Ladas, *Global Behavior of Nonlinear Difference Equations of Higher Order with Applications*, Kluwer Academic Publishers, Dordrecht, 1993.
- [20] M. R. S. Kulenovic and G. Ladas, *Dynamics of Second Order Rational Difference Equations with Open Problems and Conjectures*, Chapman & Hall / CRC Press, 2001.
- [21] B. Ogul, D. Simsek and T. Ibrahim, (2021). Solution of the Rational difference Equation, *Dynamics of Continuous, Discrete and Impulsive Systems Series, Applications and Algorithms*, 28 (2021) 125-141.
- [22] A. Sanbo and E. M. Elsayed, Some Properties of the Solutions of the Difference Equation $T_{\eta+1} = aT_{\eta} + \frac{bT_{\eta}T_{\eta-4}}{cT_{\eta-3} + dT_{\eta-4}}$, $\eta = 0, 1, \dots$, *Open Journal of Discrete Applied Mathematics*, 2(2)(2019), 31-47.
- [23] X. Yan and W. Li, Global attractivity for a class of nonlinear difference equations, *Soochow J. Math.*, 29 (3) (2003), 327-338.
- [24] X. Yang, W. Su, B. Chen, G. M. Megson and D. J. Evans, On the recursive sequence $x_{\eta+1} = \frac{ax_{\eta-1} + bx_{\eta-2}}{c + dx_{\eta-1}x_{\eta-2}}$, *Appl. Math. Comp.*, 162 (2005), 1485-1497.
- [25] L. Zhang, G. Zhang and H. Liu, Periodicity and attractivity for a rational recursive sequence, *J. Appl. Math. & Computing*, 19(1-2) (2005), 191-201.

On Matrix Sequences of modified Tribonacci-Lucas Numbers

Yüksel Soykan¹, Erkan Taşdemir², Vedat İrge³

¹ Department of Mathematics, Zonguldak Bülent Ecevit University, Zonguldak, Turkey, yuksel_soykan@hotmail.com, ORCID: 0000-0002-1895-211X, ²Pınarhisar Vocational School, Kırklareli University, Kırklareli, Turkey, erkantademir@hotmail.com, ORCID: 0000-0002-5002-3193, ³ Department of Mathematics, Zonguldak Bülent Ecevit University, Zonguldak, Turkey, vedatirge_1986@hotmail.com, ORCID: 0000-0003-2878-3505,

ABSTRACT

In this paper, we define modified Tribonacci-Lucas matrix sequence and investigate its properties.

ARTICLE INFO

Research article

Received: 10.05.2021

Accepted: 17.12.2021

Keywords: Tribonacci numbers, Tribonacci-Lucas matrix sequence, modified Tribonacci-Lucas matrix sequence.

*Corresponding author

1. Introduction and Preliminaries

Tribonacci sequence $\{T_n\}_{n \geq 0}$, Tribonacci-Lucas sequence $\{K_n\}_{n \geq 0}$ and modified Tribonacci-Lucas sequence $\{G_n\}_{n \geq 0}$ are defined, respectively, by the third-order recurrence relations

$$T_{n+3} = T_{n+2} + T_{n+1} + T_n, \quad T_0 = 0, T_1 = 1, T_2 = 1, \quad (1.1)$$

$$K_{n+3} = K_{n+2} + K_{n+1} + K_n, \quad K_0 = 3, K_1 = 1, K_2 = 3, \quad (1.2)$$

$$G_{n+3} = G_{n+2} + G_{n+1} + G_n, \quad G_0 = 4, G_1 = 4, G_2 = 10. \quad (1.3)$$

The sequences $\{T_n\}_{n \geq 0}$, $\{K_n\}_{n \geq 0}$ and $\{G_n\}_{n \geq 0}$ can be extended to negative subscripts by defining

$$T_{-n} = -T_{-(n-1)} - T_{-(n-2)} + T_{-(n-3)}, \quad (1.4)$$

$$K_{-n} = -K_{-(n-1)} - K_{-(n-2)} + K_{-(n-3)}, \quad (1.5)$$

$$G_{-n} = -G_{-(n-1)} - G_{-(n-2)} + G_{-(n-3)}, \quad (1.6)$$

for $n = 1, 2, 3, \dots$ respectively. Therefore, recurrences (1.1)-(1.3) hold for all integers n . Basic properties of Tribonacci, Tribonacci-Lucas and modified Tribonacci-Lucas sequences are given in [8].

Next, we present the first few values of the Tribonacci, Tribonacci-Lucas and modified Tribonacci-Lucas numbers with positive and negative subscripts:

Table 1. The first few values of the special third-order numbers with positive and negative subscripts.

n	0	1	2	3	4	5	6	7	8	9	10	11	12	13
T_n	0	1	1	2	4	7	13	24	44	81	149	274	504	927
T_{-n}		0	1	-1	0	2	-3	1	4	-8	5	7	-20	18
K_n	3	1	3	7	11	21	39	71	131	241	443	815	1499	2757
K_{-n}		-1	-1	5	-5	-1	11	-15	3	23	-41	21	43	-105
G_n	4	4	10	18	32	60	110	202	372	684	1258	2314	4256	7828
G_{-n}		2	-2	4	0	-6	10	-4	-12	26	-18	-20	64	-62

For all integers n , Tribonacci, Tribonacci-Lucas and modified Tribonacci-Lucas numbers can be expressed using Binet's formulas as

$$T_n = \frac{\alpha^{n+1}}{(\alpha - \beta)(\alpha - \gamma)} + \frac{\beta^{n+1}}{(\beta - \alpha)(\beta - \gamma)} + \frac{\gamma^{n+1}}{(\gamma - \alpha)(\gamma - \beta)}, \tag{1.7}$$

$$K_n = \alpha^n + \beta^n + \gamma^n, \tag{1.8}$$

$$G_n = (\alpha + 1)\alpha^n + (\beta + 1)\beta^n + (\gamma + 1)\gamma^n \tag{1.9}$$

respectively. Here, α, β and γ are the roots of the cubic equation

$$x^3 - x^2 - x - 1 = 0.$$

Moreover,

$$\alpha = \frac{1 + \sqrt[3]{19 + 3\sqrt{33}} + \sqrt[3]{19 - 3\sqrt{33}}}{3},$$

$$\beta = \frac{1 + \omega\sqrt[3]{19 + 3\sqrt{33}} + \omega^2\sqrt[3]{19 - 3\sqrt{33}}}{3},$$

$$\gamma = \frac{1 + \omega^2\sqrt[3]{19 + 3\sqrt{33}} + \omega\sqrt[3]{19 - 3\sqrt{33}}}{3}$$

where

$$\omega = \frac{-1 + i\sqrt{3}}{2} = \exp(2\pi i/3).$$

Note that

$$\begin{aligned} \alpha + \beta + \gamma &= 1, \\ \alpha\beta + \alpha\gamma + \beta\gamma &= -1, \\ \alpha\beta\gamma &= 1. \end{aligned}$$

Note that the Binet form of a sequence satisfying (1.7) and (1.9) for non-negative integers is valid for all integers n . The generating functions for the modified Tribonacci-Lucas sequence $\{G_n\}_{n \geq 0}$ is

$$\sum_{n=0}^{\infty} G_n x^n = \frac{4 + 2x^2}{1 - x - x^2 - x^3}. \tag{1.10}$$

Recently, there have been so many studies of the sequences of numbers in the literature that concern about subsequences of the Horadam (Generalized Fibonacci) numbers and generalized Tribonacci numbers such as Fibonacci, Lucas, Pell and Jacobsthal numbers; third-order Pell, third-order Pell-Lucas, Padovan, Perrin, Padovan-Perrin, Narayana, third order Jacobsthal and third order Jacobsthal-Lucas numbers. The sequences of numbers were widely used in many research areas, such as physics, engineering, architecture, nature and art. On the other hand, the matrix sequences have taken so much interest for different type of numbers. We present some works on matrix sequences of the numbers in the following Table 2.

Table 2. A few special study on the matrix sequences of the numbers.

Name of sequence	work on the matrix sequences of the numbers
Generalized Fibonacci	[2],[3],[4],[9],[10],[11],[12],[13],[16]
Generalized Tribonacci	[1],[6],[7],[14],[15]
Generalized Tetranacci	[5]

In this paper, the matrix sequences of modified Tribonacci-Lucas numbers will be defined. Then, by giving the generating functions, the Binet formulas, and summation formulas over this new matrix sequence, we will obtain some fundamental properties on modified Tribonacci-Lucas numbers. Also, we will present the relationship between matrix sequences of Tribonacci, Tribonacci-Lucas and modified Tribonacci-Lucas numbers.

Tribonacci and Tribonacci-Lucas matrix sequences are defined as follows (see [6]).

Definition 1.1 For any integer $n \geq 0$, the Tribonacci matrix (\mathcal{T}_n) and Tribonacci-Lucas matrix (\mathcal{K}_n) are defined by

$$\mathcal{T}_n = \mathcal{T}_{n-1} + \mathcal{T}_{n-2} + \mathcal{T}_{n-3}, \tag{1.11}$$

$$\mathcal{K}_n = \mathcal{K}_{n-1} + \mathcal{K}_{n-2} + \mathcal{K}_{n-3}, \tag{1.12}$$

respectively, with initial conditions

$$\mathcal{T}_0 = \begin{pmatrix} 1 & 0 & 0 \\ 0 & 1 & 0 \\ 0 & 0 & 1 \end{pmatrix}, \mathcal{T}_1 = \begin{pmatrix} 1 & 1 & 1 \\ 1 & 0 & 0 \\ 0 & 1 & 0 \end{pmatrix}, \mathcal{T}_2 = \begin{pmatrix} 2 & 2 & 1 \\ 1 & 1 & 1 \\ 1 & 0 & 0 \end{pmatrix}$$

and

$$\mathcal{K}_0 = \begin{pmatrix} 1 & 2 & 3 \\ 3 & -2 & -1 \\ -1 & 4 & -1 \end{pmatrix}, \mathcal{K}_1 = \begin{pmatrix} 3 & 4 & 1 \\ 1 & 2 & 3 \\ 3 & -2 & -1 \end{pmatrix}, \mathcal{K}_2 = \begin{pmatrix} 7 & 4 & 3 \\ 3 & 4 & 1 \\ 1 & 2 & 3 \end{pmatrix}.$$

The sequences $\{\mathcal{T}_n\}_{n \geq 0}$ and $\{\mathcal{K}_n\}_{n \geq 0}$ can be extended to negative subscripts by defining

$$\mathcal{T}_{-n} = -\mathcal{T}_{-(n-1)} - \mathcal{T}_{-(n-2)} + \mathcal{T}_{-(n-3)}$$

and

$$\mathcal{K}_{-n} = -\mathcal{K}_{-(n-1)} - \mathcal{K}_{-(n-2)} + \mathcal{K}_{-(n-3)}$$

for $n = 1, 2, 3, \dots$ respectively. Therefore, recurrences (1.11) and (1.12) hold for all integers n .

The following theorem gives the n th general terms of the Tribonacci and Tribonacci-Lucas matrix sequences.

Theorem 1.2 For any integer $n \geq 0$, we have the following formulas of the matrix sequences:

$$\mathcal{T}_n = \begin{pmatrix} T_{n+1} & T_n + T_{n-1} & T_n \\ T_n & T_{n-1} + T_{n-2} & T_{n-1} \\ T_{n-1} & T_{n-2} + T_{n-3} & T_{n-2} \end{pmatrix}, \tag{1.13}$$

$$\mathcal{K}_n = \begin{pmatrix} K_{n+1} & K_n + K_{n-1} & K_n \\ K_n & K_{n-1} + K_{n-2} & K_{n-1} \\ K_{n-1} & K_{n-2} + K_{n-3} & K_{n-2} \end{pmatrix}. \tag{1.14}$$

Proof. It is given in [6]. □

We now give the Binet formulas for the Tribonacci and Tribonacci-Lucas matrix sequences.

Theorem 1.3 For every integer n , the Binet formulas of the Tribonacci and Tribonacci-Lucas matrix sequences are given by

$$\mathcal{T}_n = A_1\alpha^n + B_1\beta^n + C_1\gamma^n, \tag{1.15}$$

$$\mathcal{K}_n = A_2\alpha^n + B_2\beta^n + C_2\gamma^n \tag{1.16}$$

where

$$A_1 = \frac{\alpha\mathcal{T}_2 + \alpha(\alpha - 1)\mathcal{T}_1 + \mathcal{T}_0}{\alpha(\alpha - \gamma)(\alpha - \beta)}, B_1 = \frac{\beta\mathcal{T}_2 + \beta(\beta - 1)\mathcal{T}_1 + \mathcal{T}_0}{\beta(\beta - \gamma)(\beta - \alpha)}, C_1 = \frac{\gamma\mathcal{T}_2 + \gamma(\gamma - 1)\mathcal{T}_1 + \mathcal{T}_0}{\gamma(\gamma - \beta)(\gamma - \alpha)},$$

$$A_2 = \frac{\alpha\mathcal{K}_2 + \alpha(\alpha - 1)\mathcal{K}_1 + \mathcal{K}_0}{\alpha(\alpha - \gamma)(\alpha - \beta)}, B_2 = \frac{\beta\mathcal{K}_2 + \beta(\beta - 1)\mathcal{K}_1 + \mathcal{K}_0}{\beta(\beta - \gamma)(\beta - \alpha)}, C_2 = \frac{\gamma\mathcal{K}_2 + \gamma(\gamma - 1)\mathcal{K}_1 + \mathcal{K}_0}{\gamma(\gamma - \beta)(\gamma - \alpha)}.$$

Proof. It is given in [6]. □

2. The Matrix Sequences of modified Tribonacci-Lucas Numbers

In this section, we define modified Tribonacci-Lucas matrix sequence and investigate its properties.

Definition 2.1 For any integer $n \geq 0$, the modified Tribonacci-Lucas matrix (\mathcal{G}_n) is defined by

$$\mathcal{G}_n = \mathcal{G}_{n-1} + \mathcal{G}_{n-2} + \mathcal{G}_{n-3}, \tag{2.1}$$

with initial conditions

$$\mathcal{G}_0 = \begin{pmatrix} 4 & 6 & 4 \\ 4 & 0 & 2 \\ 2 & 2 & -2 \end{pmatrix}, \mathcal{G}_1 = \begin{pmatrix} 10 & 8 & 4 \\ 4 & 6 & 4 \\ 4 & 0 & 2 \end{pmatrix}, \mathcal{G}_2 = \begin{pmatrix} 18 & 14 & 10 \\ 10 & 8 & 4 \\ 4 & 6 & 4 \end{pmatrix}.$$

The sequence $\{\mathcal{G}_n\}_{n \geq 0}$ can be extended to negative subscripts by defining

$$\mathcal{G}_{-n} = -\mathcal{G}_{-(n-1)} - \mathcal{G}_{-(n-2)} + \mathcal{G}_{-(n-3)}$$

for $n = 1, 2, 3, \dots$. Therefore, recurrences (2.1) holds for all integers n .

The following theorem gives the n th general terms of the modified Tribonacci-Lucas matrix sequence.

Theorem 2.2 For any integer $n \geq 0$, we have the following formula of the matrix sequence:

$$\mathcal{G}_n = \begin{pmatrix} G_{n+1} & G_n + G_{n-1} & G_n \\ G_n & G_{n-1} + G_{n-2} & G_{n-1} \\ G_{n-1} & G_{n-2} + G_{n-3} & G_{n-2} \end{pmatrix}. \tag{2.2}$$

Proof. We prove (2.2) by strong mathematical induction on n . If $n = 0$ then, since $G_{-3} = 4, G_{-2} = -2, G_{-1} = 2, G_0 = 4, G_1 = 4, G_2 = 10$, we have

$$\mathcal{G}_0 = \begin{pmatrix} G_1 & G_0 + G_{-1} & G_0 \\ G_0 & G_{-1} + G_{-2} & G_{-1} \\ G_{-1} & G_{-2} + G_{-3} & G_{-2} \end{pmatrix} = \begin{pmatrix} 4 & 6 & 4 \\ 4 & 0 & 2 \\ 2 & 2 & -2 \end{pmatrix}$$

which is true and

$$\mathcal{G}_1 = \begin{pmatrix} G_2 & G_1 + G_0 & G_1 \\ G_1 & G_0 + G_{-1} & G_0 \\ G_0 & G_{-1} + G_{-2} & G_{-1} \end{pmatrix} = \begin{pmatrix} 10 & 8 & 4 \\ 4 & 6 & 4 \\ 4 & 0 & 2 \end{pmatrix}$$

which is true. Assume that the equality holds for $n \leq k$. For $n = k + 1$, we have

$$\begin{aligned} \mathcal{G}_{k+1} &= \mathcal{G}_k + \mathcal{G}_{k-1} + \mathcal{G}_{k-2} \\ &= \begin{pmatrix} G_{k+1} & G_k + G_{k-1} & G_k \\ G_k & G_{k-1} + G_{k-2} & G_{k-1} \\ G_{k-1} & G_{k-2} + G_{k-3} & G_{k-2} \end{pmatrix} + \begin{pmatrix} G_k & G_{k-1} + G_{k-2} & G_{k-1} \\ G_{k-1} & G_{k-2} + G_{k-3} & G_{k-2} \\ G_{k-2} & G_{k-3} + G_{k-4} & G_{k-3} \end{pmatrix} \\ &\quad + \begin{pmatrix} G_{k-1} & G_{k-2} + G_{k-3} & G_{k-2} \\ G_{k-2} & G_{k-3} + G_{k-4} & G_{k-3} \\ G_{k-3} & G_{k-4} + G_{k-5} & G_{k-4} \end{pmatrix} \\ &= \begin{pmatrix} G_k + G_{k-1} + G_{k+1} & G_k + G_{k-1} + G_{k-1} + G_{k-2} + G_{k-2} + G_{k-3} & G_k + G_{k-1} + G_{k-2} \\ G_k + G_{k-1} + G_{k-2} & G_{k-1} + G_{k-2} + G_{k-2} + G_{k-3} + G_{k-3} + G_{k-4} & G_{k-1} + G_{k-2} + G_{k-3} \\ G_{k-1} + G_{k-2} + G_{k-3} & G_{k-2} + G_{k-3} + G_{k-3} + G_{k-4} + G_{k-4} + G_{k-5} & G_{k-2} + G_{k-3} + G_{k-4} \end{pmatrix} \\ &= \begin{pmatrix} G_{k+2} & G_k + G_{k+1} & G_{k+1} \\ G_{k+1} & G_k + G_{k-1} & G_k \\ G_k & G_{k-1} + G_{k-2} & G_{k-1} \end{pmatrix}. \end{aligned}$$

Thus, by strong induction on n , this proves (2.2). \square

We now give the Binet formula for the modified Tribonacci-Lucas matrix sequence.

Theorem 2.3 For every integer n , the Binet formula of the modified Tribonacci-Lucas matrix sequence is given by

$$\mathcal{G}_n = A_5\alpha^n + B_5\beta^n + C_5\gamma^n \tag{2.3}$$

where

$$A_5 = \frac{\alpha \mathcal{G}_2 + \alpha(\alpha - 1)\mathcal{G}_1 + \mathcal{G}_0}{\alpha(\alpha - \gamma)(\alpha - \beta)}, B_5 = \frac{\beta \mathcal{G}_2 + \beta(\beta - 1)\mathcal{G}_1 + \mathcal{G}_0}{\beta(\beta - \gamma)(\beta - \alpha)}, C_5 = \frac{\gamma \mathcal{G}_2 + \gamma(\gamma - 1)\mathcal{G}_1 + \mathcal{G}_0}{\gamma(\gamma - \beta)(\gamma - \alpha)}.$$

Proof. We prove the theorem only for $n \geq 0$. By the assumption, the characteristic equation of (2.1) is $x^3 - x^2 - x - 1 = 0$ and the roots of it are α, β and γ . So, it's general solution is given by

$$\mathcal{G}_n = A_5 \alpha^n + B_5 \beta^n + C_5 \gamma^n.$$

Using initial condition which is given in Definition 2.1, and also applying linear algebra operations, we obtain the matrices A_5, B_5, C_5 as desired. This gives the formula for \mathcal{G}_n . \square

The well known Binet formulas for modified Tribonacci-Lucas is given in (1.7). But, we will obtain this function in terms of modified Tribonacci-Lucas matrix sequence as a consequence of Theorems 2.2 and 2.3. To do this, we will give the formulas for these numbers by means of the related matrix sequences. In fact, in the proof of next corollary, we will just compare the linear combination of the 2nd row and 1st column entries of the matrices.

Corollary 2.4 For every integers n , the Binet's formulas for modified Tribonacci-Lucas numbers is given as

$$G_n = (\alpha + 1)\alpha^n + (\beta + 1)\beta^n + (\gamma + 1)\gamma^n.$$

Proof. From Theorem 2.2, we have

$$\begin{aligned} \mathcal{G}_n &= A_5 \alpha^n + B_5 \beta^n + C_5 \gamma^n \\ &= \frac{\alpha \mathcal{G}_2 + \alpha(\alpha - 1)\mathcal{G}_1 + \mathcal{G}_0}{\alpha(\alpha - \gamma)(\alpha - \beta)} \alpha^n + \frac{\beta \mathcal{G}_2 + \beta(\beta - 1)\mathcal{G}_1 + \mathcal{G}_0}{\beta(\beta - \gamma)(\beta - \alpha)} \beta^n \\ &\quad + \frac{\gamma \mathcal{G}_2 + \gamma(\gamma - 1)\mathcal{G}_1 + \mathcal{G}_0}{\gamma(\gamma - \beta)(\gamma - \alpha)} \gamma^n \\ &= \frac{\alpha^{n-1}}{(\alpha - \gamma)(\alpha - \beta)} \begin{pmatrix} 10\alpha^2 + 8\alpha + 4 & 8\alpha^2 + 6\alpha + 6 & 4\alpha^2 + 6\alpha + 4 \\ 4\alpha^2 + 6\alpha + 4 & 2\alpha(3\alpha + 1) & 4\alpha^2 + 2 \\ 4\alpha^2 + 2 & 6\alpha + 2 & 2\alpha^2 + 2\alpha - 2 \end{pmatrix} \\ &\quad + \frac{\beta^{n-1}}{(\beta - \gamma)(\beta - \alpha)} \begin{pmatrix} 10\beta^2 + 8\beta + 4 & 8\beta^2 + 6\beta + 6 & 4\beta^2 + 6\beta + 4 \\ 4\beta^2 + 6\beta + 4 & 2\beta(3\beta + 1) & 4\beta^2 + 2 \\ 4\beta^2 + 2 & 6\beta + 2 & 2\beta^2 + 2\beta - 2 \end{pmatrix} \\ &\quad + \frac{\gamma^{n-1}}{(\gamma - \beta)(\gamma - \alpha)} \begin{pmatrix} 10\gamma^2 + 8\gamma + 4 & 8\gamma^2 + 6\gamma + 6 & 4\gamma^2 + 6\gamma + 4 \\ 4\gamma^2 + 6\gamma + 4 & 2\gamma(3\gamma + 1) & 4\gamma^2 + 2 \\ 4\gamma^2 + 2 & 6\gamma + 2 & 2\gamma^2 + 2\gamma - 2 \end{pmatrix}. \end{aligned}$$

By Theorem 2.3, we know that

$$\mathcal{G}_n = \begin{pmatrix} G_{n+1} & G_n + G_{n-1} & G_n \\ G_n & G_{n-1} + G_{n-2} & G_{n-1} \\ G_{n-1} & G_{n-2} + G_{n-3} & G_{n-2} \end{pmatrix}.$$

Now, if we compare the 2nd row and 1st column entries with the matrices in the above two equations, then we obtain

$$\begin{aligned} G_n &= \frac{\alpha^{n-1}}{(\alpha - \gamma)(\alpha - \beta)}(4\alpha^2 + 6\alpha + 4) + \frac{\beta^{n-1}}{(\beta - \gamma)(\beta - \alpha)}(4\beta^2 + 6\beta + 4) \\ &\quad + \frac{\gamma^{n-1}}{(\gamma - \beta)(\gamma - \alpha)}(4\gamma^2 + 6\gamma + 4) \\ &= (\alpha + 1)\alpha^n + (\beta + 1)\beta^n + (\gamma + 1)\gamma^n. \quad \square \end{aligned}$$

Now, we present summation formulas for modified Tribonacci-Lucas matrix sequences.

Theorem 2.5 For all integers m and j , we have

$$\sum_{k=0}^n \mathcal{G}_{mk+j} = \frac{\mathcal{G}_{mn+m+j} + \mathcal{G}_{mn-m+j} + (1 - K_{-m})\mathcal{G}_{mn+j} - \mathcal{G}_{m+j} - \mathcal{G}_{j-m} + (K_m - 1)\mathcal{G}_j}{K_m - K_{-m}}. \tag{2.4}$$

Proof. Note that

$$\begin{aligned} \sum_{k=0}^n \mathcal{G}_{mk+j} &= \mathcal{G}_{mn+j} + \sum_{k=0}^{n-1} \mathcal{G}_{mk+j} = \mathcal{G}_{mn+j} + \sum_{k=0}^{n-1} (A_5\alpha^{mk+j} + B_5\beta^{mk+j} + C_5\gamma^{mk+j}) \\ &= \mathcal{G}_{mn+j} + A_5\alpha^j \left(\frac{\alpha^{mn} - 1}{\alpha^m - 1} \right) + B_5\beta^j \left(\frac{\beta^{mn} - 1}{\beta^m - 1} \right) + C_5\gamma^j \left(\frac{\gamma^{mn} - 1}{\gamma^m - 1} \right). \end{aligned}$$

Simplifying the last equalities in the last expression imply (2.4) as required. □

As in Corollary 2.4, in the proof of next Corollary, we just compare the linear combination of the 2nd row and 1st column entries of the relevant matrices.

Corollary 2.6 For all integers m and j , we have

$$\sum_{k=0}^n \mathcal{G}_{mk+j} = \frac{\mathcal{G}_{mn+m+j} + \mathcal{G}_{mn-m+j} + (1 - K_{-m})\mathcal{G}_{mn+j} - \mathcal{G}_{m+j} - \mathcal{G}_{j-m} + (K_m - 1)\mathcal{G}_j}{K_m - K_{-m}}. \tag{2.5}$$

Note that using the above Corollary we obtain the following well known formulas (taking $m = 1, j = 0$ and $m = -1, j = 0$ respectively):

$$\sum_{k=0}^n \mathcal{G}_k = \frac{1}{2} (\mathcal{G}_{n+1} + 2\mathcal{G}_n + \mathcal{G}_{n-1} - 6)$$

and

$$\sum_{k=0}^n \mathcal{G}_{-k} = \frac{1}{2} (-\mathcal{G}_{-n+1} - \mathcal{G}_{-n-1} + 14).$$

or

$$\sum_{k=1}^n \mathcal{G}_{-k} = \frac{1}{2} (-\mathcal{G}_{-n+1} - \mathcal{G}_{-n-1} + 6).$$

Note that the last Corollary can be written in the following form:

$$\sum_{k=1}^n \mathcal{G}_{mk+j} = \frac{\mathcal{G}_{mn+m+j} + \mathcal{G}_{mn-m+j} + (1 - K_{-m})\mathcal{G}_{mn+j} - \mathcal{G}_{m+j} - \mathcal{G}_{j-m} + (K_{-m} - 1)\mathcal{G}_j}{K_m - K_{-m}}.$$

We now give generating functions of \mathcal{G} .

Theorem 2.7 The generating function for the modified Tribonacci-Lucas matrix sequence is given as

$$\sum_{n=0}^{\infty} \mathcal{G}_n x^n = \frac{1}{1 - x - x^2 - x^3} \begin{pmatrix} 4x^2 + 6x + 4 & 2x + 6 & 2x^2 + 4 \\ 2x^2 + 4 & 2x^2 + 6x & -2x^2 + 2x + 2 \\ -2x^2 + 2x + 2 & 4x^2 - 2x + 2 & 4x^2 + 4x - 2 \end{pmatrix}.$$

Proof. Suppose that $g(x) = \sum_{n=0}^{\infty} \mathcal{G}_n x^n$ is the generating function for the sequence $\{\mathcal{G}_n\}_{n \geq 0}$. Then, using Definition 2.1, we obtain

$$\begin{aligned} g(x) &= \sum_{n=0}^{\infty} \mathcal{G}_n x^n = \mathcal{G}_0 + \mathcal{G}_1 x + \mathcal{G}_2 x^2 + \sum_{n=3}^{\infty} \mathcal{G}_n x^n \\ &= \mathcal{G}_0 + \mathcal{G}_1 x + \mathcal{G}_2 x^2 + \sum_{n=3}^{\infty} (\mathcal{G}_{n-1} + \mathcal{G}_{n-2} + \mathcal{G}_{n-3}) x^n \\ &= \mathcal{G}_0 + \mathcal{G}_1 x + \mathcal{G}_2 x^2 + \sum_{n=3}^{\infty} \mathcal{G}_{n-1} x^n + \sum_{n=3}^{\infty} \mathcal{G}_{n-2} x^n + \sum_{n=3}^{\infty} \mathcal{G}_{n-3} x^n \\ &= \mathcal{G}_0 + \mathcal{G}_1 x + \mathcal{G}_2 x^2 - \mathcal{G}_0 x - \mathcal{G}_1 x^2 - \mathcal{G}_0 x^2 + x \sum_{n=0}^{\infty} \mathcal{G}_n x^n + x^2 \sum_{n=0}^{\infty} \mathcal{G}_n x^n + x^3 \sum_{n=0}^{\infty} \mathcal{G}_n x^n \\ &= \mathcal{G}_0 + \mathcal{G}_1 x + \mathcal{G}_2 x^2 - \mathcal{G}_0 x - \mathcal{G}_1 x^2 - \mathcal{G}_0 x^2 + xg(x) + x^2 g(x) + x^3 g(x). \end{aligned}$$

Rearranging the above equation, we get

$$g(x) = \frac{\mathcal{G}_0 + (\mathcal{G}_1 - \mathcal{G}_0)x + (\mathcal{G}_2 - \mathcal{G}_1 - \mathcal{G}_0)x^2}{1 - x - x^2 - x^3}$$

which equals the $\sum_{n=0}^{\infty} \mathcal{G}_n x^n$ in the Theorem. This completes the proof. \square

The well known generating functions for modified Tribonacci-Lucas numbers is as in (1.10). However, we will obtain these functions in terms of modified Tribonacci-Lucas matrix sequence as a consequence of Theorem 2.7. To do this, we will again compare the the 2nd row and 1st column entries with the matrices in Theorem 2.7. Thus, we have the following corollary.

Corollary 2.8 The generating functions for the modified Tribonacci-Lucas sequence $\{G_n\}_{n \geq 0}$ is given as

$$\sum_{n=0}^{\infty} G_n x^n = \frac{2x^2 + 4}{1 - x - x^2 - x^3}.$$

3. Relation Between Tribonacci, Tribonacci-Lucas and modified Tribonacci-Lucas Matrix Sequences

The following theorem shows that there always exist interrelation between Tribonacci, Tribonacci-Lucas and modified Tribonacci-Lucas matrix sequences.

Theorem 3.1 For the matrix sequences $\{\mathcal{T}_n\}$ and $\{\mathcal{G}_n\}$, we have the following identities.

- (a) $22\mathcal{T}_n = 7\mathcal{G}_{n+4} - 13\mathcal{G}_{n+3} + \mathcal{G}_{n+2}$,
- (b) $22\mathcal{T}_n = -6\mathcal{G}_{n+3} + 8\mathcal{G}_{n+2} + 7\mathcal{G}_{n+1}$,
- (c) $22\mathcal{T}_n = 2\mathcal{G}_{n+2} + \mathcal{G}_{n+1} - 6\mathcal{G}_n$,
- (d) $22\mathcal{T}_n = 3\mathcal{G}_{n+1} - 4\mathcal{G}_n + 2\mathcal{G}_{n-1}$,
- (e) $22\mathcal{T}_n = -\mathcal{G}_n + 5\mathcal{G}_{n-1} + 3\mathcal{G}_{n-2}$,
- (f) $\mathcal{G}_n = 4\mathcal{T}_{n+4} - 6\mathcal{T}_{n+3}$,
- (g) $\mathcal{G}_n = -2\mathcal{T}_{n+3} + 4\mathcal{T}_{n+2} + 4\mathcal{T}_{n+1}$,
- (h) $\mathcal{G}_n = 2\mathcal{T}_{n+2} + 2\mathcal{T}_{n+1} - 2\mathcal{T}_n$,
- (i) $\mathcal{G}_n = 4\mathcal{T}_{n+1} + 2\mathcal{T}_{n-1}$,
- (j) $\mathcal{G}_n = 4\mathcal{T}_n + 6\mathcal{T}_{n-1} + 4\mathcal{T}_{n-2}$.

Proof. The proof follows from the following equalities:

$$\begin{aligned} 22\mathcal{T}_n &= 7\mathcal{G}_{n+4} - 13\mathcal{G}_{n+3} + \mathcal{G}_{n+2}, \\ 22\mathcal{T}_n &= -6\mathcal{G}_{n+3} + 8\mathcal{G}_{n+2} + 7\mathcal{G}_{n+1}, \\ 22\mathcal{T}_n &= 2\mathcal{G}_{n+2} + \mathcal{G}_{n+1} - 6\mathcal{G}_n, \\ 22\mathcal{T}_n &= 3\mathcal{G}_{n+1} - 4\mathcal{G}_n + 2\mathcal{G}_{n-1}, \\ 22\mathcal{T}_n &= -\mathcal{G}_n + 5\mathcal{G}_{n-1} + 3\mathcal{G}_{n-2} \end{aligned}$$

and

$$G_n = 4T_{n+4} - 6T_{n+3}, \tag{3.1}$$

$$G_n = -2T_{n+3} + 4T_{n+2} + 4T_{n+1}, \tag{3.2}$$

$$G_n = 2T_{n+2} + 2T_{n+1} - 2T_n, \tag{3.3}$$

$$G_n = 4T_{n+1} + 2T_{n-1}, \tag{3.4}$$

$$G_n = 4T_n + 6T_{n-1} + 4T_{n-2}. \tag{3.5}$$

\square

Theorem 3.2 For the matrix sequences $\{\mathcal{K}_n\}$ and $\{\mathcal{G}_n\}$, we have the following identities.

- (a) $2\mathcal{K}_n = -3\mathcal{G}_{n+4} + 4\mathcal{G}_{n+3} + 3\mathcal{G}_{n+2}$,
- (b) $2\mathcal{K}_n = \mathcal{G}_{n+3} - 3\mathcal{G}_{n+1}$,
- (c) $2\mathcal{K}_n = \mathcal{G}_{n+2} - 2\mathcal{G}_{n+1} + \mathcal{G}_n$,
- (d) $2\mathcal{K}_n = -\mathcal{G}_{n+1} + 2\mathcal{G}_n + \mathcal{G}_{n-1}$,
- (e) $2\mathcal{K}_n = \mathcal{G}_n - \mathcal{G}_{n-2}$,
- (f) $\mathcal{G}_n = \mathcal{K}_{n+3} - \mathcal{K}_{n+2}$,
- (g) $\mathcal{G}_n = \mathcal{K}_{n+1} + \mathcal{K}_n$,
- (h) $\mathcal{G}_n = 2\mathcal{K}_n + \mathcal{K}_{n-1} + \mathcal{K}_{n-2}$.

Proof. The proof follows from the following equalities:

$$\begin{aligned} 2\mathcal{K}_n &= -3\mathcal{G}_{n+4} + 4\mathcal{G}_{n+3} + 3\mathcal{G}_{n+2}, \\ 2\mathcal{K}_n &= \mathcal{G}_{n+3} - 3\mathcal{G}_{n+1}, \\ 2\mathcal{K}_n &= \mathcal{G}_{n+2} - 2\mathcal{G}_{n+1} + \mathcal{G}_n, \\ 2\mathcal{K}_n &= -\mathcal{G}_{n+1} + 2\mathcal{G}_n + \mathcal{G}_{n-1}, \\ 2\mathcal{K}_n &= \mathcal{G}_n - \mathcal{G}_{n-2} \end{aligned}$$

and

$$\begin{aligned} \mathcal{G}_n &= \mathcal{K}_{n+3} - \mathcal{K}_{n+2}, \\ \mathcal{G}_n &= \mathcal{K}_{n+1} + \mathcal{K}_n, \\ \mathcal{G}_n &= 2\mathcal{K}_n + \mathcal{K}_{n-1} + \mathcal{K}_{n-2}. \end{aligned}$$

□

Lemma 3.3 For all non-negative integers m and n , we have the following identities.

- (a) $\mathcal{G}_0\mathcal{T}_n = \mathcal{T}_n\mathcal{G}_0 = \mathcal{G}_n$,
- (b) $\mathcal{T}_0\mathcal{G}_n = \mathcal{G}_n\mathcal{T}_0 = \mathcal{G}_n$.

Proof. Identities can be established easily. Note that to show (a) we need to use the relations (3.1)-(3.5). □
We need the following Theorem.

Theorem 3.4 For all non-negative integers m and n , we have the following identities.

$$\begin{aligned} \mathcal{T}_m\mathcal{T}_n &= \mathcal{T}_{m+n} = \mathcal{T}_n\mathcal{T}_m, \\ \mathcal{K}_{m+n} &= \mathcal{T}_m\mathcal{K}_n = \mathcal{K}_n\mathcal{T}_m. \end{aligned}$$

Proof. It is given in [6]. □

The following theorem gives relations between the matrices \mathcal{T}_n and \mathcal{G}_n .

Theorem 3.5 For all non-negative integers m and n , we have the following identities.

- (a) $\mathcal{T}_m\mathcal{G}_n = \mathcal{G}_n\mathcal{T}_m = \mathcal{G}_{m+n}$,
- (b) $\mathcal{G}_m\mathcal{G}_n = \mathcal{G}_n\mathcal{G}_m = 16\mathcal{T}_{m+n+8} - 48\mathcal{T}_{m+n+7} + 36\mathcal{T}_{m+n+6}$,
- (c) $\mathcal{G}_m\mathcal{G}_n = \mathcal{G}_n\mathcal{G}_m = 4\mathcal{T}_{m+n+4} + 8\mathcal{T}_{m+n+3} - 4\mathcal{T}_{m+n+2} - 8\mathcal{T}_{m+n+1} + 4\mathcal{T}_{m+n}$,
- (d) $\mathcal{G}_m\mathcal{G}_n = \mathcal{G}_n\mathcal{G}_m = 16\mathcal{T}_{m+n+2} + 16\mathcal{T}_{m+n} + 4\mathcal{T}_{m+n-2}$,
- (e) $(\mathcal{G}_{m+n+2} - 2\mathcal{G}_{m+n+1} + \mathcal{G}_{m+n}) = \frac{1}{22}(2\mathcal{G}_{m+2} + \mathcal{G}_{m+1} - 6\mathcal{G}_m)(\mathcal{G}_{n+2} - 2\mathcal{G}_{n+1} + \mathcal{G}_n)$.

Proof.

(a) By Lemma 3.3, we have

$$\mathcal{T}_m \mathcal{G}_n = \mathcal{T}_m \mathcal{T}_n \mathcal{G}_0.$$

Now, from Theorem 3.4 and again by Lemma 3.3 we obtain $\mathcal{T}_m \mathcal{G}_n = \mathcal{T}_{m+n} \mathcal{G}_0 = \mathcal{G}_{m+n}$.

Similarly, it can be shown that $\mathcal{G}_n \mathcal{T}_m = \mathcal{G}_{m+n}$.

(b) Using Theorem 3.1 and Theorem 3.4, we obtain

$$\begin{aligned} \mathcal{G}_m \mathcal{G}_n &= (4\mathcal{T}_{m+4} - 6\mathcal{T}_{m+3})(4\mathcal{T}_{n+4} - 6\mathcal{T}_{n+3}) \\ &= 36\mathcal{T}_{m+3}\mathcal{T}_{n+3} - 24\mathcal{T}_{m+3}\mathcal{T}_{n+4} - 24\mathcal{T}_{m+4}\mathcal{T}_{n+3} + 16\mathcal{T}_{m+4}\mathcal{T}_{n+4} \\ &= 36\mathcal{T}_{m+n+6} - 24\mathcal{T}_{m+n+7} - 24\mathcal{T}_{m+n+7} + 16\mathcal{T}_{m+n+8} \\ &= 36\mathcal{T}_{m+n+6} - 48\mathcal{T}_{m+n+7} + 16\mathcal{T}_{m+n+8} \\ &= 16\mathcal{T}_{m+n+8} - 48\mathcal{T}_{m+n+7} + 36\mathcal{T}_{m+n+6}. \end{aligned}$$

It can be shown similarly that $\mathcal{G}_n \mathcal{G}_m = 16\mathcal{T}_{m+n+8} - 48\mathcal{T}_{m+n+7} + 36\mathcal{T}_{m+n+6}$.

Similarly, the remaining of identities can be proved by considering again using Theorem 3.1 and Theorem 3.4. \square

Comparing matrix entries and using Theorem 1.2 and Theorem 2.2 we have next result.

Corollary 3.6 For Tribonacci and modified Tribonacci-Lucas numbers, we have the following identities:

(a) $G_{m+n} = G_{n+1}T_m + G_n(T_{m-1} + T_{m-2}) + G_{n-1}T_{m-1},$

(b) $G_{n+1}G_m + G_n(G_{m-1} + G_{m-2}) + G_{n-1}G_{m-1} = 16T_{m+n+8} - 48T_{m+n+7} + 36T_{m+n+6},$

(c) $G_{n+1}G_m + G_n(G_{m-1} + G_{m-2}) + G_{n-1}G_{m-1} = 4T_{m+n+4} + 8T_{m+n+3} - 4T_{m+n+2} - 8T_{m+n+1} + 4T_{m+n},$

(d) $G_{n+1}G_m + G_n(G_{m-1} + G_{m-2}) + G_{n-1}G_{m-1} = 16T_{m+n+2} + 16T_{m+n} + 4T_{m+n-2},$

(e) $G_{m+n} - 2G_{m+n+1} + G_{m+n+2} = \frac{1}{22}(G_{n+3}(2G_{m+2} + G_{m+1} - 6G_m) + G_{n+2}(-4G_{m+2} + 15G_m - 5G_{m-1} - 6G_{m-2}) + G_{n+1}(2G_{m+2} - G_{m+1} - 11G_m + 4G_{m-1} + 12G_{m-2}) + G_n(-2G_{m+1} + G_m + 7G_{m-1} - 6G_{m-2}) + G_{n-1}(2G_{m+1} + G_m - 6G_{m-1})).$

Proof.

(a) From Theorem 3.5 (a), we have $\mathcal{T}_m \mathcal{G}_n = \mathcal{G}_n \mathcal{T}_m = \mathcal{G}_{m+n}$. Using Theorem 1.2 and Theorem 2.2, we can write this result as

$$\begin{aligned} &\begin{pmatrix} T_{m+1} & T_m + T_{m-1} & T_m \\ T_m & T_{m-1} + T_{m-2} & T_{m-1} \\ T_{m-1} & T_{m-2} + T_{m-3} & T_{m-2} \end{pmatrix} \begin{pmatrix} G_{n+1} & G_n + G_{n-1} & G_n \\ G_n & G_{n-1} + G_{n-2} & G_{n-1} \\ G_{n-1} & G_{n-2} + G_{n-3} & G_{n-2} \end{pmatrix} \\ &= \begin{pmatrix} G_{m+n+1} & G_{m+n} + G_{m+n-1} & G_{m+n} \\ G_{m+n} & G_{m+n-1} + G_{m+n-2} & G_{m+n-1} \\ G_{m+n-1} & G_{m+n-2} + G_{m+n-3} & G_{m+n-2} \end{pmatrix}. \end{aligned}$$

Now, by multiplying the left-side matrices and then by comparing the 2nd rows and 1st columns entries, we get the required identity in (a).

Similarly, the remaining of identities can be proved by considering again Theorems 3.5, 1.2 and 2.2. \square

The next two theorems provide us the convenience to obtain the powers of Tribonacci and modified Tribonacci-Lucas matrix sequences.

Theorem 3.7 For non-negative integers m, n and r with $n \geq r$, the following identities hold:

(a) $\mathcal{T}_n^m = \mathcal{T}_{mn},$

(b) $\mathcal{T}_{n+1}^m = \mathcal{T}_1^m \mathcal{T}_{mn},$

(c) $\mathcal{T}_{n-r} \mathcal{T}_{n+r} = \mathcal{T}_n^2 = \mathcal{T}_2^n.$

Proof. The proof is given in [6]. □

To prove the following theorem we need the next lemma.

Lemma 3.8 Let A_5, B_5, C_5 as in Theorem 2.3. Then the following relations hold:

$$A_5B_5 = B_5A_5 = A_5C_5 = C_5A_5 = C_5B_5 = B_5C_5 = (0) .$$

Proof. Using $\alpha + \beta + \gamma = 1, \alpha\beta + \alpha\gamma + \beta\gamma = -1$ and $\alpha\beta\gamma = 1$, required equalities can be established by matrix calculations. □

We have analogues results for the matrix sequence \mathcal{G}_n .

Theorem 3.9 For non-negative integers m, n and r with $n \geq r$, the following identities hold:

(a) $\mathcal{G}_{n-r}\mathcal{G}_{n+r} = \mathcal{G}_n^2,$

(b) $\mathcal{G}_n^m = \mathcal{G}_0^m \mathcal{T}_{mn}.$

Proof.

(a) We use Binet’s formula of modified Tribonacci-Lucas matrix sequence which is given in Theorem 2.3. So,

$$\begin{aligned} & \mathcal{G}_{n-r}\mathcal{G}_{n+r} - \mathcal{G}_n^2 \\ &= (A_5\alpha^{n-r} + B_5\beta^{n-r} + C_5\gamma^{n-r})(A_5\alpha^{n+r} + B_5\beta^{n+r} + C_5\gamma^{n+r}) \\ & \quad - (A_5\alpha^n + B_5\beta^n + C_5\gamma^n)^2 \\ &= A_5B_5\alpha^{n-r}\beta^{n-r}(\alpha^r - \beta^r)^2 + A_5C_5\alpha^{n-r}\gamma^{n-r}(\alpha^r - \gamma^r)^2 \\ & \quad + B_5C_5\beta^{n-r}\gamma^{n-r}(\beta^r - \gamma^r)^2 \\ &= 0 \end{aligned}$$

since $A_5B_5 = A_5C_5 = C_5B_5$ (see Lemma 3.8). Now, we get the result as required.

(b) By Theorem 3.7, we have

$$\mathcal{G}_0^m \mathcal{T}_{mn} = \underbrace{\mathcal{G}_0 \mathcal{G}_0 \dots \mathcal{G}_0}_{m \text{ times}} \underbrace{\mathcal{T}_n \mathcal{T}_n \dots \mathcal{T}_n}_{m \text{ times}}.$$

When we apply Lemma 3.3 (a) iteratively, it follows that

$$\begin{aligned} \mathcal{G}_0^m \mathcal{T}_{mn} &= (\mathcal{G}_0 \mathcal{T}_n)(\mathcal{G}_0 \mathcal{T}_n) \dots (\mathcal{G}_0 \mathcal{T}_n) \\ &= \mathcal{G}_n \mathcal{G}_n \dots \mathcal{G}_n = \mathcal{G}_n^m. \end{aligned}$$

This completes the proof. □

References

[1] Cerda-Morales, G., On the Third-Order Jacobsthal and Third-Order Jacobsthal–Lucas Sequences and Their Matrix Representations. *Mediterranean Journal of Mathematics*, **16** (2019) 1-12.

[2] Cıvcıv, H., Turkmen, R., On the (s; t)-Fibonacci and Fibonacci matrix sequences, *Ars Combin.* **87** (2008) 161-173.

[3] Cıvcıv, H., Turkmen, R., Notes on the (s; t)-Lucas and Lucas matrix sequences, *Ars Combin.* **89** (2008) 271-285.

[4] Gulec, H.H., Taskara, N., On the (s; t)-Pell and (s; t)-Pell-Lucas sequences and their matrix representations, *Appl. Math. Lett.* **25** (2012), 1554-1559, doi.org/10.1016/j.aml.2012.01.014.

[5] Soykan, Y., Matrix Sequences of Tetranacci and Tetranacci-Lucas Numbers, *Int. J. Adv. Appl. Math. and Mech.* **7**(2), 57-69, 2019.

[6] Soykan, Y., Matrix Sequences of Tribonacci and Tribonacci-Lucas Numbers, *Communications in Mathematics and Applications*, **11**(2), 281-295, 2020. DOI: 10.26713/cma.v11i2.1102

[7] Soykan, Y., Tribonacci and Tribonacci-Lucas Matrix Sequences with Negative Subscripts, *Communications in Mathematics and Applications*, **11**(1), 141159, 2020. DOI: 10.26713/cma.v11i1.1103.

[8] Soykan, Y., On Four Special Cases of Generalized Tribonacci Sequence: Tribonacci-Perrin, modified Tribonacci, modified Tribonacci-Lucas and adjusted

- Tribonacci-Lucas Sequences, *Journal of Progressive Research in Mathematics*, 16(3), 3056-3084, 2020.
- [9] Uslu, K., Uygun, Ş., On the (s,t) Jacobsthal and (s,t) Jacobsthal-Lucas Matrix Sequences, *Ars Combin.* **108** (2013), 13-22.
- [10] Uygun, Ş., Uslu, K., (s,t)-Generalized Jacobsthal Matrix Sequences, *Springer Proceedings in Mathematics & Statistics, Computational Analysis*, Amat, Ankara, (May 2015), 325-336.
- [11] Uygun, Ş., Some Sum Formulas of (s,t)-Jacobsthal and (s,t)-Jacobsthal Lucas Matrix Sequences, *Applied Mathematics*, **7** (2016), 61-69, <http://dx.doi.org/10.4236/am.2016.71005>.
- [12] Uygun, Ş., The binomial transforms of the generalized (s,t)-Jacobsthal matrix sequence, *Int. J. Adv. Appl. Math. and Mech.* **6**(3) (2019), 14–20.
- [13] Yazlik, Y., Taskara, N., Uslu K., Yilmaz, N., The generalized (s; t)-sequence and its matrix sequence, *Am. Inst. Phys. (AIP) Conf. Proc.* **1389** (2012), 381-384, <https://doi.org/10.1063/1.3636742>.
- [14] Yilmaz, N., Taskara, N., Matrix Sequences in Terms of Padovan and Perrin Numbers, *Journal of Applied Mathematics*, Volume 2013 (2013), Article ID 941673, 7 pages, <http://dx.doi.org/10.1155/2013/941673>.
- [15] Yilmaz, N., Taskara, N., On the Negatively Subscripted Padovan and Perrin Matrix Sequences, *Communications in Mathematics and Applications*, **5**(2) (2014), 59-72.
- [16] Wani, A.A., Badshah, V.H., and Rathore, G.B.S., Generalized Fibonacci and k-Pell Matrix Sequences, *Punjab University Journal of Mathematics*, **50**(1) (2018), 68-79.

On (α, ϕ) -weak Pata contractions

Merve Aktay¹, Murat Özdemir²

¹Department of Mathematics, Faculty of Science, Atatürk University, Erzurum, 25240, Turkey, merve.ozkan@atauni.edu.tr ²Department of Mathematics, Faculty of Science, Atatürk University, Erzurum, 25240, Turkey, mozdemir@atauni.edu.tr

ABSTRACT

In this paper, we give (α, ϕ) -weak Pata contractive mapping by using the simulation function and multivalued (α, ϕ) -weak Pata contractions and establish some fixed point results for such contractions. Also, we give an example related to (α, ϕ) -weak Pata contractive mappings via simulation function. Our results generalize some Pata type contractions and Banach contractions. Consequently, the obtained results encompass several results in the literature.

ARTICLE INFO

Research article

Received: 10.05.2022

Accepted: 01.12.2022

Keywords: fixed point, pata contraction, ϕ -weak contraction, metric spaces

*Corresponding author

1. Introduction and Preliminaries

One of the fundamental results in fixed point theory, which is called Banach's contraction principle was given by Banach [7]. Several researchers have dealt with this result. Recently, Pata [21] extended the Banach contraction principle and proved some interesting fixed point results. Chakraborty et. al. [9] got an extension of Kannan's based on the result of Pata [21]. Later Pata-Chatterjea type cyclic fixed point theorems were proved by Kadelburg et. al. [12] in metric spaces. After that coupled fixed point theorems for Pata type mappings were proved by Eshaghi [10]. This topic was extended the metric space into various different spaces by some researchers. For instance, Paknazar et. al. [20] gave Pata type fixed point theorems in modular metric space and Balasubramanian [6] obtained a fixed point theorem for Pata type mappings in cone metric spaces. Later, Aktay et. al. [2] proved some fixed point results for generalized Pata-Suzuki type contractive mappings.

Firstly, the concept of ϕ -weak contraction was defined by Alber et. al. [1] and then, Rhoades [24] studied such contractions for single-valued mappings in Banach spaces. After that, Zhang et. al. [26] introduced generalized ϕ -weak contraction and they obtained a unique common fixed point of such contractions.

Existence of fixed point for multivalued mappings in metric fixed point theory was initiated by Nadler [18]. Some notable generalizations were obtained by Hong [11].

In a recent work, Khojasteh et al. [15] introduced the notion of Z -contraction using simulation functions. Later, Karapınar [14] and Argoubi et. al. [5] studied such contractions.

Samet et. al. [25] and Karapınar et al. [13] gave respectively, the definition of α -admissible and triangular α -admissible mappings. Further, Asl et al. [4], Mohammadi et al. [17], Patel [22] and Aktay et. al. [2] gave some definitions related to α -admissibility.

The aim of this paper is to establish some fixed point results for (α, ϕ) -weak Pata contractive mapping by using the simulation function and multivalued (α, ϕ) -weak Pata contractions. Our results give existence of fixed point for a

wider class of Pata type contractions. Moreover, we give an example related to (α, ϕ) -weak Pata contractive mappings. Consequently, the obtained results encompass various well known results in the literature.

$P(W) = 2^W$ all nonempty subset of W . Let $\wp = P(W) - \{\emptyset\}$ for $U, V \in 2^W$,

$$H_{\varrho}(U, V) = \max \left\{ \sup_{u \in U} \varrho(u, V), \sup_{v \in V} \varrho(U, v) \right\}$$

where

$$\varrho(u, V) = \inf_{v \in V} \varrho(u, v)$$

H_{ϱ} is called the Hausdorff-Pompeiu functional induced by ϱ .

A point $u \in W$ is said to be a fixed point of $\tau : W \rightarrow \wp$ if $u \in \tau u$ (for single valued mapping $u = \tau u$). The set of all fixed points of τ is denoted by $F_H(\tau)$ (for single valued mapping $F(\tau)$).

Alber et. al. [1] gave the following definition.

[1] Let (W, ϱ) be a metric space. A mapping $\tau : W \rightarrow W$ is said to be ϕ -weak contraction, if there exists a map $\phi : [0, +\infty) \rightarrow [0, +\infty)$ with $\phi(0) = 0$ and $\phi(s) > 0$ for all $s > 0$ such that

$$\varrho(\tau w, \tau t) \leq \varrho(w, t) - \phi(\varrho(w, t))$$

for all $w, t \in W$.

Along this work, Ψ denotes the class of all increasing function $\psi : [0, 1] \rightarrow [0, \infty)$, which vanishes with continuity at zero. For an arbitrary $w_0 \in W$, we denote $\|w\| = \varrho(w, w_0), \forall w \in W$.

The existence of fixed point of Pata contraction mappings was proved by Pata [21] as follow.

[21] Let (W, ϱ) be a complete metric space. Let $\Lambda \geq 0, \xi \geq 1$ and $\vartheta \in [0, \xi]$ be fixed constants, $\psi \in \Psi$ and $\tau : W \rightarrow W$ be a function. If for all $w, t \in W$ the inequality

$$\varrho(\tau w, \tau t) \leq (1 - \epsilon) \varrho(w, t) + \Lambda \epsilon^{\xi} \psi(\epsilon) [1 + \|w\| + \|t\|]^{\vartheta}$$

is satisfied for all $\epsilon \in [0, 1]$, then τ has a unique fixed point, $u = \tau u$.

Samet et al. [25] and Karapinar et al. [13] gave respectively, the following definitions.

Let W be a metric space and $\tau : W \rightarrow W$ be a map and $\alpha : W \times W \rightarrow [0, +\infty)$ be a function. Then for all $w, t, z \in W$,

(i) [25] τ is said to be α -admissible if $\alpha(w, t) \geq 1$ implies $\alpha(\tau w, \tau t) \geq 1$.

(ii) [13] τ is said to be triangular α -admissible if:

- τ is α -admissible,

- $\alpha(w, z) \geq 1$ and $\alpha(z, t) \geq 1$ imply $\alpha(w, t) \geq 1$.

Further, Asl et al. [4] gave the concept of an α^* -admissible mapping which is a multivalued version of the α -admissible mapping. Later, Mohammadi et al. [17] and Patel [22] gave respectively, the definitions of α -admissible and triangular α -admissible as follows.

Let W be a nonempty set, $\tau : W \rightarrow P(W)$ and $\alpha : W \times W \rightarrow [0, \infty)$ be two given mappings. Then

(i) [17] τ is said to be an α -admissible if whenever for each $x \in W$ and $y \in Tx, \alpha(x, y) \geq 1 \Rightarrow \alpha(y, z) \geq 1$, for all $z \in Ty$.

(ii) [22] τ is said to be triangular α -admissible if τ is α -admissible and $\alpha(x, y) \geq 1$ and $\alpha(y, z) \geq 1 \Rightarrow \alpha(x, z) \geq 1, \forall z \in Ty$.

Khojasteh et. al. [15] gave the simulation function and Z -contraction in 2015 as follows.

[15] A mapping $\zeta : [0, \infty) \times [0, \infty) \rightarrow \mathbb{R}$ is called a simulation function if it satisfies the following conditions:

(ζ_1) $\zeta(0, 0) = 0$;

(ζ_2) $\zeta(w, t) < w - t$;

(ζ_3) if $\{w_n\}$ and $\{t_n\}$ are sequences in $(0, \infty)$ such that $\lim_{n \rightarrow +\infty} w_n = \lim_{n \rightarrow +\infty} t_n > 0$ then $\limsup_{n \rightarrow +\infty} \zeta(w_n, t_n) < 0$.

[15] Let (W, ϱ) be a metric space and $\tau : W \rightarrow W$ be a mapping. If there exists $\zeta \in Z$ such that

$$\zeta(\varrho(\tau w, \tau t), \varrho(w, t)) \geq 0, \text{ for all } w, t \in W$$

then τ is called Z -contraction with respect to ζ .

(ζ_1) condition was removed in above definition of simulation function by Argoubi et. al. [5] in 2015. Also, \check{Z} denotes the set of all simulation functions.

Let (W, \leq) be a partially ordered set and $w, t \in W$. Elements w and t are said to be comparable elements of W if either $w \leq t$ or $t \leq w$.

Hong [11] gave following definitions for multivalued mappings.

[11] Let W be a metric space. A subset $V \subset W$ is said to be approximative if the multivalued mapping $F_V(w) = \{v \in V : \varrho(w, v) = \varrho(w, V)\} \forall w \in W$, has nonempty values.

[11] Let $\tau : W \rightarrow 2^W$ be a multivalued mapping. Then

- (i) τ is said to have approximative values (AV), if τw is approximative for each $w \in W$.
- (ii) τ is said to have comparable approximative values (CAV), if τ has approximative values and, for each $t \in W$, there exists $u \in F_{\tau_t}(w)$ such that w is comparable to u .
- (iii) τ is said to have upper comparable approximative values (UCAV), (resp. lower comparable approximative values (LCAV)), if τ has approximative values and, for each $t \in W$, there exists $u \in F_{\tau_t}(w)$ such that $u \geq t$ (resp. $u \leq t$).

Nieto et. al. [19] gave the following definition in 2005.

[19] (H_*): Let (W, ϱ, \leq) be a partial ordered complete metric space. If $\{w_n\}$ is a non-decreasing (resp. non-increasing) sequence in W such that $w_n \rightarrow w$, then $w_n \leq w$ (resp. $w_n \geq w$) for all $n \in \mathbb{N}$.

The following Lemma 1 is used to prove our results.

[23] Let (W, ϱ) is a metric space and $\{w_n\}$ be a sequence in W such that $\varrho(w_{n+1}, w_n) \rightarrow 0$ as $n \rightarrow \infty$. If $\{w_n\}$ is not a Cauchy sequence, then there exist a $\varsigma > 0$ and sequences of positive integers $\{m_j\}$ and $\{n_j\}$ with $m_j > n_j > j$ such that $\varrho(w_{m_j}, w_{n_j}) \geq \varsigma$ and $\varrho(w_{m_j-1}, w_{n_j}) \leq \varsigma$ and $\lim_{j \rightarrow \infty} \varrho(w_{m_j-1}, w_{n_j+1}) = \varsigma$, $\lim_{j \rightarrow \infty} \varrho(w_{m_j}, w_{n_j}) = \varsigma$, $\lim_{j \rightarrow \infty} \varrho(w_{m_j-1}, w_{n_j}) = \varsigma$. From Lemma 1, we obtain

$$\lim_{j \rightarrow \infty} \varrho(w_{m_j+1}, w_{n_j+1}) = \varsigma \text{ and } \lim_{j \rightarrow \infty} \varrho(w_{m_j}, w_{n_j-1}) = \varsigma.$$

2. Main Results

In this section, we introduce the concept of (α, ϕ) -weak Pata contractions via simulation function and multivalued (α, ϕ) -weak Pata contractions in metric spaces. We establish some fixed point results for such contractions on metric spaces.

Let $\Lambda \geq 0$, $\xi \geq 1$ and $\vartheta \in [0, \xi]$ be fixed constants, $\psi \in \Psi$ and $\alpha : W \times W \rightarrow [0, +\infty)$, $\tau : W \rightarrow W$ be two functions. We say that τ is an (α, ϕ) -weak Pata contractive mapping via simulation function if there exists a function $\zeta \in \check{Z}$ such that for all $w, t \in W$, and $\epsilon \in [0, 1]$, τ satisfies the inequality

$$\zeta(\alpha(w, t) \varrho(\tau w, \tau t), (1 - \epsilon)(M(w, t) - \phi(M(w, t)) + P(w, t)) \geq 0, \tag{1}$$

where $\phi : [0, +\infty) \rightarrow [0, +\infty)$ is a continuous and nondecreasing function with $\phi(0) = 0$ and $\phi(s) > 0$, for all $s > 0$, and

$$P(w, t) = \Lambda \epsilon^\xi \psi(\epsilon) [1 + \|w\| + \|t\| + \|\tau w\| + \|\tau t\|]^\vartheta$$

and

$$M(w, t) = \max \left\{ \varrho(w, t), \varrho(w, \tau w), \varrho(t, \tau t), \frac{\varrho(w, \tau t) + \varrho(t, \tau w)}{2} \right\}.$$

Now, we state a fixed point result for (α, ϕ) -weak Pata contractive mapping via simulation function.

Let (W, ϱ) be a complete metric space. $\mathcal{T} : W \rightarrow W$ be an (α, ϕ) -weak Pata contractive mapping via simulation function. Assume that

- (i) \mathcal{T} is triangular α -admissible;
- (ii) there exists $w_0 \in W$ such that $\alpha(w_0, \mathcal{T}w_0) \geq 1$;
- (iii) \mathcal{T} is continuous;
- (iv) for all $u, v \in F(\mathcal{T})$, $\alpha(u, v) \geq 1$.

Then \mathcal{T} has a unique fixed point that is $u = \mathcal{T}u$, $u \in W$.

Proof The hypothesis (ii) of the Theorem 2, there exists $w_0 \in W$ such that $\alpha(w_0, \mathcal{T}w_0) \geq 1$. Starting at the point $w_0 \in W$, the iterative sequence $\{w_n\}$ is constructed by $w_n = \mathcal{T}w_{n-1} = \mathcal{T}^n w_0$, $n \geq 1$. If $w_{n_0} = w_{n_0+1}$ for any $n_0 \in \mathbb{N}$, then $w_{n_0} = \mathcal{T}w_{n_0}$. Consequently, we assume that successive terms are distinct i.e. $w_{n_0+1} \neq w_{n_0}$ for all $n_0 \in \mathbb{N}$. First of all, we show that $\alpha(w_n, w_{n+1}) \geq 1$ for all $n \in \mathbb{N}$. Since \mathcal{T} is an α -admissible mapping, we have

$$\alpha(w_0, w_1) \geq 1 = \alpha(w_0, \mathcal{T}w_0) \geq 1 \text{ implies } \alpha(w_1, w_2) \geq 1$$

and

$$\alpha(w_1, w_2) \geq 1 \text{ implies } \alpha(w_2, w_3) \geq 1.$$

By induction, we obtain

$$\alpha(w_n, w_{n+1}) \geq 1 \text{ for all } n \in \mathbb{N}. \tag{2}$$

Since \mathcal{T} is triangular α -admissible, we have

$$\alpha(w_n, w_{n+1}) \geq 1 \text{ and } \alpha(w_{n+1}, w_{n+2}) \geq 1 \text{ imply } \alpha(w_n, w_{n+2}) \geq 1.$$

Thus, by induction, we get

$$\alpha(w_n, w_m) \geq 1 \text{ for all } m > n \geq 0. \tag{3}$$

Now, we will show that $\{\varrho(w_{n+1}, w_n)\}$ is a decreasing sequence. Since \mathcal{T} is an (α, ϕ) -weak Pata contractive mapping via simulation function, we have

$$\zeta(\alpha(w_{n-1}, w_n)\varrho(w_n, w_{n+1}), (1 - \epsilon)(M(w_{n-1}, w_n) - \phi(M(w_{n-1}, w_n))) + P(w_{n-1}, w_n)) \geq 0.$$

From ζ_2 and together with (2.2), we obtain

$$\begin{aligned} \varrho(w_n, w_{n+1}) &\leq \alpha(w_{n-1}, w_n)\varrho(w_n, w_{n+1}) \\ &\leq (1 - \epsilon)(\max\{\varrho(w_n, w_{n-1}), \varrho(w_{n+1}, w_n), \varrho(w_n, w_{n-1}), \\ &\quad \frac{\varrho(w_n, w_n) + \varrho(w_{n-1}, w_{n+1})}{2}\} - \phi(\max\{\varrho(w_n, w_{n-1}), \\ &\quad \varrho(w_{n+1}, w_n), \varrho(w_n, w_{n-1}), \frac{\varrho(w_n, w_n) + \varrho(w_{n-1}, w_{n+1})}{2}\})) \\ &\quad + \Lambda \epsilon^\xi \psi(\epsilon) [1 + \|w_{n-1}\| + \|w_n\| + \|w_{n+1}\|]^\theta \\ &\leq (1 - \epsilon)(\max\{\varrho(w_n, w_{n-1}), \frac{\varrho(w_{n+1}, w_n) + \varrho(w_n, w_{n-1})}{2}\} \\ &\quad - \phi(\max\{\varrho(w_n, w_{n-1}), \frac{\varrho(w_{n+1}, w_n) + \varrho(w_n, w_{n-1})}{2}\})) \\ &\quad + K \epsilon^\xi \psi(\epsilon), \end{aligned}$$

for some $K > 0$. If $\varrho(w_n, w_{n-1}) \leq \varrho(w_{n+1}, w_n)$, then we obtain $\varrho(w_{n+1}, w_n) \leq (1 - \epsilon)(\varrho(w_{n+1}, w_n) - \phi(\varrho(w_{n+1}, w_n))) + K \epsilon^\xi \psi(\epsilon)$. In this way, we obtain $\varrho(w_{n+1}, w_n) = 0$, is a contraction. Therefore we have

$$\varrho(w_{n+1}, w_n) < \varrho(w_n, w_{n-1}) < \dots < \varrho(w_1, w_0) = \|w_1\|,$$

that is $\{\varrho(w_{n+1}, w_n)\}$ is a decreasing sequence. Since $\{\varrho(w_n, w_{n+1})\}$ is decreasing, and so, it is convergent to $\varrho \geq 0$ and $\lim_{n \rightarrow \infty} \varrho(w_n, w_{n+1}) = \varrho$. Now, we will demonstrate that $\{\|w_n\|\}$ is a bounded sequence. By the triangle inequality, we have

$$\|w_n\| = \varrho(w_n, w_0) \leq \varrho(w_n, w_{n+1}) + \varrho(w_{n+1}, w_1) + \varrho(w_1, w_0).$$

Since \mathbb{T} is an (α, ϕ) -weak Pata contractive mapping via simulation function, we have

$$\begin{aligned} 0 &\leq \zeta(\alpha(w_0, w_n)\varrho(\mathbb{T}w_0, \mathbb{T}w_n), (1 - \epsilon)(M(w_0, w_n) - \phi(M(w_0, w_n))) + P(w_0, w_n)) \\ &\leq (1 - \epsilon)(M(w_0, w_n) - \phi(M(w_0, w_n))) + P(w_0, w_n) - \alpha(w_0, w_n)\varrho(\mathbb{T}w_0, \mathbb{T}w_n). \end{aligned}$$

Using (2.3), we obtain

$$\begin{aligned} \varrho(w_1, w_{n+1}) &= \alpha(w_0, w_n)\varrho(\mathbb{T}w_0, \mathbb{T}w_n) \\ &\leq (1 - \epsilon)(\max\{\varrho(w_n, w_0), \varrho(w_n, w_{n+1}), \varrho(w_0, w_1), \\ &\quad \frac{\varrho(w_n, w_1) + \varrho(w_0, w_{n+1})}{2}\} - \phi(\max\{\varrho(w_n, w_0), \varrho(w_n, w_{n+1}), \\ &\quad \varrho(w_0, w_1), \frac{\varrho(w_n, w_1) + \varrho(w_0, w_{n+1})}{2}\})) \\ &\quad + \Lambda\epsilon^\xi \psi(\epsilon) [1 + \|w_n\| + 0 + \|w_{n+1}\| + \|w_1\|]^\vartheta \\ &\leq (1 - \epsilon)(\max\{\varrho(w_n, w_0), \varrho(w_n, w_{n+1}), \varrho(w_0, w_1), \\ &\quad \frac{\varrho(w_n, w_0) + \varrho(w_1, w_0) + \varrho(w_{n+1}, w_n) + \varrho(w_n, w_0)}{2}\} \\ &\quad - \phi(\max\{\varrho(w_n, w_0), \varrho(w_n, w_{n+1}), \varrho(w_0, w_1), \\ &\quad \frac{\varrho(w_n, w_0) + \varrho(w_1, w_0) + \varrho(w_{n+1}, w_n) + \varrho(w_n, w_0)}{2}\})) \\ &\quad + \Lambda\epsilon^\xi \psi(\epsilon) [1 + 2\|w_n\| + 2\|w_1\|]^\vartheta \\ &\leq (1 - \epsilon)(\max\{\|w_n\|, \|w_1\|, \|w_n\| + \|w_1\|\} - \phi(\max\{\|w_n\|, \|w_1\|, \\ &\quad \|w_n\| + \|w_1\|\})) + \Lambda\epsilon^\xi \psi(\epsilon) [1 + 2\|w_n\| + 2\|w_1\|]^\vartheta \\ &\leq (1 - \epsilon)(\|w_n\| + \|w_1\| - \phi(\|w_n\| + \|w_1\|)) \\ &\quad + \Lambda\epsilon^\xi \psi(\epsilon) [1 + 2\|w_n\| + 2\|w_1\|]^\vartheta. \end{aligned}$$

Since $\vartheta \leq \xi$, we get

$$\|w_n\| \leq (1 - \epsilon)(\|w_n\| + \|w_1\| - \phi(\|w_n\| + \|w_1\|)) + 2\|w_1\| + \Lambda\epsilon^\xi \psi(\epsilon) [1 + 2\|w_n\| + 2\|w_1\|]^\xi$$

and

$$\epsilon \|w_n\| \leq k\epsilon^\xi \psi(\epsilon) \|w_n\|^\xi + l,$$

for some $k, l > 0$. By the same reason as in [21], $\{\|w_n\|\}$ is a bounded sequence. Using (2.2), we have

$$\begin{aligned} \varrho(w_n, w_{n+1}) &\leq \alpha(w_{n-1}, w_n)\varrho(w_n, w_{n+1}) \\ &\quad (1 - \epsilon)(\max\{\varrho(w_n, w_{n-1}), \varrho(w_{n+1}, w_n), \varrho(w_n, w_{n-1}), \\ &\quad \frac{\varrho(w_n, w_n) + \varrho(w_{n-1}, w_{n+1})}{2}\} - \phi(\max\{\varrho(w_n, w_{n-1}), \varrho(w_{n+1}, w_n), \\ &\quad \varrho(w_n, w_{n-1}), \frac{\varrho(w_n, w_n) + \varrho(w_{n-1}, w_{n+1})}{2}\})) \\ &\quad + \Lambda\epsilon^\xi \psi(\epsilon) [1 + \|w_n\| + \|w_{n-1}\| + \|w_{n+1}\| + \|w_n\|]^\vartheta \\ &\leq (1 - \epsilon)(\max\left\{\varrho(w_n, w_{n-1}), \frac{\varrho(w_{n+1}, w_n) + \varrho(w_n, w_{n-1})}{2}\right\} \\ &\quad - \phi(\max\left\{\varrho(w_n, w_{n-1}), \frac{\varrho(w_{n+1}, w_n) + \varrho(w_n, w_{n-1})}{2}\right\})) + K\epsilon^\xi \psi(\epsilon), \end{aligned}$$

for some $K > 0$. Taking limit as $n \rightarrow \infty$, we obtain $\varrho \leq K\epsilon^\xi \psi(\epsilon)$ and thus $\varrho = 0$.

Next, we demonstrate that $\{w_n\}$ is a Cauchy sequence. We assume that $\{w_n\}$ is not a Cauchy sequence. From Lemma 1, there exist subsequences $\{w_{m_j}\}$ and $\{w_{n_j}\}$ with $n_j > m_j > j$ such that $\lim_{j \rightarrow \infty} \varrho(w_{m_j-1}, w_{n_j+1}) = \varsigma$, $\lim_{j \rightarrow \infty} \varrho(w_{m_j}, w_{n_j}) = \varsigma$, $\lim_{j \rightarrow \infty} \varrho(w_{m_j-1}, w_{n_j}) = \varsigma$, $\lim_{j \rightarrow \infty} \varrho(w_{m_j+1}, w_{n_j+1}) = \varsigma$ and $\lim_{j \rightarrow \infty} \varrho(w_{m_j}, w_{n_j-1}) = \varsigma$. Since \mathbb{T} is an (α, ϕ) -weak Pata contractive mapping via simulation function, we have

$$\begin{aligned} \varsigma &\leq \varrho(w_{m_j}, w_{n_j}) = \alpha(w_{m_j-1}, w_{n_j-1})\varrho(\mathbb{T}w_{m_j-1}, \mathbb{T}w_{n_j-1}) \\ &\leq (1 - \epsilon) (\max\{\varrho(w_{m_j-1}, w_{n_j-1}), \varrho(w_{m_j-1}, w_{m_j}), \varrho(w_{n_j-1}, w_{n_j}), \\ &\quad \frac{\varrho(w_{n_j-1}, w_{m_j}) + \varrho(w_{m_j-1}, w_{n_j})}{2}\} - \phi(\max\{\varrho(w_{m_j-1}, w_{n_j-1}), \\ &\quad \varrho(w_{m_j-1}, w_{m_j}), \varrho(w_{n_j-1}, w_{n_j}), \frac{\varrho(w_{n_j-1}, w_{m_j}) + \varrho(w_{m_j-1}, w_{n_j})}{2}\})) \\ &\quad + \Lambda \epsilon^\xi \psi(\epsilon) [1 + \|w_{m_j}\| + \|w_{n_j}\| + \|w_{n_j+1}\| + \|w_{m_j+1}\|]^\theta. \end{aligned}$$

Taking the limit as $j \rightarrow \infty$, we obtain

$$\varsigma \leq (1 - \epsilon) (\varsigma - \phi(\varsigma)) + K\epsilon\psi(\epsilon)$$

and

$$\varsigma \leq (1 - \epsilon) \varsigma + K\epsilon\psi(\epsilon),$$

then

$$\varsigma \leq K\psi(\epsilon),$$

is a contradiction. Hence, $\{w_n\}$ is a Cauchy sequence in (W, ϱ) . By the completeness of W , $w_n \rightarrow u \in W$ as $n \rightarrow +\infty$. Since \mathbb{T} is continuous, $\mathbb{T}w_n \rightarrow \mathbb{T}u$ as $n \rightarrow +\infty$. By the uniqueness of the limit, we obtain $u = \mathbb{T}u$, that is, $u \in F(\mathbb{T})$.

Now we demonstrate that fixed point of \mathbb{T} is unique. Assume that u and v are fixed points of \mathbb{T} . Since \mathbb{T} is an (α, ϕ) -weak Pata contractive mapping via simulation function, we have

$$\begin{aligned} 0 &\leq \zeta(\alpha(u, v))\varrho(\mathbb{T}u, \mathbb{T}v), (1 - \epsilon) (M(u, v) - \phi(M(u, v))) + P(u, v) \\ &\leq (1 - \epsilon) (M(u, v) - \phi(M(u, v))) + P(u, v) - \alpha(u, v)\varrho(\mathbb{T}u, \mathbb{T}v). \end{aligned}$$

Since \mathbb{T} satisfies the hypothesis (iv) of Theorem 2, we have

$$\begin{aligned} \varrho(\mathbb{T}u, \mathbb{T}v) &\leq \alpha(u, v)\varrho(\mathbb{T}u, \mathbb{T}v) \\ &\leq (1 - \epsilon) (\max\left\{\varrho(u, v), \varrho(u, \mathbb{T}u), \varrho(v, \mathbb{T}v), \frac{\varrho(u, \mathbb{T}v) + \varrho(v, \mathbb{T}u)}{2}\right\} \\ &\quad - \phi(\max\left\{\varrho(u, v), \varrho(u, \mathbb{T}u), \varrho(v, \mathbb{T}v), \frac{\varrho(u, \mathbb{T}v) + \varrho(v, \mathbb{T}u)}{2}\right\})) + K\epsilon\psi(\epsilon). \end{aligned}$$

We obtain that $\varrho(u, v) \leq K\psi(\epsilon)$, and so, $u = v$. Thus, \mathbb{T} has a unique fixed point in W . □

The following theorem does not require the continuity of \mathbb{T} .

Let (W, ϱ) be a complete metric space. $\mathbb{T} : W \rightarrow W$ be an (α, ϕ) -weak Pata contractive mapping via simulation function. Assume that

- (i) \mathbb{T} is triangular α -admissible;
- (ii) there exists $w_0 \in W$ such that $\alpha(w_0, \mathbb{T}w_0) \geq 1$;
- (iii) if $\{w_n\}$ is a sequence in W such that $\alpha(w_n, w_{n+1}) \geq 1$, for all n and $w_n \rightarrow u \in W$ as $n \rightarrow +\infty$, then $\alpha(w_n, u) \geq 1$ for all n ;
- (iv) for all $u, v \in F(\mathbb{T})$, $\alpha(u, v) \geq 1$.

Then \mathbb{T} has a unique fixed point that is $u = \mathbb{T}u$, $u \in W$.

Proof Following the proof of Theorem 2, we have already shown that $\{w_n\}$ is a Cauchy sequence in W . Since W is complete, we have $w_n \rightarrow u \in W$ as $n \rightarrow +\infty$. Next, we prove that $u \in F(\mathbb{T})$, that is, $u = \mathbb{T}u$. From (2.2) and the hypothesis (iii) of Theorem 2, we have $\alpha(w_n, u) \geq 1$ for all n . Also, we have

$$0 \leq \zeta(\alpha(w_n, u)\varrho(\mathbb{T}u, w_{n+1}), (1 - \epsilon)(M(w_n, u) - \phi(M(w_n, u)) + P(w_n, u))$$

and

$$\begin{aligned} \varrho(\mathbb{T}u, u) &= \varrho(\mathbb{T}u, w_{n+1}) + \varrho(w_{n+1}, u) \\ &\leq \alpha(w_n, u)\varrho(\mathbb{T}u, w_{n+1}) + \varrho(w_{n+1}, u) \\ &\leq (1 - \epsilon)\left(\max\left\{\varrho(u, w_n), \varrho(u, \mathbb{T}u), \varrho(w_n, w_{n+1}), \frac{\varrho(u, w_{n+1}) + \varrho(w_n, \mathbb{T}u)}{2}\right\}\right) \\ &\quad - \phi\left(\max\left\{\varrho(u, w_n), \varrho(u, \mathbb{T}u), \varrho(w_n, w_{n+1}), \frac{\varrho(u, w_{n+1}) + \varrho(w_n, \mathbb{T}u)}{2}\right\}\right) \\ &\quad + \Lambda\epsilon^\xi \psi(\epsilon) [1 + \|w_n\| + \|u\| + \|\mathbb{T}u\| + \|w_{n+1}\|]^\theta + \varrho(w_{n+1}, u). \\ &\leq (1 - \epsilon)\left(\max\left\{\varrho(u, w_n), \varrho(u, \mathbb{T}u), \varrho(w_n, w_{n+1}), \frac{\varrho(u, w_{n+1}) + \varrho(w_n, \mathbb{T}u)}{2}\right\}\right) \\ &\quad - \phi\left(\max\left\{\varrho(u, w_n), \varrho(u, \mathbb{T}u), \varrho(w_n, w_{n+1}), \frac{\varrho(u, w_{n+1}) + \varrho(w_n, \mathbb{T}u)}{2}\right\}\right) \\ &\quad + K\epsilon^\xi \psi(\epsilon), \end{aligned}$$

for some $K > 0$. We take the limit as $n \rightarrow \infty$, we get

$$\varrho(\mathbb{T}u, u) \leq (1 - \epsilon)(\varrho(\mathbb{T}u, u) - \phi(\varrho(\mathbb{T}u, u))) + K\epsilon^\xi \psi(\epsilon).$$

Thus, we obtain that $\mathbb{T}u = u$ and that is $u \in F(\mathbb{T})$. Similar to the proof of Theorem 2, the uniqueness of fixed point of \mathbb{T} can be obtained. \square

Let $W = [0, 1]$ with the usual metric and define the mappings $\mathbb{T} : W \rightarrow W$ by $\mathbb{T}(w) = \frac{w^2}{4}$, $w \in [0, 1]$ and $\phi : [0, \infty] \rightarrow [0, \infty]$, $\phi(s) = \frac{s}{3}$. Let $\alpha : W \times W \rightarrow [0, +\infty)$ be defined as $\alpha(w, t) = \begin{cases} 1, & w, t \in [0, 1] \\ 0, & \text{otherwise} \end{cases}$. It is clear that \mathbb{T} is triangular α -admissible. Our goal is to show that \mathbb{T} satisfies (2.1). For $w, t \in [0, 1]$, we have

$$\varrho(w, t) - \phi(\varrho(w, t)) = \varrho(w, t) - \frac{1}{3}\varrho(w, t) = \frac{2}{3}\varrho(w, t)$$

and

$$\begin{aligned} \varrho(\mathbb{T}w, \mathbb{T}t) &\leq \alpha(w, t)\varrho(\mathbb{T}w, \mathbb{T}t) \\ &= \frac{w^2}{6} - \frac{t^2}{6} \\ &= \frac{1}{6}(|w - t|)(w + t) \\ &\leq \frac{1}{3}(|w - t|) \\ &= \frac{1}{3}\varrho(w, t). \end{aligned}$$

Since $\varrho(w, t) \leq M(w, t)$, we obtain

$$\varrho(\mathbb{T}w, \mathbb{T}t) \leq \frac{1}{3}M(w, t) = \frac{1}{2}\left(\frac{2}{3}M(w, t)\right) = \frac{1}{2}(M(w, t) - \phi(M(w, t))).$$

For arbitrary $\epsilon \in [0, 1]$, we can write the above inequality as follows

$$\begin{aligned} \varrho(\mathbb{T}w, \mathbb{T}t) &\leq (1 - \epsilon) (M(w, t) - \phi(M(w, t))) + \left(\frac{1}{3} + \epsilon - 1\right) M(w, t) \\ &\leq (1 - \epsilon) (M(w, t) - \phi(M(w, t))) \\ &\quad + \left(\frac{1}{3} + \epsilon - 1\right) (1 + \|w\| + \|t\| + \|\mathbb{T}w\| + \|\mathbb{T}t\|). \end{aligned}$$

Our goal is to prove that $\gamma \geq 0$ and $\Lambda \geq 0$ such that

$$\left(\frac{1}{3} + \epsilon - 1\right) (1 + \|w\| + \|t\| + \|\mathbb{T}w\| + \|\mathbb{T}t\|) \leq \Lambda \epsilon^{\gamma+1} (1 + \|w\| + \|t\| + \|\mathbb{T}w\| + \|\mathbb{T}t\|),$$

satisfies for all $w, t \in [0, 1]$ and every $0 \leq \epsilon \leq 1$. We can find $\Lambda \geq 0$ such that

$$\Lambda = \frac{\left(\frac{1}{3} + \epsilon - 1\right)}{\epsilon^{\gamma+1}},$$

satisfies for each $0 \leq \epsilon \leq 1$ and some $\gamma \geq 0$. If we choose γ such that $\frac{\gamma}{\gamma+1} > 1 - \frac{1}{3}$, then

$$\Lambda = \frac{\gamma^\gamma}{(\gamma+1)^{\gamma+1} \left(1 - \frac{1}{3}\right)^\gamma}.$$

Thus, we have that

$$\alpha(w, t) \varrho(\mathbb{T}w, \mathbb{T}t) \leq (1 - \epsilon) (M(w, t) - \phi(M(w, t))) + \Lambda \epsilon^{\gamma+1} \left(\begin{array}{l} 1 + \|w\| + \|t\| \\ + \|\mathbb{T}w\| + \|\mathbb{T}t\| \end{array} \right)$$

and

$$\zeta \left(\alpha(w, t) \varrho(\mathbb{T}w, \mathbb{T}t), (1 - \epsilon) (M(w, t) - \phi(M(w, t))) + \Lambda \epsilon^{\gamma+1} \left(\begin{array}{l} 1 + \|w\| + \|t\| \\ + \|\mathbb{T}w\| + \|\mathbb{T}t\| \end{array} \right) \right) \leq 0,$$

satisfies for all $w, t \in [0, 1]$, $\zeta \in \mathcal{Z}$ and each $\epsilon > 0$. If $\epsilon = 0$, it can be seen that (2.1) is satisfied. Also, the conditions of Theorem 2 are satisfied with $\psi(\epsilon) = \epsilon^\gamma$, $\xi = \vartheta = 1$. Hence, \mathbb{T} has a unique fixed point in $W = [0, 1]$. It is seen that, $u = 0$ is the unique fixed point of \mathbb{T} in W .

Now, we state a fixed point result for multivalued (α, ϕ) -weak Pata contractive mapping.

Let (W, ϱ) be an ordered complete metric space and satisfy (H_*) . Let $\Lambda \geq 0$, $\xi \geq 1$ and $\vartheta \in [0, \xi]$ be fixed constants, $\psi \in \Psi$ and $\alpha : W \times W \rightarrow [0, +\infty)$ be two functions. Assume that $\mathbb{T} : W \rightarrow 2^W$ be a multivalued mapping has UCAV and if for all $w, t \in W$ with w and t comparable, and $\epsilon \in [0, 1]$, \mathbb{T} satisfies the inequality

$$\alpha(w, t) H_\varrho(\mathbb{T}w, \mathbb{T}t) \leq (1 - \epsilon) (M(w, t) - \phi(M(w, t))) + P(w, t), \tag{4}$$

where $\phi : [0, +\infty) \rightarrow [0, +\infty)$ is a continuous and nondecreasing function with $\phi(0) = 0$ and $\phi(s) > 0$, for all $s > 0$, and

$$P(w, t) = \Lambda \epsilon^\xi \psi(\epsilon) [1 + \|w\| + \|t\| + \|\mathbb{T}w\| + \|\mathbb{T}t\|]^\vartheta$$

and

$$M(w, t) = \max \left\{ \varrho(w, t), \varrho(w, \mathbb{T}w), \varrho(t, \mathbb{T}t), \frac{\varrho(w, \mathbb{T}t) + \varrho(t, \mathbb{T}w)}{2} \right\},$$

and also, assume that \mathbb{T} satisfies the following conditions

- (i) \mathbb{T} is triangular α -admissible;
- (ii) there exists $w_0 \in W, w_1 \in \mathbb{T}w_0$ such that $\alpha(w_0, w_1) \geq 1$;
- (iii) \mathbb{T} is continuous;

(iv) for all $u, v \in F_H(\mathbb{T})$, $\alpha(u, v) \geq 1$.

Then \mathbb{T} has a unique fixed point that is $u \in \mathbb{T}u$, $u \in W$.

Proof The hypothesis (ii) of the Theorem 2, there exists $w_0 \in W$ such that $\alpha(w_0, \mathbb{T}w_0) \geq 1$. Starting at the point $w_0 \in W$, if $w_0 \in \mathbb{T}w_0$, proof is clearly completed. Since $\mathbb{T}w_0$ has UCAV, there exists $w_1 \in \mathbb{T}w_0$ with $w_1 \neq w_0$ and $w_1 \geq w_0$ such that

$$\varrho(w_0, w_1) = \inf_{w \in \mathbb{T}w_0} \varrho(w, w_0) = \varrho(\mathbb{T}w_0, w_0).$$

Continuing this process, the iterative sequence $\{w_n\}$ is constructed by $w_{n+1} \in \mathbb{T}w_n$ with $w_{n+1} \neq w_n$ and $w_{n+1} \geq w_n$, for all $n \geq 1$ such that

$$\varrho(w_n, w_{n+1}) = \varrho(\mathbb{T}w_n, w_n).$$

Furthermore

$$\varrho(\mathbb{T}w_n, w_n) \leq \sup_{w \in \mathbb{T}w_{n-1}} \varrho(\mathbb{T}w_n, w) \leq H_\varrho(\mathbb{T}w_n, \mathbb{T}w_{n-1}).$$

Thus, we have

$$\varrho(w_n, w_{n+1}) \leq H_\varrho(\mathbb{T}w_{n-1}, \mathbb{T}w_n), \text{ for } n \geq 2.$$

We denote $\|w_n\| = \varrho(w_n, w_0)$ for $n \geq 1$. If $w_{n_0} = w_{n_0+1}$ for any $n_0 \in \mathbb{N}$, then $w_{n_0} \in \mathbb{T}w_{n_0}$. First of all, we show that $\alpha(w_n, w_{n+1}) \geq 1$, for all $n \in \mathbb{N}$. Since \mathbb{T} is an α -admissible mapping, $w_0 \in W$, $w_1 \in \mathbb{T}w_0$ we have

$$\alpha(w_0, w_1) \geq 1 \text{ implies } \alpha(w_1, w_2) \geq 1, \text{ for } w_2 \in \mathbb{T}w_1$$

and

$$\alpha(w_1, w_2) \geq 1 \text{ implies } \alpha(w_2, w_3) \geq 1, \text{ for } w_3 \in \mathbb{T}w_2.$$

By induction, we obtain

$$\alpha(w_n, w_{n+1}) \geq 1, \text{ for } w_{n+1} \in \mathbb{T}w_n, n \in \mathbb{N}. \tag{5}$$

Since \mathbb{T} is triangular α -admissible, we have

$$\alpha(w_n, w_{n+1}) \geq 1 \text{ and } \alpha(w_{n+1}, w_{n+2}) \geq 1 \text{ imply } \alpha(w_n, w_{n+2}) \geq 1, w_{n+2} \in w_{n+1}.$$

Thus, by induction, we get

$$\alpha(w_n, w_m) \geq 1 \text{ for all } m > n \geq 0. \tag{6}$$

Now, we will show that $\{\varrho(w_{n+1}, w_n)\}$ is a decreasing sequence. Using (2.5),

$$\begin{aligned} \varrho(w_n, w_{n+1}) &\leq H_\varrho(\mathbb{T}w_{n-1}, \mathbb{T}w_n) \\ &\leq \alpha(w_{n-1}, w_n)H_\varrho(\mathbb{T}w_{n-1}, \mathbb{T}w_n) \\ &\leq (1 - \epsilon)(\max\{\varrho(w_n, w_{n-1}), \varrho(w_{n+1}, w_n), \varrho(w_n, w_{n-1}), \\ &\quad \frac{\varrho(w_n, w_n) + \varrho(w_{n-1}, w_{n+1})}{2}\} - \phi(\max\{\varrho(w_n, w_{n-1}), \\ &\quad \varrho(w_{n+1}, w_n), \varrho(w_n, w_{n-1}), \frac{\varrho(w_n, w_n) + \varrho(w_{n-1}, w_{n+1})}{2}\})) \\ &\quad + \Lambda \epsilon^\xi \psi(\epsilon) [1 + \|w_{n-1}\| + \|w_n\| + \|w_n\| + \|w_{n+1}\|]^\theta \\ &\leq (1 - \epsilon)(\max\{\varrho(w_n, w_{n-1}), \frac{\varrho(w_{n+1}, w_n) + \varrho(w_n, w_{n-1})}{2}\} \\ &\quad - \phi(\max\{\varrho(w_n, w_{n-1}), \frac{\varrho(w_{n+1}, w_n) + \varrho(w_n, w_{n-1})}{2}\})) \\ &\quad + K \epsilon^\xi \psi(\epsilon), \end{aligned}$$

for some $K > 0$. If $\varrho(w_n, w_{n-1}) \leq \varrho(w_{n+1}, w_n)$, then we obtain $\varrho(w_{n+1}, w_n) \leq (1 - \epsilon)(\varrho(w_{n+1}, w_n) - \phi(\varrho(w_{n+1}, w_n))) + K \epsilon^\xi \psi(\epsilon)$. In this way, we obtain $\varrho(w_{n+1}, w_n) = 0$, is a contraction. Therefore, we have

$$\varrho(w_{n+1}, w_n) \leq H_\varrho(\mathbb{T}w_{n-1}, \mathbb{T}w_n) < \varrho(w_n, w_{n-1}).$$

If we continue this process, we get

$$\varrho(w_{n+1}, w_n) < \varrho(w_n, w_{n-1}) < \dots < \varrho(w_1, w_0) = \|w_1\|,$$

that is $\{\varrho(w_{n+1}, w_n)\}$ is a decreasing sequence and so, this sequence is convergent to $\varrho \geq 0$ and $\lim_{n \rightarrow \infty} \varrho(w_n, w_{n+1}) = \varrho$. Now, we will demonstrate that $\{\|w_n\|\}$ is a bounded sequence. By the triangle inequality, we have

$$\|w_n\| = \varrho(w_n, w_0) \leq \varrho(w_n, w_{n+1}) + \varrho(w_{n+1}, w_1) + \varrho(w_1, w_0),$$

is a contradiction. Since \mathbb{T} is a multivalued (α, ϕ) -weak Pata contractive mapping with (2.6), we obtain

$$\begin{aligned} \varrho(w_1, w_{n+1}) &\leq H_\varrho(\mathbb{T}w_0, \mathbb{T}w_n) \\ &\leq \alpha(w_0, w_n)H_\varrho(\mathbb{T}w_0, \mathbb{T}w_n) \\ &\leq (1 - \epsilon) (\max\{\varrho(w_n, w_0), \varrho(w_n, w_{n+1}), \varrho(w_0, w_1), \\ &\quad \frac{\varrho(w_n, w_1) + \varrho(w_0, w_{n+1})}{2}\} - \phi(\max\{\varrho(w_n, w_0), \varrho(w_n, w_{n+1}), \\ &\quad \varrho(w_0, w_1), \frac{\varrho(w_n, w_1) + \varrho(w_0, w_{n+1})}{2}\})) \\ &\quad + \Lambda \epsilon^\xi \psi(\epsilon) [1 + \|w_n\| + 0 + \|w_{n+1}\| + \|w_1\|]^\vartheta \\ &\leq (1 - \epsilon) (\max\{\varrho(w_n, w_0), \varrho(w_n, w_{n+1}), \varrho(w_0, w_1), \\ &\quad \frac{\varrho(w_n, w_0) + \varrho(w_1, w_0) + \varrho(w_{n+1}, w_n) + \varrho(w_n, w_0)}{2}\} \\ &\quad - \phi(\max\{\varrho(w_n, w_0), \varrho(w_n, w_{n+1}), \varrho(w_0, w_1), \\ &\quad \frac{\varrho(w_n, w_0) + \varrho(w_1, w_0) + \varrho(w_{n+1}, w_n) + \varrho(w_n, w_0)}{2}\})) \\ &\quad + \Lambda \epsilon^\xi \psi(\epsilon) [1 + 2\|w_n\| + 2\|w_1\|]^\vartheta \\ &\leq (1 - \epsilon) (\max\{\|w_n\|, \|w_1\|, \|w_n\| + \|w_1\|\} - \phi(\max\{\|w_n\|, \|w_1\|, \\ &\quad \|w_n\| + \|w_1\|\})) + \Lambda \epsilon^\xi \psi(\epsilon) [1 + 2\|w_n\| + 2\|w_1\|]^\vartheta \\ &\leq (1 - \epsilon) (\|w_n\| + \|w_1\| - \phi(\|w_n\| + \|w_1\|)) \\ &\quad + \Lambda \epsilon^\xi \psi(\epsilon) [1 + 2\|w_n\| + 2\|w_1\|]^\vartheta. \end{aligned}$$

Since $\vartheta \leq \xi$, we get

$$\|w_n\| \leq (1 - \epsilon) (\|w_n\| + \|w_1\| - \phi(\|w_n\| + \|w_1\|)) + 2\|w_1\| + \Lambda \epsilon^\xi \psi(\epsilon) [1 + 2\|w_n\| + 2\|w_1\|]^\xi$$

and

$$\epsilon \|w_n\| \leq k \epsilon^\xi \psi(\epsilon) \|w_n\|^\xi + l,$$

for some $k, l > 0$. By the same reason as in [21], $\{\|w_n\|\}$ is a bounded sequence. Using (2.5), we have

$$\begin{aligned} \varrho(w_n, w_{n+1}) &\leq \alpha(w_{n-1}, w_n)H_\varrho(\mathbb{T}w_{n-1}, \mathbb{T}w_n) \\ &\quad (1 - \epsilon) (\max\{\varrho(w_n, w_{n-1}), \varrho(w_{n+1}, w_n), \varrho(w_n, w_{n-1}), \\ &\quad \frac{\varrho(w_n, w_n) + \varrho(w_{n-1}, w_{n+1})}{2}\} - \phi(\max\{\varrho(w_n, w_{n-1}), \varrho(w_{n+1}, w_n), \\ &\quad \varrho(w_n, w_{n-1}), \frac{\varrho(w_n, w_n) + \varrho(w_{n-1}, w_{n+1})}{2}\})) \\ &\quad + \Lambda \epsilon^\xi \psi(\epsilon) [1 + \|w_n\| + \|w_{n-1}\| + \|w_{n+1}\| + \|w_n\|]^\vartheta \\ &\leq (1 - \epsilon) (\max\left\{\varrho(w_n, w_{n-1}), \frac{\varrho(w_{n+1}, w_n) + \varrho(w_n, w_{n-1})}{2}\right\} \\ &\quad - \phi(\max\left\{\varrho(w_n, w_{n-1}), \frac{\varrho(w_{n+1}, w_n) + \varrho(w_n, w_{n-1})}{2}\right\})) + K \epsilon^\xi \psi(\epsilon), \end{aligned}$$

for some $K > 0$. Taking limit as $n \rightarrow \infty$, we obtain $\varrho \leq K \epsilon^\xi \psi(\epsilon)$ and thus $\varrho = 0$.

Next, we demonstrate that $\{w_n\}$ is a Cauchy sequence. We assume that $\{w_n\}$ is not a Cauchy sequence. From Lemma 1, there exist subsequences $\{w_{m_j}\}$ and $\{w_{n_j}\}$ with $n_j > m_j > j$ such that $\lim_{j \rightarrow \infty} \varrho(w_{m_j-1}, w_{n_j+1}) = \varsigma$, $\lim_{j \rightarrow \infty} \varrho(w_{m_j}, w_{n_j}) = \varsigma$, $\lim_{j \rightarrow \infty} \varrho(w_{m_j-1}, w_{n_j}) = \varsigma$, $\lim_{j \rightarrow \infty} \varrho(w_{m_j+1}, w_{n_j+1}) = \varsigma$ and $\lim_{j \rightarrow \infty} \varrho(w_{m_j}, w_{n_j-1}) = \varsigma$. Since \mathbb{T} is a multivalued (α, ϕ) -weak Pata contractive mapping with (2.6), we have

$$\begin{aligned} \varsigma &\leq \varrho(w_{m_j}, w_{n_j}) \leq \alpha(w_{m_j-1}, w_{n_j-1})H_{\varrho}(\mathbb{T}w_{m_j-1}, \mathbb{T}w_{n_j-1}) \\ &\leq (1 - \epsilon) (\max\{\varrho(w_{m_j-1}, w_{n_j-1}), \varrho(w_{m_j-1}, w_{m_j}), \varrho(w_{n_j-1}, w_{n_j}), \\ &\quad \frac{\varrho(w_{n_j-1}, w_{m_j}) + \varrho(w_{m_j-1}, w_{n_j})}{2}\} - \phi(\max\{\varrho(w_{m_j-1}, w_{n_j-1}), \\ &\quad \varrho(w_{m_j-1}, w_{m_j}), \varrho(w_{n_j-1}, w_{n_j}), \frac{\varrho(w_{n_j-1}, w_{m_j}) + \varrho(w_{m_j-1}, w_{n_j})}{2}\})) \\ &\quad + \Lambda \epsilon^{\xi} \psi(\epsilon) [1 + \|w_{m_j}\| + \|w_{n_j}\| + \|w_{n_j+1}\| + \|w_{m_j+1}\|]^{\vartheta}. \end{aligned}$$

Taking the limit as $j \rightarrow \infty$, we obtain

$$\varsigma \leq (1 - \epsilon) (\varsigma - \phi(\varsigma)) + K\epsilon\psi(\epsilon)$$

and $\varsigma \leq (1 - \epsilon) \varsigma + K\epsilon\psi(\epsilon)$. We obtain that

$$\varsigma \leq K\psi(\epsilon),$$

is a contradiction. Hence, $\{w_n\}$ is a Cauchy sequence in (W, ϱ) . Since W is complete metric space, we get $w_n \rightarrow u \in W$ as $n \rightarrow +\infty$. Since \mathbb{T} is continuous, $\mathbb{T}w_n \rightarrow \mathbb{T}u$ as $n \rightarrow +\infty$. By the uniqueness of the limit, we obtain $u \in \mathbb{T}u$, that is, $u \in F_H(\mathbb{T})$.

Now, we demonstrate that fixed point of \mathbb{T} is unique. Assume that u and v are fixed points of \mathbb{T} . Since \mathbb{T} satisfies the hypothesis (iv) of Theorem 2 and \mathbb{T} is a multivalued (α, ϕ) -weak Pata contractive mapping, we have

$$\begin{aligned} \varrho(\mathbb{T}u, fv) &\leq \alpha(u, v)H_{\varrho}(\mathbb{T}u, fv) \\ &\leq (1 - \epsilon) (\max\left\{\varrho(u, v), \varrho(u, \mathbb{T}u), \varrho(v, fv), \frac{\varrho(u, fv) + \varrho(v, \mathbb{T}u)}{2}\right\} \\ &\quad - \phi(\max\left\{\varrho(u, v), \varrho(u, \mathbb{T}u), \varrho(v, fv), \frac{\varrho(u, fv) + \varrho(v, \mathbb{T}u)}{2}\right\})) + K\epsilon\psi(\epsilon). \end{aligned}$$

Thus, we obtain that $\varrho(u, v) \leq K\psi(\epsilon)$, and so, $u = v$. Thus \mathbb{T} has a unique fixed point in W . □

If we take $M(w, t) = \varrho(w, t)$, for all $w, t \in W$ in Theorem 2, then we get the following corollary.

Let (W, ϱ) be a complete metric space, $\Lambda \geq 0, \xi \geq 1$ and $\vartheta \in [0, \xi]$ be fixed constants, $\psi \in \Psi$ and $\alpha : W \times W \rightarrow [0, +\infty)$, $\mathbb{T} : W \rightarrow W$ be two functions. If for all $w, t \in W$, and $\epsilon \in [0, 1]$, \mathbb{T} satisfies the inequality

$$\alpha(w, t)\varrho(\mathbb{T}w, \mathbb{T}t) \leq (1 - \epsilon)(\varrho(w, t) - \phi(\varrho(w, t)) + \Lambda \epsilon^{\xi} \psi(\epsilon) [1 + \|w\| + \|t\| + \|\mathbb{T}w\| + \|\mathbb{T}t\|]^{\vartheta},$$

where $\phi : [0, +\infty) \rightarrow [0, +\infty)$ is a continuous and nondecreasing function with $\phi(0) = 0$ and $\phi(s) > 0$, for all $s > 0$, and

- (i) \mathbb{T} is triangular α -admissible;
- (ii) there exists $w_0 \in W$ such that $\alpha(w_0, \mathbb{T}w_0) \geq 1$;
- (iii) \mathbb{T} is continuous;
- (iv) for all $u, v \in F(\mathbb{T})$, $\alpha(u, v) \geq 1$.

Then \mathbb{T} has a unique fixed point $u = \mathbb{T}u$.

If we take $M(w, t) = \varrho(w, t)$ and $\alpha(w, t) = 1$, for all $w, t \in W$ in Theorem 2, then we get the following corollary.

Let (W, ϱ) be a complete metric space, $\Lambda \geq 0, \xi \geq 1$ and $\vartheta \in [0, \xi]$ be fixed constants, $\psi \in \Psi$, $\mathbb{T} : W \rightarrow W$ be a function. If for all $w, t \in W$, and $\epsilon \in [0, 1]$, \mathbb{T} satisfies the inequality

$$\varrho(\mathbb{T}w, \mathbb{T}t) \leq (1 - \epsilon)(\varrho(w, t) - \phi(\varrho(w, t)) + \Lambda \epsilon^{\xi} \psi(\epsilon) [1 + \|w\| + \|t\| + \|\mathbb{T}w\| + \|\mathbb{T}t\|]^{\vartheta},$$

where $\phi : [0, +\infty) \rightarrow [0, +\infty)$ is a continuous and nondecreasing function with $\phi(0) = 0$ and $\phi(s) > 0$, for all $s > 0$, and \mathbb{T} is continuous. Then \mathbb{T} has a unique fixed point $u = \mathbb{T}u$.

Corollary 2 generalizes the results of Pata [21] and Banach [7]. For $\epsilon = 0$, we get the results of [26] and in addition to this, if $\epsilon = 0$ and we take $M(w, t) = \varrho(w, t)$, for all $w, t \in W$ in Theorem 2, then we get the results of [1].

If we take $\alpha(w, t) = 1$, for all $w, t \in W$ in Theorem 2, then we get the following corollary.

Let (W, ϱ) be an ordered complete metric space and satisfy (H_*) . Let $\Lambda \geq 0$, $\xi \geq 1$ and $\vartheta \in [0, \xi]$ be fixed constants, $\psi \in \Psi$ be a function. Assume that $\mathbb{T} : W \rightarrow 2^W$ be a multivalued mapping has UCAV and if for all $w, t \in W$ with w and t comparable, and $\epsilon \in [0, 1]$, \mathbb{T} satisfies the inequality

$$H_{\varrho}(\mathbb{T}w, \mathbb{T}t) \leq (1 - \epsilon)(M(w, t) - \phi(M(w, t))) + P(w, t),$$

where $\phi : [0, +\infty) \rightarrow [0, +\infty)$ is a continuous and nondecreasing function with $\phi(0) = 0$ and $\phi(s) > 0$ for all $s > 0$, and

$$P(w, t) = \Lambda \epsilon^{\xi} \psi(\epsilon) [1 + \|w\| + \|t\| + \|\mathbb{T}w\| + \|\mathbb{T}t\|]^{\vartheta}$$

and

$$M(w, t) = \max \left\{ \varrho(w, t), \varrho(w, \mathbb{T}w), \varrho(t, \mathbb{T}t), \frac{\varrho(w, \mathbb{T}t) + \varrho(t, \mathbb{T}w)}{2} \right\},$$

and also, \mathbb{T} is continuous, then \mathbb{T} has a unique fixed point, that is, $u \in \mathbb{T}u, u \in W$.

If we take $M(w, t) = \varrho(w, t)$ and $\alpha(w, t) = 1$, for all $w, t \in W$ in Theorem 2, then we get the following corollary.

Let (W, ϱ) be an ordered complete metric space and satisfy (H_*) . Let $\Lambda \geq 0$, $\xi \geq 1$ and $\vartheta \in [0, \xi]$ be fixed constants, $\psi \in \Psi$ be a function. Assume that $\mathbb{T} : W \rightarrow 2^W$ be a multivalued mapping has UCAV and if for all $w, t \in W$ with w and t comparable, and $\epsilon \in [0, 1]$, \mathbb{T} satisfies the inequality

$$H_{\varrho}(\mathbb{T}w, \mathbb{T}t) \leq (1 - \epsilon)(\varrho(w, t) - \phi(\varrho(w, t))) + P(w, t),$$

where $\phi : [0, +\infty) \rightarrow [0, +\infty)$ is a continuous and nondecreasing function with $\phi(0) = 0$ and $\phi(s) > 0$, for all $s > 0$, and

$$P(w, t) = \Lambda \epsilon^{\xi} \psi(\epsilon) [1 + \|w\| + \|t\| + \|\mathbb{T}w\| + \|\mathbb{T}t\|]^{\vartheta},$$

and also \mathbb{T} is continuous, then \mathbb{T} has a unique fixed point, that is, $u \in \mathbb{T}u, u \in W$.

Corollary 2 generalizes the results of Kolagar [16] and Nadler [18].

References

- [1] Alber Ya.I., Guerre-Delabriere S., "Principle of weakly contractive maps in Hilbert spaces", in: I. Gohberg, Yu. Lyubich (Eds.), New Results in Theory Operator Theory, in Advances and Appl., Birkhauser, Basel 98, (1997), 7–22.
- [2] Aktay M., Özdemir M., "Common fixed point results for a class of (α, β) -Geraghty contraction type mappings in modular metric spaces", Erzincan University Journal of Science and Technology, 13 (Special Issue-I), (2020), 150-161.
- [3] Aktay M., Özdemir M., "Some results on generalized Pata–Suzuki type contractive mappings", Journal of Mathematics, (2021), Article ID 2975339, 9.
- [4] Asl J.H., Rezapour S., Shahzad N, "On fixed points of $\alpha - \psi$ -contractive multifunctions", Fixed Point Theory Appl., (2012), 212.
- [5] Argoubi H., Samet B., Vetro C., "Nonlinear contractions involving simulation functions in a metric space with a partial order", J. Nonlinear Sci. Appl., 8, (2015), 1082-1094.
- [6] Balasubramanian S., "A Pata-type fixed point theorem", Math. Sci., 8, (2014), 65-69.
- [7] Banach S., "Sur les opérations dans les ensembles abstraits et leur application aux équation intégrales", Fundam. Math., 3, (1922), 133-181.
- [8] Beg I., Azam A., "Fixed points of asymptotically regular multivalued mappings", J. Austral. Math. Soc. (Series-A), 53, (1992), 313-326.
- [9] Chakraborty M., Samanta S.K., "On a fixed point theorem for a cyclical Kannan-type mapping", Facta Univ. Ser. Math. Inform., 28, (2013), 179–188.
- [10] Eshaghi M., Mohsen S., Delavar M.R., De La Sen M., Kim G.H., Arian, A., "Pata contractions and coupled type fixed points", Fixed Point Theory Appl., 1, (2014), 130.

- [11] Hong S.H., "Fixed points of multivalued operators in ordered metric spaces with applications", *Nonlinear Anal.*, 72, (2009), 3929-3942.
- [12] Kadelburg Z., Radenovic S., "Fixed point theorems under Pata-type conditions in metric spaces", *J. Egypt. Math. Soc.*, 24, (2016), 77-82.
- [13] Karapinar E., Kumam P., Salimi P., "On $\alpha - \psi$ -Meir-Keeler contractive mappings", *Fixed Point Theory and Applications*, 94, (2013).
- [14] Karapinar E., "Fixed points results via simulation functions", *Filomat*, 30(8), (2016), 2343-2350.
- [15] Khojasteh F., Shukla S., Radenovic S., "A new approach to the study of fixed point theorems via simulation functions", *Filomat*, 29(6), (2015), 1189-1194.
- [16] Kolagar S.M., Ramezani M., Eshaghi M., "Pata type fixed point theorems of multivalued operators in ordered metric spaces with applications to hyperbolic differential inclusions", *U.P.B. Sci. Bull., Series A*, 78(4), (2016).
- [17] Mohammadi B., Rezapour S., Shahzad N., "Some results on fixed points of $\alpha - \psi$ -Ciric generalized multifunctions", *Fixed Point Theory Appl.*, (2013), 24.
- [18] Nadler S.B., Multivalued contraction mappings, *Pacific J Math.*, 30, (1969), 475-488.
- [19] Nieto J.J., Rodriguez-Lope R., "Contractive mapping theorems in partially ordered sets and applications to ordinary differential equations", *Order*, 72, (2005), 223-239.
- [20] Paknazar M., Eshaghi M., Cho Y.J., Vaezpour S.M., "A Pata-type fixed point theorem in modular spaces with application", *Fixed Point Theory Appl.*, (2013), 239.
- [21] Pata V., "A fixed point theorem in metric spaces", *J. Fixed Point Theory Appl.*, 10, (2011), 299-305.
- [22] Patel D.P., "Fixed points of multivalued contractions via generalized class of simulation functions", *Bol. Soc. Paran. Math.*, 38(3), (2020), 161-176.
- [23] Radenovic S., Kadelburg Z., Jandrlic D., Jandrlic A., "Some results on weakly contractive maps", *Bull. Iranian Math. Soc.*, 38(3), (2012), 625.
- [24] Rhoades B.H., "Some theorems on weakly contractive maps", *Nonlinear Analysis*, 47, (2001), 2683-2693.
- [25] Samet B., Vetro C., Vetro P., "Fixed point theorem for (α, ψ) -contractive type mapping", *Nonlinear Analysis*, 75, (2012), 2154-2165.
- [26] Zhang Q., Song Y., "Fixed point theory for generalized φ -weak contractions" *Applied Mathematics Letters*, 22, (2009), 75-78.